Nanoneedle-based Gene Transfer for Cardiac Regeneration

&

Biophysical Regulation of Cellular State

Vincent Leonardo

A thesis submitted for the degree of Doctor of Philosophy

and the Diploma of Imperial College

Department of Materials

Faculty of Engineering

Imperial College London

Declaration of Authenticity

I declare that the work presented in this thesis was conducted by the author unless stated otherwise by reference in the text.

Some of the results presented in this thesis have been published and presented at various conferences and seminars.

Copyright Declaration

The copyright of this thesis rests with the author and is made available under a Creative Commons Attribution Non-Commercial No Derivatives licence. Researchers are free to copy, distribute or transmit the thesis on the condition that they attribute it that they do not use it for commercial purposes and that they do not alter transform or build upon it. For any reuse or redistribution, researchers must make clear to others the licence terms of this work.

Abstract

In recent years the advances in biomaterial science have made possible to use micro- and nano-fabrication techniques such as electro-spinning, soft- and photo-lithography to create numerous biomaterials with increasing sophistication in the ability to tune, mimic and manipulate complex physical and biological properties related to the cell niche. Modern biomaterials have a wide array of applications including but not limited to their use in surgical implants, medical devices, advanced applications in tissue engineering, biosensing and drug delivery, and as aids to understandthe interaction between cells and their niche to enablethe manipulation of cellular behaviour and identity.

This thesis aims to show how the combination of advanced biomaterials and biological tools can lead to the development of novel therapeutic tools and provides insight into cellular mechanosensing and cellular identity.

Firstly, the thesis aims at developing a proof-of-concept *in vivo* therapeutic tool targeted at rejuvenating the damaged myocardium post-myocardial infarction (MI) by nanoinjection of cardiac reprogramming factors to the epicardial layer of the heart. For this purpose, this study used a previously developed nanodelivery platform based on porous silicon nanoneedles (nN) that are capable of delivering a cargo in an efficient, safe and spatially resolved manner. An effective strategy was established through this study to uniformly load the nN with high concentrations of pDNA that are capable of rapid release under physiological conditions. A single polycistronic transposon-based plasmid containing the three cardiac transcription factors, MEF2C, GATA4 and TBX5 (MGT), was developed and used to initiate the direct conversion of the epicardial cells towards cardiomyocyte lineage. An *in vitro* study successfully demonstrated the ability of the nN to load and deliver the MGT containing transposon and the transposase to the epicardial derived cells (EPDC) and the transgenes were successfully integrated into the genome showing sustained prolong expression which in turn directed the EPDC to differentiate to cardiomyocytes. The i*n vivo* proof of principle study further demonstrates the mostly successful nN-mediated intracellular gene delivery to the heart epicardium.

The purpose of the second study is to provide further insight into the cellular response to external biophysical cues from a global perspective. External biophysical cues can be

transferred via the cytoskeletal networks to alter the nuclear matrix mechanically. The mechanisms that underlie this phenomenon have just started to be elucidated however there are still substantial processes that are not entirely understood. To address this issue, mouse embryonic fibroblasts (MEFs) were cultured on a high aspect ratio silicon-based nanomaterial with defined geometry and physical properties, namely nanoneedles. The close interaction with the nN induced substantial alteration on the nuclear shape and structure.

Furthermore, the positioning of the nucleosomes was also altered and the nanoneedles also induced significant changes in the histone modifications specifically the methylation patterns. RNA sequencing performed on MEFs grown on nN revealed enrichment in genes associated with cytoskeletal organisation, chromosomes organisation, response to oxidative stress and nuclear division and cell cycle. These results were mirrored by the label-free mass spectrometry proteomic analysis performed on cells cultured under the same conditions. The changes observed through the different analysis methodologies indicate that the cells were in a different state as oppose to cells cultured on conventional tissue culture plastic (TCP) potentially adopting a more responsive and open epigenetic state.

In conclusion, the work in this thesis demonstrates how biomaterials could be used in conjunction with robust biology to further advanced regenerative medicine and the understanding of complex biological problems.

Acknowledgements

First and foremost, I would like to thank God Almighty for all His blessing and for giving me strength, knowledge, ability and opportunity to undertake this research study and to persevere and complete it satisfactorily, without which, this achievement would not have been possible.

To my family, thank you for encouraging and supporting me in my pursuits and inspiring me to follow my dreams. I am especially grateful to my parents, who supported me emotionally and financially.

I am deeply grateful to my supervisor Professor Molly Stevens for all the advice, guidance and the opportunity to perform research in such a stimulating and incredible environment.

I would also like to thank Dr Paola Campagnolo, Dr Ciro Chiappini and Dr Manuel Mazo for all their help, advice, guidance and stimulating discussions throughout my degree.

Moreover, I would like to acknowledge Katie Hansel, Sahana Gopal, Wang Ye, Hsu Chia Chen, Worrapong Kit-Anan, Yi Yang, Stephanie Maynard, Eunjung Kim and Melisse Chee not only for all their help, stimulating discussions and very fruitful collaborations, but also for their friendship.

Finally, I would like to dedicate this thesis to my mom and dad, who have always been there for me through thick and thin and for loving me unconditionally.

Contents

Declaration of Authenticity....2
Copyright Declaration....2
Abstract....3
Acknowledgements....5
List of Figures....11
List of Tables....14
List of Abbreviations....15
1. Chapter 1: Introduction....18
1.1. Gene Delivery Strategies....20
1.1.1. Viral Delivery Carriers....20
1.1.2. Mechanical and Physical Methods for Gene Delivery....22
1.1.3. Biomaterials Based Carriers....24
1.1.3.1. Nanoparticles Based Delivery Systems....24
1.1.3.2. Microfabricated Nanostructures....25
1.1.3.2.1. Nanoneedle Fabrication and Characterisation....25
1.1.3.2.2. Nanoneedles as Delivery Tools....27
1.2. Material Systems Enabling the Study of Mechanobiology....28
1.2.1. Two-Dimensional Systems with Tunable Properties....30
1.2.1.1. Tunable Surface Geometry and Topography....30
1.2.1.2. Tunable Matrix Stiffness....32
1.2.1.3. Dynamic Extracellular Forces....33
1.2.2. Three-Dimensional Systems....33
1.2.3. Microfabricated Nanostructures: Novel Tools in Mechanobiology....34
1.2.3.1. Cell-Nanoneedle Interactions....37
1.3. Hypothesis, aims and scope of thesis....39
2. Chapter 2: Nanoneedle-based Gene Transfer for Cardiac Regeneration....40
2.1. Introduction....40
2.2. Pathology of Myocardial Infarction....40
2.3. Heart Regeneration....43
2.3.1. Regeneration Potential in Amphibian and Fish....43

2.3.2. Limited Regeneration Capacity of Mammalian Heart 43
2.4. Therapeutic Strategies for Cardiac Regeneration....44
2.4.1. Endogenous Progenitor Cells and their Role in Cardiac Regeneration....46
2.4.2. Transplantation of Exogenous Cells....47
2.4.3. Tissue Engineering Approaches 50
2.4.4. Exosomes for Cardiac Regeneration 51
2.4.5. Direct Cardiac Reprogramming....52
2.5. Cocktails for Direct Cardiac Reprogramming....53
2.5.1. Basal Cocktails....53
2.5.2. Additional Factors and Combinations....54
2.5.3. Factors for Human Direct Cardiac Reprogramming from Fibroblasts 56
2.5.4. *In vivo* Direct Cardiac Reprogramming....57
2.6. Strategies to Enhance Direct Cardiac Reprogramming 59
2.6.1. Reprogramming Factors Optimisation....59
2.6.2. Modulation of Epigenetic Barriers 60
2.6.3. Modifications of Cellular Signalling....61
2.6.4. Manipulations of the Microenvironment 62
2.7. The Epicardium and its Role in Cardiac Regeneration....66
2.7.1. Cellular Contribution of Epicardium in Adult Heart....67
2.7.2. Role of Epicardium-derived Mitogens in Adult Heart....68
2.7.3. Role of Epicardium in Cardiac Repair....69
2.7.4. Stimulations and Clinical Applications of the Epicardium 72
2.8. Aims....75
2.9. Hypotheses 76
2.10. Materials and Methods....77
2.10.1. Nanoneedle Fabrication 77
2.10.2. Nanoneedle Chip Surface Modifications....77
2.10.3. DNA Loading and Release Optimisation....78
2.10.4. Plasmids Used in The Study....79
2.10.5. Animal Surgical Procedures....79
2.10.6. Isolation of Rat EPDCs....80

2.10.7. *In Vitro* Nanoinjection of pDNA 81
2.10.8. *In Vitro* Assay for Rho-pDNA Delivery with Nanoneedles 81
2.10.9. Transposon Stable Integration Assay 81
2.10.10. *In Vitro* Direct Cardiac Reprogramming of Rat EPDCs 82
2.10.11. *In Vivo* Nanoinjection and Reprogramming 83
2.10.12. RNA Expression Analysis 83
2.10.12.1. RNA Isolation from Tissue Explants and Cell Lines 83
2.10.12.2. cDNA Synthesis and Quantitative qRT-PCR 84
2.10.13. Protein Expression Analysis 85
2.10.13.1. Protein Isolation 85
2.10.13.2. Western Blot 86
2.10.13.3. Immunostaining of Cultured Cells 86
2.10.13.4. Immunostaining of Histology Slices 87
2.10.13.5. Statistical Analysis 87
2.11. Results 90
2.11.1. Optimisation of pDNA Transfection with The Nanoneedle 90
2.11.2. Transposon Reprogramming Systems 94
2.11.2.1. Construction and Validation of the Transposon System 94
2.11.3. *In vitro* Nanoinjection and Reprogramming of Primary rEPDCs 100
2.11.4. *In vivo* Nanoinjection of the Post-MI Epicardium 105
2.12. Discussion 109
3. Chapter 3: Biophysical Regulation of Cellular State by Nanoneedles 112
3.1. Introduction 112
3.2. Cellular Behaviour and Its Regulation by Extracellular Cues 112
3.2.1. The Principle of Cellular Mechanosensing 112
3.2.2. Cellular Membrane – Matrix Interactions 114
3.2.3. Mechanotransduction and the Actin Cytoskeleton 115
3.2.4. Nuclear Mechanotransduction 117
3.3. Biophysical Regulation of the Epigenome 122
3.3.1. Epigenetic Codes 122
3.3.1.1. Chromatin 122

3.3.1.2. DNA Methylation 124
3.3.1.3. Histone Post-Translational Modifications 125
3.3.2 The Effects of Biophysical Cues on Chromatin 130
3.3.3 Biophysical Regulation of Epigenetic State in Cell Reprogramming 132
3.4. Aims 135
3.5. Hypotheses 135
3.6. Materials and Methods 136
3.6.1. Cell Culture 136
3.6.2. Cells Viability Assays 136
3.6.3. RNA Expression Analysis 137
3.6.3.1. RNA Isolation from *In Vitro* Cells 137
3.6.3.2. cDNA Synthesis and Quantitative RT-PCR 138
3.6.3.3. RNA Sequencing and Analysis 139
3.6.4. Protein Expression Analysis 140
3.6.4.1. Protein Isolation 140
3.6.4.2. Western Blotting 140
3.6.4.3. Immunostaining 141
3.6.4.4. Label-Free Mass Spectrometry 142
3.6.5. Statistical Analysis 143
3.7. Results 144
3.7.1. The Viability of Cells Cultured on Nanoneedle Chips 144
3.7.2. Nanoneedle Induced Nuclear Remodelling 147
3.7.3. Nanoneedle Induced Global Alterations 153
3.7.3.1. Overview of the Transcriptomic Profile 153
3.7.3.2. Overview of the Proteomic Profile 155
3.7.4. Pathway Analysis 158
3.7.4.1. Transcriptomic Pathway Analysis 158
3.7.4.2. Proteomic Pathway Analysis 164
3.7.4.3. Integrative Transcriptomic and Proteomic Analysis 165
3.7.5. Oxidative Stress Response on Nanoneedles 169
3.7.6. Nanoneedle and Cell Cycle Control 177

3.7.7. Histones and DNA Modifications on Nanoneedle Chips.....187
3.8. Disscussion.....195
4. Conclusions.....199
5. References.....206

List of Figures

Figure 1. An overview of vectors used for gene delivery 23
Figure 2. Fabrication process and properties of porous silicon nanoneedles 27
Figure 3. Biomaterial Systems for the Study of Mechanobiology 30
Figure 4. Cell Behaviour across different vSNA densities 37
Figure 5. Cellular and Molecular Events Following MI 43
Figure 6. Regenerative-based therapeutics for MI 46
Figure 7. Summary of direct reprogramming by transcription factors. 54
Figure 8. Summary of the role of the epicardium during development 67
Figure 9. Role of Epicardium in Cardiac Injury and the Signals and Factors Involved 72
Figure 10. Overview of the nanoinjection strategy for direct cardiac reprogramming 77
Figure 11. Optimizing the efficiency of nanoinjection 93
Figure 12. Map of the piggyBac transposon-based polycistronic vector 95
Figure 13. Overexpression of the MGT transgenes in RNA and protein levels 97
Figure 14. Nanoinjection mediates integration 99
Figure 15. Characterisation of isolated primary rat epicardial cells 100
Figure 16. qRT-PCR of rEPDCs transfected with MGT+HaHy or blank Ctl via FuGene 102
Figure 17. nN mediated delivery and transfection of epicardial cells 103
Figure 18. Nanoinjection and reprogramming of epicardial cells 104
Figure 19. *In vivo* nanoinjection of Rho-pDNA, early time point (30 min) 106
Figure 20. *In vivo* nanoinjection of Rho-pDNA, later time point (Day 4) 106
Figure 21. *In vivo* nanoinjection of MGT+HaHy to the epicardium for genes regulation 108
Figure 22. Schematic depicting the complexity of the cellular microenvironment 113
Figure 23. Cell-Matrix Interface. 115
Figure 24. Nuclear Mechanotransduction 121
Figure 25. Chromosomal Organisation and Modifications 123
Figure 26. Single Nucleosome with Histone Post-Translational Modifications 125
Figure 27. Histone post-translational modifications and their histone modifying enzymes 128
Figure 28. Chromatin Status 134
Figure 29. Epigenetic Landscape of Cellular Reprogramming 129
Figure 30. Characterisation of MEFs viability on nanoneedle 147

Figure 31. Nanoneedle-induced nuclear deformation 149
Figure 32. Quantitative analysis of nanoneedle-induced nuclear deformation 150
Figure 33. Nanoneedle-induced nuclear deformation did not cause nuclear condensation 151
Figure 34. FRAP experiments on H1-GFP diffusion kinetics 152
Figure 35. Heat map of genes expression 154
Figure 36. Volcano plot displaying DEGs between nN and TCP samples 154
Figure 37. Principal component analysis of the dataset 155
Figure 38. Hierarchical clustering analysis 156
Figure 39. Volcano plot displaying DEPs between nN and TCP samples 157
Figure 40. GO enrichment analysis of differentially upregulated expressed genes 158
Figure 41. GO enrichment analysis of differentially downregulated expressed genes 159
Figure 42. Global Functional Analysis 160
Figure 43. Canonical pathway analysis of upregulated DEGs 162
Figure 44. Canonical pathway analysis of downregulated DEGs 163
Figure 45. GO enrichment analysis of differentially expressed proteins 164
Figure 46. Interactions between mRNA and proteins samples 165
Figure 47. Comparative Global Functional Analysis 168
Figure 48. Comparative Canonical Pathway Analysis 169
Figure 49. NRF2-mediated oxidative stress response 172
Figure 50. NRF2-Upstream analysis 173
Figure 51. ELISA assay of pERK 174
Figure 52. MGST1 differential expression 174
Figure 53. DNA damage investigated by the level of γH2Ax 175
Figure 54. G2/M transition pathway 179
Figure 55. Differential expression of kinetochore complex 180
Figure 56. Mitotic pathways 182
Figure 57. Investigation of cell division 183
Figure 58. Cell Cycle Upstream Regulators 186
Figure 59. The screen of histone modifying enzymes 188
Figure 60. H3K4me3 immunofluorescence 188
Figure 61. Quantification of H3K4me3 189

Figure 62. Quantification of H3K4me3 modifying enzymes 190
Figure 63. H3K27me3 immunofluorescence 191
Figure 64. Quantification of H3K27me3 191
Figure 65. Quantification of H3K27me3 modifying enzymes 192
Figure 66. Quantification of H3K4/K19Ac 193
Figure 67. mRNA level of HDAC11 193
Figure 68. Effect of nanoneedle on the level of DNA 5-mc 194
Figure 69. Expression levels of DNMTs 195

List of Tables

Table 1. List of clinical trials using transplantation of adult stem cells mentioned in the text 50

Table 2. List of known cardiac reprogramming factors used 65-66

Table 3. Composition of Cardiac Reprogramming Medium.....84

Table 4. TaqMan qRT-PCR reaction mix.....85

Table 5. Taqman qRT-PCR thermal cycling profiling 86

Table 6. TaqMan probes used in this study.....86

Table 7. Immunofluorescence blocking solution recipe. 88

Table 8. Primary antibodies used for immunofluorescence (IF) and western blot (WB)...88-89

Table 9. List of Secondary antibodies for the detection of primary antibodies in IF and WB. 89

Table 10. Different classes of histones modifications known and their associated functions 126

Table 11. SYBR Green qRT-PCR reaction mix 139

Table 12. SYBR Green qRT-PCR thermal cycling profile.....139

Table 13. SYBR primers used in this study 140

Table 14. Primary antibodies used for immunofluorescence (IF) and western blot (WB) 142

Table 15. Immunofluorescence blocking solution recipe.....143

Table 16. Secondary antibodies used for immunofluorescence (IF) and western blot (WB) 143

Table 17. Statistically significant genes regulated at the same level in both mRNA and protein levels 166

Table 18. Over-represented pathways involved in oxidative stress response.....170

Table 19. Over-represented pathways involved in cell cycle regulation.....177

List of Abbreviations

7F	GATA4-MEF2C-TBX5-ESSRG-MESP1-MYOCD-ZFPM2
9F	CHIR99021-A83-01-BIXO1294-AS8351-SC1-Y27632-OAC2-SU16F-JNJ
AAVs	Adeno-associated virus
APTES	3-aminopropyltrieoxysilane
BMNCs	Bone marrow-derived mononuclear cells
CDCs	Cardiosphere derived cells
CFs	Cardiac fibroblasts
CMs	Cardiomyocytes
CPCs	Cardiac progenitor cells
CRFVPT	CHIR99021-RepSox-Forskolin-VPA-Parnate-TTNPB
cTnT	Cardiac Troponin T
DAPI	4’6-diamidino-2-phenylindole
DEGs	Differentially expressed genes
DEPs	Differentially expressed proteins
ECM	Extracellular matrix
EFs	Ejection fraction
EMT	Epithelial-to-mesenchymal transformation
EPDC	Epicardial derived cells
ESCs	Embryonic stem cells
EVs	Extracellular vesicles
FAK	Focal adhesion kinases
FBS	Foetal bovine serum
FGF	Fibroblasts growth factor
FHF	First heart field
FRAP	Fluorescence recovery after photobleaching
GAGs	Glycosaminoglycans
GMT	GATA4-MEF2C-TBX5
GMTMM	GATA4-MEF2C-TBX5-MESP1-MYOCD
GMTMSMS	GATA4-MEF2C-TBX5-MYOCD-SRF-MESP1-SMARCD3
GO	Gene ontologies

HA	Hyaluronic acid
HBSS	Hank’s balanced salt solution
HDAC	Histone deacetylase
HF	Hydrofluoric acid
HNGMT	HAND2-NKX2.5-GATA4-MEF2C-TBX5
HSCs	Hematopoietic stem cells
iCMs	Induced cardiomyocytes
IF	Immunofluorescence
IPA	Ingenuity pathway analysis
iPSCs	Induced pluripotent stem cells
ITR	Inverted terminal repeat sequences
LVEF	Left ventricle ejection fraction
MEFs	Mouse embryonic fibroblasts
MGT	MEF2C-GATA4-TBX5
MI	Myocardial Infarction
MMPs	Matrix metalloproteases
MTM	MEF2C-TBX5-MYOCD
nN	Nanoneedle
OX	Oxidised
PB-GFP	PiggyBac GFP plasmid
PB-MGT	PiggyBac MGT plasmid
PBS	Phosphate buffer saline
PDMS	Polydimethylsiloxane
pDNA	Plasmid DNA
PE	Proepicardium
PEG	Poly (ethylene glycol)
PGs	Proteoglycans
PTMs	Post-translational modifications
qRT-PCR	Quantitative real-time polymerase chain reactions
RA	Retinoic acid
ROS	Reactive oxygen species

RT	Reverse temperature
SDS-PAGE	Sodium dodecyl sulfate-polyacrylamide gel electrophoresis
SHF	Second heart field
shRNA	Short hairpin RNA
SIM	Structured illumination microscopy
siRNA	Small inhibitory RNA
SP	Side population
TCP	Tissue culture plastic
TIMPs	Tissue inhibitors of metalloproteases
TTF	Tail-tip fibroblasts
Tβ4	Thymosin beta-4
VEGF	Vascular endothelial growth factors
VPA	Valproic acid
WB	Western blot

Chapter 1: Introduction

Biomaterials play various crucial roles in medical applications and can be generated from numerous sources including natural sources, such as collagen, gelatine or other purified matrixes, and synthetic materials including polymers, silica or metals [20].

Biomaterials have evolved from a simple physico-mechanical construct to second generation materials with inherent bioactivity and resorbable behaviour followed by third generation biomaterials capable of stimulating and regulating specific cell responses [21]. Moreover, the recent advances in nanotechnology and microfabrication techniques have made possible to design biomaterial-based drug delivery systems and scaffolds [20]. Nanoscale architectural features are incorporated to mimic the native extracellular matrix (ECM) to simulate the cell microenvironment and drive specific cellular functions [22].

Substantial research efforts have been focused on developing biomaterials for applications in tissue engineering. In orthopaedics, one of the most prominent usages of biomaterials, a variety of materials such as metal alloys, polymers, and ceramics have been used [23]. Also, naturally derived or synthetic scaffolds have been used, for example to replace damaged valves or reopen blocked arteries in the cardiovascular systems [24]. More recently, the combination of cell therapy and tissue engineering has shown great promise as a potential therapy to induce cardiac repair following injuries [25]. Furthermore, bioengineered skin grafts made of cells seeded on biocompatible and biodegradable 3D scaffolds have slowly been adopted as viable strategies for the repair of skin injuries [25].

The use of biomaterials in drug-delivery systems is one of the fastest growing areas. Many studies have explored the creation and design of devices capable of controlled and targeted delivery of molecules *in situ* in a living system. The design of these carriers should be in-line with the target sites, the disease phenotype and the type of molecules to be delivered. Some of these constructs incorporate smart polymeric materials, and more recently, nanofabricated materials have emerged as another viable option to achieve controlled and targeted delivery [26].

In the past decade, the growing appreciation and understanding of the importance of physical properties, including topological and mechanical cues, in modulating cellular response has risen to an unprecedented level [27]. Mounting evidence shows that physical features of varying length and dimension from tens of nanometers to tens of micrometres can influence

how cells perceive, interact and respond to certain stimuli. The mechanisms responsible for these effects are only beginning to be unravelled. New approaches in biomaterial fabrication techniques which enable the incorporation of physical as well as chemical moieties to construct physiologically relevant materials have become indispensable tools to study how the cell phenotype is regulated by this dynamic interplay between the cell and its surrounding microenvironment.

In the following sections, two main concepts comprising the core of this thesis are highlighted:

- Microfabricated nanostructures as gene delivery systems.
- Microfabricated nanostructures as tools to study cell-ECM interactions.

The work presented in this thesis aims to present a proof-of-concept study to show efficient gene delivery *in vitro* and *in vivo* via nano-structured materials and investigates the global functional changes of material-induced remodelling including epigenetic and inner chromatin structure. To fulfil these aims, the present work utilises porous high-aspect ratio nanoneedles designed and fabricated in-house as the material used to answer these questions.

1.1. Gene Delivery Strategies

Gene therapy holds high therapeutic potential due to the prolonged and sustained beneficial effect that it can achieve unlike the transient effect of most pharmacotherapies. Gene therapy involves the delivery of therapeutic and functional nucleic acid-like plasmid DNA, si/shRNA or miRNA or nucleases to modulate the gene expression profile of cells, tissues or organs for the prevention or treatment of diseases, or to fix genetic defects. Nevertheless, the advancement of gene therapy is hampered by the limitation of the current delivery vectors. The ideal delivery vector should be non-cytotoxic and non-immunogenic, and with a high nucleic acid loading capacity and localised effect.

In general, viral or non-viral vectors are the most commonly used vehicles for gene therapy, and both have advantages and limitations (Fig. 1). More recently, the advancement of microfabrication techniques has also led to the development of unique nanomaterial-based nucleic acid delivery systems.

1.1.1. Viral Delivery Carriers

Currently viral delivery methods are the most widely used gene therapy delivery carriers for clinical use [28]. This is partly due to their ease of production, high functional titer, ability to infect a wide variety of cell types and capability to protect the therapeutic payload within the viral capsid shell. Some of the viruses that have been used for human gene therapy include adenovirus, adeno-associated virus, retroviruses and lentiviruses (Fig. 1).

Adenoviruses were among the first viruses used in gene therapy due to their excellent transduction efficiency and have been widely used for cardiac gene therapy applications [29]. Although adenovirus vectors are able to successfully deliver therapeutic genes for treating the vasculature problems, they induce the activation of both innate and humoral immune response, and show some level of toxicity [29]. Further modifications to the first-generation adenoviruses, unfortunately, did not sufficiently alleviated the adverse effects [30]. Thus they are no longer commonly used for gene therapy but have procured a new role in cancer treatment as an oncolytic virus where robust immune responses are beneficial for therapeutic outcomes [30].

The use of adeno-associated virus (AAVs) vectors for gene therapy have yielded many successes [29]. This is partly due to their ability to infect non-dividing cells and to integrate

into the host genome for sustained modification, and their much lower immunogenicity in comparison with adenoviruses. Several studies have investigated and proposed several AAVs serotypes, like AAV-6,8 and 9, for efficient delivery of cardiac tissue [29]. Many efforts are still conducted to find novel serotypes to induce tissue-specific transduction profiles and expand the existing repertoire of AAV viruses to circumvent the issues of immunogenicity and innate tropism [30]. The capability to transduce both dividing and non-dividing cells, and the ability to cause stable, persistent transgene expression have catapulted lentivirus-based vectors as a suitable delivery vehicle for end-point differentiated cells, such as cardiomyocytes [29].

To increase the safety of this method of delivery, a system utilising several plasmids that expresses lentiviral proteins, produces viral capsids and the desired transgenes separately has been developed [31]. Modification to the noncoding sequences on the ends of the lentivirus-based vectors has also reduced the risk of side effects caused by insertional mutagenesis (genotoxicity). However, the use of lentivirus-based vectors might still lead to transduction induced cell transformation (oncogenesis) and heterogeneous transduction due to its preferred route of delivery [29].

In the case of *in vivo* direct cardiac reprogramming, where resident cardiac fibroblasts are converted into *de novo* cardiomyocytes with defined cardiogenic factors, retroviruses have been used to deliver the reprogramming factors [32-35]. The rationale is to exploit retroviruses' inherent properties to only infect proliferating cells, thus making sure that only dividing cells in the heart (mostly fibroblasts) are transduced since adult cardiomyocytes no longer enter the cell cycles. In terms of safety and side effects, retroviruses are considered to be inferior than lentivirus-based vectors.

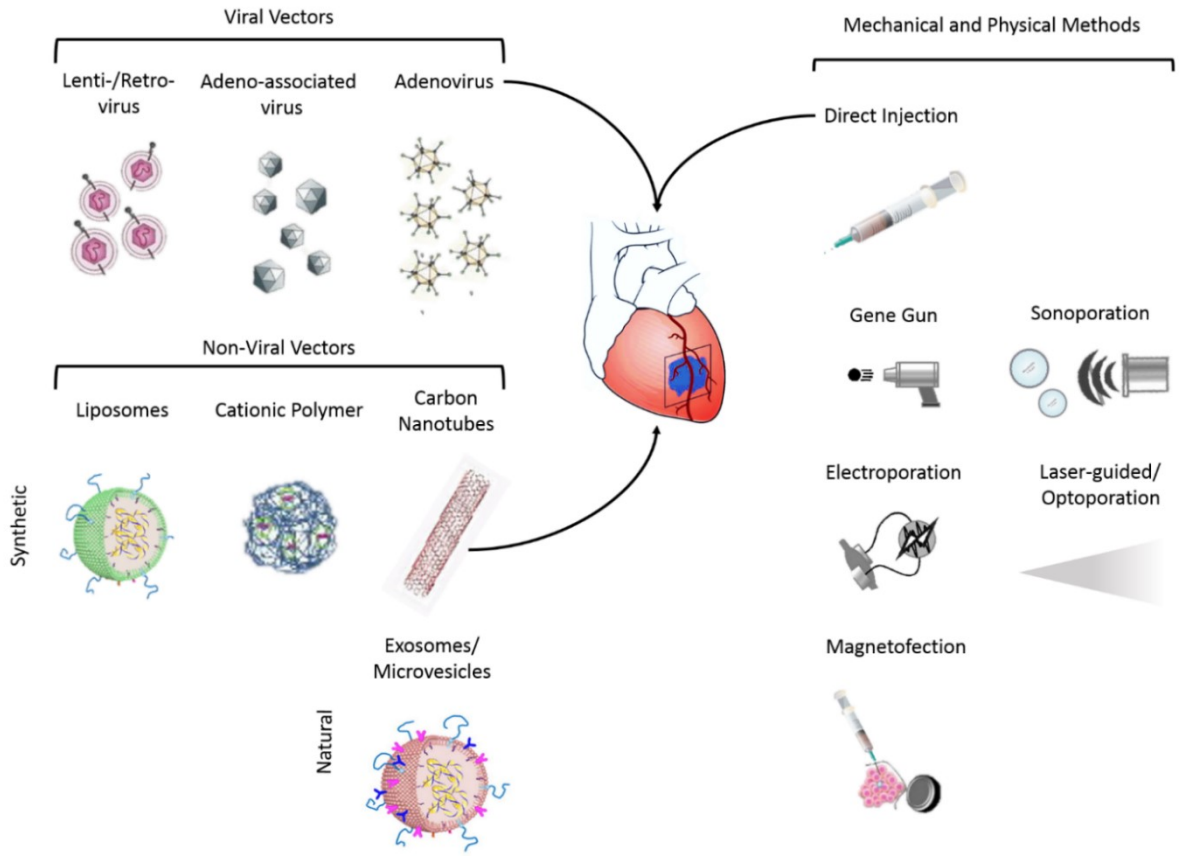


Figure 1. An overview of vectors used for gene delivery. Classically viruses, including adenovirus, AAV and lenti-/retro- viruses have been used as a gene therapy delivery tool. However, due to safety concerns, alternative approaches have been developed over the years. Non-viral vectors have risen in popularity due to improved safety and ease of modifications, but the efficiency of delivery is still far below than that of viral vectors. Non-viral vectors can be separated into synthetic and natural systems. Direct mechanical and physical methods offer the users more precise controls over the spatiotemporal delivery of the genetic load *in vivo*, nonetheless, these methods can induce tissue damage and activate the immune response.

1.1.2. Mechanical and Physical Methods for Gene Delivery

A range of physical-based delivery strategies has also been used to deliver therapeutic nucleic acids to the heart (Fig. 1). Direct needle injection of naked pDNA might be the most simple and straightforward method. Several studies have used this technique for delivering pDNA to the heart [36]. However, due to premature degradation, poor cellular uptake across the cell membrane, and inflammation in response to needle injury have to led to the loss of interest in this therapeutic activity [36].

The ballistic DNA transfer or gene gun method is based on the use of pressurised gas to accelerate nucleic acid coated nanoparticles to achieve transfection in target cells by direct penetration through the cell membrane [36]. Using this technology, DNA-coated gold particles were successfully delivered to beating rat hearts and resulted in the expression of GFP transgenes [36]. The expression was only detected in the bombarded region and not in the collateral organs, demonstrating the level of specificity that can be achieved.

The electroporation method entails the use of small-interval high-intensity electric pulses to create transient pores on the cell membrane in combination with DNA injection. The delivery of VEGF expressing plasmid to porcine heart was enhanced five-fold through electroporation [37].

Sonoporation is another physical method that uses ultrasound in the presence of gas-filled microbubbles. The microbubbles are coated with the nucleic acid of interest, and upon the application of ultrasound waves, the bubbles are mechanically destroyed within the target tissue and diffused into the cell [38]. The ultrasound also enhances the permeability of the cell membrane, and the transfection efficiency dramatically depends on the strength of the acoustic waves and the duration of the exposure to ultrasound [38]. Using this technique, Bekeredjian *et al.* have demonstrated the feasibility of delivering microbubbles containing luciferase expressing plasmids in the rat heart with high spatiotemporal specificity [39]. In another study, the delivery of hepatocyte growth factor in conjunction with the application of ultrasound after MI successfully prevented left ventricular remodelling and reduced scar size [40].

The laser beam has also been used to circumvent the rate-limiting cell membrane step, by creating a local thermal effect that enhances the permeability of the cell membrane [41]. In a porcine model of chronic ischemia, the combined treatment of VEGF(121) plasmid injection and transmyocardial laser lead to a three-fold increase in expression, and subsequently, pigs that received the combined treatment showed increased regional myocardial perfusion and restoration of function [42].

Finally, another technique worth mentioning is magnetofection. This method uses the external magnetic control to deliver systemically administered paramagnetic nanoparticles containing DNA complexes into the target tissue. A study conducted in a murine model

demonstrated that the delivery of these particles under the guidance of a magnetic field had a 36-85 fold increase on transfection efficiency compared with the control group [43].

1.1.3. Biomaterials Based Carriers

Although the use of viral vectors and physical methods have significantly advanced the field of gene therapy, a few side effects and limitations associated with those techniques, such as immunogenicity, oncogenicity, broad tropism, limited packaging capacity, and physiological damages have put a brake on their wide-spread clinical usage. In response, biomaterials based nano-carriers including liposomes, cationic polymers, and nano-structured material were developed to potentially address some of the limitations.

1.1.3.1. Nanoparticles Based Delivery Systems

Liposomes made of cationic lipids are the most effective nonviral gene delivery system. The liposomes can be tailored to meet specific DNA size requirements, and the lipid bilayer protects the nucleic acid from nuclease-mediated degradation. Moreover, the surface of the liposomes can be decorated with cues to enable specific targeted delivery [44]. As an example, the conjugation of monoclonal anti-myosin antibody and TAT peptide significantly enhanced the transfection of cardiomyocytes in the ischemic heart [45]. It can also be engineered to release cargo upon exposure to external forces, for instance in microbubble-liposomes the use of ultrasonic waves break up the microbubble and release waves which disrupt the nearby cell membranes and increase their permeability leading to enhanced uptake of the liposomes. This method has been successfully applied in murine and dogs cardiac disease models [46, 47].

The use of cationic polymers to deliver nucleic acids *in vivo* shows some promise. The structural and functional groups of polymeric vectors can be easily modified to offer the ability to fine-tune the system to specific needs and to enable higher transfection efficiency. As an example, the use of dexamethasone-conjugated polyethyleneimine enables the complex to be safely relocated into the nucleus by binding to the glucocorticoid receptor upon cell entry [48]. Oligopeptides modified polymers have been used to deliver human erythropoietin genes into infarcted hearts and have been shown to prevent fibrosis, apoptosis and to have cardioprotective effects on post-infarct rats [49].

Besides the use of lipids and polymers to form nanoparticles for the delivery of nucleic acid, the use of inorganic nanomaterials such as gold, graphene oxide and quantum dots has also been explored. In general, these materials are easy to functionalise, possess unique electrical and optical properties, are biocompatible and have low cytotoxicity [50].

1.1.3.2. Microfabricated Nanostructures

Despite recent advances, non-viral carriers are still not as capable as viral carriers in delivering nucleic acids *in vivo*. The use of non-viral carriers could also result in the activation of the host immune response. Thus, much effort has been put on developing a more sophisticated platform for nucleic acid delivery, and advances in biomaterial fabrication techniques and the convergence of multiple disciplines including biology, medicine, engineering and material sciences have yielded a new range of nanoscale materials with precise geometry, texture and rigidity, namely nanoneedles and nanopillars.

One of the main characteristics of nanoneedles is the high aspect ratio, which enables them to interact with the intracellular space of a large number of cells simultaneously without affecting to their physiological processes. Nanoneedles can exist as single needles (*i.e*. nanowires) or as an array supported on a substrate. Nanoneedles can be fabricated to have different structures to fit specific needs. For example, nanowires enable multiple probing sites across a cell simultaneously due to their disordered structure. Nanopillars with defined geometry can be modified to have a variety of mechanical properties to modulate their profile of cellular interaction and to accurately sense forces applied by cells. Nanostraws are a type of nanotubes with an open end at both sides, with one end connected to a reservoir. They can be used to create a sustained and controlled exchange of contents between the intracellular and extracellular space. The conical structure of nanocones improve stability while making them porous provides an extra surface area for interaction with molecules.

1.1.3.2.1. Nanoneedle Fabrication and Characterisation

There are many fabrication strategies used to create the broad variety of nanoneedle structures.

This section will briefly describe the fabrication steps used to create the nNs that were used in this thesis (Fig. 2). The nanoneedles were fabricated with a metal-assisted chemical etch and standard microfabrication technique to achieve a high throughput homogeneous

synthesis of porous silicon nN arrays [9]. The geometry has been optimised to meet the requirement for intracellular delivery (Fig. 2). The nNs used are 5 µm in length with an apical tip diameter of 50 nm and a base diameter of 600 nm. This geometry is below the dimensions known to induce nanoneedle cytotoxicity [51]. The nanoneedles are supported by a solid base and have a 2 µm spacing between each nanoneedle. The nanoneedles are porous to increase the surface area and to maximise the volume of molecules that can be loaded. The nNs are also biodegradable due to the porosity introduced into the structure, an essential property for *in vivo* application. The nNs have robust mechanical properties and are able to withstand forces two orders of magnitude higher than the forces required for cell penetration [9].

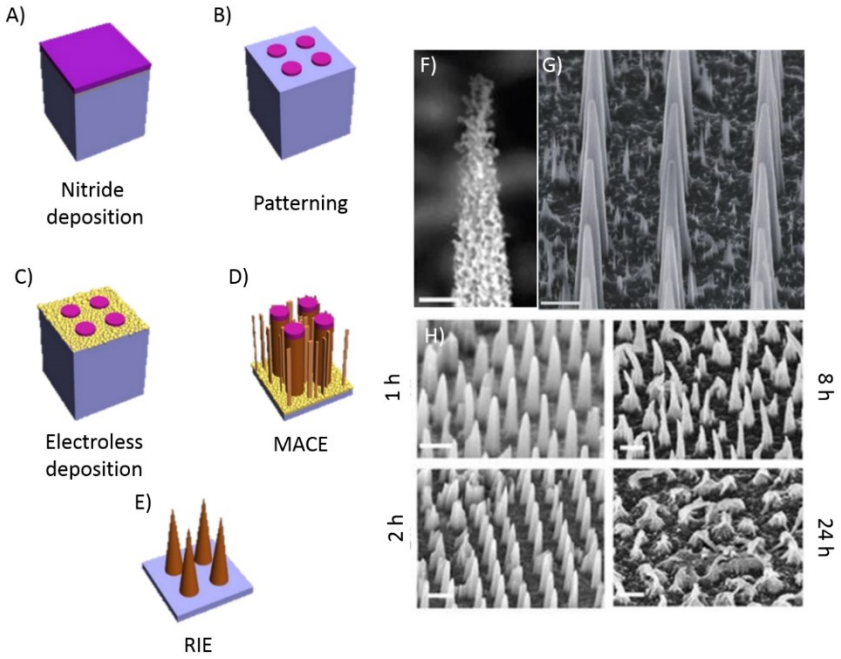


Figure 2. Fabrication process and properties of porous silicon nanoneedles. The fabrication process starts with (A) the deposition of a thin film of low-stress silicon nitride by low-pressure chemical vapour deposition. (B) A 600 nm circular nitride pattern is created by reactive ion etching (RIE), (C) followed by selective deposition of Ag dendrites over the surface by electroless deposition from $AgNO_3$ salts. (D) pSi pillars and nanowires are created by metal assisted chemical etch (MACE) in oxidising solution of HF. (E) The pillars are shaped into conical structures by reactive ion etching in SF_6 plasma. This step also removes the nanowires. (F-G) Scanning electron microscopy (SEM) images showing the morphology of the nanoneedles. (F) The high-resolution SEM images show the porosity of the nanoneedle structure with a tip diameter of 100 nm (Scale bar= 200 nm). (G) The nanoneedle used in the study has an array of 2 µm pitch (Scale bar= 2 µm). (H) SEM micrographs showing the progressive degradation of the nanoneedles over time in cell culture medium at 37^{o}C, with a complete loss of structural integrity between 8 – 24 hours (Scale bars= 2 µm). Figures adapted from [9, 10].

1.1.3.2.2. Nanoneedles as Delivery Tools

The nanoneedles have rapidly emerged as a tool with tremendous potential owing to their ability to efficiently deliver cell impermeant molecules [9, 52, 53] and nanoparticles [10] directly to the cytosol, and sense the state of the intracellular microenvironment [54, 55] across biological systems ranging from cells [56] to tissues within living organisms [57] without eliciting immune reactions.

The most relevant application of the nanoneedles in the context of this thesis is their ability to deliver cell-impermeant payloads (pDNAs, siRNAs, peptides, proteins and nanoparticles) across the cell membrane and directly into the cytosolic space. This method allows the molecules to circumvent the cell membrane and the endolysosomal system, thus overcoming one of the most significant obstacles in nanoparticle-based therapeutics. Although a host of methods has been developed to deliver these various molecules, unfortunately, most of the approaches have proven to be ineffective. Shalek and colleagues demonstrated that vertical silicon nanowires (NWs) could be used to deliver an array of biomolecules without disturbing the normal physiological function of the cells [52, 53]. Through the use of membrane-labelled cells and fluorescently conjugated dyes of different wavelength on the tip of the NWs, they demonstrated that direct cellular penetration of the loaded NWs is the mode of delivery into the cells [52]. They also demonstrated that the molecules delivered can exert their proper function within the cells. As an example, in their subsequent study, they utilised NW-mediated transfection to deliver siRNA to silence LEF1 in various primary immune cells to investigate its role in chronic lymphocytic leukaemia [53].

A recent study has generated a magnetic nanospear that uses a magnet to precisely control the positioning and 3D rotation of the particles for targeted intracellular gene delivery [58]. One advantage of this system is that it would enable the clinician to remotely control a systemically injected magnetic nanospear to the site of interest.

A seminal study by Chiappini *et al.* [9] demonstrated for the first time the use of porous degradable nanoneedles to deliver molecules in a highly uniform and localised manner in an *in vivo* context without causing any morphological tissue damage and any inflammatory responses. Furthermore, this study demonstrated that nanoinjection of VEGF-165 expressing plasmid into the muscle of mice resulted in neovascularisation that was far superior in terms

of gene expression, number of de novo nodes and overall blood perfusion than the direct injection of the same amount of naked plasmid [9].

The same group showed that the nNs can also be used to load and deliver cell impermeant quantum dots both *in vitro* and *in vivo* [10]. They managed to achieve transfection as quick as 30 min post-interfacing in a cell culture system, and only required 2 min of application to the skin and muscle of mice to efficiently deliver the quantum dots [10]. However, the exact mechanism of how nanoneedles efficiently deliver cargo directly into the intracellular space is still an ongoing debate.

1.2. Material Systems Enabling the Study of Mechanobiology

The creation, characterisation and manipulation of *in vitro* generated models isessential to understand in depth the complex interaction between cells and their microenvironment. Over the past two decades, different types of *in vitro* model systems have been established to provide dynamic modulation and stimulation of various biochemical and biophysical cues to cultured cells. Micro- and nano-engineered functional biomaterials have been of great help to allow researchers to understand in great detail the effects of individual biophysical signals present in the microenvironment, such as cell shape and geometry, stiffness, topography, external forces and spatial patterning extracellular proteins (Fig. 3). Working at the interface between biology, medicine and materials science, we are now entering a new era of science using these functional biomaterials to propel our understanding of mechanobiological responses and mechanotransduction pathways. Such systems can be categorised into 2D and 3D, taking into account the dynamic and multiparametric nature of the cellular microenvironment (Fig. 3).

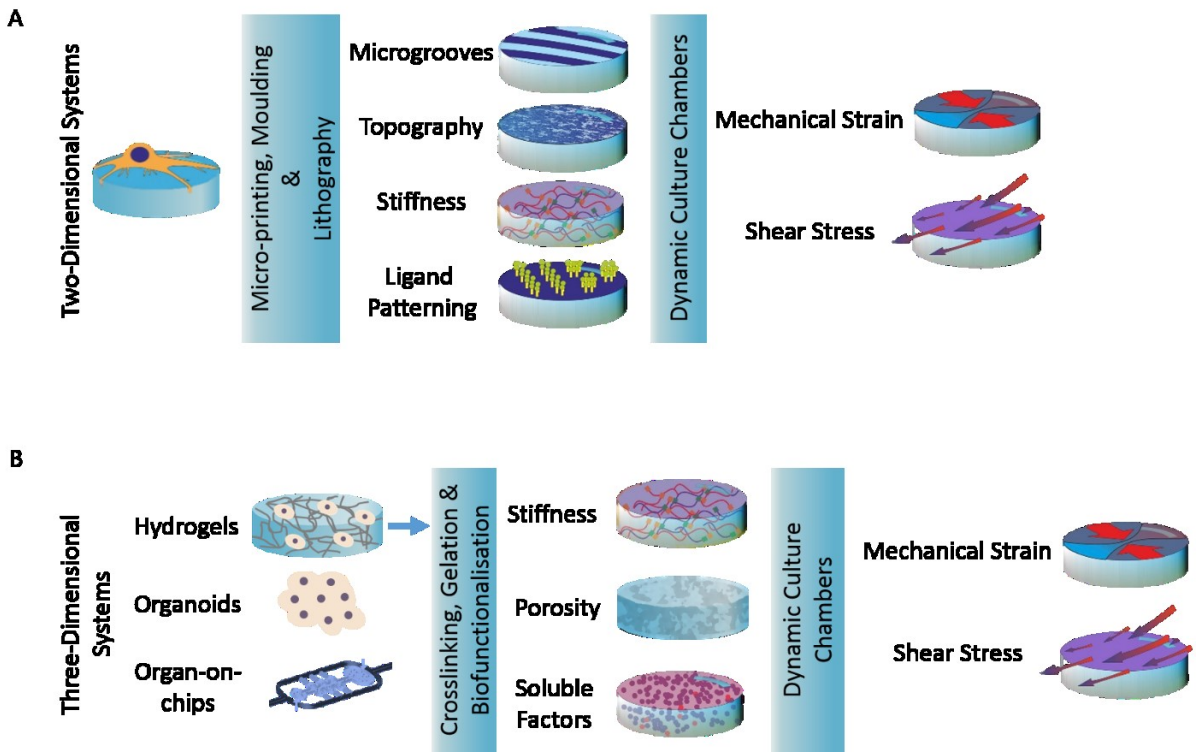


Figure 3. Biomaterial systems for the study of mechanobiology. The systems can be classified in 2D and 3D, and both types can be modified to have variety of biochemical and biophysical properties present in the *in vivo* environment albeit with slight variation in the methods used to achieve them. (A) In a 2D system, it is possible to introduce topographical cues such as micro- or nano-surface roughness through acid-assisted etching, and micro- or nanoscale structures like grooves, pits, pillars or conical structures using advanced lithography techniques. Patterning of ECM components or instructive biochemical cues can also be used to modulate cellular behaviour. (B) Cells can be seeded inside hydrogels, aggregated into an organoid or seeded inside pre-designed microfluidic chips, to form a 3D culture model. 3D hydrogel systems allow the modification of stiffness and porosity by modulating the crosslinking and gelation parameters. Additionally, instructive soluble cues can be distributed across the system by simple diffusion or cross-linked into the structures. In both 2D and 3D systems, external mechanical strains and fluid shear can be introduced using 3D strain systems and fluid flow cell, respectively.

1.2.1. Two-Dimensional Systems with Tunable Properties

1.2.1.1. Tunable Surface Geometry and Topography

In vivo, cells reside in a complex 3D microenvironment with a vast topographical architecture. Ranging from porous honeycomb to fibrous networks, these structures can range from micro- to nanometers in dimension. Various biomaterials with micro- or nanoscale surface topography have been developed to help reveal different cellular phenotypes. Roughness and patterns on the material surface are some of the factors affecting substrate topography. MSC differentiation towards an osteogenic lineage was shown to be enhanced upon culture on substrates with a surface roughness ranging from 0.7 to 1 µm despite the presence or absence of osteogenic inducers [59, 60].

Interestingly, the introduction of nanoscale roughness in the range of 100 nm by acid etching has been reported to be enough to positively influence the osteogenic differentiation of osteoblastic cells [61, 62]. For simplicity, surface topography is classified into two major categories based on their orientation (*i.e.* anisotropic or isotropic). An anisotropic surface is defined as a surface with precise orientation such as grooves or ridges, and an isotropic surface, on the other hand, is a surface without any orientation such as pillars and pits.

On a microscale level, several studies have demonstrated the ability of microgrooved substrates in modulating cell fate. For example, culturing MSCs on 15 µm ridges enhances the differentiation potential towards the adipogenic lineage whereas 2 µm ridges enhances osteogenic differentiation [63] and grooves in a similar range can also enhance myogenic differentiation [64]. Also, microgrooved substrates have been used to guide the neuronal differentiation of hESCs and the extent of the dendritic outgrowth [65]. With advances in material sciences and fabrication techniques, recent studies have started to use nanoscale ridges and grooves instead. A landmark paper by Downing *et al.* showed that MEFs cultured on parallel microgrooves lead to alignment and nuclear elongation which is correlated with an increase in active epigenetic marks on pluripotency genes that result in higher induced pluripotent stem cells (iPSCs) reprogramming efficiency [66]. Nano-grooved topography is of great use when it comes to neuronal tissue engineering. As an example, the use of 350 nm nanograted surface has been demonstrated to differentiate hMSCs into neuronal lineage with or without the presence of retinoic acids as shown by the significant upregulation of neuronal markers [67].

However, the use of isotropic surfaces to control cellular behaviour often results in a highly heterogeneous response and is partly due to the variation in cell types, culture conditions and the materials properties itself. Pillars, pits, nanotubes and unaligned nanofibers are some of the typical examples of isotropic architectures. Dimensions and distributions of these features are some of the elements that can be varied in the design of the material surfaces. In general, the use of nanopillars or islands synergistically enhances the differentiation capacity of MSCs toward the osteogenic lineage in the presence of an inductive media [68-70]. A study by Dalby *et al.* reported that the specific distribution of the topographical features might also influence stem cell behaviour with disordered nanopits resulting in the highest osteogenic induction in comparison to irregular or highly organised topographies [71].

Advances in fabrication techniques have made possible to create a new class of nanomaterials for cellular-interfacing, namely nanoneedles and nanopillars. This type of nanostructures have an exact geometry, texture and rigidity and can be produced in a variety of different formats, from nanostructures with a hollow cores (nanostraws) [72] to high-aspect ratio porous needles [9]. This type of materials can be used in a wide range of biological applications such as intracellular delivery of biomolecules, electrophysiological recordings [72], and pH sensing [54].

Electrospun fibres can be designed to create both anisotropic and isotropic architectures to control specific cellular behaviours, as shown by a recent study which demonstrated that anisotropic fibres lead to tendon-like tissue regeneration, while randomly aligned fibres lead to the formation of bone [73].

1.2.1.2. Tunable Matrix Stiffness

Over the years, there have been many functional biomaterial platforms that can be used to modulate mechanical properties in an *in vitro* microenvironment. Polyacrylamide (PaAM) based hydrogels have been widely used to study how cells sense and respond to the mechanical cues of their environment due to their ease of use and versatility.

By adjusting the cross-linking ratio of acrylamide to bis-acrylamide, it is possible to modulate the bulk stiffness of the gels from 0.1 – 200 kPa. Alteration in the stiffness of the polyacrylamide gels can impact a variety of cellular behaviours such as cell spreading [74], shape [75], the maturity of cardiomyocytes [76, 77] and hepatocytes[78], and differentiation potential [79]. Polyacrylamide hydrogels can further be used in a method such as traction force microscopy (TFM) to measure cell-generated forces. PEG- and PDMS based hydrogels are also another popular system to study cellular response to matrix stiffness. Researchers have developed elegant methods using arrays of PDMS microposts which enable researchers to define the effective stiffness a cell is experiencing by modulating their deformability, while simultaneously monitoring the force exerted by the cells based on the displacement of the posts [80]. More recently, using more advanced techniques such as photo-cross-linking or microfluidic-assisted fabrication, hydrogels were generated with more precise mechanical properties and even stiffness gradients within the gels [81, 82].

Advances in photo-assisted realtime crosslinking or degradation of hydrogels *in situ*, allow to better mimic the dynamic nature of the *in vivo* 3D microenvironment. In general, the strategy involves the modification of the hydrogel backbone with a light-sensitive group (*e.g.* methacrylate group) post the initial gelation. Then, the material properties can be altered *in situ* upon irradiation by UV-light ideally at a dose tolerated by live cells [83, 84]. In the case of photo-assisted softening, proteolytically cleavable crosslinkers or photodegradable monomers can be incorporated into the structure of the hydrogels to achieve subsequent degradation [85, 86]. The study of this type of dynamic hydrogel system has shed light on cellular mechanical memory [87-89].

1.2.1.3. Dynamic Extracellular Forces

In the body, tissues are subjected to deformations and external forces that may vary in strength and periodicity. A range of systems has been developed which allow the application of mechanical strains in two-dimensional cultures.

There are two types of strains a cell can experience, static and dynamic (defined as a periodic loading cycle). Using strains relevant to a particular cell type,an experiment could reveal a range of exciting phenomena. For example, the cyclic straining of vascular smooth muscle cells resulted in the increased expression of HDAC7 and repression of HDAC3/4 expression leading to AcH3 hyperacetylation and inhibited migration [90]. Application of tensile cyclic strain to MSCs cultured on collagen-coated silicon substrates enhanced their osteogenic differentiation capacity and appeared to be regulated through stretch-activated ion channels [91]. Tissue explants, 3D tissue engineered scaffolds, or whole organ culture systems are commonly used to recapitulate better the *in vivo* mechanical environment. These constructs can also be externally stimulated *in vitro*. For example, the moderate compressive load on bovine cartilage explants inhibits pro-catabolic response such as apoptosis and enhance anabolic gene expression in the presence of inflammatory cytokines [92].

1.2.2. Three-Dimensional Systems

Significant efforts have been put toward the development of 3D cell culture systems that better mimic the *in vivo* physiology. Nowadays, 3D cell cultures are used in a variety of applications from drug discovery, disease modelling, cellular differentiation and maturation and also therapeutic applications.

Some of the most common forms of 3D cell culture technologies include spheroids, organoids, scaffolds, hydrogels and organs-on-chips. With specific advantages and disadvantages, all these technologies have the standard function of restoring the architectural and functional features of living tissues and organs. In the scope of this thesis, only scaffolds and hydrogels are going to be discussed. The 3D scaffolds can be modified to incorporate biochemical cues such as ECM proteins or specific ligands and can also be engineered to possess specific mechanical properties (Fig. 2. For example, using elegant chemistry and two-photon microscopy has provided a means of controlling the addition and removal of the notch ligand, delta and vitronectin in guiding stem cell fate [93]. In a 3D environment, cells can either be

encapsulated and dispersed throughout the substrate homogeneously or seeded on to the 3D scaffolds to allow them to migrate into the scaffold naturally. This more physiologically relevant environment has brought about various changes and advantages to cellular behaviour, including growth and survival, differentiation capacity and maturation of *in vitro* generated constructs. As an example, MSCs seeded in either soft or stiff 3D hydrogels encourage differentiation toward adipogenic and osteogenic pathways, respectively, as observed in the classical 2D culture system [94]. However, the effect does not seems to be regulated by actomyosin cytoskeletal tension or cell shape, since cells remain spherical in both conditions [95]. The use of adult cardiac ECM derived 3D scaffolds has also been shown to promote the maturation of iPSCs derived cardiomyocytes shown by their calcium handling potential [96].

1.2.3. Microfabricated Nanostructures: Novel Tools in Mechanobiology

Advances in techniques used in biomaterial fabrication have pushed forth the development of a new sub-type of nanostructures with precise geometry, textures and mechanical properties. These emerging class of nanomaterials are nanoneedles and nanopillars and can be designed in different formats, from a single needle structure (nanowires), nanostraws with a hollow core, to the high-aspect ratio porous needles. These nanostructures have been used in several biological applications such as the delivery of cell-impermeable biomolecules, electrophysiological recording, pH sensing, biomolecule recognition, and detection of cell forces [97].

The nanoneedles form strong intimate interactions with the cell membrane and the intracellular space of the cells owing to the nanoscale dimensions and high aspect ratio. The physical properties of the nanoneedles including length, density, diameter and composition of the needles can be customised to provide isolated and specific systems to mimic naturally occurring biophysical cues and to understand their mode of action in cells. Thus, this architecture provides a large number of mechanical cues that the cell can sense and react to. As an example, nanowire density was shown to affect the morphology of the cells [98]. Qualitative results from scanning ion electron microscopy and quantitative measurement reveal that as the nanowire density decreases, the cell area increases. Cells cultured on the highest nanowire density (29 nanowires/100 μm^2 = 2 μm spacing), appeared to adopt a much

rounder and smaller morphology, whereas on lower densities nanowire chips (5, 7, 10 µm spacing) cells are significantly more spread out, elongated and have a larger surface area [98]. Suggesting that by modulating the density of nanowires, one could easily modulate the shape of the cells and thus affecting the fate of the cells.

Furthermore, it is possible also to achieve different morphological cell responses by merely altering the diameter of the pillars. Cells grown on 2 µm diameter pillars displayed higher circularity index and lower elongation (more rounded), compared to cells grown on 500 nm pillars [99]. More recently, a systematic study was conducted by the group of Karen L Martinez to investigate the overall cell behaviour and detailed adhesion molecules variance across geometrically different vertical silicon nanocolumn arrays (vSNA) [11]. All parameters of the vSNA were kept constant except the density of the vSNA (3, 10, 80, 170, and 700 nanocolumns per 100 μm^2). They observed three distinct cellular behaviours across the range of investigated vSNA densities (Fig. 4). In lower density vSNA array, cells deformed tightly around the full length of the nanocolumns, appeared rounder, showed decreased mobility, and increased actin localisation and FA density. As the density of vSNA array increases, cells appeared to be more spread out, formed more elongated FAs, the deformed cell membrane adhered tightly and actin colocalised on the side of the nanocolumns.

In the array with highest nanocolumns density, the cell membrane did not appear to be deformed and appeared to have a similar attachment profile as cells cultured on a flat substrate. The nanopillars can also be used to study the mechanical stability and deformability of the cell nucleus *in situ* in live cells. The geometry of nanopillars arrays can be customised to induce desired nuclear deformation parameters such as depth, width and curvature. A study by Hanson *et al.* showed that larger nanopillar radii induce shallower and broader deformation; whereas smaller radii lead to deeper and narrower deformation [100]. Moreover, they showed that the average nuclear deformation is drastically increased from 0.23 µm to 0.95 µm as the pitch is increased from 2 µm to 6 µm, suggesting that the pitch of nanopillar arrays has a stronger effect on nuclear deformation than the radius [100]. Detailed understanding on cell-to-nanoneedle type structure interface and the impact on cellular processes could serve as a guide to improve the design of the nanostructure array for the desired cell manipulation.

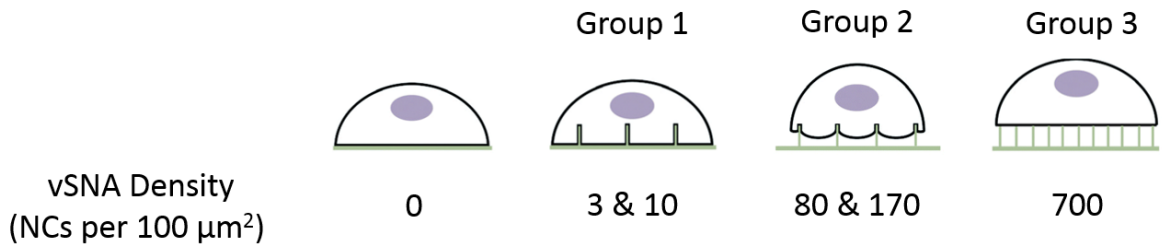


Figure 4. Cell behaviour across different vSNA densities. Cells can be grouped into three main categories depending on the density of the vSNA density. Cells adopt a group 1 morphology in low density arrays, group 2 in medium density array, and in high density arrays (group 3) cells appeared to adopt similar morphology and behaviour as cells cultured on flat surfaces. Figure adapted from [11].

Mechanical forces from inside the cell (*i.e.* cytoskeletal forces) and their interplay with external forces are crucial in regulating cellular processes including adhesion, cell-cell contact and migration. The ability to sense forces applied by the cells to their surrounding is needed to provide essential insights to improve our understanding of their role within these cellular processes.

Due to the high density, nanoscale size, and wide range of stiffness, the nanoneedles have been applied to detect forces at nanoscale levels with high spatial resolution. As an example, nanoimprinted polycarbonate pillars in combination with scanning electron microscopy technique were used to detect cellular forces. These techniques were able to distinguish the dissimilarity in the arrangement of forces exerted by cells with different morphological structures. The system is also sensitive enough to record forces at a single cell level, revealing a higher traction force at the edge than at the centre of the cell [99]. In addition, gallium phosphide nanowire mats coated with gold nanodots were used to measure cellular forces down to 15 pN [101]. The forces generated by the cells were recorded by quantifying the deflection of the tip of the nanowire with confocal microscopy in live cells. The array can detect more than 20,000 points in a 140 x 140 μm^2 chip with a resolution of 1 µm, and it is possible to measure forces across a broader range by merely altering the length and diameter of the nanowires [101].

1.2.3.1. Cell-Nanoneedle Interactions

A study using transmission electron microscopy demonstrates there is very close contact between nanoneedles and the cell membrane wraps arounsd the entirety of the nanoneedle structures without the nanoneedles penetrating into the intracellular space of the cell [102]. Another study combines the use of stable cell line expressing the kappa-opioid receptor, a transmembrane protein, fused to a SNAP-tag (SNAP-KOR) and confocal z-stack imaging, demonstrated that nanowires of various lengths, spacings and surface coatings commonly used do not get in direct contact with the interior of the cell [103].

However, a study by Shalek *et al.* showed a lack of cellular membrane enveloping the nanowires as evidenced by confocal microscopy [52]. In another study using NW electrode arrays, the application of short voltage pulse was required to enable transient intracellular access for the recording of intracellular action potentials [55], further supporting the hypothesis that cellular penetration does not occur naturally. An elegant study using nanostraws to deliver the membrane-impermeant Co^{2+} to locally quench the fluorescence of GFP expressing cells to quantify the frequency of nanoneedle penetration, estimated that only 1-10% of nanostraws have direct access to the cytosol [104].

Further studies with the same system showed that a combination of dimethyl sulfoxide (DMSO) and Latrunculin A to permeabilise the cell membrane and destabilise cytoskeletal assembly, respectively, leads to significant increase in the percentage of nanostraws penetration from 8% to 13% [105]. This study along with others mentioned above suggestthat the cell membrane and the underlying cytoskeletal network represent a barrier at the cell nanoneedle interface to prevent direct cytosolic access.

Current evidence suggests that seeding cells over nanoneedles do not necessarily lead to direct intracellular penetration but do lead to intimate interaction between the nanoneedle and the cellular membrane that facilitates the delivery. It is possible that the initial contact between cells and nanoneedles caused membrane rupture and allowed direct delivery to the cytosol. However, the membrane will reclose within a relatively short time. It is also possible that enhanced cytosolic delivery of biomolecules by nanoinjection is mediated by enhanced cellular endocytosis.

This notion is supported by a recent study which demonstrated that membrane curvature induced by nanopillars attracts and localises proteins involved in clathrin-mediated

endocytosis [106]. Interestingly, the application of external forces increases the transfection efficiency of the nanoinjection. Various strategies to exert a force on arrays of nanoneedles such as hypergravity, manual application of forces, and oscillating actuator have been tested and have shown to improve the ability of nanoneedles to deliver cargoes into the cells.

The application of 12.8 to 35.5g of hypergravity through centrifugation significantly improve the efficiency of delivery from 5% to 80%, without inducing cell death [107]. Another study uses a custom linear manipulator to precisely control the mode and force applied to the cells [108]. The nanoneedle array was positioned directly above the cells in a parallel fashion in order to maximise the number of interacting cells, and then lower at a constant speed until it makes contact to the cells. The array was then retracted and oscillated at about 5 kHz for 1 min to allow the absorbed molecules to be released into the cells [108]. This method leads to the direct insertion of the nanoneedles into the cytosol of the cell and improves the transfer of molecules, as measured through the efficiency of gene expression post-delivery of pDNA. This suggests that external forces might enable direct intracellular access to the cytosol by promoting nanoneedle penetration of the cell membrane. Other parameters such as the geometry of the nanoneedles [109], force and speed of interfacing [110], cell stiffness, membrane fluidity [110] and nanoneedle surface modifications and decorations [97] can further impact upon delivery efficiency.

1.3. Hypothesis, aims and scope of thesis

This thesis focusses around two main premises:

- Biomaterials can be used as an efficient delivery tool for *in vitro* and *in vivo* gene delivery.
- Biomaterials can be used to understand the complex dynamic interplay between cell and its physical surrounding.

This prompts to ask two main questions: firstly, can microfabricated nanostructures (*i.e.* nanoneedles) be used to efficiently deliver nucleic acids into cells? If so, could they be used in a therapeutic concept to promote cardiac regeneration via gene transfer induced direct cardiac reprogramming? Secondly, can nanoneedles be used as a model to further understand how cells react to the presence of high-aspect ratio nanostructures? Furthermore, can the information gathered be used to modulate cell behaviour?

To answer these questions the thesis is organised around two main chapters that contain their own detailed literature review which support their specific objectives.

Chapter 2 (Nanoneedle-based Gene Transfer for Cardiac Regeneration) is dedicated to demonstrating the potential of nanoneedle chips as efficient gene delivery tools both *in vitro* and *in vivo*. To demonstrate this, a nanoneedle chip is used to deliver plasmid encoding cardiac reprogramming factors to induce the reprogramming of the epicardial derived cells (EPDCs) into induced cardiomyocytes (iCMs) *in vitro* and *in vivo*.

Chapter 3 (Biophysical Regulation of Cellular State by Nanoneedles) is dedicated to the analysis of the potential effects of nanoneedles on a cell behaviour including the inner nuclear structure and epigenome. The purpose of this chapter is to identify the main modifications in cellular signalling, pathways and chromatin following exposure to specific extracellular biophysical cues.

Chapter 2: Nanoneedle-based Gene Transfer for Cardiac Regeneration

2.1. Introduction

Significant advances in preventative and intervention medicine have seen the survival rate of myocardial infarction (MI) steadily improving over the past decades [111]. However, it remains one of the leading causes of death worldwide. This is partly due to the limitation of current treatments just able to alleviate symptoms associated with the progression of heart failure and cardiac deterioration. Currently, the primary focus of cardiovascular science is moving toward preserving and restoring the functionality of the post-MI hearts. Functional recovery of the heart is severely limited due to the limited regenerative capacity of the heart and to scar tissue formation. In recent years, clinical interventions aimed at improving cardiac regeneration that have shown significant progress include the injection of new cardiomyocytes or progenitor stem cells, stimulating resident *in situ* progenitors, gene therapy and new drug treatments. Nonetheless, most are still far from optimal clinical usage, and thus there is a great need for constant refinement of current methods and development of novel therapeutic approaches.

2.2. Pathology of Myocardial Infarction

Cardiovascular disease which includes MI was the cause of death of 17.5 million individuals in 2012, with MI responsible for almost a third of the deaths. The number of deaths caused by cardiovascular diseases is expected to continue to rise in the next decade.

The heart is a core organ in the body that requires a constant supply of oxygen and has a strict metabolic requirement to maintain its normal function. The partial or total obstruction of the coronary artery by atherosclerosis and/or thrombi leads to the disruption of the blood flow carrying oxygen and nutrients to the myocardium and, in turn, causes the onset of MI (Fig. 5). Due to the imbalance of the supply and demand for oxygen and nutrients, the myocardium shifts to anaerobic metabolism resulting in the acidification of the infarct zone [112]. Consequently, the blockage will lead to a loss of contractile function due to the loss of approximately 25% of the cardiomyocytes [113].

On the long run, in combination with the onset of interstitial fibrosis, as a result of the inflammatory responses, the heart will undergo a geometrical and organisational alteration which can lead to heart failure in the future. Following an ischemic event, the heart relies

heavily on the remodelling of the microenvironment and structure, to meet the increased metabolic and contractile load. Cardiac remodelling post-MIan be further broken down into three main phases, the inflammatory, proliferative and late maturation phase (Fig. 5).

The first step after an ischemic injury can be characterised by the activation of the innate immune response [114]. Mononuclear cells and neutrophils are recruited to the site of injury to phagocytose dead cells and debris. Numerous inflammatory cytokines such as TNF-α, IL-1β and IL-6 are released, and this leads to the initiation of the ECM remodelling through the activation of matrix metalloproteases (MMPs).

During the proliferative stage, several mechanisms are involved in promoting the active revascularisation and remodelling of the infarct zone. For example, vascular progenitor cells are recruited to the site of injury in response to the release of chemo-attractants such as SDF-1 and IL-8 [115]. Also, resident cardiac fibroblasts are also activated and start to deposit new matrix, mainly collagen fibres [116]. Prolonged the proliferative stage and profibrotic response ultimately lead to the formation of mature scar tissues and in conjunction with the increased mechanical load will lead to the remodelling of the ventricle.

In the final scar maturation phase, myofibroblasts continue to play a role in stabilising the initial matrix deposited at the early stages of remodelling by releasing tissue inhibitors of metalloproteinases (TIMPs) which stabilises the extracellular matrix (ECM) [117]. Additionally, the body sympathetic adrenergic system kicks in and along with the morphological alterations acts as a response to prevent ventricular dilation and heart rupture [117]. However, as time progresses, these alterations can lead to cardiac arrhythmias, chronic heart failure and even sudden death.

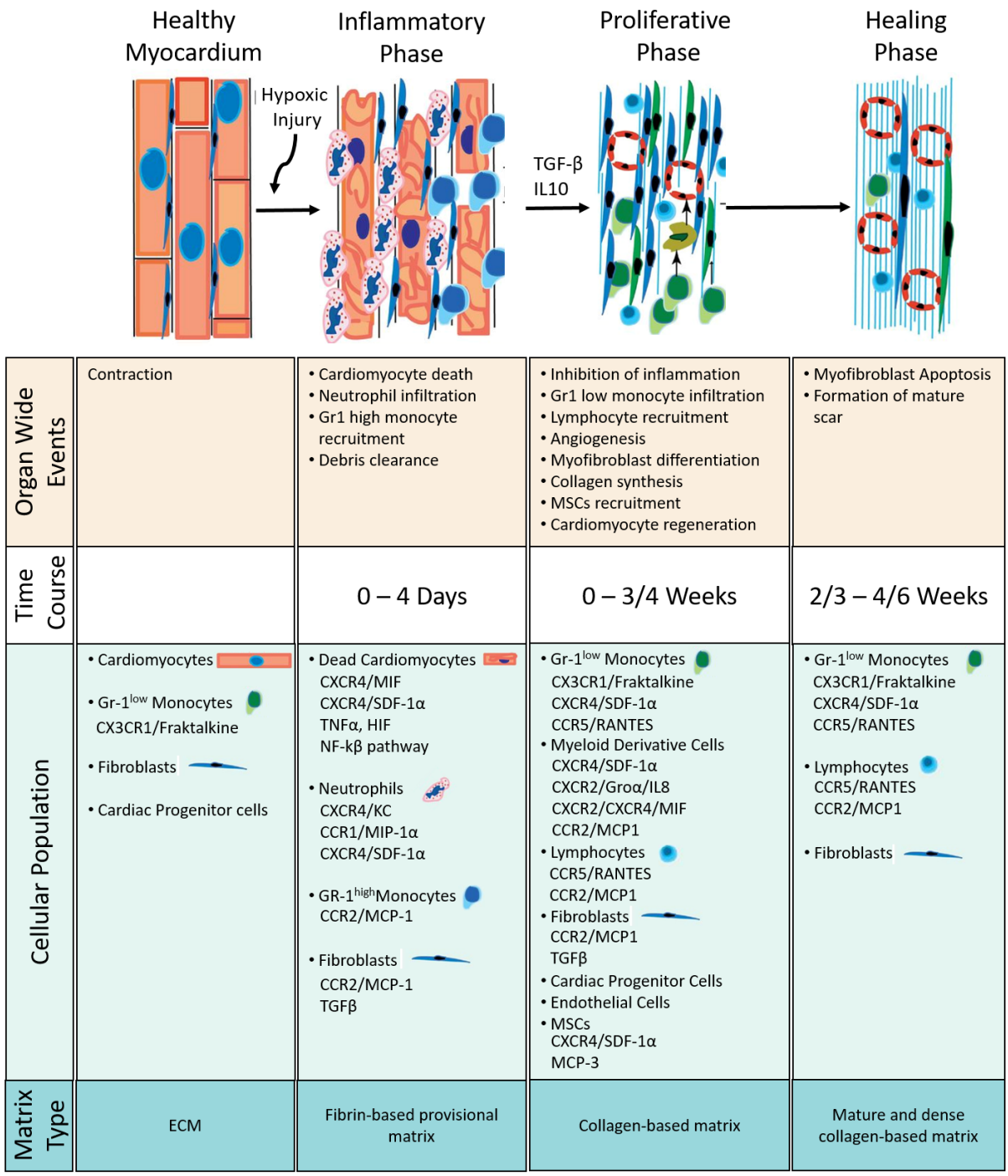


Figure 5. Cellular and molecular events following MI. Responses after MI involve 3 overlapping phases: an inflammatory phase which occur immediately following injury, then a proliferative phase that can last for approximately 3-4 weeks and finally a healing phase. Hypoxia due to the MI induces the death of cardiomyocytes and triggers an array of inflammatory responses. Each step of the process can be characterised by the occurrence of specific events involving different cells and controlled by set of chemokines. The known chemokines and respective receptors can be found listed under each cellular target involves. Figure adapted from [13].

2.3. Heart Regeneration

2.3.1. Regeneration Potential in Amphibian and Fish

Many amphibians and fishes possess the ability to regenerate their limbs and internal organs following injury.

Zebrafish has been studied extensively in regards to their ability to efficiently regenerate their heart following amputation of up to 20% of their ventricle [118]. There have been a few theories proposed to explain the phenomenon, including the activation of progenitor or stem cells around the infarct zone, and the proliferation of resident cardiomyocytes. Only until recently, studies using lineage tracing demonstrated that cardiac regeneration in zebrafish occurs by the proliferation of existing cardiomyocytes [119, 120]. The current consensus is that following cardiac injury, the pre-existing cardiomyocytes undergo dedifferentiation and re-enter the cell cycle to give rise to *de novo* cardiomyocytes.

2.3.2. Limited Regeneration Capacity of Mammalian Heart

Unlike amphibian and fish, the mammalian heart is considered to be a post-mitotic organ that is incapable of regeneration. It is thought that soon after birth, cardiomyocytes withdraw from the cell cycle and are incapable of re-entry.

However, this hypothesis was challenged by a seminal study by Bergmann and colleagues. Through the use of an excellent isotopic study they determined that in young healthy adults, cardiomyocytes are renewed at about 1% per year, this number reduces progressively as people age to about 0.45% in the old adult [121]. Indeed, the neonatal mammalian heart regeneration capacity seems to be greater in comparison to that of the adult heart, and this is thought to occur through cardiomyocyte proliferation. A recent study indicates that this intrinsic capacity of repair post myocardial damage is also present in newborn humans [122]. The downregulation of Meis1 and upregulation of neuregulin-1 (NRG-1) signalling pathways have been demonstrated to play an essential role in the activation of neonatal cardiomyocyte cell division [123, 124]. Knockout of Hippo pathway can also be another potential therapeutic avenue since it has been shown to elevate cardiomyocyte proliferation extensively [177]. However, the mechanisms involved in cardiac regeneration in the adult heart are not as clear-cut. An early study using Myh6 Cre-Lox transgenic mice in a genetic pulse-chase study showed that new myocytes arose from the stem or progenitor cells differentiation and expansion

[125]. However, a later study by the same group appears to contradict their previous findings [126].

Another study using genetic fate mapping to label the resident cardiomyocytes in conjunction with a long-term BrdU pulsing demonstrated that in normal heart cardiomyocyte regeneration predominantly occurs via the proliferation of *in situ* cardiomyocytes. However post MI, *de novo* cardiomyocytes seems to arise from both progenitors as well as the proliferation of the pre-existing cardiomyocytes [127]. The activation of ERBB2, NRG-1 co-receptors appear to be sufficient to reactivate the postnatal cardiomyocytes regenerative capacity via dedifferentiation of binucleated cardiomyocytes, proliferation and redifferentiation [128].

In summary, the studies demonstrated a limited capability of the heart to self-renew although the exact degree of the regeneration is still an ongoing debate and is postulated to be insufficient to repair damages caused by either acute or chronic injuries. On a positive note, many successful strategies have also been discovered to boost this endogenous regenerative capacity of the heart.

2.4. Therapeutic Strategies for Cardiac Regeneration

Due to the limited regenerative capacity of the adult mammalian heart, researchers have developed various strategies to promote healing and functional regeneration of the heart following injuries (Fig. 6). This chapter will provide a brief overview of the different therapeutic strategies currently employed.

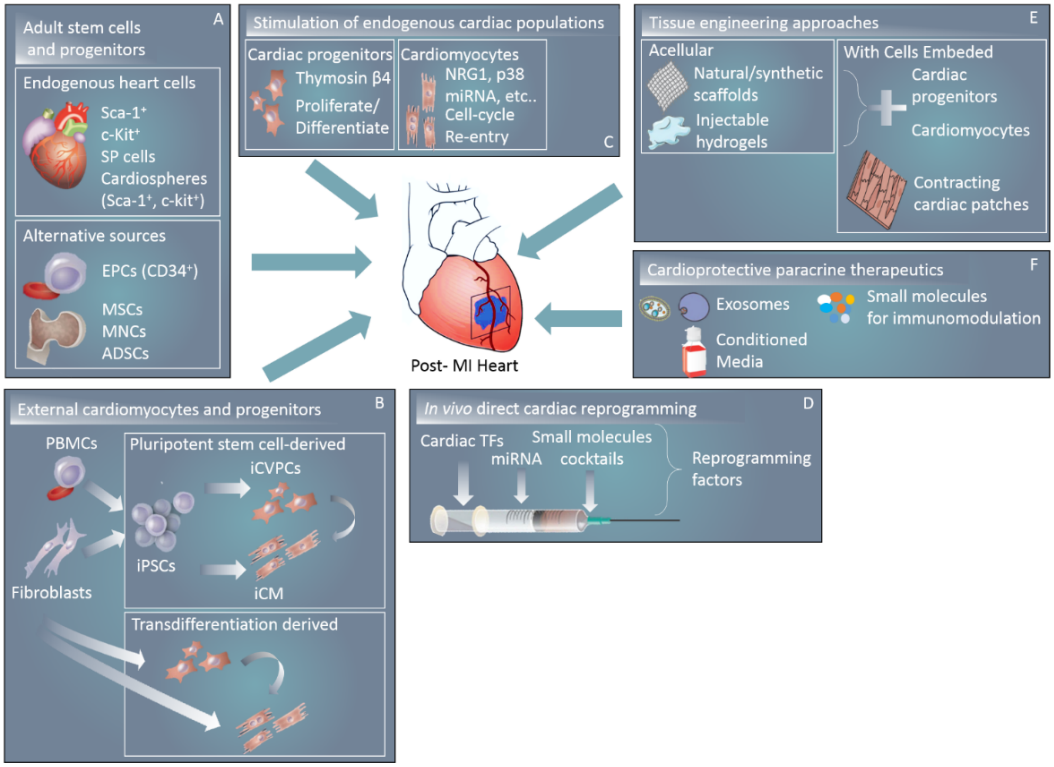


Figure 6. Regenerative-based therapeutics for MI. (A) Adult stem cells and progenitors can be isolated from various sources within the body and expanded in an *in vitro* culture and used in cellular transplantation. The cells listed in (A) are currently used in clinical trials. (B) Pluripotent stem cells and transdifferentiation strategies involve the expansion and conversion of the primary cell source into functional cardiomyocytes prior to transplantation. (C) Small molecules and other bioactive molecules can also be administered intravenously or locally to stimulate the endogenous regeneration capacity of the cardiomyocytes and cardiac stem cells. (D) The enormous reservoir of resident cardiac fibroblasts can be reprogrammed into functional cardiomyocytes *in vivo* with the use of various reprogramming factors. (E) The use of biomaterials alone or in combination with cells has also been investigated as another promising strategy. (F) More recently from the results observed in trials involving cellular transplantation, researches have realised that most of the effect can be recapitulated with just the use of paracrine factors that the cells secrete (*i.e.* conditioned media and exosomes) and this discovery have fuelled the recent boom in the field of acellular therapeutics. In addition, the use of immunomodulatory chemicals has been shown to boost the outcomes of trials involving cellular transplantation.

2.4.1. Endogenous Progenitor Cells and their Role in Cardiac Regeneration

The rising interest in stem cell biology in the past two decades has reaped interest among cardiovascular researchers. This led to the discovery of several populations of cardiac non-myocytes cells coined cardiac progenitor cells (CPCs) in the adult heart. They are categorised based on the expression of the cell surface markers and represent about 0.005% to 2% of the adult cellular content. One of the first population to be isolated is the c-Kit-positive progenitors isolated by Beltrami and colleagues [129]. Their study shows that this population of stem cell progenitors are scarce, only present in 1 per 10,000 myocytes and are quite heterogeneous in their expressions of cardiac markers. These cells can differentiate into biochemically mature cardiomyocytes albeit lacking the ultrastructure and spontaneous contractility [129]. The Sca-1 positive cells are another well-characterised adult cardiac progenitors. These cells require the supplementation of demethylating agent 5-azacytidine [130] or oxytocin [131] for four weeks to differentiate them into beating cardiomyocytes. Multiple groups have also identified the side population (SP), a subset of stem cells with characteristic scatters on fluorescent activated cell sorting (FACS) [132-134]. They expressed proteins associated with the ABC transporter superfamily on their surface which provides a neat method to characterise and isolate them based on their ability to exclude dye such as Hoechst. Upon coculture with adult rat ventricular cardiomyocytes, these SP cells can differentiate into fully functional cardiomyocytes [134]. Finally, the cardiospheres, a heterogeneous population of cells positive for c-Kit, Sca-1 and KDR, form clonal, multicellular clusters in suspension culture [135]. They were first isolated from a surgical biopsy of the human atrium and ventricle, although newer techniques with higher efficiency has been developed [136]. These cells are capable of differentiating into endothelial, smooth muscle cells and cardiomyocytes [135, 137]. These so-called CPCs reside within a specialised microenvironment that provides homeostasis between survival, proliferation and self-renewal [138]. These cells (c-Kit$^+$, Sca-1$^+$ and SP) appear to be phenotypically distinct from one another and expressed different surface markers. However, a recent study by Hans Clever's group through the use of single cell sequencing and lineage tracing found no evidence of CPCs contribution to *de novo* cardiac regeneration post-injury. Furthermore, the study demonstrated that various markers associated with CPCs are widely expressed by non-cardiomyocyte cardiac lineages.

2.4.2. Transplantation of Exogenous Cells

There have been a substantial number of clinical studies conducted since the early 2000s which looked into the functional benefit of autologous cell transplantation to regenerate the injured hearts (Table. 1).

One of the first few trials was conducted using the intracoronary infusion of bone marrow-derived mononuclear cells (BMNCs). Trials such as the BOOST [139] and REPAIR-AMI [140] showed improved diastolic function in patients with MI following an intracoronary autologous BMNC injection. The effect was thought to be mediated by CD34+ hematopoietic stem cells. However, transplantation of the cells only improved left ventricle ejection fraction (LVEF) by 1.8%, while transplantation of BMNC led to a 4.41% improvement [141]. However, there are also several studies which show that patients who received an infusion of BMNCs did not show any sign of improvement [142-144]. In general, it seems that intracoronary transfusion of BMNCs did induce a small increase in LVEF and reduced the infarct size although without much impact on ventricular remodelling [145].

hMSCs were also trialled in patients with MI due to their potent therapeutic properties such as angiogenic, anti-inflammatory and immunomodulatory effects [146]. An intracoronary infusion of bone marrow-derived autologous hMSCs showed an LVEF improvement of 5.9% in comparison to the control group which showed a 1.6% improvement six months post-intervention [147]. In the PROCYMAL trial, allogenic cells were used instead of autologous bone marrow-derived MSCs. Following the intravenous transfusion of the cells, patients treated showed increase LVEF, a reversal in the ventricular remodelling, improvement in pulmonary function and also marked a reduction in the episodes of ventricular tachycardia [148].

Another approach was to utilise cardiac-committed progenitor/stem cells with the rationale that by using cells phenotypically close to the cells intended to be replaced and rescued might lead to a more efficacious treatment [149]. So far only c-Kit^{+} (SCIPIO trial) [150] and cardiosphere derived cells (CADUCEUS trial) [151] have been used in the clinical setting to treat MI. In both trials, only a modest effect was observed in patients who received the cellular transfusion [145]. This could be because c-Kit+ cells preferentially differentiate into vascular cells instead of cardiomyocytes *in vivo* [152], and become senescent during the expansion phase in the culture thus losing their therapeutic potential [153].

Approaches using embryonic stem cells (ESCs) or induced pluripotent stem cells (iPSCs) derived cardiomyocytes are also being explored. This approach allows for the tight and robust control of the differentiation pathway and thus enable transplantation of cells at the desired cardiomyogenic commitment. Transplantation of cardiac-enriched hESCs progeny into the left ventricular wall of rats showed their ability to repopulate and form a human myocardium [154]. In a mouse infarct model, despite the ability of hESC derived cardiomyocytes to engraft into the host and improve contractile function of the infarcted hearts, these beneficial effects were short-lived [155] and correlated to the degree of vascularisation and not graft size [156]. As more focus is put on the use of iPSCs, recent studies with iPSCs-CMs have also shown successful survival and engraftment of these cells to the host's hearts [157]. Another relevant study of interest in large animal model involves the intra-myocardial delivery of cryopreserved hESC-CMs into a non-human primate infarct model. The delivery of one billion hESC-CM into the wounded heart generated great revascularisation, and the graft displayed a well connected electromechanical integration with the hosts, although non-fatal ventricular arrhythmias were observed in the engrafted primates [158].

So far clinical trials of cell therapy for cardiac repair and regeneration conducted on MI have demonstrated safety and feasibility of these types of treatments. However, functionallythese treatments have yielded neutral or at best marginally positive outcomes. As the most common delivery methods such as intravenous infusion, intracoronary injection and direct epicardial injection have all showed poor cellular retention and problems with homing [159]. Furthermore, the microenvironment of the heart following an MI is very acidic and highly inflammatory, and thus transplantation of unprotected cells into this environment would result in significant cell death. As such, important issues such as optimal cell source and number, the timing of delivery and the route of application should be further investigated and optimised.

Table 1. List of clinical trials using transplantation of adult stem cells mentioned in the text.

Name of clinical trial	Cell Type/dose ($x10^8$)	Route of injection	Time of delivery	Functional outcome	Refs
BOOST	Autologous BMNC/24.6±0.94	IC	4-6 days after PCI	Minor improvement in EF 6 months in, but further follow up showed no changes.	[160]
REPAIR-AMI	Autologous BMNC/2.36±1.74	IC	3-6 days after PCI	3% increase in LVEF after four months but the improvement dissipate soon after.	[161, 162]
PROCYMAL	Allogenic BMSCs	IC	3-10 days after AMI	hMSC treated group showed an increase in LVEF by 5.2% at 12 months.	[148]
SCIPIO	c-kit+ cells/0.005-0.01	IC	113 days after CABG	Showed an improved EF and decreased infarct size even after 12 months post-treatment.	[150]
CADUCEUS	CDCs/0.125-0.25	IC	45-90 days after MI	Reduction in infarct size and local improvements in function, but no differences in LVEF between treated and control.	[163]

2.4.3. Tissue Engineering Approaches

Tissue engineering approaches have gained considerable momentum in the past few years as a way to improve clinical outcomes of cardiac regeneration therapies. Tissue engineering can be acellular or in combination with cell transplantation to improve survival and grafting.

The use of acellular biomaterials in the form of injectable hydrogels and patches to provide regenerative cues and mechanical support post-MI have been heavily evaluated. Acellular constructs can be generated from various biomaterials, naturally occurring or synthetic, but in general, they should be able to provide mechanical stability, host cell integration and vascularisation, exhibit mechanical properties matching that of the heart, be non-immunogenic and most importantly support physiological function and the regeneration of the tissues. Collagen type I scaffolds are one of the most common scaffolds being used in regenerative medicine due to collagen's presence in almost all connective tissue. The transplantation of 3D collagen type I scaffolds with optimised mechanical properties onto the surface of the heart post-MI leads to significant improvement in cardiac function, diminished fibrosis and inhibition of left ventricle dilation and wall thinning [164]. Additionally, collagen gels have also been used for controlled release of thymosin β4 in the infarcted heart to induce EPDCs activation and induce angiogenesis post-MI [165].

Moreover, the application of injectable hydrogels made of fibrin 1-2 days post-infarction preserved infarct wall thickness, reduced infarct size, induced neovasculature and improved cardiac EFs [166, 167]. The use of ECM derived scaffolds has also gained much attention recently. The use of urinary bladder ECM (UB-ECM) as an epicardial patch has been established to be capable of promoting cardiomyocyte differentiation and migration, and formed a highly vascularized tissue enriched in collagen and myofibroblasts to improve the mechanical functionality of the heart regionally [168]. Efraim and colleagues recently designed a biohybrid cardiac ECM-based hydrogel, aimed at leveraging the natural therapeutic properties of cardiac ECM, while strengthening its limited mechanical strength with genipinand chitosan for the treatment of acute and long-term chronic MI [169].Their scaffolds not only preserve but also improve cardiac function in eight-week post-treatment and this is partly possible due to the biological properties of the infiltrating progenitor cells. Scaffolds derived from synthetic materials such as, poly(ethylene glycol)(PEG) [170], poly(caprolactone)(PCL) and poly(N-isopropylacrylamide) (PNIPAM) [171] have also been

used for cardiac tissue implants. The ability to modify the synthetic polymers with high precision to meet specific therapeutic needs is one of the reasons why they have been widely used in tissue engineering applications.

The incorporation of cells into biomaterials in most cases showed further improvement over the use of the material alone. Moreover, biomaterials can provide a 3D environment that could enhance cell survival, proliferation, and differentiation, and provide protection from the injection-associated stresses and the highly inflammatory microenvironment. The encapsulation of cardiac stem cells within hydrogels enriched with fibronectin and fibrinogen positively affected the long-term survival and retention of the transplanted cells and improved cardiac function post-MI [172]. In a recent study, transplantation of an IGF-1 microsphere-loaded fibrin patch in combination with human cardiac tri-lineage significantly improved survival and retention of transplanted cells and even improved cardiac function without inducing arrhythmias [173]. A seminal study by Zimmerman and colleagues for the first-time generated engineered heart tissues (EHTs) from neonatal rate heart capable of generating sizeable contractile force and upon transplantation resulted in improvement of cardiac function [174]. More recently, they have successfully generated EHTs from embryonic and iPSC-CMs with advanced maturation profiles mimicking that of adult myocytes [175].

Tissue engineering methods, either on its own or in combination with stem cells, show positive approaches for cardiac regeneration.

2.4.4. Exosomes for Cardiac Regeneration

Conditioned medium from stem cells has long been suggested to have beneficial effects on the damaged heart. Several studies have demonstrated that stem cells can produce and release a wide range of cardioprotective cytokines, growth factors and chemokines [176, 177]. It is postulated that the long-term functional improvement in cardiac function post-cellular transplantation is due to the secreted paracrine factors since almost 90% of transplanted cells are flushed out of the system 24 h post-injection. Researchers have started to assess whether reliance on the paracrine mechanism, mainly extracellular vesicles (EVs), might be able to replace the use of cells as the transplanted agents.

Exosomes, a class of EVs, are rich in nucleic acids primarily the noncoding type, lipid rafts, and protein fragments, that can cross into target cells and elicit changes in the behaviour of the recipient cells [178]. A study by Ibrahim *et al.* demonstrated that CDCs derived exosomes

exhibit a range of cardioprotective properties such as enhancing angiogenesis, decreasing fibrosis and promoting cardiomyocyte proliferation, and showed that the injection of exosomes into murine hearts post-MI recapitulates the regenerative and functional effects produced by CDCs transplantation [179]. Mouse ESC-derived exosomes mediated at least partly by miRNA-294 were shown to enhance endogenous repair and preserves cardiac function following MI. Furthermore, these exosomes were able to increase proliferation of CPCs up to four weeks post-MI [180]. Another study supporting this notion comes from the lab of Philippe Menasche. They demonstrated that the functional benefits of human embryonic stem cells derived cardiac progenitors transplantation can be mimicked by their secreted EVs [181]. The EVs induced similar changes in the pattern of cardiac gene expression that could be linked to the functional recovery observed in the post-infarct model of heart failure. They have also successfully isolated EVs from iPSCs derived cardiac progenitors and demonstrated that the EVs injected not only mimic the paracrine effect of the parent cells but are also better at improving the ejection fraction of murine chronic heart failure model [182]. Although the exact mechanism of EV therapy is still unclear, it is clear that it isas good as, if not more, effective than direct cell transplantation. If this holds true, EV therapy may have significant advantages in the costs, feasibility and safety compared with direct cellular transplantation.

2.4.5. Direct Cardiac Reprogramming

The initial concept of direct reprogramming was demonstrated in the late 1980s, with overexpression of MyoD led to the direct conversion of murine fibroblast into skeletal muscle cells [183]. The field gained significant momentum since the discovery of iPSCs back in 2006 by Takashi and Yamanaka [184, 185]. The findings inspired a new approach in generating specific cell types without the need to transition through a stem cell state by introducing combinations of lineage-specific factors, a term called direct reprogramming. Many groups have demonstrated the direct conversion of fibroblasts to various cell types including, macrophages [186], hepatocytes [187], neuronal cells [188] and hematopoietic stem/progenitor cells [189] (Fig. 7). All of these findings have fundamentally challenged and re-shaped our traditional understanding of cellular plasticity and epigenetic stability of differentiated cells.

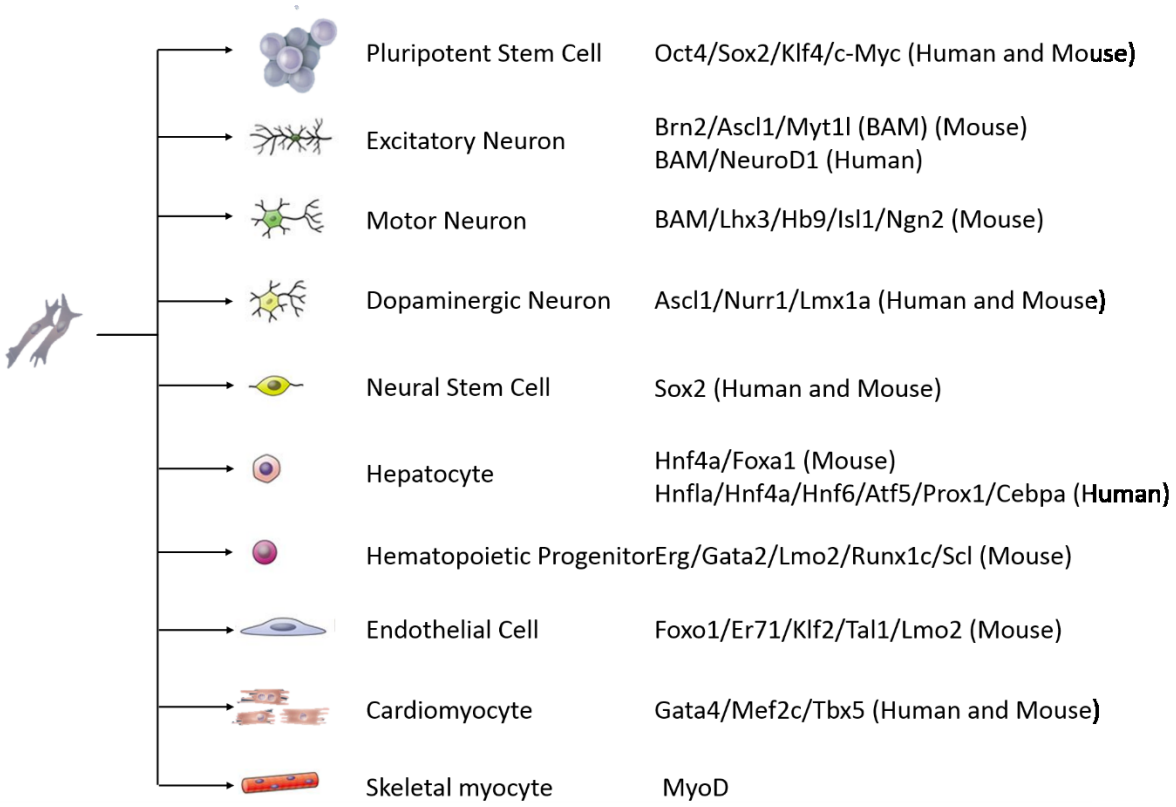


Figure 7. Summary of direct reprogramming by transcription factors. The overexpression of lineage-specific transcription factors in committed adult cells can directly reprogram them into a diverse range of cells including various subtypes of neurons, cardiomyocytes, endothelial cells, hematopoietic cells and skeletal myocytes without having to revert into a progenitor state. Figure adapted from [1].

2.5. Cocktails for Direct Cardiac Reprogramming

2.5.1. Basal Cocktails

Although cardiac mesoderm can be induced into cardiomyocytes, there has been no information regarding the master regulators required for cardiomyocyte transdifferentiation. In 2010, Ieda and colleagues developed an *in vitro* assay to identify the multiple factors that could activate the cardiac program [32]. Through the use of α-myosin heavy chain promoter-driven green fluorescence protein expression (α-MHC-GFP) transgenic mice, they quantitatively analysed and sorted cells that have successfully turned on their cardiac genes program as they will be GFP^+. They employed an iterative screening approach starting with an original pool of 14 retrovirally expressed transcription factors in purified cardiac fibroblasts (CFs), and the factors were removed one by one to identify the minimal number of factors

required to transdifferentiate the nonmyocyte cells into a cardiomyocyte. The expression of 14 different transcription factors known to play a role in cardiac development did yield a small pool of GFP^+ cells, suggesting successful conversion. Eventually, after a series of serial deletion, the overexpression of three transcription factors GATA4, MEF2C and TBX5 (GMT) yielded 15-20% GFP^+ cells. As expected the induced cardiomyocytes (iCMs) generated were very heterogeneous, and the vast majority of cells were only partially reprogrammed, since only a fraction of the cells expressed the classical cardiac markers such as cardiac Troponin T (cTnT) and sarcomeric α-actinin, and even fewer cells showed spontaneous beating four weeks post-induction. On the bright side, these cells showed epigenetic and transcriptional shifts towards that of neonatal cardiomyocytes and a lineage tracing experiment further demonstrated that fibroblasts were directly reprogrammed towards cardiomyocytes without passing through a progenitor cell as shown by the lack of Isl1 and Mesp1 expression. Ieda and colleagues also successfully reprogrammed neonatal tail-tip fibroblasts (TTFs) with the GMT cocktails, and the iCM produced also showed expression of cTnT, Ca^{2+} transient, albeit no spontaneous beating was observed. The efficiency of the direct cardiac reprogramming remained highly variable but is in line with that of iPSCs generation [1]. For example, the lentiviral expression of GMT did not successfully reprogram adult mouse CFs and TTFs into iCMs, and only partial reprogramming was observed. It has been shown that cells with a neonatal origin are more prone to reprogramming in comparison to their adult counterpart [190].It should be noted that as with all reprogramming protocols, variables in culture conditions, primary cell types used, dose of viruses and the extent of reprogramming cocktail overexpression may be key determinants in the success of the transdifferentiation.

2.5.2. Additional Factors and Combinations

There have been many studies aimed at improving the efficiency of direct cardiac conversion using additional factors or modifications of transcription factors, miRNAs and small molecules, andcombinations of all the above (Table. 2).

Soon after the first report by Ieda *et al*. using a similar screening approach, a study by Song *et al.* identified that the addition of Hand2 to the basal GMT reprogramming cocktail yielded a three-fold increase in the percentage of reprogrammed iCMs than any other combinations [191]. The GHMT cocktails were able to faster reprogram adult CFs and TTFs into fully functional iCMs, and the cells produced displayed a cardiomyocyte-like transcriptional profile,

a fully assembled sarcomeric structured, $Ca2^{+}$ transients and even spontaneous beating. Another study showed that *in vitro* reprogramming of MEFs into cardiomyocytes with the GHMT factors lead to the generation of all three types of immature cardiomyocytes, atrial, ventricular, and pacemaker cells, determined by multiplex immunostaining and electrophysiology. Thus it seems that Hand2 plays a role at the early stage of reprogramming. The sequential subtraction of factors and the screening of α-MHC-GFP reporter expression to screen optimal cocktails may identify some reprogramming factors, however this approach suffers from biased identification of factors that can activate the α-MHC promoter and execute those that may promote full reprogramming [192]. To address this issue, Protze *et al.* tested all possible triplet combinations of ten reprogramming factors and used qPCR to identify three factors that can induce the broadest range of cardiac genes and settled on the combination Tbx5, Mef2c and Myocd [193]. Cells reprogrammed with these cocktails displayed all the classical cardiac phenotypes except for spontaneous beating. Furthermore, the addition of Myocd and SRF to the three GMT reprogramming cocktail enhanced cTnT mRNA expression by almost five-fold, but no spontaneous contractile activity was observed [194]. Finally, using a cTnT promoter derived GCaMP calcium reporter as a screening method for candidate reprogramming factors, Addis *et al.* identified that Hand2, Nkx2.5, Gata4, Mef2c, and Tbx5 (HNGMT) were able to induce robust calcium oscillation and increase the percentage of spontaneously beating iCMS compared to the basal GMT factor alone [195].

The fusion of a dominant transactivation domain of the MyoD to Mef2c in combination with the delivery of wild-type Gata4, Hand2 and Tbx5 generated fully functional beating clusters of iCMs with an efficiency of 3.5%, which was 15-fold higher than the wild-type combinations [196].

While the most studies focus on the use of transcription factors as the critical tool for cardiac transdifferentiation, Jayawardena and colleagues reported the successful generation of reprogrammed iCMS with a cocktail of microRNA [197]. They screened six microRNAs chosen for their regulatory role in cardiomyocyte differentiation and developed all 41 possible permutations of singlet, doublet and triplet combinations. The combination of miR-1, miR-133, miR-208, and miR-499 (miR Combo) were able to reprogram cardiac fibroblasts into cardiomyocytes.

Another approach to direct reprogramming uses a combination of chemical cocktails, circumventing the risks associated with genetic manipulation in transcription factors and microRNA methodologies. In an attempt to generate chemically induced iPSCs, Fu *et al.* noticed a spontaneous cluster of contracting cells resembling that of cardiomyocytes and developed a two-step reprogramming process to induce and stabilise iCM reprogramming [198]. The process involves cells passing through a cardiac progenitor phase before further differentiating into a cardiomyocyte. Using this method, Fu and colleague showed that spontaneous beating was observed as early as day 6-8 after the addition of the chemical reprogramming cocktails, as opposed to other methodologies in which the first sign of beating was typically observed at around day 20.

Finally, the combinations of the factors discussed above have been shown to produce a synergistic effect and enhance reprogramming efficiency. The use of a chemical cocktail in addition to the overexpression of Oct4 in MEFs was able to directly reprogram MEFs into iCMs without going through a pluripotent state, but in this method, cells were differentiated down the cardiac progenitor lineage first [199]. Additionally, the addition of a single small molecule inhibitor of TGFβ enhanced the reprogramming efficiency of the HNGMT reprogramming cocktail by five-fold [200]. The addition of miR-1 or miR-133 in combination with the GMT cocktail produced a six-fold increase in efficiency in comparison to GMT alone [201]. Finally, Jayawardena *et al.* showed that the addition of JAK inhibitor I to the same four microRNA cocktails they initially used led to an increase in reprogramming efficiency by ten-fold [197].

Much focus is still placed on the discovery of methodologies that can improve the reprogramming efficiency and perhaps an improved understanding of the normal cardiac developmental process might provide some novel ideas.

2.5.3. Factors for Human Direct Cardiac Reprogramming from Fibroblasts

Despite the numerous successes to reprogram murine fibroblasts, the attempts for direct reprogramming of human somatic cells have not seen similar results and appear to be more difficult to achieve (Table. 2). In human fibroblasts reprogramming towards cardiomyocytes required the addition of Myocd on top of the GHMT factors to initiate the expression of cardiac genes profile [202]. In the same study, the researchers also showed that Mef2c could be eliminated in the presence of 2 additional muscle-specific microRNAs, miR-1, and miR-133, and this combination further improved the conversion rate to about 10 to 20% although only

a small subset of the cells displayed spontaneous contractile activity after 11 weeks of culture. The group that first pioneered the reprogramming protocol in murine cells also discovered that GMT was not sufficient for cardiac reprogramming in human fibroblasts and required the addition of Mesp1 and Myocd [203]. The addition of Mesp1 and Myocd led to the increased expression of intracellular $Ca2^{+}$ oscillations and sarcomeric genes, respectively. The human CFs and dermal fibroblasts transduced with the GMT, Mesp1, and Myocd displayed a structural and electrophysiological mature phenotype although no spontaneous beating was observed.

Moreover, the suppression of fibroblastic gene circuits by miR-133 mediated Snail1 repression further promoted the reprogramming of human fibroblasts [201]. A study by Fu *et al.* showed that transient expression of GMT along with Essrg, Mesp1, Myocd, and ZFPM2 in human fetal cardiac fibroblasts and neonatal dermal fibroblasts enhance cardiac reprogramming and even a small proportion of iCMs showed proper sarcomere assembly, calcium handling and action potentials [204]. Another combinatorial partial direct reprogramming approach reported that transient expression of Ets2 and Mesp1, after the addition of activin A and bmp2, could reprogram human dermal fibroblasts into cardiac-progenitor cells that can be further differentiated into cardiomyocyte-like cells upon prolonged culture [205]. The use of chemical cocktails that consists of CHIR99021 (a WNT pathway activator), A83-01 (potent inhibitor of TGF-β), BIX01294 (methyltransferase inhibitor), AS8351 (histone demethylase inhibitor), SC1 (ERK and RAS-GAP inhibitor), OAC2 (Oct4 activator), SU16F (PDGFRβ inhibitor), and JNJ1098409 (PDGFRTK inhibitor) were shown to be able to direct human foreskin fibroblasts *in vitro* into iCMs [206].

To further advance the use of direct cardiac reprogramming strategy towards clinical applications, more emphasis should be put on developing protocols to enhance human cardiac reprogramming.

2.5.4. *In vivo* Direct Cardiac Reprogramming

The possibility of performing *in vivo* direct cardiac reprogramming of a large pool of endogenous cardiac CFs is fascinating. One could hypothesise that the *in vivo* cardiac microenvironment might help enhance the reprogramming process and generate more mature iCMs compared to *in vitro* environments. There have been a few studies investigating this possibility with a variable success rate (Table 2).

In the first study, Qian *et al.* delivered GMT via retroviral vectors to mice post ligation of the coronary artery and demonstrated *in vivo* cardiac reprogramming and more importantly saw functional improvement [33]. They also showed that approximately 35% of the cardiomyocytes by the peri-infarct zone were derived from the infected CFs or nonmyocytes and not due to cell fusion with pre-existing myocytes asdemonstrated by the lineage tracing experiments performed. The *in vivo* generated iCMs showed a highly mature ventricular-like phenotype in term of electrophysiological properties and displayed binucleation, fully assembled sarcomere and remarkable electrical coupling with the endogenous cardiomyocytes. The GMT treated mice showed significant improvement of cardiac function and reduction in fibroblast as shown byMRI, echocardiography and histological analysis.

Another study by Song *et al*. [191] also demonstrated the retroviral injection of GHMT successfully converted endogenous CFs into newly generated iCMS with visible striations and functional properties of that of ventricular myocytes. They also observed an increase of the heart EFs by nearly 2-fold and reduction in scar size by 50% in GHMT-treated mice compared to controls.

Ingawa *et al.* also reported the same results as the previous two articles [34]. However, they constructed and used retroviruses containing the polycistronic GMT under a single promoter to have a more homogeneous expression of the individual transgenes. This modification lead to the reprogramming of CFS into more mature iCMs compared to injecting the GMT vectors separately. This concept was also adopted by Mathison *et al.* [207], and they demonstrated that polycistronic GMT delivery to infarcted rat hearts led to a two-fold increase in *in vivo* iCMs reprogrammed as well as improvement in ventricular function.

Pre-treatment of the infarcted myocardium with intramyocardial injection of vascular endothelial growth factors (VEGFs) three weeks before GMT gene delivery led to significantly decreased fibrosis and 4-fold increase in ejection fraction [208]. The benefits observed might be because of the induction of neovascularisation thus improving the chance of survival of the newly formed iCMs in the infarcted hearts. The addition of a fibroblast activator, thymosin β4, on top of the basal GMT reprogramming factors also significantly increased the efficiency and the functional recovery of the infarcted hearts [209].

The direct administration of lentiviruses expressing a combination miR-1, miR-133, miR-208 and miR-499 into the infarcted hearts of mice led to the *in vivo* conversion of resident CFs

into iCMs with a mature ventricular like cardiac phenotype [210]. The study also showed a progressive improvement of ventricular function starting 1 to 2 months post-surgery and further enhanced at three months check-up.

Taken together these novel approaches to *in vivo* cardiac reprogramming suggest that the resident CFs can be used as a cell source for the generation of new iCMs. Also, *in vivo* reprogramming showed significantly greater reprogramming efficiency in comparison to *in vitro*. The results from *in vivo* reprogramming further demonstrate the vital role of the microenvironment and surrounding cells in providing the necessary paracrine agents, mechanical forces and appropriate ECM support to facilitate the reprogramming and also the maturation of the newly formed iCMs.

2.6. Strategies to Enhance Direct Cardiac Reprogramming

Despite the success of direct cardiac reprogramming, the efficiency remains low. Many methods have been developed aimed at increasing the conversion rate (Table. 2). These can be classified into four main categories: reprogramming factors optimisation, modulation of epigenetic barriers, modification of cellular signalling and manipulation of the microenvironment.

2.6.1. Reprogramming Factors Optimisation

The procedure of direct reprogramming often involves the forced overexpression of the reprogramming factors by multiple retroviral or lentiviral vectors. It means that the initial cells must take up each of the individual viruses to be reprogrammed. Additionally, individual cells can also receive different ratios of the reprogramming factors. Statistically speaking, only a small proportion of the starting cells receive the ideal ratio and dose to achieve successful cell fate conversion. These methods often result in crude, heterogeneous and artificial dosage, as opposed to the delicate balance of transcription factor expression that is required to initiate and maintain cardiac lineage commitment during the developmental process *in vivo*.

Wang *et al*. [35] took on the challenge and determined the optimal ratio of the basal Gata4, Mef2c and Tbx5 transcription factors for efficient reprogramming. They generated polycistronic constructs with every possible splicing order separated by 2A peptide cleavage sites in between the factors. They showed that only Mef2c-Gata4-Tbx5 (MGT) and Mef2c-Tbx5-Gata4 (MTG) constructs enhanced the reprogramming efficiency in comparison to the

infection of the individual factors separately. Suggesting that the high transcriptional activity of Mef2c and low expression of Gata4 and Tbx5 is critical to increased cardiac induction. Furthermore, a follow-up study by the same group demonstrated that optimal stoichiometry of the three transcription factors using the polycistronic construct (MGT) also leads to the increased efficiency of *in vivo* reprogramming and improves cardiac function following MI than reprogramming with separate viruses [211]. Two independent studies also generated polycistronic constructs. Inagawa *et al.* [34] placed the factors in the order Tbx5-Mef2c-Gata4 and saw no difference in the amount of α-Actinin positive cells but did observe that more of the reprogrammed cells had assembled sarcomeres. While a study by Mathison *et al.* [207] used the order Gata4-Mef2c-Tbx5 and saw a slight increase in the number of transformed cells *in vitro* and enhanced cardiac function *in vivo* post-MI. However, in both of these studies, only a modest improvement was observed and could be due to the non-optimal ratio between the reprogramming factors.

2.6.2. Modulation of Epigenetic Barriers

The conversion of cellular phenotypes from one type to another requires the activation and repression of various genetic circuits. Epigenetic codes dictate the accessibility of TFs to their target DNA and are crucial in the determination of reprogramming efficiency. The epigenetic marks have to recode to alter the structure of the chromatin and repress the fibroblasts gene signature while activating cardiac genes. Recent studies have shown that during direct cardiac reprogramming, the inactive histone marker trimethyl lysine 27 of histone 3 (H3K27me3) increases at the promoter region of fibroblastic genes and decreases at cardiac promoters while the H3K4me3, which marks active chromatin, shows the opposite pattern [212]. A few studies have demonstrated the possibility to further enhance the reprogramming process by modulating the epigenome.

Developmental studies demonstrated the importance of inhibiting class IIa histone deacetylase (HDAC) to promote cardiomyogenesis [213, 214]. Christoforou *et al.* showed that the expression of reprogramming factors in conjunction with the inhibition of HDAC with valporic acid, a non-specific HDAC inhibitor, increased the number of cTnT or α-Actinin positive, positive cells by two-fold.

During microRNA mediated cardiac reprogramming, the level of H3K27me3 was significantly reduced globally, and a 50% reduction was observed at the promoter of the MGT. Inhibition

of the H3K27 methyltransferases le to increased expression of cardiac markers in the level of genes and proteins, while knockdown of H3K27 demethylase inhibited the expression of cardiac genes and block reprogramming [215]. Additionally, the timing of histone methyltransferase inhibition is critical to enhancing reprogramming [216]. Inhibition of Ezh2, the catalytic component of the complex responsible for the methylating H3K27me2/3, in the first three days of reprogramming increased the conversion rate of fibroblasts to iCMs. Conversely, maximal generation of iCM clusters was only observed G9a was inhibited at a later stage. Inhibition at other times resulted in no effect or even a decrease in efficiency [216].

A study by Zhou *et al.* [217] showed that the early inhibition of Bmi1, a polycomb group protein that interact with cardiac loci and suppresses their expression, prime fibroblasts adopted cardiac fate and subsequently resulted enhanced the efficiency. The inhibition of Bmi1 also enables reprogramming to occur with only exogenous expression of Mef2c and Tbx5. Mll1, an H3K4 methyltransferase, has also been identified as another epigenetic barrier to direct cardiac reprogramming [218]. The inhibition of Mll1 not only increases the expression of αMHC-GFP by 1.5-fold, an indicator of successful iCM conversion, but also the maturation of the iCMs.

These results highlight the complexity of the reprogramming process and the importance that the epigenetic landscape has on the process of cell fate conversion.

2.6.3. Modifications of Cellular Signalling

The process of direct reprogramming requires the activation of target cell gene expression and must also be accompanied by the complete repression of the original cell expression signature. Indirect cardiac reprogramming, the leftover fibroblast gene expression represents a roadblock to the success of the reprogramming protocol.

miRNA-1 and miRNA-133 have been shown to enhance direct cardiac reprogramming by suppressing fibrotic gene expression [201, 219]. The iCMs produced by the addition of miRNA cocktails also showed a more mature and functional phenotype. miRNA-133 work through the suppression of Snai1 and this leads to the suppression of fibroblast genes expression and simultaneously enhance cardiac gene expression during the reprogramming [201]. Using chemical inhibitors to TGFβ and Rho-associated kinase (ROCK) to suppress fibroblast identity, have also lead to an increase in total iCMs produced and a decrease in the time required. A

recent study by Mohamed *et al.* [220] demonstrated that inhibition of TGFβ signalling with SB431542 a day after GMT infection followed by the inhibition of Wnt signalling with XAV939 (day 2 of reprogramming) resulted in an 8-fold increase in cardiac reprogramming and iCMs that are transcriptionally more similar to adult cardiomyocytes. The combination of GMT transcription factor cocktail with the TGFβ and Wnt inhibition also enhanced reprogramming and improved cardiac function *in vivo* as early as one-week post-MI.

Furthermore, the activation of Akt1 signalling pathway during GHMT transcription factor-mediated reprogramming not only increased the reprogramming efficiency but also produced iCMs that exhibited an increase in calcium flux, spontaneous beating, polynucleation, mitochondrial function, size and sarcomere assembly [221]. Zhou *et al*. showed that Akt1 activation resulted in downstream mTOR activation and Foxo3a inhibition which together play a role in the regulation of myocyte development and mitochondrial function.

During development, Notch signalling plays a crucial role in the regulation of cardiomyocyte differentiation and proliferation. One of the ways it regulates this process is by blocking the binding of Mef2c to promoter regions. Thus it comes as no surprise that the addition of the Notch inhibitor DAPT to the GHMT transcription factor cocktail during reprogramming leads to the enhanced conversions [222]. Moreover, Notch inhibition via DAPT and Akt1 activation worked synergistically to increase the acquirement of mature myocyte phenotypes [222].

2.6.4. Manipulations of the Microenvironment

Several studies have demonstrated that *in vivo* reprogrammed iCMs displayed far superior phenotypes and are more similar to endogenous cardiomyocytes in comparison to that of *in vitro* reprogrammed iCMs [33, 34, 191, 211]. Additionally, the higher conversion efficiency was noted in *in vivo* reprogramming strategies over *in vitro*. Suggesting that cues present in the *in vivo* microenvironment such as topographical cues, mechanical forces, and soluble factors play an essential role in promoting the generation and maturation of iCMs.

In the presence of serum-based reprogramming media, several studies have noted that most of the iCMs generated were only partially reprogrammed and failed to assemble α-Actinin or cTnT sarcomeric structure in culture [194, 223]. To address this problem, Yamakawa *et al.* [223] performed a screening of cardiogenic compounds to create a serum-free cell culture media and found that the addition of fibroblast growth factor (FGF) 2, FGF10, and vascular endothelial growth factor (VEGF) significantly improved the functionality and maturity of the

in vitro generated iCMs. This cocktail of growth factors is critical for late-stage maturation and works by activating cardiac transcription regulators, the p38 MAPK pathway and the PI3K/AKT pathways which have been shown to be important in the acquisition of mature phenotypes [221-223]. Despite the increase in the percentage of cells with fully assembled sarcomeres, the use of low serum growth media was insufficient for the reprogrammed iCMs to maintain their striated sarcomere overtime [194] suggesting the importance of growth factors in iCMs maturation.

Apart from soluble factors, biophysical cues are also crucial in the establishment of functional maturity of iCMs. It is well known that cells including cardiomyocytes can sense and respond by reorganising their actocystoskeletal assembly in response to different substrate stiffness. A softer stiffness closer to the *in vivo* healthy heart (10-30 kPa) promotes cardiomyocytes to adopt a more rectangular shape that forms well organised sarcomeres, compared to cells on a stiffer substrate [224]. However, it appears that the efficiency of GMT cocktail mediated cardiac reprogramming of adult tail tip fibroblasts was not influenced by substrate stiffness despite inducing morphological differences [225]. Similarly, the application of cyclic uniaxial stretch also fails to increase the reprogramming efficiency [225].

On the other hand, topographical cues were able to enhance reprogramming efficiency and maturation through histone acetylation and transcriptional activation mechanism [225, 226]. Reprogramming in microgrooved substrates led to translocation of the mechanosensitive transcription factor Mlk1 into the nucleus and the activation of the downstream effector genes. Also, GMT reprogrammed cells on microgrooves showed an increase in histone three acetylations. Sia *et al.* showed that simultaneous HDAC inhibition with valporic acid (VPA) and Mlk1 overexpression mimicked the effect of microgrooved substrates and enhanced reprogramming on the flat substrates [225].

The composition of the ECM directly influences cardiac reprogramming. Reprogramming efficiency was improved when cells were cultured on hydrogels supplemented with fibrin and collagen I [227]. These combination promotes cardiac differentiation and increases the number of contractile colonies.

The use of 3D fibrin hydrogels to more accurately mimic *in vivo* stimuli enhanced direct cardiac reprogramming by 20-fold [228]. The mechanism behind this observation appears to be mediated through the upregulation of MMPs expression, suggesting that increased MMPs

in infarcted hearts could be one of the contributing factors to the higher efficiency observed *in vivo* [228].

Table 2. Summary of cardiac reprogramming factors reported in the literature.

Rep Factors	Mouse/ Human	*In vitro/In vivo*	Expression System	Reported Efficiency	Functional Assay	Time	Ref
Transcription Factor Cocktails							
GMT	Mouse	Both	Retroviruses / Lentiviruses	4.8% $cTnT^+$ (*in vitro*) and 17% αMHC^+ (*in vitro*)	Ca^{2+} flux, Electrical activity, Beating and cell transplantation	4 – 5 weeks	[32, 33]
GMHT	Mouse	Both	Retroviruses	27.6% $cTnT^+$ (*in vitro*)	Calcium flux and beating	5 weeks	[191, 202]
MTM	Mouse	*In vitro*	Lentiviruses	12% $cTnT^+$	Electrical activity and Beating	2 weeks	[193]
GMTMSMS	Mouse	*In vitro*	Lentiviruses	2.4% αMHC^+	Ca^{2+} transient	NB	[194]
HNGMT	Mouse	*In vitro*	Lentiviruses	1.6% $GCaMP^+$	Ca^{2+} oscillations, Beating	11-16 days	[95]
GMHT, *MyoD* transactivation Domain	Mouse	*In vitro*	Retroviruses	19% $cTnT^+$	Ca^{2+} oscillations and Beating	2 weeks	[196]
Stoichiometry of MGT	Mouse	*In vitro*	Retroviruses	25% $cTnT^+$, 15% αMHC^+ (after Pur selection)	Ca^{2+} transient and Beating	3-4 weeks	[35]
Mesp1 + *Ets2*	Human	*In vitro*	Retroviruses	9% of $Nkx2.5^+$	Ca^{2+} transient	8-14 days	[205]
GMTMM	Human	*In vitro*	Retroviruses	± 6%$cTnT^+$	Ca^{2+} transient and action potential	4 weeks	[203]
7F	Human	*In vitro*	Retroviruses	15-20% αMHC^+	Ca^{2+} transient	2-4 weeks	[195]
MicroRNA Cocktail							
miR Combo	Mouse	Both	Transient *in vitro,* Lentivirus *in vivo*	28% αMHC^+ *in vitro*, 1% iCM *in vivo*	Beating and Ca^{2+} transient *in vitro*, cardiac function improvement *in vivo*	3-4 weeks	[197, 210]

Chemical Cocktails							
CRFVPT	Mouse	*In vitro*	Transient	9% αMHC^{+}	Beating and Ca^{2+} transient	1 week	[198]
9C	Human	*In vitro*	Transient	6.6% cTnT^{+}	Beating, Ca^{2}+ transient and electrophysiology	1 week	[206]
Combined Cocktails							
GMT or GMTMM +miR-133	Both	*In vitro*	Rertroviruses	25% αMHC^{+}, 8% αMHC^{+}/cTnT^{+} in MEFs, 27.8% cTnT^{+} in HCFs	Beating and Calcium transient	10 days	[201]
MGT+ WNT/TGFβ inhibitior	Mouse	Both	Polycistronic Retrovirus	30% αMHC^{+} after 2 weeks,	Beating and Ca^{2+} transient	1 week	[220]
miR Combo + JAK inhibitorI	Mouse	Both	Transient *in vitro* and Lentivirus *in vivo*	28% αMHC^{+} *in vitro*, 1% iCM *in vivo*	Beating and Ca^{2+} transient *in vitro*, cardiac function improvement *in vivo*	3-4 weeks	[197]
GMT + Bmi1 inhibitor	Mouse	*In vitro*	Retrovirus	±22% αMHC^{+}/ cTnT^{+}	Calcium transient	2-4 weeks	[217]
HGMT2m+ anti fibrotic signal	Mouse	*In vitro*	Retrovirus and adenoviruses	70% cTnT^{+} (from MEF) 20% cTnT^{+} (from ACFs), 35% cTnT^{+} (from ATTFs) (after 2 weeks)	Beating, calcium transient and Action Potentials	8 days	[219]
GMT + Thymosin β4	Mouse	*In vivo*	Retrovirus	35% iCM on infarct zone, 98% of iCMs were α-actinin^{+}, 90% of iCMs were Cx43^{+}	Calcium transient, Action Potentials and improvement in cardiac function	4 weeks	[209]

2.7. The Epicardium and its Role in Cardiac Regeneration

The development of the heart is a complicated process. The heart receives cellular contributions from three primary sources [229]. Firstly, the cardiogenic mesoderm of the cardiac crescents, *i.e.* first heart field (FHF) and second heart field (SHF), contributes to the cellular contents of the heart.Following looping of the heart tube, the cardiac neural crest cells, which contribute to vascular cells and play a pivotal role in aorticopulmonary septation [230]. Finally, cells originating from the proepicardium (PE) contribute to various cellular subpopulations including the adult epicardial lining.

This chapter will provide an overview of the role of epicardium development, the current evidence on the role of epicardium role in regenerating the damaged heart and ways to enhance and harness the regenerative property (Fig. 8).

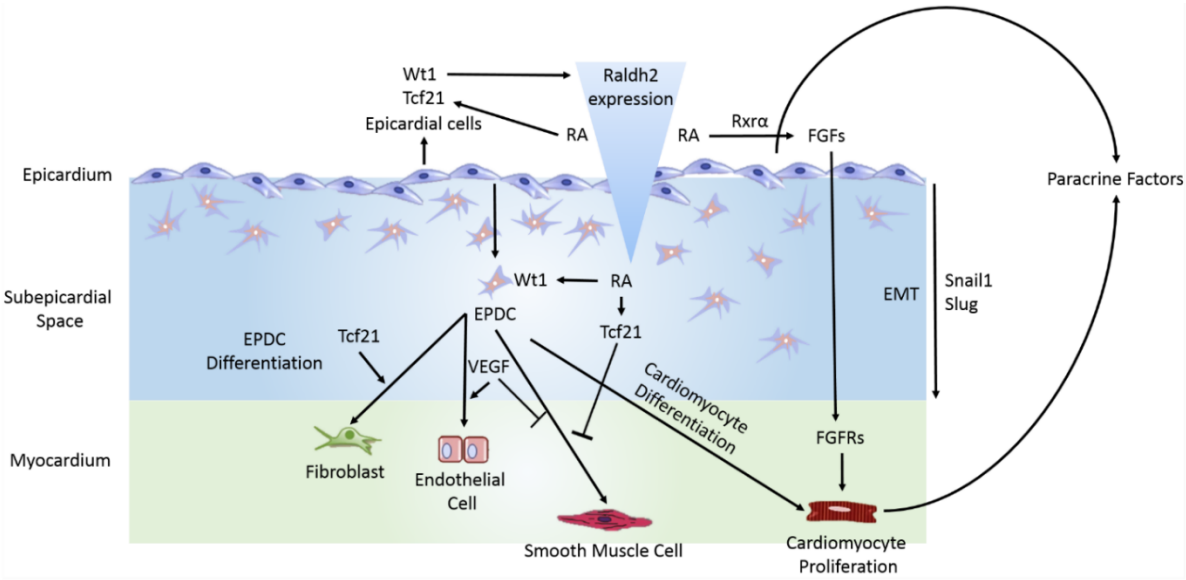


Figure 8. Summary of the role of the epicardium during development. Epicardial cells can be identified by the expression of Wt1 and Tcf21 which is regulated by retinoic acid (RA) signalling. The epicardial cells have two major roles in supporting normal cardiac development. Firstly, they act a major source of paracrine signals such as Fgf2, 9 and 16 to support the proliferation of cardiomyocytes. The epicardium-myocardium crosstalk is very important not only during development but also in the maintenance of normal cardiac function. Secondly, the epicardial cells can undergo EMT and give rise to cardiac fibroblasts, smooth muscle cells, endothelial cells and cardiomyocytes.

2.7.1. Cellular Contribution of Epicardium in Adult Heart

During development, the epicardium undergoes epithelial-to-mesenchymal transformation (EMT) and invade the myocardial walls, giving rise to epicardial-derived cells (EPDCs) [231]. The EPDCs are characterised by the expression of the Wt1, Tbx18 and Tcf21 transcription factors in addition to Raldh2, a retinoic acid (RA) synthesising enzyme [232]. EPDCs are classified as multipotent cardiac progenitors, due to their potential to differentiate and give rise to endothelial cells [233], coronary vascular smooth muscle cells [234], cardiac fibroblasts [235] and pericytes [231, 236]. However, their involvement in cardiomyocytes and coronary endothelial cells remained controversial.

Using a Tbx18 lineage tracing, Cai *et al.* [237] demonstrated that epicardial $Tbx18^{+}$ cells not only contributed to EPDC-derived lineages as previously reported but also to *in vivo* ventricular cardiomyocytes. However, previous studies showed that fetal cardiomyocytes also expressed Tbx18 thus casting doubt on experiments utilising $Tbx18^{+}$ epicardial lineage tracing technology [238, 239].

$Wt1^{+}$ epicardial cells have also been reported to give rise to endothelial cells and cardiomyocytes [236]. However, the studies were challenged by a more recent discovery of the presence of Wt-1 derived cardiomyocytes before PE/epicardial formation [240]. Two more recent studies using a Tcf21 lineage tracing in the zebrafish model [241] and a label cell transplant experiments [242] also support the theory that epicardial cells do not contribute to the myocardium.

Equally unresolved controversies have also arisen on the topic of the contribution of EPDCs to coronary endothelium. Previous studies suggested the involvement of epicardium [243, 244], however, recently it is increasingly reasoned that only a limited amount, if any, is derived from the PE or epicardium layer [245, 246]. A detailed discussion can be found in a recent review by Riley and Smart [247].

2.7.2. Role of Epicardium-derived Mitogens in Adult Heart

In addition to their contribution to the cellular components of the heart, the epicardium also serves as an indispensable source of paracrine signals. Some of the critical signals such as retinoic acid (RA), FGFs, VEGFs and endothelin act as essential mitogens to support proper cardiac development (Fig. 4) [232].

The tight regulation of RA signalling is critical for early heart development. Mice lacking the RA signalling showed reduced proliferation of cardiomyocytes in the outer ventricular chamber wall and fail to form the compact zone, resulting in midgestation lethality [248]. This phenotype is associated with the lack of epicardial specific RA signalling. *In vitro*, the inhibition of RA signalling with RA receptor antagonist suppressed the proliferation of cardiomyocytes in chick fetal heart slices, and this phenotype can also be recapitulated by the removal of the epicardium layer [249]. The addition of RA to cultured mouse embryonic epicardial cells and stable epicardial cell lines also induced the cells to secrete further factors that stimulate proliferation of cultured CMs [250]. Recent studies worth noting demonstrated the cross-talk between the hepatic and cardiac system in mice. In response to RA, the liver secretes erythropoietin (EPO) into the bloodstream, which in turn leads to the production of insulin growth factor 2 (IGF2) in the epicardium [251]. IGF2 released by the epicardium induces CM proliferation.

The RA-Epo signalling acts synergistically on the epicardium to initiate and present mitogens for the heart development[249]. Surprisingly, four days post birth, both the ability of the epicardial to release mitogens in the presence of RA and the ability of CMs to undergo division in response to the mitogens were lost [250]. The loss of this proliferative capacity coincided with the loss of the regenerative capacity of the mouse heart [252].

As discussed, one of the roles of the epicardium is to regulate the growth and survival of the myocardium, and this process depends on the intrinsic RA and Epo signals. These signals act on the epicardium and regulate the production and the release of FGFs, and the epicardial derived FGF signals, in turn, regulate the proliferation of the myocardium during midgestation of the heart development [253]. Moreover, during development, the epicardium underwent epithelial-mesenchymal transformation (EMT) and gave rise to precursor cells that later became cardiac fibroblasts and other cell types. FGF molecules secreted by the myocardium are required to induce and initiate this process in the epicardium [254]. Subsequently, the

embryonic cardiac fibroblasts formed exert collaborative cues in the form of ECM components (*i.e*. fibronectin, collagen, and heparin-binding EGF-like growth factor) to stimulate myocyte proliferation [255]. Epicardial-myocardial FGF signalling is a critical pathway not only during fetal development but also in adulthood to maintain myocardial homeostasis [256] and proper phenotype and functionality [257].

Thymosin beta-4 (Tβ4), and actin monomer-binding protein has gained some traction in recent years due to its involvement in both the developing epicardium [258] and response post-injury [259]. Through the use of short hairpin RNA (shRNA) to knockdown the expression of Tβ4 in the embryonic mice CMs, Smart *et al.* [258] demonstrated that both epicardial development and vasculogenesis were severely disrupted. This observation was associated with the reduction in EPDC differentiation and migration towards the vascular lineages and the phenotypes associated with the knockout can be rescued following the addition of Tβ4 and further optimised by parallel treatment with VEGF and FGF7 [7, 258]

2.7.3. Role of Epicardium in Cardiac Repair

At the end of gestation, the epicardium enters a state of quiescence. Embryonic epicardial markers were silenced, except for very low levels in the epicardium surrounding the atria and atrioventricular sulcus in the mouse [260, 261]. As mentioned in the previous chapter, in the adult zebrafish the epicardium remained active and contributed to myocardial homeostasis via FGF mediated signalling with CMs throughout life [256]. However, the role of the epicardium in the healthy adult mammalian heart remains poorly characterised.

Following injury, early studies of resection injury in zebrafish demonstrated that the epicardial activation and mobilisation of the EPDCs are some of the first events that take place in the post-injury repair mechanism [262]. The epicardial layer reactivates its embryonic gene programme to provide a rapid and robust response to help repair the heart (Fig. 9). Van Wijk *et al.* [260] reported that immediately after the induction of ischemia the epicardial layer over the infarct is lost, but this event is followed by the re-activation of the epicardium on the border zone. The re-activated epicardium transiently expresses embryonic epicardial markers genes such as Wt1, Tbx18 and Raldh and begins proliferating and expanding, and by day three post infarction the newly expanded epicardium completely ensheath the exposed myocardium over the infarct zone [260]. The newly formed epicardium undergo EMT to populate the sub-epicardial space with $Wt1^{+}$ mesenchymal cells, and a small portion of these

cells differentiate further into myofibroblasts, coronary endothelial cells and cardiomyocytes [260]. On the other hand, in a study by Zhou *et al.* EPDCs did not contribute to new CMs and coronary endothelium but rather $Wt1^+$ EPDCs secreted pro-angiogenic paracrine signals containing a high level of VEGF and FGF2 that were further shown to improve cardiac remodelling following MI [261].

Additionally few studies have also revealed a new role for the epicardium in establishing a microenvironment that supports heart regeneration. Through loss-of-function experiments, Wang *et al.* showed that the fibronectin secreted by the epicardium in response to cardiac injury is crucial for the regeneration of the zebrafish heart [263]. Furthermore, the study of cardiac regeneration in newt heart revealed the role of the epicardium in remodelling the ECM to provide a more regeneration-specific matrix that supports cardiomyocyte re-entry to the cell cycle and the migration of progenitor cells following injury [264]. This process occurs as early as three days post-amputation and the matrix is composed mainly of tenascin-C, hyaluronic acid (HA) and fibronectin [264].

The re-activation of the embryonic signature in adult epicardium is partly mediated by the CCAAT/enhancer binding protein (C/EBP) signalling, and its binding sites were found to be present in the promoter regions of both *Wt1* and *Raldh2* [265]. Surprisingly, the disruption of C/EBP signalling in the adult murine epicardial cells following injury led to a reduction in inflammatory response, specifically the injury-induced neutrophil infiltration into the myocardium and led to improvement in cardiac function [265]. These findings reveal the dual role of the C/EBP signalling in the epicardium; first as a signal required for the re-activation of embryonic gene signature, and also for the regulation of the inflammatory response by the epicardium.

A more recent study by Ramjee *et al*. [266] provides another support for the role of the epicardium in modulating the immune responses following injury. This study described the previously unappreciated role of the Hippo signalling within the epicardium in suppressing deleterious post-infarct inflammatory response through the recruitment of a subset of $CD4^+$, T-regulatory cells (Tregs). The Tregs have been shown to repress the immune response and prevent adverse remodelling following cardiac injury. Following MI the mice developed extensive pericardial inflammation, myocardial fibrosis and fewer suppressive Tregs in the injured myocardium, all of which resulted in cardiomyopathy and death [266]. The studies

mentioned provide strong evidence linking the epicardium and the immune system. However, the precise mechanisms by which the epicardium modulates the immune cell following injury remain elusive.

Interestingly, following myocardial necrosis, unidentified soluble factors present in the pericardial fluids have also been shown to re-activate the embryonic signature of EPDCs and promote cell proliferation [267]. The re-activated adult EPDCs can restore the expression of the embryonic gene signature. However, re-activated adult EPDCs are distinct from their embryonic counterpart [268]. The adult EPDCs population expresses a higher level of Sca-1, CD90, CD44 and CD105 in comparison to the embryonic cells, and is also very heterogeneous, consisting of many subpopulations with different cardiogenic differentiation potential [268].

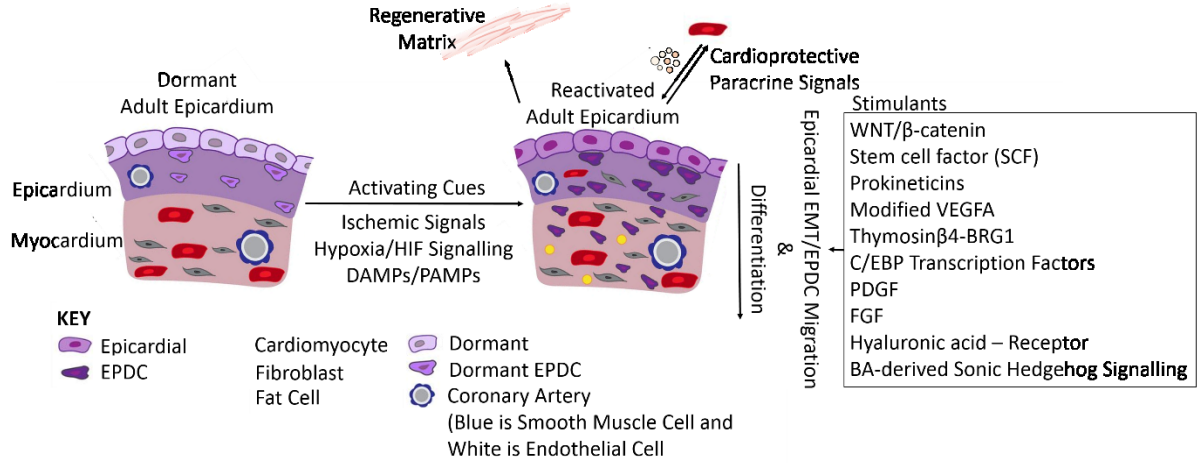


Figure 9. Role of the epicardium in cardiac injury and the signals and factors involved. Following ischemic injury, signals such as hypoxia mediated signalling, and paracrine factors such as DAMPs and PAMPs, activate the epicardium. The epicardium reactivates its embryonic molecular signature Wt1, Tbx18 and RA and undergo rapid proliferation and expansion. The activated epicardial cells contribute to cardiac repair through direct cellular contribution as they undergo EMT, migrate into the myocardium and differentiate towards cardiac lineage cells. Secondly, the epicardium acts via paracrine signalling, inducing proliferation of cardiomyocytes, angiogenesis and survival or cardiomyocytes. More recently, it was revealed that the EPDCs actively remodel the matrix of the myocardium to provide a regenerative microenvironment that promotes healing. The physiological activation of the EPDCs in cardiac repair is limited, however, various stimulants have been shown to be able to further drive and enhance the reparatory functions and contributions of the epicardial cells in cardiac injury. Figure adapted from [7].

2.7.4. Stimulations and Clinical Applications of the Epicardium

Although the EPDCs possess the ability to differentiate into various cell types of cardiovascular lineage and play a vital role in post-injury cardiac response, these beneficial properties are insufficient to repair damages incurred on the mammalian hearts. Thus various groups have explored ways to externally stimulate the EPDCs regenerative potential as a novel strategy for cardiac regeneration (Fig. 9).

The first of this approaches was demonstrated in mice cardiac explant studies by Smart *et al.* [258]. They identified Tβ4 as an essential molecule for the development of coronary vasculature in the development of mice, and demonstrated that stimulation of quiescent adult epicardial explants with Tβ4 significantly enhanced cellular outgrowth, restored pluripotency and even initiated differentiation towards smooth muscle, fibroblast lineages and vascular progenitors [258]. As well as inducing organ-wide activation of the embryonic program in the adult epicardium, Tβ4 treatment in adult mice also led to the expression of factors that promote EMT in the epicardium [259].

Around the same time, two independent studies demonstrated the capability of Tβ4 in facilitating epicardial neovascularisation of the injured adult hearts [269, 270]. In both studies, Tβ4-treated hearts led to dramatic epicardial thickening accompanied by an increase of progenitors and a large number of endothelial cells (ECs) and vascular smooth muscle cells (VSMCs) which assembled into a perfused, functional network of vasculatures at the border and the remote zone. Some of the newly generated ECs and VSMCs were shown to be of $WT1^+$ origin, re-affirming the role of the EPDCs in neovascularisation. Tβ4 induced arteriogenesis mediated partly by the epicardium may, therefore, be a beneficial treatment post-MI, to enhance the relatively weak and inadequate endogeneous capillary response.

A follow-up study by Smart *et al.* demonstrated that the administration of Tβ4 resulted in enhancing cardiac repair by promoting $Wt1^+$ cells to differentiate into cardiomyocytes [271]. In this study Tβ4 was administered prior to MI to reactivate the adult Wt1 EPDC population, and between day 2-7 post-injury, $WT1^+$ EPDCs, including some cardiac progenitors were seen migrating from the epicardium to the site of injury, and by day 14, these $WT1^+$ EPDCs started to express sarcomeric markers and adopt phenotype resembling the mature cardiomyocytes within the myocardium [271]. More importantly, the bona fide *de novo* cardiomyocytes were functionally integrated with the resident myocardium, and this treatment led to significant

improvement in cardiac function following MI [271]. Nevertheless, this approach requires patients to be primed with Tβ4 before the injury, since no new cardiomyocytes from EPDCs were formed without pretreatment [271] or if the Tβ4 was administered after MI [272]. This method of 'priming' the heart with Tβ4 has also been shown to extend the cardiac regenerative capacity of neonatal mice. A study by Rui *et al.* demonstrated that daily intraperitoneal injection of Tβ4 for six days before apical resection at P7, led to complete regeneration of the heart by day 19 and was mediated by an increase of $WT1^+$ cells [273]. The mechanism behind Tβ4 induced re-activation of epicardial fetal gene programme was recently revealed and highlighted the importance of chromatin remodelling [274]. Through the use of chromatin immunoprecipitations (CHIP), the catalytic subunit of the SWI/SNF chromatin remodelling complex, BRG1, was demonstrated to physically interact with Tβ4, and was recruited to the regulatory region of *Wt1* and other epicardial loci, such as *Raldh2*, *Tbx18*, *Tcf21* by the C/EBP, and these BRG1-Tβ4 co-operative interaction promoted the expression of the embryonic epicardial genes [274].

Additionally, cardiomyocyte-specific overexpression of the membrane-associated human stem cell factor (hSCF) has been shown to promote epicardial activation both *in vitro* and *in vivo*, to increase $Wt1^+$ EPDCs migration into the infarcted myocardium and to enhance arteriogenesis post-MI [275]. The prokineticin receptor-1 (PKR1) and its ligand prokineticin-2 (PKC-2) have also emerged as potential targets to induce cardioprotective machinery post-MI [276]. The overexpression of PKR1 in cardiomyocytes *in vivo* resulted in an increase in the number of EPDCs and the formation of neovasculature and vascular remodelling. This effect was thought to be mediated by the activation of the prokineticin signalling pathways in EPDCs inducing the endothelial and smooth muscle cells differentiation programme [276].

Interestingly, the use of exosomal clusterin derived from the pericardial fluid of infarcted patients can also improve the cardiac function post-MI [277]. The study suggested that clusterin containing exosomes acts through the activation of EMT in epicardial cells, the induction of arteriogenesis and the reduction in cardiomyocyte apoptosis [277]. A pivotal study recently reported by Wei *et al.* demonstrated that epicardial follistatin-like 1 (Fstl1) marker is a potent molecule that can promote cardiogenic activity [278]. Application of collagen patches seeded with epicardial derived Fstl1 onto the mouse epicardium following MI injury stimulated cell cycle re-entry and division of pre-existing cardiomyocytes in the

border zone, and improved cardiac function and survival in murine and swine models of MI [278]. In a standard MI response, the epicardial cells lost Fstl1 expression and were replaced by the myocardial expression. Surprisingly only epicardially derived Fstl1 could provide the helpful responses observed, whereas myocardial Fstl1 failed to evoke CM cell division. Moreover, the effect of Fstl1 induced cellular division was transient and only specific to immature CMs.

A recent study using a cardiac cell patch loaded with MSCs transplanted onto the epicardium promoted repair and regeneration of the infarcted myocardium through various modalities including epicardial activation [279]. The MSCs seeded on the PCL/gelatin electrospun patch secreted high concentrations of paracrine factors such as, HIF-1α, Tβ4, VEGF and SDF-1, which not only enhanced the survival of the transplanted cells but also stimulated the activation of EPDCs which later migrated deep into the myocardium and differentiated into endothelial cells, smooth muscle cells and potentially a small number of cardiomyocytes [279]. This approach also led to an increased recruitment of c-kit$^+$ cardiac progenitors into the infarcted myocardium.

In conclusion, previous research has demonstrated the role of epicardium in regenerating the myocardium and paved the way for the discovery and use of novel compounds such as Fstl1, Tβ4 and RA and novel materials and strategies to more efficiently promote the epicardial activation and engagements in the various aspects of cardiac regeneration. Continued investigation into these avenues may provide the key to unveiling a cure for cardiac failure.

2.8. Aims

- Generate transposon-based polycistronic plasmid containing the cardiac reprogramming factors (MEF2C, GATA4 and TBX5)
- Develop a strategy to efficiently load and release transposon-based cardiac reprogramming cocktails
- Use nanoneedle-mediated delivery (nanoinjection) to target gene therapy to the epicardial cells
- Directly reprogram EPDCs into cardiomyocyte both *in vitro* and *in vivo*

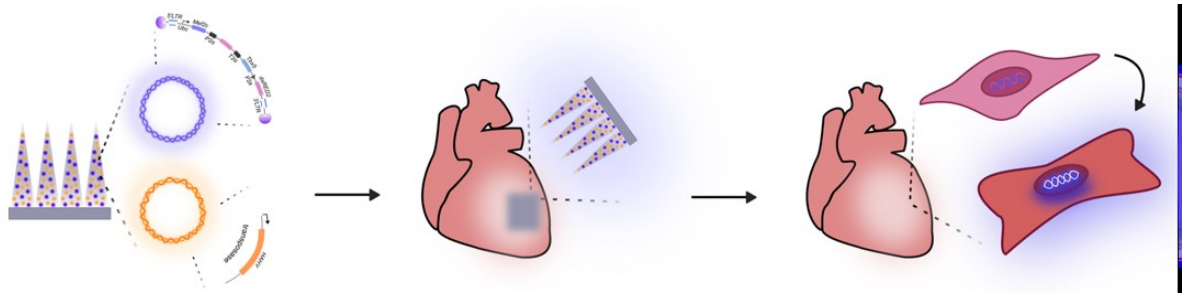


Figure 10. Overview of the nanoinjection strategy for direct cardiac reprogramming. The nanoneedle chip is loaded with a polycistronic integrative transposon plasmid coding for the cardiac reprogramming factors Mef2c, Gata4 and Tbx2 along with the transposase plasmid to enable integration. Nanoinjection of the cardiac reprogramming factors occurs by applying the loaded nanoneedle chip for 30 seconds onto the epicardium, in the area surrounding the infarct. The delivery of the reprogramming factors aims to initiate the transdifferentiation of cells residing in the epicardium into cardiomyocyte-like cells that contribute to tissue regeneration post myocardial infarction.

2.9. Hypotheses

- **First of all, the nanoneedles (nN) can be used to load and deliver pDNA efficiently.** Fluorescently labelled plasmid was used to evaluate the binding and release kinetics from the nanoneedles.
- **Secondly, the use of the polycistronic transposon vector can lead to the sustained expression of transgenes.** Long-term culture followed by sequential analysis with FACS and end-point gDNA insertion assays was performed to validate this point.
- **Furthermore, the integrative transposon plasmid containing the Mef2c, Gata4 and Tbx5 (MGT) can reprogram the epicardial cells into cardiomyocytes.** The expression of transgenes and several vital cardiac markers was used to validate this hypothesis.
- **Lastly, nanoinjection can transfect cells *in vitro* and accurately target and transfect cells on the epicardial layer of infarcted hearts.** The expression of transgenes evaluated through qRT-PCR and histology of cardiac tissue slices post-nanoinjection were analysed to provide a concrete conclusion.

2.10. Materials and Methods

2.10.1. Nanoneedle Fabrication

Nanoneedles were fabricated by Dr Ciro Chiappini according to the established protocol published in [9]. In brief, a 120 nm layer of silicon nitride was deposited over a 100 mm, 0.01-0.02 Ω-cm, p-type silicon wafers (University Wafer) by low-pressure chemical vapour deposition (Scottish Microelectronics Centre). Followed by a patterning step using a 250 nm thick negative photoresist (NR9-250P from Futurrex, USA) as a mask transfer layer, the substrate was patterned with 0.6 µm diameter dots with a 2 µm pitch over the entire surface. The pattern was later transferred into the silicon nitride layer by reactive ion etching in CF_4 plasma for 120 s. Ag nanoparticles were selectively deposited on the exposed silicon by electroless deposition from $AgNO_3$ salt (0.002 M) in an aqueous solution of 10% hydrofluoric acid (HF) for two minutes. Metal-assisted chemical etching of the substrate in 10% HF, 1% H_2O_2 aqueous solution (total 400ml) for 8.5 min was used to form the porous structures. Finally, the substrate was shaped into the final conical structure by reactive ion etching in SF_6 plasma for 2.5 min. The nanoneedle wafer was diced into 8 x 8 mm chips (Disco Dicing Saw) for further use and stored in air.

2.10.2. Nanoneedle Chip Surface Modifications

Before the adsorption of the pDNA/molecules onto the nanoneedle, the surface of the nanoneedle was chemically modified. The nanoneedles were subjected to 20 min of oxygen plasma treatment to increase the hydrophilicity of the surface (PlasmaPrep5, Gala Instrumente GmBH) at an oxygen pressure between 0.4 – 0.6 mbar. Then the nanoneedles were either further functionalised with 3-aminopropyltrietoxysilane (APTES) by immersion for 2 hours in 2% APTES in a solution of 100% ethanol (APTES-nN) or remained unmodified (OX-nN). Following this, both types of nanoneedles were treated with 2 M HCl solution for 10 min and rinsed in DI water and dried with N_2 gas. The nanoneedles were then exposed to direct UV light for 30 min to sterilise them before usage.

2.10.3. DNA Loading and Release Optimisation

pDNA was covalently linked to Rhodamine to allow visualisation and quantification of the loading and release capacity by fluorescent microscopy. The conjugation was performed following the instructions provided by the Label IT Nucleic Acid Labelling CX-Rhodamine Kit (Mirus Bio LLC) with a 1:1 conjugation ratio.

Functionalised nanoneedles were incubated with 10 µg Rho-pDNA using the dry or wet method for 30 min to allow the pDNA absorption to occur. In the dry method, the plasmid was diluted in molecular grade water and drop cast onto the nanoneedle and left to dry on the bench, whereas in the wet method, the nanoneedles were placed inside a humidified chamber. To further improve upon the adsorption and the distribution of the pDNA to OX-nN, the pDNA including the Rho-pDNA, the transposon plasmids and the transposases used in the study were diluted with either Buffer 1 (0.25 M Glycine and 400 mM KCl, adjusted to pH 5.0 with either HCl or KOH solution) or Buffer 2 (10 mM Acetic Acid, 1 mM $CaCl_2$ and 9 mM NaCl, adjusted to pH 5.0) and loaded onto the nanoneedles using the wet method. Next, the loaded nanoneedles were washed once in the respective pDNA loading buffer (lacking pDNA), followed by a final wash in RPE buffer (QIAGEN). The nanoneedles were dried in between washes with N_2 gas. To evaluate the loading efficiency, the Rho-pDNA loaded nNs were imaged at this point.

As for the pDNA-release experiments, the Rho-pDNA loaded nN chips were incubated in HEPES buffer for 30 sec, 5 min, 30 min or overnight. Following the incubation, the nN chips were dried under a N_2 stream and imaged with an Olympus IX 71 fluorescent microscope with a Texas Red filter cube while maintaining constant acquisition parameters throughout all the chips and at all times. For each chip at each time point, five images were acquired in random locations to ensure fair representation of both the central and the peripheral region of the chip. The remaining fluorescence on each chip at each time point and its standard deviation were calculated by averaging the mean fluorescence of each image. These values were then used to compare the relative loading and release profile for each loading condition.

2.10.4. Plasmids Used in The Study

A piggyBac expressing GFP plasmid (PB-GFP) was acquired from (SystemBioSciences), the pPB-UbC plasmid backbone and pCMV-HaHyPBase (HaHy transposase) were obtained from the Sanger Institute. The pPB-MGTdsRED (MGT) were designed in-house and constructed in three steps. First, the MEF2C was amplified from Dharmacon cDNA clone (MHS6278-202806738) to remove the stop codon, and BamHI inserted in the 3' end. The fragment was then ligated via the BamHI site to the P2A-GATA4-T2A fragment synthesised by Genscript. The MEF2C-P2A-GATA4-T2A construct was then ligated to the ClaI restriction site located on the 3' of the fragment to the TBX5 fragment. The TBX5 fragment was previously amplified from Dharmacon cDNA clone (MHS6278-202801327) and had the stop codon removed and ClaI restriction site added to the 5' end. The final step was to ligate the MEF2C-P2A-GATA4-T2A-TBX5 construct to the P2A-dsRED sequence synthesised by Genscript via the 5' XbaI and 3' ClaI restriction sequences.

2.10.5. Animal Surgical Procedures

These procedures were performed by Camille A. Marijon.

All animal procedures were carried out in accordance with the UK Home Office Animals (Scientific Procedures) Act 1986 and Directive 2010/63/EU of the European Parliament on the protection of animals used for scientific purposes. The rats used in the study were purchased from Charles River Laboratories and were allowed to acclimatise to the new surrounding before any procedures were performed. The rats were anasthesised with 5% (v/v) isoflurane (Zoetis, UK) and confirmed by the loss of standing and pedal reflexes. The coats covering the left part of the thorax were shaved using clippers (Harvard Apparatus, UK) and the eyes were hydrated with Lacri-lube (Allergan, UK). For analgesia, prevention of infection and fluid therapy, a combination of Buprenorphine (0.05 mg/kg, Vetergesic®, Ceva, UK), Carprofen (5 mg/kg, Rimadyl®, Zoetis, UK) and Enrofloxacin (5 mg/kg, Baytril®, Bayer, UK) diluted in saline was injected subcutaneously. The rats were intubated with an appropriate cannula (Williams Medical Supplies, UK) and mechanically ventilated (Harvard Apparatus, UK). The ventilation parameters were adjusted based on the animal weight and chest movement. Body temperature was maintained during the whole procedure using an adjustable heating mat. The surgical site was then scrubbed using a diluted iodine solution, and the level of isoflurane

was then reduced and maintained at 2% (v/v) during the whole procedure. The heart was exposed by a horizontal incision of the skin followed by the dissociation of the thorax and intercostal muscles to allow access to the base of the left ventricle. The pericardium was dissociated, and MI was induced by ligation of the left anterior descending coronary artery (LAD), ligated 1-2 mm distal to the inferior border of the left atrium using a 6/0 Prolene suture. Effective ligation was confirmed by blanching and cyanosis of the left ventricular free wall and apex. At this stage, the nanoneedles were applied for 30 sec onto the epicardium layer on top of the infarct zone. Following the treatment, the anaesthesia was turned down to 1% (v/v) isoflurane, and the skin was closed with the same suture. At the end of the surgery, the anaesthetic gas was turned off, and the animal was extubated and placed in a heat chamber until full recovery. Animals were checked regularly for signs of pain/distress and analgesia was maintained for two days using Carprofen (5 mg/kg, Rimadyl®, Zoetis, UK). At the designated time point for the experiment, the animals were sacrificed, and the heart was collected for RNA isolation and histological sampling.

2.10.6. Isolation of Rat EPDCs

MI induction surgeries as described above were performed four days before cells isolation to allow the activation and proliferation of the epicardium. On the day of the collection, post-MI hearts were isolated and repeatedly rinsed in 1X Hank's Balanced Salt Solution (Gibco, Thermo Fischer Scientific) supplemented with 1% (v/v) Pen-Strep (Gibco, Thermo Fisher Scientific) in order to wash off the blood and any dead cells on the surface or circulating. Isolation of epicardium-derived cells was adapted from protocol published by Zhou *et al.* [280]. The epicardial layer was peeled off from the surface of the heart and was subjected to enzymatic digestion in an aqueous solution composed of 0.08% (w/v) Collagenase IV, 0.05% (v/v) Trypsin and 1% (v/v) FBS in 1x HBSS solution. The digestion was conducted at 37 °C for 6 min with rotation, and this process was repeated 7 times. In between digestion, the supernatant containing dissociated cells was collected and placed on ice, and the digestion was stopped by the addition of fresh Heat Inactivated Fetal Bovine Serum. The final digestion solutions were filtered through a 70 µm cell SmartStrainer (MACS Miltenyl Biotech) and then pelleted at 500 rcf for 10 min. The cell pellet was re-suspended in 1 ml of MSC20 medium (Mesenchymal Stem Cell Growth Medium 2, PromoCell, supplemented by 10% (v/v) FBS and 1% (v/v) Pen-Strep). 1X RBC lysis buffer (155 mM NH_4CL, 12 mM $NaHCO_3$, 0.1 mM EDTA) was

added to the cell suspension, and the mixture was incubated at 4 °C for 10 min to remove the red blood cells. Final centrifugation was performed at 500 rcf for 5 min, and the cell pellet was re-suspended in MSC20 medium and plated onto a previously coated 2% (w/v) Gelatin type B coated tissue culture plastic. EPDC culture was maintained in MSC20 medium in a 5% CO_2 incubator at 37 °C and was passaged every 3-5 days.

2.10.7. *In Vitro* Nanoinjection of pDNA

OX-nN chips prepared as mentioned above were treated with 2 M HCl solution for ten minutesand rinsed in DI nuclease free water and dried with N_2 gas. The nanoneedles were then exposed to direct UV light for 30 min for sterilisation before the pDNA deposition.

The desired pDNA diluted in B1 was added onto the nanoneedles and incubated inside a humidified chamber for 30 min to allow the adsorption of the pDNA to the surface of the nanoneedles. Following the incubation, the chips were washed once in B1 (without plasmid) and RPE buffer with a drying step in between washes with N_2 gas.

1 x 10^5 cells were then seeded over the loaded nanoneedle chips and cultured for between 2 – 24 hours at 37°C in a cell culture incubator to allow the transfection to occur. The next day, the cells were trypsinised off the chips and were either analysed or plated on tissue culture plastic (TCP) for further maintenance or manipulation.

2.10.8. *In Vitro* Assay for Rho-pDNA Delivery with Nanoneedles

10 µg of Rho-pDNA was added onto the nanoneedles using the dry method or first diluting in either buffer 1 or buffer 2 and incubated in the humidified chamber for 30 min and washed as described above. 1 x 10^5 HEK 293T cells were seeded over the loaded nanoneedle chips and cultured for two hours or overnight at 37 °C. At the desired time-point, the cells were trypsinised, pelleted, washed once and re-suspended in PBS for further analysis with flow cytometry. A BD Fortessa equipped with 561 nm excitation laser and 610/20 collection filter was used to record the percentage of Rho^+ cells.

2.10.9. Transposon Stable Integration Assay

HEK293T cells were transfected with either PB-GFP (7.2 µg) + HaHy (2.8 µg) or PB-GFP (10 µg) only with the nanoneedles. 24 h post-transfection, the cells were lifted off the nanoneedles using 0.05% (w/v) Trypsin-EDTA 1X (Gibco, Thermo Fischer Scientific) for 7 min at 37 °C. Cells

from each chip were plated into a single well of a 24-well plate and were cultured for the next five days. At day 6, the cells were sorted (BD FACSAria III), and the GFP positive cells were collected and cultured for an additional 15 days. At day 21, images of the cells were acquired on a Widefield Zeiss Cell Observer Live Cell Imaging System. Also, a fraction of the cells was collected for analysis via flow cytometry (BD Fortessa) to determine the level of GFP positive cells in the different conditions. Final sorting was performed 30 days post-transfection, and the GFP positive fraction was collected and cultured for another ten days before gDNA isolation. The cells were trypsinised, and 5 x 10^6 cells were pelleted by centrifuging for 5 min at 300 rcf at 4°C and washed once in ice-cold PBS and re-pelleted. The gDNA was isolated with the DNeasy Blood & Tissue Kit (QIAGEN) with the following modification: before the digestion and dissociation of the cells, the samples were resuspended in 200 µl of PBS and treated with 400 µg of RNase A for 2 min at RT. The PiggyBac copy number kit (SystemBioscience) was used to check for successful integration via PCR. The end reaction from the PCR was then run on the 2% E-Gel General Purpose Agarose gel (Thermo Fisher Scientific) with the pre-designed settings along with a 100 bp DNA Ladder (Promega) and imaged on the E-Gel Imager (Thermo Fisher Scientific).

2.10.10. *In Vitro* Direct Cardiac Reprogramming of Rat EPDCs

Approximately 1 x 10^5 of rat EPDCs were plated on nanoneedles loaded with 7.2 µg PB-MGT and 2.8 µg HaHy and were cultured in MSC20 media for 24 h to allow the nanoneedle mediated transfection to occur. The next day, the cells were trypsinised from the nanoneedles chip with 0.5% (v/v) Trypsin-EDTA for 7 min and plated on a 2% (w/v) gelatin-coated well of a 24-well plate. The MSC20 medium was then replaced by Cardiac Reprogramming Medium (Table 3) to initiate the reprogramming. The cardiac reprogramming medium used in this study has been previously used and described by Zhao *et al.* [219]. The medium was changed every 2-3 days until the cells were examined. As a control experiment, rat EPDC was also transfected with the PB-MGT and HaHy plasmids via FuGENE. RNA samples were collected at day 4 and day 18 post-transfection for analysis.

Table 3. Composition of Cardiac Reprogramming Medium.

Cardiac Reprogramming Medium	
DMEM/M199 (4:1)	4:1 ratio
FBS	10% (v/v)
Horse Serum	5% (v/v)
Antibiotics	1X
Non-Essential Amino Acids	1X
Essential Amino Acids	1X
B-27	1X
Insulin-Selenium-Transferin	1X
MEM Vitamin Solution	1X
Sodium Pyruvate	1X

2.10.11. *In Vivo* Nanoinjection and Reprogramming

Control nNs (Blank), nNs loaded with Rho-pDNA (10 µg) or nNs loaded with the PB-MGT (14 µg) and HaHy (6 µg) were prepared following the same procedure as for*in vitro* nanoinjection. The nN chips were then applied to the epicardium for 30 sec. At the designated time point for the experiment, the animals were sacrificed, and the heart was collected for RNA isolation and histological sampling.

2.10.12. RNA Expression Analysis

2.10.12.1. RNA Isolation from Tissue Explants and Cell Lines

RNA was isolated with TRIzol Reagent (Thermo Fischer Scientific, 15596026) in combination with the Direct-zol Miniprep isolation kit (Zymo Research, R2052).

The following modifications were made to the Direct-zol Miniprep isolation procedures: the cell pellets were dissolved, and the tissue fragments were homogenised with a tissue homogeniser in 1 ml TRIzol. The supernatant was immediately snap-frozen on dry ice, and before isolation, the samples were thawed on ice. Following that, 0.2 ml chloroform/isoamyl alcohol 24:1 (Across Organic, ACRO327155000) was added and shook vigorously for a few secondsthen incubated for 10 min at room temperature (RT). The samples were centrifuged at 12,000 rcf for 15 min at 4°C, and the aqueous phase containing the RNA was carefully

removed and transferred to a new DNA lo-bind tube (Eppendorf). An equal volume of absolute ethanol (Across Organic, 10517694) was added to the collected aqueous solution and mixed to form a homogeneous solution. The solution was then applied to the column, and the remaining step of the isolation process was as described in the isolation procedures provided with the kit. The eluted RNA was stored at -80 °C.

2.10.12.2. cDNA Synthesis and Quantitative qRT-PCR

RNA samples were gently thawed on ice, and the concentration was quantified with a NanoDrop 2000/2000c UV-Vis spectrophotometer (Thermo Fischer Scientific). RNA was reverse transcribed into a single-stranded cDNA with the QuantiTect Reverse Transcription Kit (Qiagen, 205313).

Quantitative RT-PCR was carried out with TaqMan chemistry. Single Taqman Gene Expression Assays (Applied Biosystems) was carried out in 384-well plates in a reaction volume of 10 µl as listed in Table 4. A list of TaqMan probes used in this study can be found in Table 6.

Table 4. TaqMan qRT-PCR reaction mix.

TaqMan based qRT-PCR reaction	
2X TaqMan Fast Advanced Master Mix	5 µl
TaqMan Gene Expression Probe	0.5 µl
cDNA (10 ng for cell line, 100ng for tissue)	X µl
Nuclease-free water	10-x µl
Total per reaction	**10 µl**

All quantitative qRT-PCR reactions were performed on the QuantStudio 6 Flex Real-Time PCR System (Thermo Fischer Scientific) according to the thermal cycling profile in Table 5.

Table 5. Taqman qRT-PCR thermal cycling profiling.

TaqMan based reaction	Step 1	Step 2	Step 3	Step 4
Cycles	1 x	1 x	40 x	40 x
Temperature (°C)	50	95	95	60
Time	2 min	2 min	1 sec	20 sec

Table 6. TaqMan probes used in this study.

TaqMan	**Catalogue Number**	**TaqMan**	**Catalogue Number**
Human *Gapdh*	Hs02758991_g1	**Rat *Gapdh***	Rn01775763_g1
Human *Mef2c*	Hs00231149_m1	**Rat *Hand2***	Rn00575515_m1
Human *Gata4*	Hs00171403_m1	**Rat *Nkx2.5***	Rn00562059_m1
Human *Tbx5*	Hs00361155_m1	**Rat *Nppa***	Rn00664637_g1
		Rat *Actnt2*	Rn01470228_m1
		Rat *Tnnt2*	Rn00562059_m1

2.10.13. Protein Expression Analysis

2.10.13.1. Protein Isolation

The total protein lysates were isolated using RIPA buffer (Santa Cruz, sc-24948) supplemented with 1x Phosphatase Inhibitors (Roche Applied Biosystems, 04906845001) and 1X Protease Inhibitor Cocktail (Roche Applied Biosystems, 04693159001). The protein lysates were homogenised for 20 sec on ice and centrifuged at 12,000 rcf for 10 min. The supernatant was then transferred to a protein lo-bind tube. The protein concentration was determined by the DC Protein Assay Kits (Bio-Rad, 500-0112).

2.10.13.2. Western Blot

Protein samples were denatured for 10 min at 95°C in 4x Sample Buffer (Bio-Rad, 1610747) supplemented with 0.1 M β-mercaptoethanol. The proteins were separated by denaturing sodium dodecyl sulfate-polyacrylamide gel electrophoresis (SDS-PAGE) in 4-20% Mini-PROTEAN TGX Precast Protein Gels (Bio-Rad, 4561094) for up to 1 h. The proteins were transferred to a low fluorescence PVDF membrane (Bio-Rad,1704274) with the Trans-Blot Turbo following the protocol recommended by the kit. The membrane containing proteins was blocked for two hours in Blocking Solution that contained either 5% (v/v) semi-skimmed milk or 5% (v/v) BSA in 0.1% (v/v) TBS-Tween-20 (Sigma, P5927) at RT. Following this step, the respective primary antibody diluted in blocking solution was added to the membrane and was left to incubate overnight at 4°C with gentle agitation. Post incubation with the primary antibody, the membrane was washed five times in 0.1% (v/v) TBS-Tween-20 solution for 5 min each and incubated with the appropriate infrared labelled secondary antibody (LiCor) diluted in the blocking solution for one hour at RT. The membrane was once again washed following the same step as before and scanned and analysed with the Odyssey imaging system and software (LiCor). The list of antibodies used in the study is listed in Table 8.

2.10.13.3. Immunostaining of Cultured Cells

Cells grown on TCP were initially washed with PBS and fixed with freshly prepared 4% (v/v) paraformaldehyde in PBS (pH 7.4) for 10 min at RT. Then, cells were washed three times with PBS for 5 min each and permeabilised with 0.4% (v/v) Triton X-100 (Sigma, X100) for 10 min at RT on a rotating platform. The samples were then blocked for 2 hours in the IF blocking solution (see Table 7) at RT with gentle agitation. Primary antibody diluted in IF blocking solution as shown in Table 8 was added to the samples and left to incubate overnight at 4 ^{o}C. The samples were washed five times with 0.1% (v/v) PBS-Tween-20 for 5 min each before the addition of species-specific secondary antibody conjugated with Alexa fluorophores (Table 9). After one hourr of incubation and wash, the samples were counter-stained with 4 µg/ml 4'6-diamidino-2-phenylindole (DAPI; Sigma, D9542) in PBS for 5 min at RT. Thesolution containing DAPI was removed and replaced with VECTASHIELD Antifade Mounting Medium (Vector Laboratories, H-1000) to prevent the bleaching of the fluorophores. Samples were covered

with aluminium foil and stored at 4°C. Images were acquired using an Inverted Widefield Axio Observer (Zeiss) and an Elyra PS1 (Zeiss) microscope.

Table 7. Immunofluorescence blocking solution recipe.

Immunofluorescence Blocking Solution	
5% (v/v) BSA	Invitrogen (B14)
0.1% (v/v) Tween-20	Sigma Aldrich (P1379)
0.3M Glycine	Sigma Aldrich (50046)
PBS	Thermo Fisher Scientific (10010023)

2.10.13.4. Immunostaining of Histology Slices

The collected tissues were embedded in Tissue Freezing Medium (Leica Biosystems) and flash frozen in pre-chilled 2-Methylbutane solution (Sigma, M32631). The frozen samples were cryosectioned with the Cryostar NX70 Cryostat (Thermo Fisher Scientific) with the following settings, -18°C specimen temperature, -25°C for the temperature of the blade. After initial trimming, 10 µm slices were collected onto superfrost plus microscope slides (Thermo Fisher Scientific). Slides containing the tissue slices were first washed once in PBS for 5 min and stained following the protocol listed for the immunostaining of cultured cells.

2.10.13.5. Statistical Analysis

Statistical analyses were performed with GraphPad Prism software (version 5). All results are displayed as the mean ± standard deviation (SD). One-Way ANOVA analysis followed by Tukey and Bonferroni post-hoc test was used unless stated otherwise.

As for the results of the in vivo nanoinjection and reprogramming; based on the qRT-PCR data, MGT+HaHy nanoinjected rats were separated to responders (n=6) and non-responder (n=3) according to where their genes expression value (Gata4 and Tbx5) fell in comparison to control animals. Responders were those animals in the current study whose level of expression above 1 standard deviation (SD) of the mean expression value of the TBX5 gene of the control group (i.e., above Tbx5 Mean of = 1 + 0.4904 SD). Analyses between control,

responder and non-responder groups were done using multiple student t-test, corrected for multiple comparison using the Holm-Sidak method.

Table 8. Primary antibodies used for immunofluorescence (IF) and western blot (WB).

Antigen Target	Species Raised	Isotype	Application used (conc in µg/ml)	Company	Product Code
Cardiac Transcription factors and co-factors					
Mef2c	Rabbit	IgG	WB (1)	Abcam	ab64644
Gata4	Rabbit	IgG	WB (1)	Abcam	ab84593
Tbx5	Goat	IgG	WB (1)	Santa Cruz	sc-17866
Wt-1	Rabbit	IgG	IF (10)	Abcam	ab89901
Whole Cell Loading Control					
GAPDH	Rabbit	IgG	WB (1)	Santa Cruz	sc-25778

Table 9. List of Secondary antibodies for the detection of primary antibodies in IF and WB.

Antigen Target	Species Raised	Isotype	Application used (conc in µg/ml)	Company	Product Code
Anti-rabbit-IRDye 800CW	Goat	IgG	WB (0.1)	LI-COR	P/N 925-32211
Anti-rabbit-IRDye 680RD	Goat	IgG	WB (0.1)	LI-COR	P/N 925-68071
Anti-goat-IRDye 800CW	Donkey	IgG	WB (0.1)	LI-COR	P/N 925-32214
Anti-goat-IRDye 680CW	Donkey	IgG	WB (0.1)	LI-COR	P/N 925-68074
Anti-mouse-IRDye 800CW	Goat	IgG	WB (0.1)	LI-COR	P/N 925-32210

Anti-mouse-IRDye 680CW	Goat	IgG	WB (0.1)	LI-COR	P/N 925-68070
Anti-mouse IgG, Alexa 488	Goat	IgG	IF (1)	Thermo Fischer	A-11001
Anti-rabbit IgG Alexa 488	Goat	IgG	IF (1)	Thermo Fischer	A-11008

2.11. Results

The concept of this study and results presented in the following chapter were acquired by the author of this thesis, unless stated otherwise.

2.11.1. Optimisation of pDNA Transfection with The Nanoneedle

High aspect ratio nanostructures are increasingly used as a tool to deliver cargoes intracellularly both *in vitro* and *in vivo* owing to their ability to deliver in a safe, efficient and high-throughput manner [52, 97]. The nanoneedle array used in this study has been previously demonstrated [9] to be able to deliver pDNA *in vivo* in a highly localised manner and without inducing any adverse immune reaction. The success of direct cardiac reprogramming is dictated in part by the expression level of the reprogramming factor. A higher level of transgene overexpression correlates positively with the outcome of the procedure [190, 207, 211]. In order to maximise the efficiency of nN mediated delivery, two criteria needed to be met and optimised. First, the loading of pDNA onto the nN has to be fully maximised, and second, the majority of the pDNA needs to be released within seconds of interfacing.

Initially the same protocol of previous study was used [9]. The nN were treated with either oxygen plasma (OX-nN) alone or further modified by the addition of 3-aminopropyltriethoxysilane (AP-nN). This treatment resulted in a difference in surface charge. The oxygen plasma treatment created a slight negative surface while the APTES modification led to a positively charged surface.

A solution containing the rhodamine labelled pDNA was directly applied on the surface and left to dry (dry method), and the fluorescence was measured to determine the relative concentration of pDNA present on the nanoneedles following loading. The AP-Dry were approximately three-fold more effective at adsorbing the pDNA in comparison to the OX-Dry (Fig. 11a,b). However, the dry-method displayed a highly heterogeneous deposition of the pDNA, with preferential accumulation at the edge of the nN chip. To improve the distribution of the loaded pDNA on the nNs, a highly-concentrated solution containing the pDNA was used, and the loaded nNs were incubated inside a humidified chamber (wet method). Using this method, the AP-H_20 was capable of a higher level of adsorption, while the OX-H_2O yielded lower levels of pDNA adsorption in comparison to the dry counterparts (Fig. 11a,b).

These results highlight the difference in the mechanism behind the dry and wet adsorption method. Although dry adsorption can load large amounts of pDNA regardless of the electrostatic interaction between the nN and the pDNA, however, the drying process leads to a highly heterogeneous distribution of pDNA across the chip. The wet method, on the other hand, relies solely on the electrostatic interaction between the pDNA and the substrate. In this instance, the strong attractive interaction between the positively-charged AP-nN and the negatively charged pDNA would enable high efficient loading, but the same interaction would ultimately prevent the rapid and efficient release of the cargo. On the contrary, in a repulsive interaction like that of the OX-nN and pDNA, loading becomes highly inefficient. To achieve nanoneedle mediated delivery, the total release capacity of the various chemically modified nNs and the buffer used for loading over time were analysed. Firstly, the release capacity and the kinetics of the pDNA from the surface of the nanoneedle was determined.

In both AP-Dry and AP-H_2O, despite being able to bind a high quantity of pDNA, showed slow release kinetics (Fig. 11c). Most of the loaded pDNA was still firmly bound to the surface of the nN chip even after overnight incubation in physiological buffer. This is due to the strong electrostatic interaction between the positively charged surface and the negatively charged pDNA (Fig. 11a,c). In OX-Dry and OX-H_2O condition, the loaded pDNA was released within the first 30 seconds of incubation (Fig. 11a,c).

To further improve upon the loading efficiency while still able to rapidly release the cargo, established methods used in the column-based nucleic acids isolation procedures were adopted to modulate the electrostatic interaction between the nN and the pDNA [281]. Two high ionic strength buffers with pH 5.0 were generated to match the isoelectric point of DNA: Buffer 1 (B1) containing 0.25 M glycine salt and 400 mM KCl and Buffer 2 (B2) containing 10 mM acetic acid, 1 mM $CaCl_2$ and 9 mM NaCl as loading buffer. To test this hypothesis, the labelled pDNA was loaded on OX-nN in either B1 or B2 and then simulated the release in physiological conditions of low ionic strength and pH 7.4 solution (HEPES). The use of B1 as loading buffer for pDNA deposition on OX-nN significantly improved the loading capacity comparable to that of AP-nN (Fig. 11b). The use of B2, however, did not result in any significant improvement in the loading capacity when compared to OX-Dry and OX-H_2O (Fig. 11b). Also, the loading of pDNA with B1 and B2 on the nanoneedle resulted in anhomogenous distribution throughout the chip (Fig. 11c).

The loaded nN chips were then immersed in HEPES buffer for a duration ranging from 30 sec to overnight (18 h) to investigate the release kinetics. OX-B1 showed a rapid burst release with approximately 40-50% of the total release occurring within 30 sec followed by gradual, continual release over time. OX-B2 showed similar release kinetic as OX-B1 but with only half of the loading capacity (Fig. 11c).

Next, a series of nanoinjection experiments in a human cell model was conducted to investigate the correlation between the loading and release results observed in Figure 11a-c with transfection efficiency. The HEK 293T cells were seeded on OX-Dry, OX-B1 or OX-B2 nN loaded with rhodamine labelled pDNA and cultured the cells for 2 hours or overnight. Following 2 hours incubation with the nN, FACS analysis revealed that OX-B1 were the most efficient at delivering pDNA into the cells with approximately 40 fold improvement over OX-Dry (Fig. 11d).

Despite lower loading capacity, the use of OX-B2 still leads to improvement in cellular transfection compared to OX-Dry owing to the rapid release kinetics (Fig. 11d). This observation confirms that maximal loading and, more importantly, the rapid release of pDNA from the nNs contributed positively to cellular transfection. However, prolonged overnight incubation showed that extended interaction between the nNs and the cells lead to 100% transfection efficiency regardless of the buffers used (Fig. 11d). This observation could be due to several reasons such as the degradation of the dye from the pDNA which allows rapid diffusion to occur, and the activation of endocytotic pathways which lead to active phagocytosis of the cargo directly from the nN surface. In the context of epicardium gene transfer, the nNs would need to be applied to the epicardial layer during an open or keyhole surgery, and thus the duration of the interfacing must be kept as short as possible to ensure safety. With this in mind, the high loading, rapid release and higher transfection efficiency achieved by using the B1 strongly supported the selection of this buffer for the study.

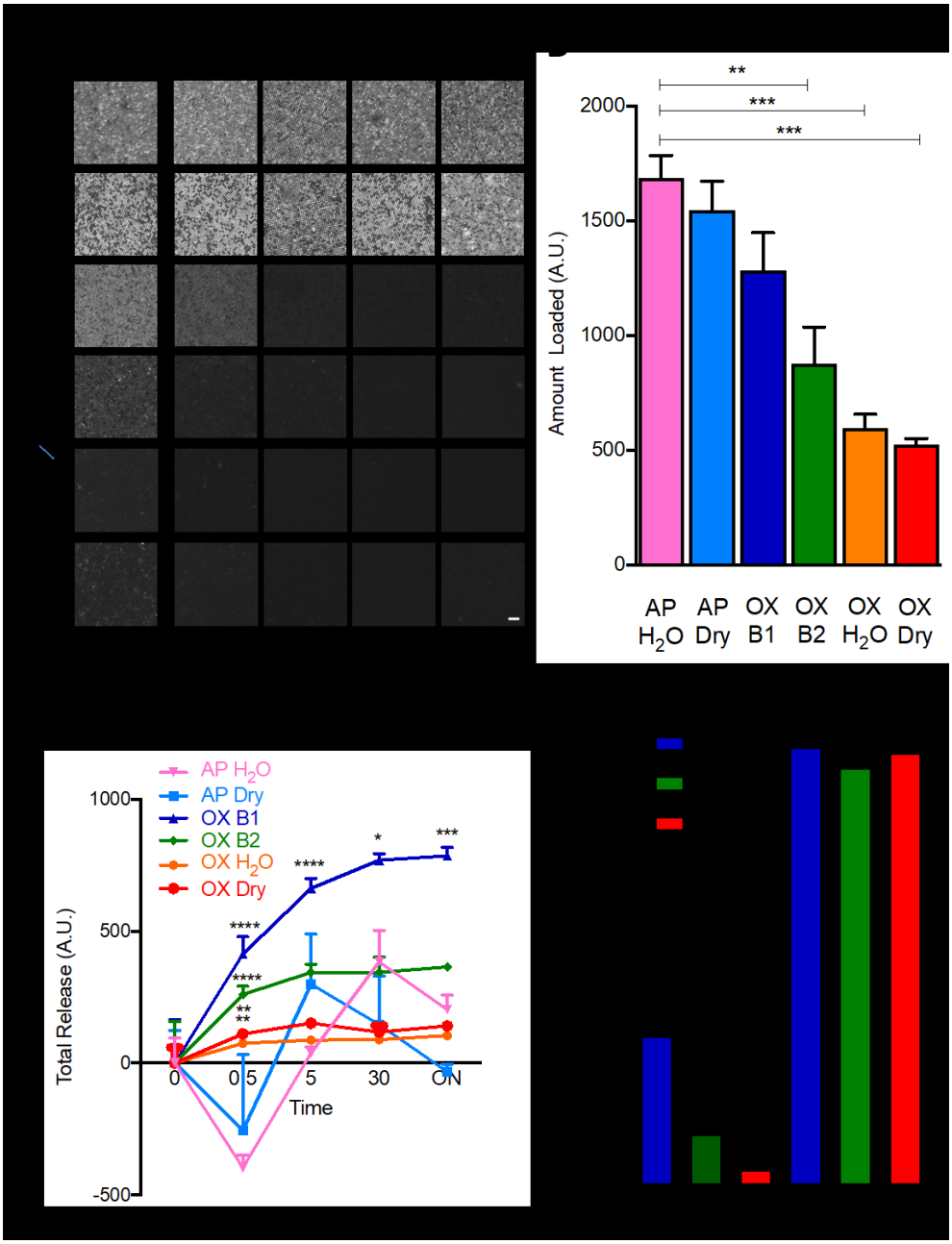


Figure 11. Optimizing the efficiency of nanoinjection. (A-C) Fluorescence microscopy images (A) and analysis (B-C) showing the relative concentration of pDNA present on nanoneedles following loading (A-B) and the release in HEPES buffer (A, C). The data is reported as a function of the nanoneedle surface chemistry (AP=APTES, OX=Oxidised) and the buffer used for loading (H_2O= water incubation, B1 =Buffer 1, B2 = Buffer 2, Dry = water drying). (D) Flow cytometry analysis of the uptake of rhodamine labelled pDNA by HEK 293T at 2 hours and 18 hours as a function of the loading condition. Data shown as mean ± s.e.m., n = 3. Differences tested by one-way (B, D) or 2-way (C) ANOVA with Bonferroni's multiple comparisons test, *p<0.05, **p<0.01, ***p<0.001, ****p<0.0001 among shown pairs (B,D) or vs. AP H_2O (C). Scale bar 10µm.

2.11.2. Transposon Reprogramming Systems

In order to induce direct cardiac reprogramming in epicardial-derived cells, integrative transposon systems containing the classical cardiac reprogramming genes MEF2C, GATA4 and TBX5 (MGT) in a single polycistronic vector was employed. The polycistronic vector was first constructed and then validated in an *in vitro* cell culture model system at both RNA and protein level. Lastly, the integrative properties of the transposon systems was validated.

2.11.2.1. Construction and Validation of the Transposon System

Transposons are naturally occurring integrative elements present in the genome and are evolutionary conserves throughoutspecies [282]. Years of research into transposon systems have led to the development of various transposon-based plasmid systems such as the Sleeping Beauty and piggyBac.

Transposon plasmids such as Sleeping Beauty and piggyBac along with the transposase-expressing plasmid have been successfully used for *in vivo* gene therapy by direct injection to target tissues [283-285]. Despite the rise of more recent gene editing systems, such as CRISPR/CAS9, the transposon systems still possess unique traits that make them better suited for epicardial reprogramming. The piggyBac transposon system used in this study can carry and insert large-cargoes over 200 kb [286], enabling the efficient integration of our 10,540 bp polycistronic construct containing the MGT reprogramming factors.

Furthermore, the piggyBac transposase integrates the transposon specifically at 'TTAA' sites which are present in 1 in every 256 bp of DNA sequences throughout the genome. This ability allows the insertion of multiple copies of transposons in the genome to achieve the high level of gene expression required for efficient cardiac reprogramming. Lastly, the transposase also enables a complete seamless removal of the transposons from the genome, leaving no residual sequences or mutations behind [286]. The reprogramming factors and a fluorescent reporter, dsRED2, were incorporated into a single polycistronic transposon-based vector (Fig. 12). As previous studies have demonstrated, the used of single polycistronic plasmid significantly increases cardiac reprogramming efficiency in comparison to the use of multiple plasmids [207, 211]. To generate the polycistronic transcript, the 2A-peptide sequences were inserted in between the genes to enable the genes to be transcribed as a single mRNA. Upon translation, the 2A peptide sequence causes a ribosomal skip resulting in the expression of all

four independent gene products. Furthermore, the reprogramming factors sequences used were of *homo sapiens* origin, and were arranged in the order reported by Wang *et al*. [35], Mef2c-Gata4-Tbx5, to achieve the optimal expression ratio amongst the factors and thus increasing the odds of reprogramming. Finally, piggyBac transposon-specific inverted terminal repeat sequences (ITR) were placed on the 3' and 5' end of the constructs to enable the cut-and-paste function of the transposase.

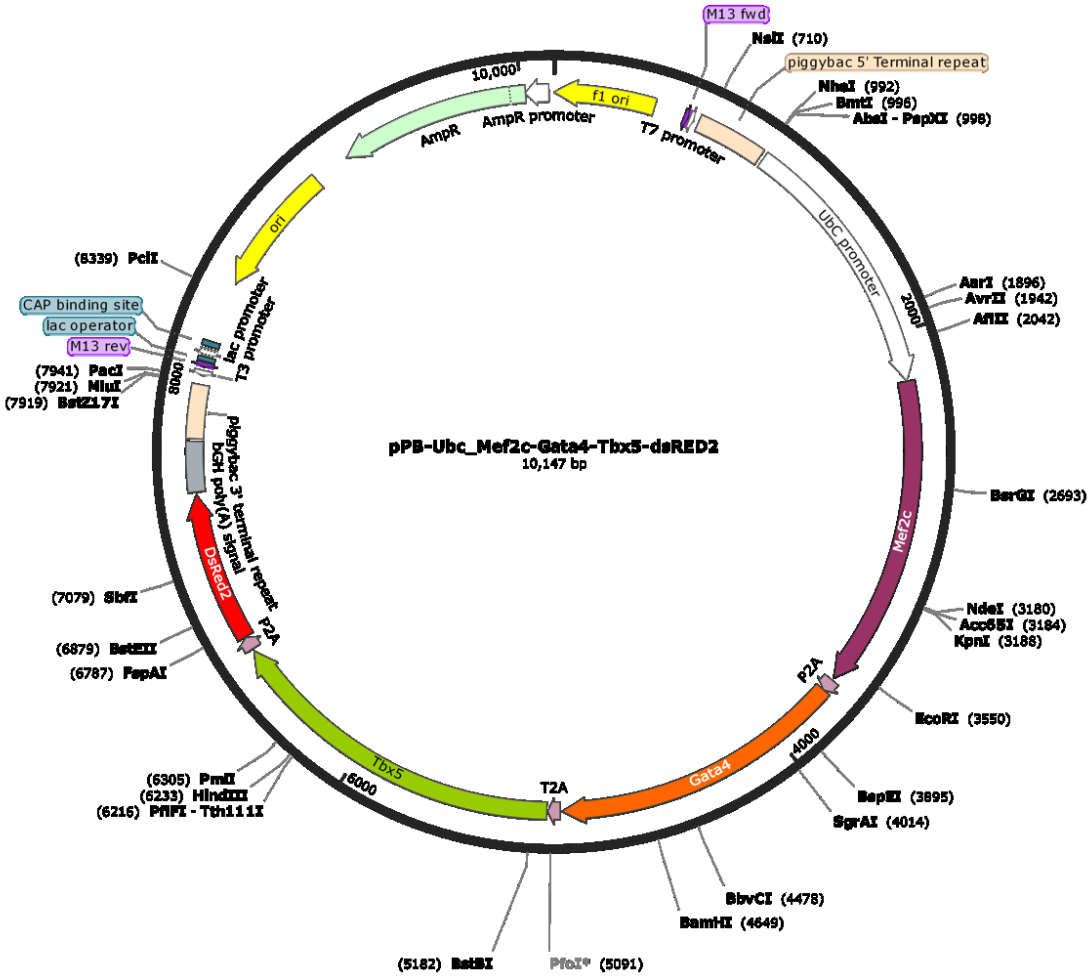


Figure 12. Map of the piggyBac transposon-based polycistronic vector encoding the Mef2c-Gata4-Tbx5-dsRED2 reprogramming factors under the control of the constitutively active UbC promoter. The 2A peptide sequences, P2A and T2A, were inserted in between the genes to enable the genes to be transcribed as a single transcript.

Next, HEK 293T cells were transfected with the PB-MGT with FuGene to investigate the level of transgenes expression. A plasmid encoding the dsRED2 in the same backbone was used as a control. *In vitro* gene transfer showed a high level of expression of the cardiac transcription factors, Mef2c, Gata4 and Tbx5, at both gene (Fig. 13a) and protein level (Fig. 13b). A robust dsRED2 signal emitted by the transfected cells upon exposure to the 561 nm laser in a live setting was also observed (Fig. 13c).

Although a similar design strategy to the one used by Wang *et al*. [35] was adopted in this study, the construct showed the opposite trend in expression profiles. Our design resulted in high expression of Tbx5, followed by Gata4 and Mef2c, while the construct produced by Wang *et al.* resulted in high Mef2c and low Tbx5 expression. According to the results observed by Wang *et al*. high level of Tbx5 and low level of Mef2c still lead to a slight increase in percentage of cTnT and α-MHC positive cells when compared to GMT but not as effective as a construct with a high level of Mef2c expression.

Next, the nanoneedle chip was loaded with the PB-MGT and used it to transfect HEK 293T as a proof-of-principle to demonstrate the potential of nNs for transposon-mediated gene therapy. Gene expression analysis confirmed the overexpression of the transgene 24 h post-transfection (Fig. 13d). However, nanoinjection led to a much lower level of overexpression compared to FuGene mediated transfection due to the lower rate of transfection achieved by nanoinjection (Fig. 13a,d). Despite the difference in the level of overexpression, the two methods shared similar expression trends, *i.e.* high Tbx5 and low Mef2c.

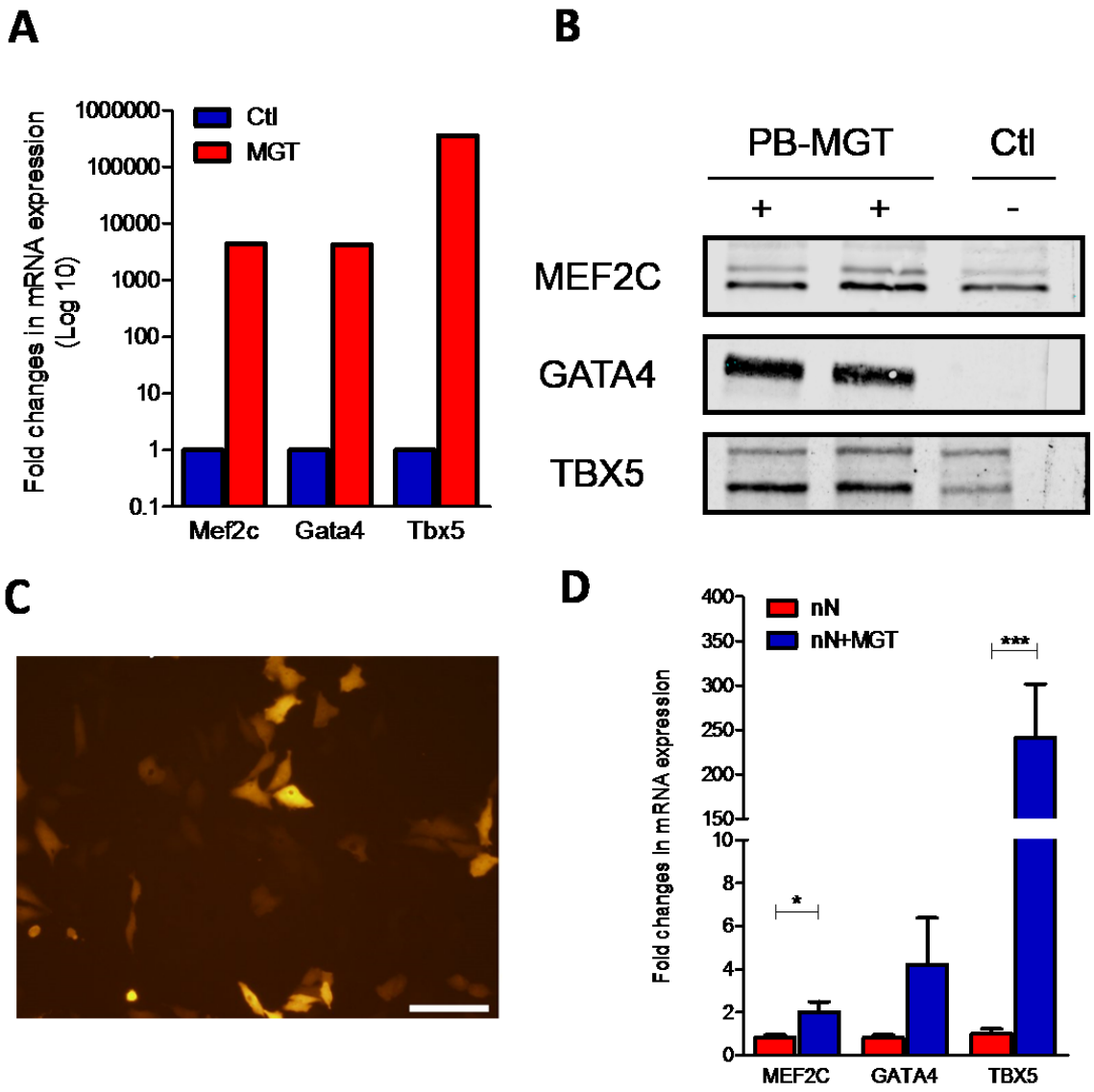


Figure 13. Overexpression of the MGT transgenes in RNA and protein levels. (A) qRT-PCR of transgenes expression 48 h post transfection with pPB-Ubc-dsRED (Ctl) or PB-MGT with FuGene in HEK 293T, showing robust overexpression of the reprogramming genes. N= 1. (B) Western blot showing the protein level expression of MEF2C, GATA4 and TBX5 48 h post transfection with Ctl or PB-MGT in HEK 293T cells. (C) A representative fluorescence image of live HEK293T cells expressing the dsRED2 (Scale bar = 100 µm). (D) qRT-PCR of the transgenes 24 h post nanoinjection of MGT+HaHy in HEK 293T, showing the upregulation of the MGT genes confirming successful nanoinjection mediated transposon expression. N = 3, n = 9. * $p \leq 0.05$, ** $p \leq 0.001$.

As mentioned previously, the piggyBac comprises two separate components, a transposon and a transposase. The transposase is responsible for facilitating the integration of the transposon into the genome. The functionality of the transposase used in this study (HaHy) to recognise the ITR sequences on the plasmids and their ability to integrate the construct into the cellular genome was validated. To confirm this, a piggyBac plasmid encoding green fluorescent protein (GFP) (PB-GFP) alone or in combination with a plasmid encoding the HaHy transposase was loaded on the nN and used to transfect HEK 293T by direct plating (onto nNs).

Following the nanoinjection, GFP expressing (GFP+)cells were sorted at day 6 and cultured for further 24 days. Flow cytometry results at day 30 reveal that two out of the four cultures nanoinjected with the (PB-GFP+HaHy) continued to express the GFP, while none of the cultures nanoinjected with just the (PB-GFP) remained positive for green (Fig. 14a,b). Fluorescence microscopy showed GFP expression following nanoinjection of PB-GFP either with or without the transposase plasmid. However, the only nanoinjection with the transposase shows high, frequent and sustained expression of the GFP up to 21 days, while in the absence of transposase, GFP expression is limited and transient (Fig. 14d).

To further support this claim, the genomic DNA from all the nanoinjected cultures at day 30 were isolated, and PCR with primers specific to the sequences present only on the transposon was performed. The results from the genetic analysis further confirmed the successful integration of the transposon in two out of the four cultures nanoinjected with the (PB-GFP+HaHy) combination and no insertion in the absence of the transposase (Fig. 14c). Taken together these results validated the specificity of the integration process and demonstrated the first stable viral-free transfection mediated by nanoneedles.

The results showed the feasibility of this strategy, which enables the simultaneous transfer and long-term expressions of three large reprogramming genes, thus overcoming the low co-expression observed when the genes are delivered using multiple viral vectors and simultaneously bypasses the safety and ethical concerns associated with viral gene transfer.

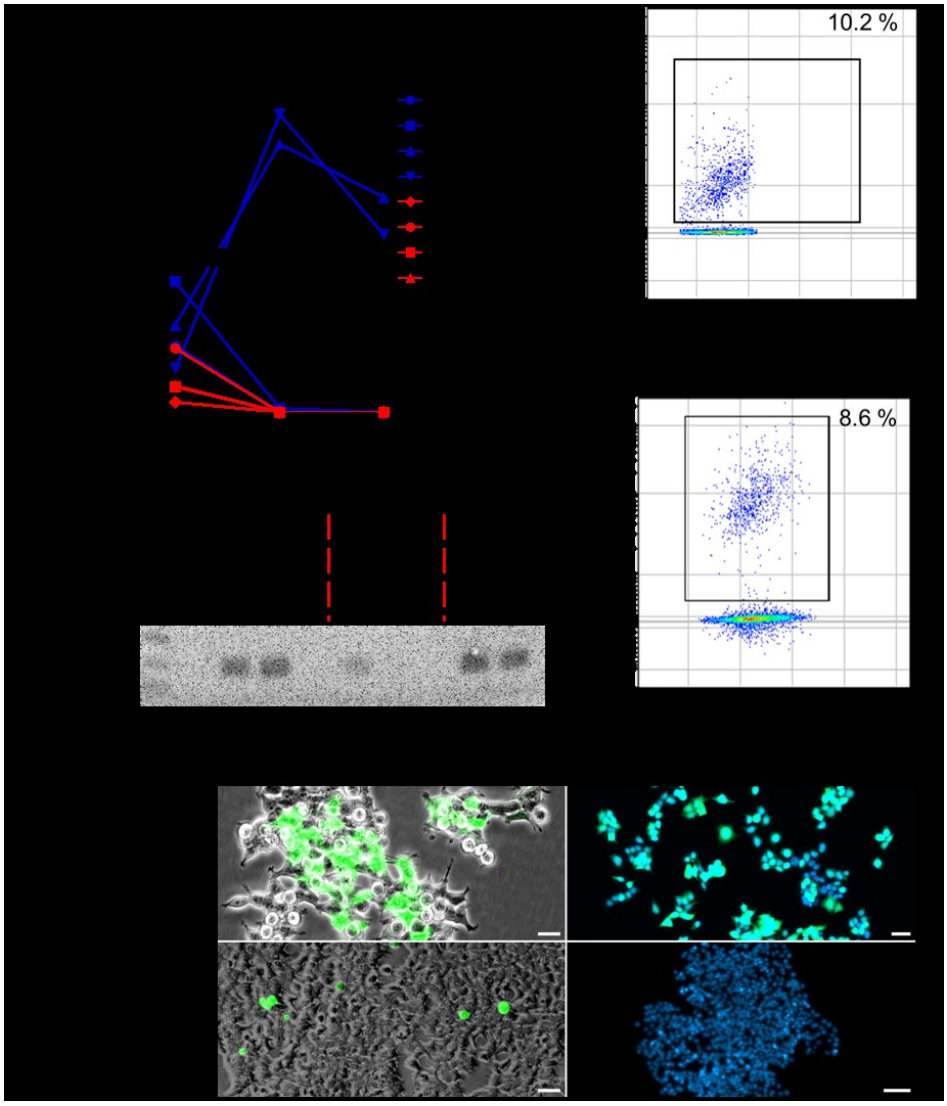


Figure 14. Nanoinjection mediates integration. (A) Flow cytometry results of HEK 293T cells at Day 6, Day 21 and Day 30 post-nanoinjection with PB-GFP+HaHy or PB-GFP only showing that 2 out of 4 nanoinjections with GFP+HaHy showed a sustained GFP expression compatible with the genomic integration of the transposable element. (B) Representative FACS plot of HEK 293T cells at Day 21 and 30 post-nanoinjection with GFP+HaHy showing sustained GFP. (C) Agarose gel showing the integration and persistence of the transposon element in the genomic DNA for two out of four nanoinjections with HaHy. (D) Fluorescence microscopy showing GFP protein expression following nanoinjection of GFP transposon with or without the transposase plasmid. Nanoinjection with transposase shows high, and prolonged expression of GFP up to 21 days, while the absence of transposase leads to sporadic and transient GFP expression. Scale bars Day 4 = 10 µm and Day 21 = 100 µm.

2.11.3. *In vitro* Nanoinjection and Reprogramming of Primary rEPDCs

As a next step, the feasibility of nanoinjecting and reprograming of primary cells isolated from the epicardium was investigated. As discussed in chapter 3.1.2.4, the epicardial undergoes massive expansion and re-activation of their embryonic-gene signature post-MI to participate in the reparatory processes post-injury. Maximum activation is in between 2-4 days post-infarction [258, 280]. To have an accurate cellular representation for our *in vitro* transfection and reprogramming assay, rEPDCs from 2 days post-MI hearts were isolated by physical epicardial tissue peeling followed by enzymatic digestion as described elsewhere [280]. The rEPDCs isolated expressed the canonical epicardial markers WT-1, TCF21 and GATA5, indicative of the successful re-activation of their embryonic gene signature and multipotency (Fig. 15).

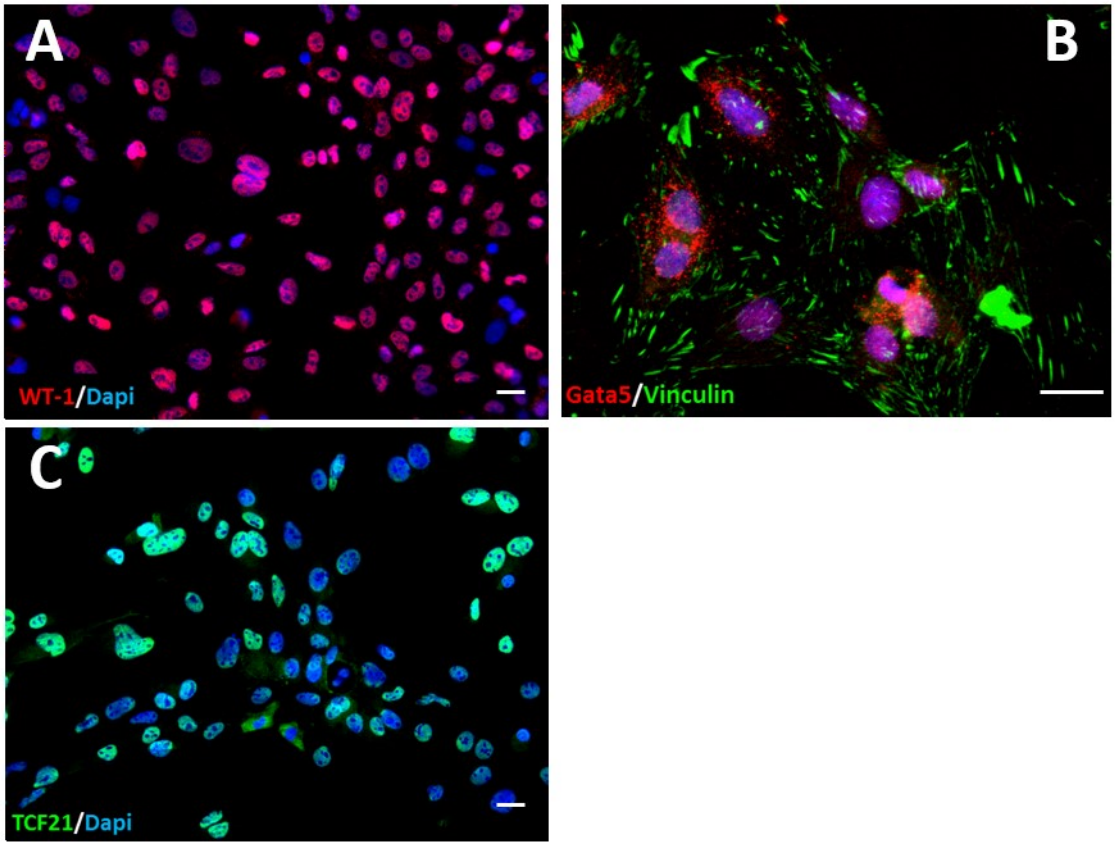


Figure 15. Characterisation of isolated primary rat epicardial cells (rEPDCs). Immunofluorescence images of *in vitro* cultured rEPDCs isolated from 48h post-MI hearts showed the characteristic activated epicardial markers (A) WT-1 (red) Dapi (blue), (B) Gata5 (red), Vinculin (green). (C) TCF21 (green), Dapi (blue). Scale bars 50 µm. Images acquired by Dr. Nicola Smart.

To access transfection and reprogramming potential of the cells, the rEPDCs were first transfected with a combination of the PB-MGT and the transposase plasmids (MGT+HaHy) or a blank control (CTL), using a cationic polymer FuGene. Following overnight incubation with the FuGene particles, the cells were cultured in cardiac reprogramming media for 18 days with a media change every two days. RNA samples were collected 4 and 18 days post-transfection.

Gene expression analysis showed a robust high overexpression of the transgenes ranging from 123 to 5500 fold over control at day 4, and sustained expression from 60 to 3400 fold at 18 days, suggesting the successful integration of the transposon (Fig. 16a).

When cultured in cardiac differentiation media after the transfection, rEPDCs transfected with the (MGT+HaHy) showed significant upregulation of the early cardiac marker NPPA ($p \leq 0.001$) on day 4. However, despite the high level of cardiac reprogramming factor overexpression, which are on-par with studies from other group [35, 190]; the cells did not undergo complete cardiac conversion by day 18 as shown by the lack of ACTNT2 and TNNT2 expression (Fig. 16b).

There are a few reasons why complete cardiac reprogramming was not observed in the study. Firstly, studies using similar reprogramming factors [1, 32, 35] only observed complete cardiac fate conversion between week 3 – 4 after the initiation of the reprogramming. So, by day 18 the cells might still be in the early/mid-stages of reprogramming and have not fully expressed the definitive cardiac markers . Secondly, it is well known that the efficiency of direct cardiac reprogramming with only the three basal transcription factors (MGT) is < 1% and was not detected by the qRT-PCR assay used. Finally, additional factors such as microRNAs, additional transcription factors, epigenetic modifiers and inhibitors are required to promote the complete conversion of rEPDCs to cardiomyocytes.

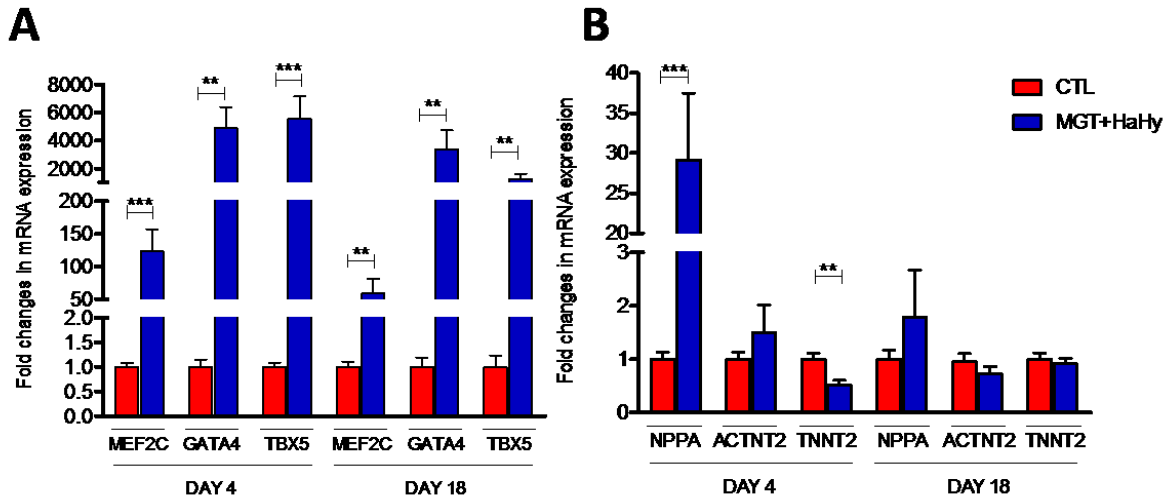


Figure 16. qRT-PCR of rEPDCs transfected with MGT+HaHy or blank Ctl via FuGene shows the sustained prolong expression of the cardiac reprogramming genes over 18 days (A) and the upregulation of early cardiac reprogramming genes. N= 6, n= 16 (B) suggesting the initiation of direct cardiac reprogramming of these cells. N = 5, n = 14. * $p \leq 0.05$, ** $p \leq 0.01$, ** $p \leq 0.001$.

After establishing the viability of transfection and the initiation of direct cardiac reprogramming in primary rEPDCs via Fugene, the ability of the nNs to mediate the gene transfer in rEPDCs were evaulated. To understand the mode of nN mediated nucleic acid delivery, pDNA were conjugated with a covalently linked fluorescence dye (Rhodamine), loaded it onto the nN and used it to transfect the rEPDCs. After 4 hours of incubation with cells seeded on top of the nNs to allow transfection to occur, the samples were fixed and imaged. Using confocal microscopy, the fluorescently labelled pDNA can be found around and inside the nuclei of the cells (Fig. 17a). To further confirm the functionality of this pDNA, the primary epicardial cells were nanoinjected with a GFP-expressing transposon plasmid and observed several cells expressing the transgene 48 hr post-nanoinjection (Fig. 17b). These results suggest that the pDNA delivered via the nNs can travel into the nucleus and subsequently have the ORF transcribed and translated.

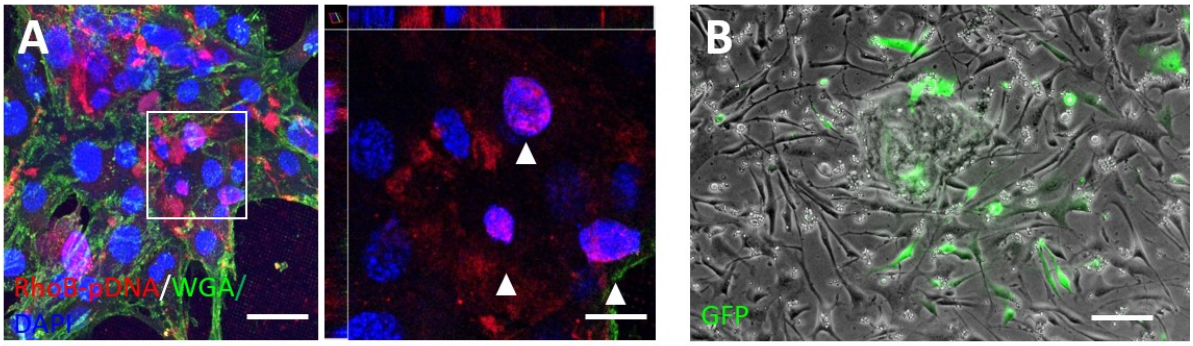


Figure 17. nN mediated delivery and transfection of epicardial cells. (A) Confocal fluorescence microscopy of Rhodamine labelled pDNA (in red) highlights the localisation of the transposon within the nucleus of cells at 4 h post-nanoinjection. Wheat germ agglutinin (in green) highlights the cell membrane. DAPI in blue highlights the cell nucleus. Scale bars, left panel = 50 µm, right panel = 10 µm. (B) Combined epifluorescence and phase contrast microscopy of rEPDC at 48 h post-nanoinjection of PB-GFP+HaHy showing GFP protein expression present in numerous cells. Scale bar = 200 µm.

Having proved the ability of the nanoneedle to transfer genetic material into the primary epicardial cells, the rEPDCs were transfected with the GMT+HaHy via nanoinjection and cultured the cells in the cardiac reprogramming media to induce direct cardiac reprogramming.

Nanoneedle-based injection of GMT+HaHy leads to sufficient overexpression of the reprogramming genes at day 4, except the Mef2c which showed no difference between the control and the MGT+HaHy trasfected samples (Fig. 18a). The high endogenous basal expression of the MEF2C in the starting population and the inability of the primers to distinguish between the *Homo sapiens* transgene and *Rattus norvegicus* endogenous expression due to the high homology (90% sequence identity) might be responsible for the undetectable overexpression of Mef2c plasmid integration.

However, compared to FuGene mediated MGT+HaHy transfection in the rEPDCs (Fig. 16a), the level of overexpression achieved was 100 – 1000 fold lower. Despite the modest upregulation of transgenes following the nanoinjection, when cultured in cardiac reprogramming media the rat epicardial cells were able to upregulate the expression of Tnnt2 ($p \leq 0.05$) at day 4 and several other cardiac markers including Nppa, Actnt2 (significant, $p \leq 0.05$) and Tnnt2 at day 18 over similarly-cultured controls (Fig. 18b).

Suggesting that overexpression of reprogramming factors in the range of 100x folds might be enough to initiate early reprogramming. Furthermore, the nanoinjection methods proof to be more beneficial for the purpose of specifically targeting the epicardial layer in live animals which is only a single-cell layer thick; compare to the use of FuGene which needs to be administered systemically thus do not offer the same level of specificity and spatial control as the nanoneedle based methods.

These results indicate that the nanoinjection of the three cardiac reprogramming genes Mef2c, Gata4 and Tbx5 can initiate the direct cardiac reprogramming program in the primary epicardial cells. However, these factors alone are insufficient to support the complete conversion of the rEPDCs into fully functional cardiomyocytes, and additional transcription factors or pathway inhibitors might be required to fully optimise the ideal protocol for epicardial cell reprogramming, which is not within the scope of this thesis. To date, this is the first report of stable gene expression achieved by transfecting primary heart cells with a nanomaterial-based approach. Previously, high-aspect-ratio nanostructures were shown by our and other groups to be an efficient method for nucleic acid delivery (both siRNA and pDNA), but within strategies for transient, non-integrative gene expression.

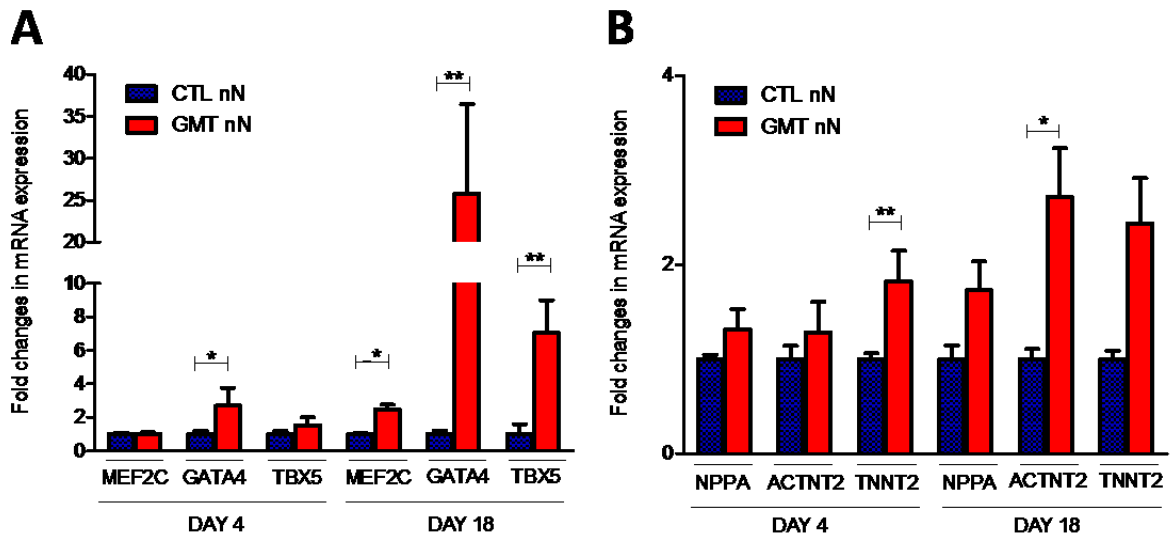


Figure 18. Nanoinjection and reprogramming of epicardial cells. (A, B) qRT-PCR of rEPDCs nanoinjected with MGT+HaHy show the robust and sustained overexpression of transgenes over 18 days (A) except for Mef2c which did not show any difference in expression profile at day 4, and the upregulation of early cardiac reprogramming genes (B). For day 4, N = 4, n = 12. For day 18, N = 3, n = 8. * $p \leq 0.05$, ** $p \leq 0.01$.

2.11.4. *In vivo* Nanoinjection of the Post-MI Epicardium

A pre-clinical small animal study was performed to investigate the feasibility of nN mediated gene transfer to the post-MI epicardium in live rats. As shown in the previous study, the nNs are capable of delivering cargoes in an efficient and spatially defined manner [9, 10]. Since the epicardial layer is only a few cell layers thick, the first experiment was to determine the level of accuracy that the nNs can achieve in delivering pDNA directly into the epicardium.

To answer this question, the nN chip was loaded with the rhodamine-labelled pDNA as described in the method section and applied it in the area downstream of the coronary ligation (on the infarct zone) in live rats at the time of intervention. Histological samples were collected at 30 min and 4 days post-treatment to understand the spatial distribution of the pDNA at the initial time point and their subsequent redistribution at the later timepoint. Rat injected with the rhodamine-labelled pDNA (Rho-PB) via the nanoinjection show clear punctate rhodamine positive signals localised on the epicardial layer of the infarcted zone during the initial delivery (30 min), whereas samples from the control rat lack the signals. This observation confirms the ability of the nanoinjection method to deliver with high precision to the epicardium (Fig. 19).

At a later time-point, 4 days post-nanoinjection, the cells that were successfully transfected and uptaken the rhodamine labelled pDNA (Rho-PB) migrated and spread deeper into the myocardium infarct zone (Fig. 20). This phenomenon is consistent with the remodelling of the epicardial layer, activation and contribution of the epicardial-derived cells in the reparative process post-MI. The diffuse red fluorescent signals observed in the control sample at day 4 post-nanoinjection is the inherent cardiac tissue background fluorescent, different from the punctate signals observed in samples from rat that received the Rho-PB via nanoinjection (Fig. 20). The ability to specifically target the epicardial layer is a unique trait that can only be achieved through the nanoneedle based transfection, since other transfection strategies such as FuGene based will not offer the same level of specificity and spatial control.

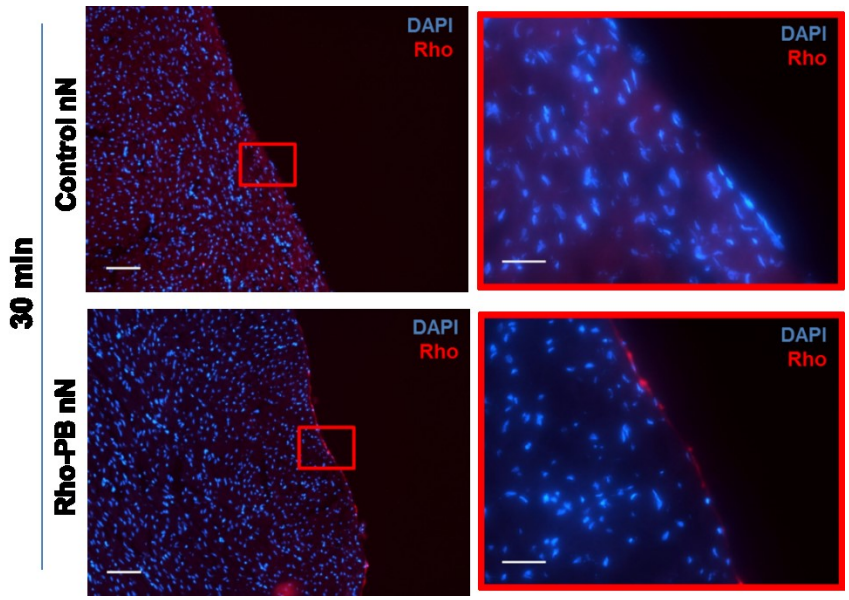


Figure 19. *In vivo* nanoinjection of Rho-pDNA at early time point (30 min). Representative immunofluorescence images of histological slices across the infarcted area that received treatment at 30 min show an initial delivery of the labelled DNA to the epicardium layer. Scale bar = 100 µm for the left panel and 400 µm for the right panel. The panels on the right (highlighted in red) correspond to the red outlined insets in the left panel. Rhodamine signal (red) and DAPI (blue).

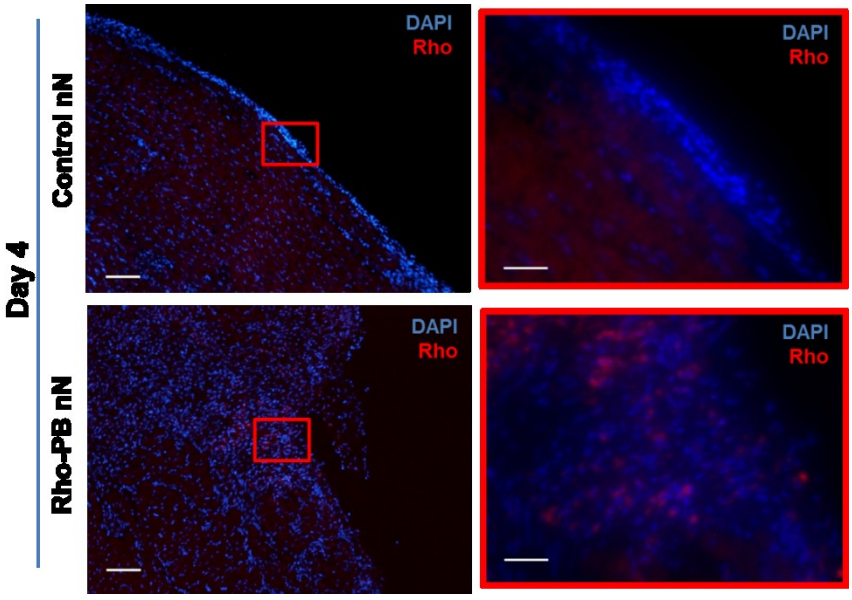


Figure 20. *In vivo* nanoinjection of Rho-pDNA at a later time point (Day 4). Representative immunofluorescence images of histological slices across the infarcted area that received treatment at 4 days show the redistribution and migration of the transfected cells following the activation and remodelling of the epicardial layer. Scale bar = 100 µm for the left panel and 400 µm for the right panel. The panels on the right (highlighted in red) correspond the red outlined insets in the left panel. Rhodamine signal (red) and DAPI (blue).

After confirming the viability for efficient and accurate epicardial delivery, proof-of-concept experiments were performed to deliver the transposon plasmids encoding the reprogramming factors and the accompanying transposase plasmid via nanoinjection to the epicardium of live rats post-MI. The experiments were separated into control group *i.e.* blank nanoinjection, and treatment group *i.e.* nanoinjection with MGT+HaHy. Following nanoinjection, the rats were kept alive and sacrificed at day 2 and day 7 post-intervention. Gene expression analysis of samples collected at day two and seven from the treated area demonstrated an overall variability of the level and efficiency of the gene transfer (Fig. 21a and b, respectively). Two days post-treatment, 6 out of the 9 animals treated with the MGT+HaHy nanoinjection had Gata4 and Tbx5 expression value higher than the sum of the mean and standard deviation of all the control samples (Responder group); with an increase from 1.3 to 14 fold (Fig. 21a). The analysis of the Mef2c overexpression was hindered by the same challenges mentioned above. The inconsistency observed in the transfection efficiency can be attributed to several parameters including the variability of the manual application of the nN chips on the beating heart, the manual tissue dissection, the isolation of the tissues from the targeted area and the intrinsic variability from one rat to the other. By day 7 post-nanoinjection, the treated (MGT+HaHy) samples collected showed overall reduced expression of the transgenes to a non-significant level (Fig. 21b).

The results observed from the *in vivo* experiments indicate that gene delivery to the heart epicardium via nN-mediated nanoinjection is mostly successful. The rapid expansion and activation of the EPDCs which relies on signalling molecules initiated post-infarction might have contribuded to the survival and potential expansion of the transfected cells on the epicardium.

However, in the long term, the transgenes overexpression was diminished. These findings may be attributed to either unstable transfection or to the fact that the transfected cells somehow suppressed the gene expression, or migrated outside the collected area. Additionally, since the epicardium layer targeted by the nanoneedle is directly downstream of the coronary ligation; the lack of blood supply to the area although lead to EPDCs activations also lead to increase cellular stress and the death of other resident cells that might have been transfected in the epicardium layer, and thus effecting the efficiency of the transfection and direct reprogramming.

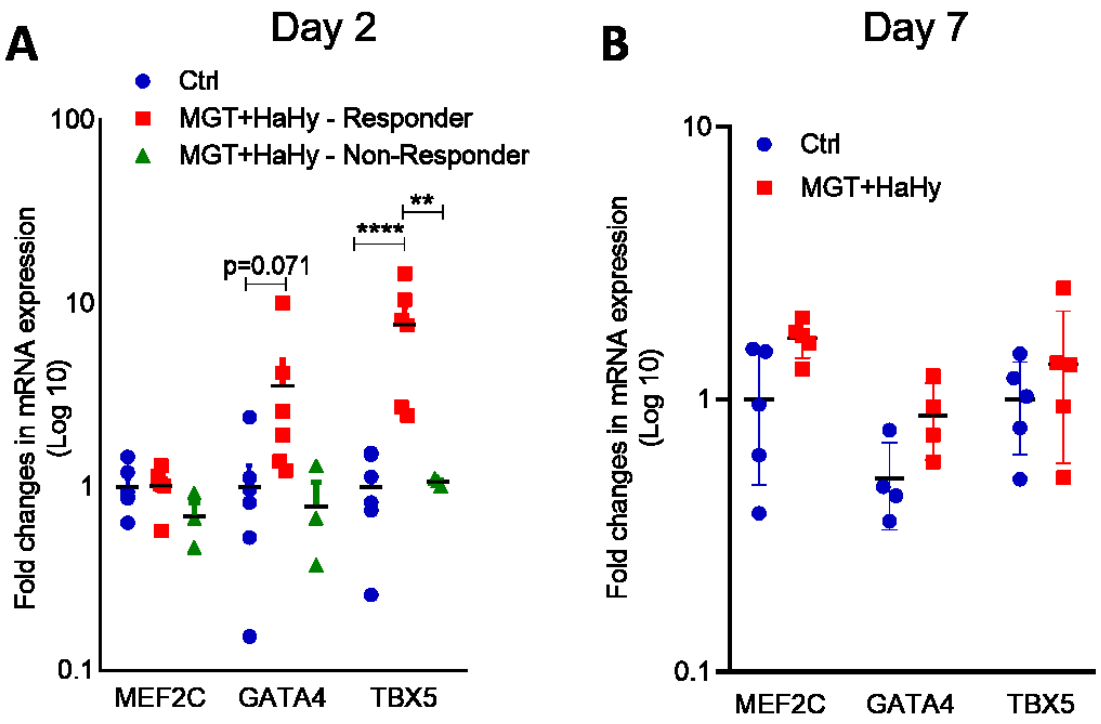


Figure 21. *In vivo* nanoinjection of MGT+HaHy to the epicardium for gene regulation. (A, B) qRT-PCR of cardiac tissue harvested from the myocardial infarction region following treatment with either empty nanoneedles (Ctrl, blue) and nanoneedles loaded with pDNA (MGT+HaHy). (A) Overall 4 out of the 7 rats injected responded to the treatment showing overexpression of transgenes at day 2 (Responders= expression values greater than the mean+SD of the control group for each genes, red) while the remaining nanoinjected rats did not show overexpression (Non-Responders= expression value is equal or less than the mean+SD of the control group for each genes, green); (B) transgenes expression in nanoinjected animals at day 7 was at basal levels. Data shown as mean ± s.e.m., n≥5. Differences tested by multiple student t-test corrected for multiple comparison, *p<0.05, **p<0.005.

2.12. Discussion

Direct cardiac reprogramming represents a promising approach for cardiac regeneration and would benefit patients with myocardial infarction. Here a nanoneedle-mediated delivery was proposed as an effective and unique strategy to specifically target gene therapy to epicardial cells *in vivo*. A method to efficiently load and rapidly release pDNA from the nanoneedles to mediate efficient transfection was revealed. The nanoinjection of the polycistronic transposons encoding for direct cardiac reprogramming genes along with the transposases leads to the sustained expression of the transgenes and the upregulation of endogenous early cardiac reprogramming genes in isolated primary epicardial cells. Upon application of the nanoneedle containing the treatment (GMT expressing transposon + transposase plasmid) to the epicardium layer on top the infarcted region *in vivo*, leads to transgene overexpression in live animals. This work shows that the combination of nanoneedle and transposon offers an unprecedentedly powerful gene editing tool, not limited by the size of insertion, and capable of targeting specifically desired tissue layers, in this case, the epicardium.

The epicardium becomes active following ischemic injury and can be characterised by the activation of embryonic gene signatures such as Wt-1, Tcf21 and Gata5. These cells have been shown to be involved in various reparative and restorative functions following an ischemic injury [7, 232], and upon activation acquired the potential to differentiate into different cell types in the cardiac lineages including smooth muscle, endothelial cells, fibroblasts and cardiomyocytes. In this study, the EPDCs was specificially targeted due to these properties and force them to differentiate into cardiomyocytes via the nanoinjection and integration of the transposon encoding the Mef2c, Gata4 and Tbx5 cardiac reprogramming factors.

While our work did not aim at establishing the ideal protocol for epicardial cell reprogramming; our data reveal that these factors can induce and initiate the early stages of the cardiac reprogramming factors. Our reprogramming experiments were terminated by day 18 post-transfection, and perhaps if the reprogramming procedure were to be kept running for up to 4 weeks, a more complete conversion could have been possible since most studies using the Mef2c, Gata4 and Tbx5 based reprogramming strategies only noticed complete conversion from 3 – 4 weeks. Since the start of this project, several other combinations of transcription factors, miRNAs cocktails and additional inducers of cardiac reprogramming have been described. The addition of transcriptional factors and pathway inhibitors might be

necessary for complete and efficient reprogramming of the epicardium cells. As an example, the addition of Hand2 might promote a higher number of cells entering the early phases of cardiac reprogramming, whereas the addition of MyoCD might help consolidate the expression of definitive cardiac markers such as Actnt2 and Tnnt2 and genes involved in the calcium handling, action potential and contractility of cardiomyocytes. The modulation of cellular signalling pathways with small molecules has also been shown to be beneficial in improving the efficiency of cardiac reprogramming. For example the inhibition of pro-fibrotic pathways, such as the TGF-β signalling with A83-01 in combination with the GHMT reprogramming factors induced ~4,400 functional cardiomyocytes from 5,000 MEFs by 4 weeks. Modulation of the Wnt signalling pathway with SB431542 and CHIR99021 has also been reported to increase reprogramming efficiency. Also, since the conversion of one cell type to another is mostly dependent on significant chromatin/epigenetic alterations, more recent studies have focussed on the addition of epigenetic modifiers that promote open-chromatin states such as forskolin to boost the rate of cardiac reprogramming from fibroblasts.

Previous *in vivo* cardiac reprogramming studies using retrovirus-based strategies to deliver the reprogramming factors in the infarcted area of the heart have yielded some level of success in terms of functional improvement post-MI. By genetic tracing, researchers demonstrated that cardiac fibroblasts are the cells targeted by the therapies and that eventually convert to the *de novo* cardiomyocytes. However, their approach did not allow for the targeting of a specific cell type or tissue layer. Our proof-of-concept *in vivo* study demonstrates the feasibility of tissue-specific delivery of integrative pDNA to the epicardium. Further studies are necessary to establish the cellular identities of the cells that were transfected in the epicardium layer of the heart. The information obtained could help design superior reprogramming cocktails. Additionally, the nanoneedles enable the loading of different types of cargoes simultaneously, including nucleic acids and chemical inhibitors and specifically targeting the epicardium. Future studies will explore the use of nanoneedles to deliver TF-based reprogramming factors along with small molecule inhibitors that have been shown to promote cardiac reprogramming. Furthermore, a thorough tracing of the fate of the transfected cells *in vivo* and an investigation of the functional cardiac recovery following nanoinjection is necessary.

Since, an *in vivo* study using Tβ4 to stimulate the EPDCs to differentiate into cardiomyocytes showed that a significant and meaningful functional recovery of the cardiac function could be achieved with as little as < 1% conversion rate [271], this would be interesting standard to compare the outcome of our strategy. Lastly, a further optimisation into the strategy for interfacing nanoneedles with the epicardium might provide more uniform and accurate results.

Chapter 3: Biophysical Regulation of Cellular State by Nanoneedles

3.1. Introduction

The cellular niche is made of a sophisticated ensemble of soluble factors, extracellular matrix and mechanical stimuli that influence a wide variety of intracellular functions.

Extensive research using *in vivo* models and/ or specific substrates with defined mechanical properties *in vitro* have shed light on the importance of biophysical cues and cellular mechanosensing in influencing cells decision-making processes. These processes range from a primary cellular function, lineage commitment, to epigenetic status. In recent years, artificial biomaterial systems have been used to probe a range of outside-in signalling events, and it is now well known that biophysical signals can modulate the epigenome. However, details of the signal transduction pathways and epigenetic alterations are just starting to emerge, and further understanding of the underlying vital processes could accelerate the development of increasingly sophisticated investigative and therapeutic tools.

3.2. Cellular Behaviour and Its Regulation by Extracellular Cues

3.2.1. The Principle of Cellular Mechanosensing

The extracellular matrix (ECM) niche is composed of a multitude of stimuli ranging from soluble biochemical factors, cell-cell interaction, physical and mechanical forces that act in symphony (Fig. 22) [287].

For many years, the focus has been on the role of soluble factors such as growth factors, hormones and cytokines that can activate intracellular signals through specific receptors and, thus, alter the behaviour of cells. However, cells not only respond to chemical signals but also have the innate and sophisticated ability to sense and react to mechanical cues in their environment. In a process referred to as mechanotransduction,the physical signals are translated into biochemical signals. Mechanical properties surrounding the ECM play essential roles in modulating a broad range of cellular phenomena (Fig. 22). These include but are not limited to cellular morphology [75, 288], cell motility [289-291], cell proliferation [292, 293] and apoptosis [294], and tissue and organ development [295, 296]. Another exciting aspect is the importance of biophysical cues on cellular differentiation and stem cell fate.

One of the first studies by Engler *et al.* showed that MSCs differentiate towards soft-tissue lineages, such as fat, when cultured on a soft substrate, and toward stiff-tissue lineages, such

as bone, when on the stiff substrate [79]. Changing substrate topography has also been shown to increase the expansion and stemness of haemopoietic stem cells (HSCs) [297, 298]. The external mechanical strain has also been demonstrated to promote self-renewal and retained pluripotency of human embryonic stem cells (ESCs) [299].

At the other range of the spectrum, abnormal cellular or tissue-level forces and material properties, and/or dysfunctional mechanosensing capability can lead to abnormal physiological responses that could lead to diseases such as atherosclerosis [300, 301], arthritis [302, 303], cancer [304] and developmental disorders such as Hutchinson-Gilford progeria syndrome [305-307].

Substantial progress has been made in understanding pathways, and components involved in cellular mechanosensing in the past decade. Mechanical cues which influence cellular behaviour range from nano- to micrometre scale, and these signals have to be regulated with exquisite spatial and temporal accuracy to give rise to the specific desired changes at the molecular level [308]. Thus one can picture the complexity of the components and pathways involved in this process, ranging from cues present in the ECM, and receptors on the cell membrane and all the way to the nucleus (Fig. 22).

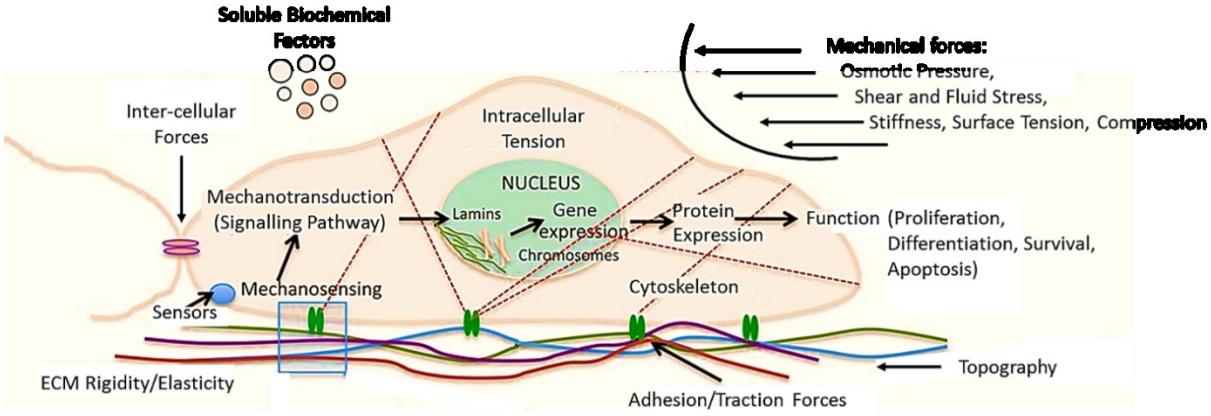


Figure 22. Schematic depicting the complexity of the cellular microenvironment. Cells are exposed to several types of cues, such as soluble paracrine factors, shear forces, tensile/traction forces through the ECM, compressive forces and intracellular tension. Mechanical forces can stimulate cells through the activation of specific mechanosensors which then activate certain signalling pathways leading to modulation in gene expression. Mechanotransduction can influence cellular functions ranging from proliferation, cell survival and death, and even differentiation potential. Adapted from [4].

3.2.2. Cellular Membrane – Matrix Interactions

The ECM is a complex meshwork which comprises proteins, glycoproteins and proteoglycans (PGs) which act as a support to which cells adhere [309]. The ECM provides mechanical support to cells and tissues mainly through elastic fibres, fibrillar collagens, glycosaminoglycans (GAGs) and the related PGs present [310]. It also provides sources of growth factors, cytokines and enzymes. Thus it comes as no surprise that the ECM influences many cellular functions, from motility, growth, differentiation all the way to survival [311]. The relationship between cells and ECM is a very dynamic and mutual one. The interactions are mediated by membrane-spanning heterodimeric proteins called integrins. Integrins act as a bridge that connects the ECM through its extracellular domain which can recognise and bind to specific signals in the ECM, such as RGD peptide to the cytoskeleton through focal adhesions (FA) [312, 313] (Fig. 23). Integrins propagate the mechanical signals by forming clusters [314] and recruiting adhesomes, a cluster of proteins which includes focal adhesion adapters, shuttling proteins and kinases that can influence gene transcription in addition to the actin cytoskeleton since it does not possess any enzymatic activity [315]. Prominent components of the adhesome are focal adhesion kinases (FAK) which act as a phosphorylation-regulated signalling scaffold [316], talin [317], vinculin[318], and p130Cas [319] (Fig. 23). The integrin-mediated mechanosensing through the adhesomes can change cellular fate and activity by altering the activity of various downstream signalling cascades (Fig. 23). The mitogen-activated protein kinase (MAPK) family is one such pathway and is an established regulator in osteoblasts [320, 321], vascular endothelial and smooth muscle cells [322] mechanoresponses and myocyte differentiation from human mesenchymal stem cells (hMSCs) [323]. Another example is the Hippo pathway whose central components consist of YAP1 and TAZ transcription co-activators [8]. Furthermore, E-cadherin, a protein present in the cell-cell junctions which play a crucial role in the formation of the epithelial monolayer, has been shown to be a crucial mechanosensor [324]. Various other molecules such as PECAM 1, VE-cadherin and VEGFR2 [325] and G protein-coupled receptors (GPCR) [326] have been demonstrated to be mechanosensors in response to fluid shear stress. A specific class of ion channels has also been demonstrated to respond to mechanical cues [327], for example the TRPV4 channel has been implicated in chondrocytes ECM biosynthesis in response to mechanical loading [328] and the remodelling of the cytoskeleton in endothelial cells upon

application of cyclic stretch [329]. The membrane/lipid rafts (MLR) can also interact with the actin cytoskeleton complex to transduce mechanical cues from the environment [330]. For example, the MLR has been shown to induce protective autophagy in HeLa cells upon shear stress [331] and play a role in the regulation of chemotaxis [332].

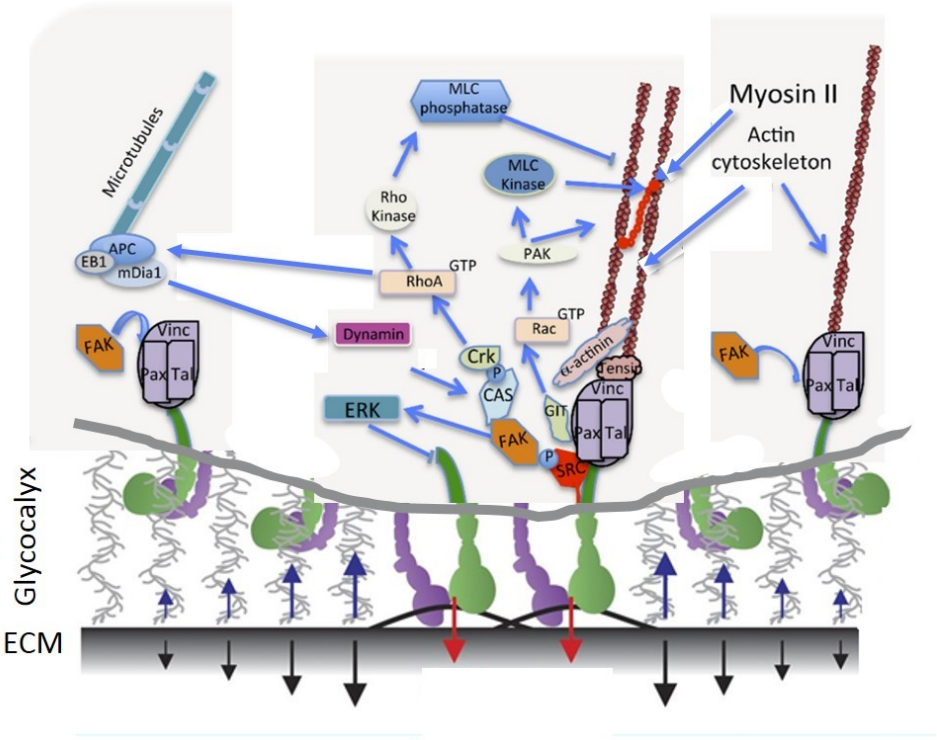


Figure 23. Cell-matrix interface. The interaction between the ECM and the cell starts at the cell membrane interface and is mediated primarily by integrin. Upon binding, the FAs, which are connected to the actin cytoskeleton via adaptor proteins such as vinculin and talin, are formed. The FA complex via FAK and paxillin act as signalling adaptors to activate various downstream signalling pathways and translate the external biomechanical cues into changes in cellular behaviour. Figure adapted from [2, 3].

3.2.3. Mechanotransduction and the Actin Cytoskeleton

The model of cellular tensegrity proposed by Ingber emphasised the importance of cytoskeletal structures and tensions in cellular response [27]. The actin cytoskeleton can sense mechanical tensions, and its response is very sensitive to the strength, direction and duration of the mechanical loading [310]. For example, fibroblasts increase the degree of the actin crosslinking and bundling to allow them to adapt to the high stiffness of their niche [333]. Also, upon exposure to cyclic loading, the cells actively re-model and re-orient the actin

cytoskeleton [334]. However, no remodelling is observed on the very compliant substrate [335]. The actin fibres can propagate the mechanical properties of their environment over long-distances and are much faster (> 40-fold) in comparison to signalling induced by soluble factors [336].

Moreover, actin fibres can communicate these mechanical cues all the way into the nucleus [337]. This function is mediated by specialised actin cap stress fibres which sit on top of the nucleus and are connected to the nuclear envelope through the LINC complexes [338]. Microtubules also contribute to cellular mechanosensation although not much has been discovered. One study has demonstrated the influence of microtubules on the degree of cell spreading in a 3D, low tension environment [339]. Microtubules also affect the state of maturation of the focal adhesion by regulating traction forces [340]. Intermediate filaments (IF) are another large family of proteins that have a role in cellular mechanosensing. IF can be categorised into five different classes based on their self-assembly behaviour [341].For example, vimentin, a type of IF important in mesenchymal cells, can interact with actin and microtubules [342] and also link α6 integrin directly with the cell nucleus via plectin and nesprin [343]. It has been shown that vimentin regulates adhesion of endothelial cells in response to shear stress [344]. Vimentin knockout leads to impaired fibroblast migration [345]. In addition to external forces, the forces generated inside the cells mainly by the myosin II-based contractile machinery are also an essential aspect of mechanotransduction. Myosin II is a hexameric protein and is the primary actin-dependent molecular motor that regulates actomyosin contractility. Myosin II assembles into bipolar filaments and by pulling actin filaments together generates cortical tension [346]. Classically, myosin-II based contractility has been associated to cellular migration, by generating the necessary force for locomotion of the cell body and the disassembly of the cell adhesions on the leading edge of the cells [347]. It also contributes to cell polarity by modifying the positioning of the nucleus [348]. However, more recently actomyosin contractility has been shown to dictate cell differentiation [349], and dysfunctional tension homeostasis promoting tumorigenesis [350]. Furthermore, different isoforms of the myosin II heavy chain might exhibit a different role within a cell in both *in vitro* and *in vivo* scenarios [351]. There is, therefore, a continuous mechanical connection between the cellular niche and the nucleus that is mediated by the integrins-focal adhesion-actocytoskeletal complexes.

3.2.4. Nuclear Mechanotransduction

The nucleus is a highly organised structure with a well defined spatial and temporal regulation where the cell blueprint is stored and transcription occurs (Fig. 24). It is established that the nucleus is the largest and stiffest organelle and can be regulated by mechanical forces from outside or generated within the cells.

In recent years, some experiments have shown the ability of mechanical cues in modulating gene expression. One such example is a study using magnetic twisting cytometry which showed that the application of local stresses on the integrins on the cell surface directly unfold and stretch chromatin and elevate the transcription of a GFP-tagged transgene [16]. However, very little is known about the underlying mechanisms of nuclear mechanics and mechanotransduction (Fig. 24). The nucleus is physically tethered to the ECM through the linker of the nucleoskeleton and cytoskeleton (LINC) complex, thereby allowing the direct transmission of mechanical cues as shown by the Ingber group in their seminal paper [352-354]. This complex is composed of the SUN and KASH membrane protein families that reside on the inner nuclear envelope and the outer nuclear envelope, respectively [355]. The KASH domain proteins bind to cytoskeletal constituents, including IF, actin filaments and microtubules, whereas SUN domain proteins are associated with the lamins, the main structural component of the nuclear envelope [356].

The nuclear envelope is dynamic and forces sensitive interface occupied by cytoplasmic cytoskeletal components on the cytoplasmic side, and dense heterochromatin, DNA, lamins and lamin-associated proteins on the nucleoplasmic side [357]. There are two main families of lamin proteins: lamin-A (type A and C derived from alternative splicing of the *LMNA* gene) and lamin-B (type B1 and B2 transcribed from *LMNB1* and *LMNB2,* respectively). These have a slightly different role within the cells but work in cohorts to provide structural integrity to the nucleus. Lamin-A primarily possesses a more viscous response, whereas Lamin-B promotes elasticity [358].

A recent study with quantitative label-free mass spectrometry (MS) showed that the ratio of nuclear lamina type-A and –B correlates strongly with the stiffness of the extracellular matrix. The nuclei of cells in soft tissues and hematopoietic systems tend to have a higher proportion of lamin-B, while cells in a stiff microenvironment such as the bone or cartilage are dominated by lamin-A [5]. Also, the nuclei of embryonic stem cells (ESCs) have been shown to be very

soft and have low lamin-A, and as they differentiated into a lineage-specific fate, the levels of the lamin-A increases and the nucleus become stiffer [359, 360].

Engler demonstrated that the stiffness of the ECM could influence cell fate [79]. This same effect can be mimicked and further enhanced by nuclear lamina modifications [5]. Lamin-A deficient mouse embryonic fibroblasts (MEFs) caused defective mechanotransduction and lower viability under mechanical strain [305]. This effect was also observed in emerin, a protein which is involved in the mechanically sensitive process, deficient MEFs [6, 361]. Also, the accessibility of a specific epitope on the lamin-A/C protein was shown to be regulated mechanically. During high strain such as, osteogenic differentiation, cell spreading, or presence of compressive forces the Ig-domain of lamin-A/C is less accessible in the basal nuclear envelope relative to the apical, whereas this epitope was actually available in equal proportion during adipogenic differentiation, or in cells cultured on soft surfaces (low strain). This epitode overlaps with critical binding sites for efficient mechanotransduction [362].

One of the possible mechanisms of nuclear mechanoregulation of gene expression is through the translocation of transcription factors (Fig. 24). Stiffness dependent nuclear translocation of the transcripton factors RARG and YAP1 directly regulates the transcription of *LMNA* and initiates the differentiation signalling cascade of MSCs down the osteogenic lineage [8]. Also, the expression of nuclear protein 1 (Nupr1), a recently discovered tumour suppressor, was also linked to the nuclear translocation of the YAP1 and depend upon mechanical forces from the matrix [363]. The modulation of actin polymerisation by nuclear envelope protein Lamin-A and emerin has also been shown to be crucial in controllingmegakaryoblastic leukaemia 1 (MKL1) nuclear translocation and SRF dependent transcription, while impaired signalling leads to diseases such as Emery-Dreifus muscular dystrophy (EDMD) and dilated cardiomyopathy (DCM) [364]. The nuclear envelope is also decorated by many nuclear pore complexes (NPC) which control the transport of various molecules in and out of the nucleus. The NPCs which linethe nuclear envelope control the traffic of various molecules in (*e.g.* YAP/TAZ or TWIST1) and out of the nucleus (*e.g.* nuclear actin). One hypothesis is that the application of external force which leads to the deformation of the nuclear structure activates the nuclear complexes through a direct mechanical link with the actocytoskeletal complexes and allows the import or export of transcriptional regulators which in turn control various physiological cell responses [365].

Mechanoregulation of 3D nuclear organisation can also be another method for mechanically regulating gene transcription (Fig. 24). It has been recently recognised that 3D organisation of chromatin within the nucleus is crucial in the regulation of the genome [366, 367]. Each chromosome occupies a distinct territory within the nucleus, and transcriptionally inactive heterochromatin tends to be localised on the nuclear periphery and around nucleoli, while transcriptionally active euchromatin is primarily localised on the centre and near the nuclear pores [368]. Although nanonewton forces are typically required to deform the nucleus structure in adherent cells [369], only piconewton forces arerequired to induce biochemical alteration such as the level of the histone-acetylation [370] and the alteration in protein-protein interaction and displacement of nuclear components [371]. An elegant study using the fluorescence *in situ* hybridisation (FISH) technique by the Shivanshankar group demonstrated that the relative positioning of chromosome territories within the nucleus is dependent on the mechanical state of the nucleus and was able to affect the transcriptional activity of the intermingled chromosomes [372]. In their study, interphase fibroblasts plated on different substrate geometries (anisotropic or isotropic) showed differential nuclear morphologies where cells on anisotropic surface had a flat and ellipsoidal nucleus, whilst cells on isotropic surfaces had a more spherical nucleus. Yet in both scenarios their chromosomes tended to orient themselves along the mechanical axis of the nucleus. The differential positioning of the chromosomes territories is due to the level of lamin-A/C. The cells cultured on isotropic substrates showed a downregulation of lamin A/C expression leading to the reduction in the cellular tension applied to the nucleus and increased nuclear dynamics. This enabledmore free movement of the chromosomes within the nucleus and led to the formation of new interactions thus altering gene expression. Another study with magnetic twisting cytometry on the surface of engineered single-cells in culture demonstrated that stress-induced chromatin stretches and the transcription upregulation depended on the direction of the load and the magnitude of the stretch and required intact actomyosin contractility and the presence of nuclear envelope proteins [16].

Nuclear membrane dilation and rupture has also been proposed as another mechanism of mechanoregulation of gene expression [17] (Fig. 24). One can speculate that substantial changes in nuclear shape and/or increase in volume might lead to increased tension in the nuclear envelope. As an example, tissue damage induced osmotic nuclear swelling in

zebrafish, led to the dilation of the nuclear membrane and in turn activated cytosolic phospholipase A2 (cPLA2), a signalling pathway important in tissue damage repair [373]. This process is mediated by perinuclear F-actin and the nuclear lamina, once again demonstrating the critical role of mechanical tension in the nuclear envelope on the downstream tissue repair response.

Nuclear rupture has been shown to regulate the translocation of transcription factors RELA into and OCT1 out of the nucleus [374]. A loss in the physiological function of lamin-A/C can lead to a transient non-lethal nuclear rupture in cells cultured on the rigid substrate [375]. The entry or exit of proteins/factors through the transiently ruptured nucleus does not seem to be a selective process. However 'primed' mechanosensitive factors under high-strain conditions might be able to access and accumulate more readily upon rupture than others [17]. In summary, the extracellular mechanical cues through modulation of integrin and actomyosin contractility can not only alter the nuclear morphology but also modulate the spatial organisation of the chromosomes and the shuttling of transcription factors, thereby resulting in differential activation or inactivation of gene expression circuits. However, it is very tricky to segregate whether changes observed are a direct result of the force propagation and impact on the nucleus or an indirect result via the cytoplasmic biochemical activity.

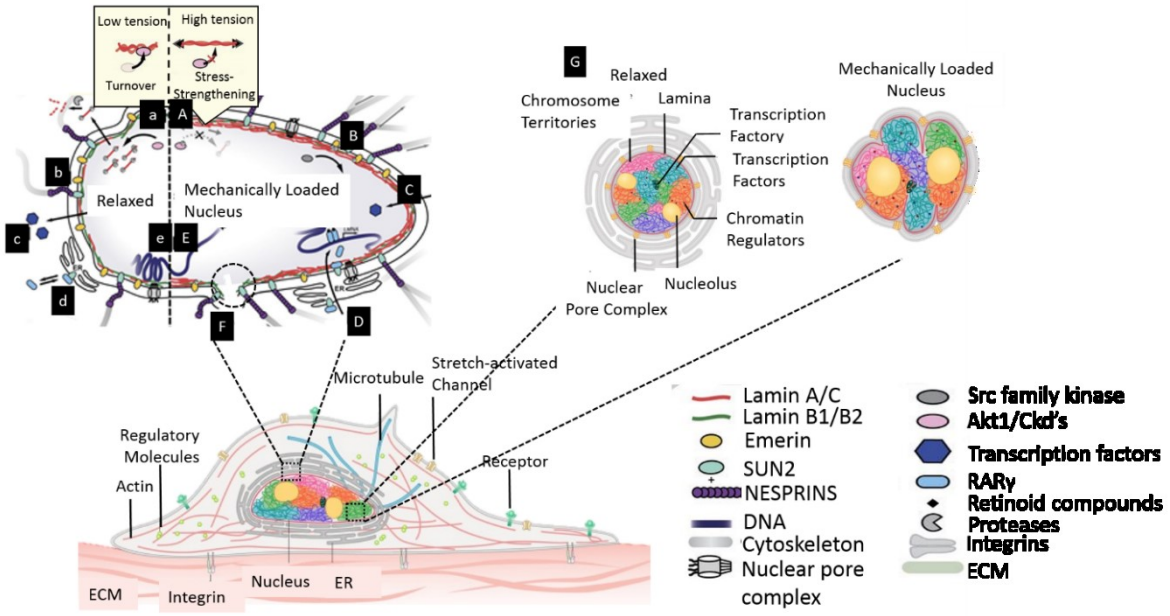


Figure 24. Nuclear mechanotransduction. The nucleus is the epicentre of the cells and is mechanically coupled to the cell surface via the actin-cytoskeleton and microtubules. The effect of biomechanical cues transferred through these intermediates affect the nucleus via several modes. The left side of the zoom in nucleus indicates a relaxed nucleus and the right side indicates a mechanically loaded nucleus. (a, A) In a soft nucleus, lamins are highly phosphorylated which lead to more solubilisation; conversely, high nuclear tension leads to lower levels of phosphorylation due to the inaccessibility by kinases and thus reduces the solubility and mobility of lamins and lead to tension induced strengthening of the lamina [5]. (b, B) Emerin is phosphorylated by Src kinases upon application of tension on nesprin-1 and results in stiffening of the nucleus and activation of various downstream mechanoresponses including the modulation of stress fibres, migration and localisation of YAP/TAZ [6]. (c, C) (d, D) Shuttling of mechanosensitive transcription factors such as YAP, TAZ [8] and RARG [5] in and out of the nucleus is another method of nuclear mechanoregulation. (e, E) External mechanical force can also lead to alteration in chromatin conformation, thereby changes transcriptional profile [16]. (F) Excessive force may induce dilation of the nuclear membrane and in some cases lead to transient ruptures, allowing the free diffusion and exchange of nucleoplasmic and cytoplasmic factors [17]. (G) Mechanical cues can also affect the higher structural organisation of the chromosomes and chromosomal territories [18]. Figure modified from [17, 19].

3.3. Biophysical Regulation of the Epigenome

Biophysical cues including static and dynamic mechanical properties, and micro/nano topographies present in the cellular niche have been widely accepted to be able to regulate a variety of cellular functions, including transducing signals from the surface of the cell to the nucleus. This phenomenon can regulate signalling molecules and lead to the regulation of transcriptional factors that alter gene expression and cell functions. More recently, several studies have also demonstrated that biophysical cues can influence cellular phenotypes, the differentiation potential of stem cells and the cellular reprogramming by regulating the epigenetic state of the cells. The following section presents a brief overview of epigenetics and highlights the potential mechanisms by which mechanotransduction may lead to epigenetic modifications.

3.3.1. Epigenetic Codes

Epigenetics refer to a series of molecular codes in cells that alter gene expressions without changing the underlying DNA sequences. Generally the DNA modifications occur through methylations and changes in chromosomal proteins like histone post-translational modifications which modulate the accessibility of specific DNA sequences by activating or silencing transcriptional factors.

3.3.1.1. Chromatin

The eukaryotic genomes are folded in a series of hierarchical packagings to form chromatins, *i.e.* highly ordered structures that contain DNAs, histones and other chromosomal proteins, in order to fit a large amount of DNA into the small nuclear compartment. The basic subunit of eukaryotic chromatin is the nucleosome, which consists of 147 base pairs (bp) of DNA wrapped around a complex of core histones (Fig. 25). Core histone is composed of H2A, H2B, H3, and H4 that assemble as one H3-H4 tetramer and two H2A-H2B dimers (Fig. 25). The genomic DNA sequence is wrapped 1.6 turns around the octamer resulting in a five- to tenfold compaction of the DNA [376, 377]. Adjacent nucleosomes are separated by a linker DNA sequence, which ranges from several kilobase pairs to as little as a few base pairs. In its compact state, the DNA is only partially accessible to regulatory proteins and is generally transcriptionally inactive. The compact nucleosome structure can be selectively unfolded by

conformational alteration of the nucleosomes, or if the DNA unwound to a certain extent from the histones to activate gene transcription. Additionally, histone tails hanging off the core complex are readily available and can be chemically modified by specific enzymes to create docking points to recruit a wide range of proteins involved in nucleosome remodelling and DNA unwinding, which can eventually lead to changes on the structure of the chromatin complex and downstream genomic regulations [378]. In general, the chromatin and nucleosomes can be altered by two main methods, and one accessory way (Fig. 25). First, the nucleosome can be directly remodelled by specific chromatin remodelling complexes which utilise ATP in the process. Second, the histone tails hanging off the nucleosome can be covalently modified by specific enzymes designed explicitly for the task of recruiting further chromatin remodelling complexes. Finally, different histone variants can replace one or more of the core histones present in the nucleosomal complex.

The location, timing and type of the modifications helped define the shape of the chromatin and the cellular epigenetic landscape and based on this the chromatin can be typically described in two forms: the transcriptionally active, euchromatin, and the transcriptionally repress, heterochromatin.

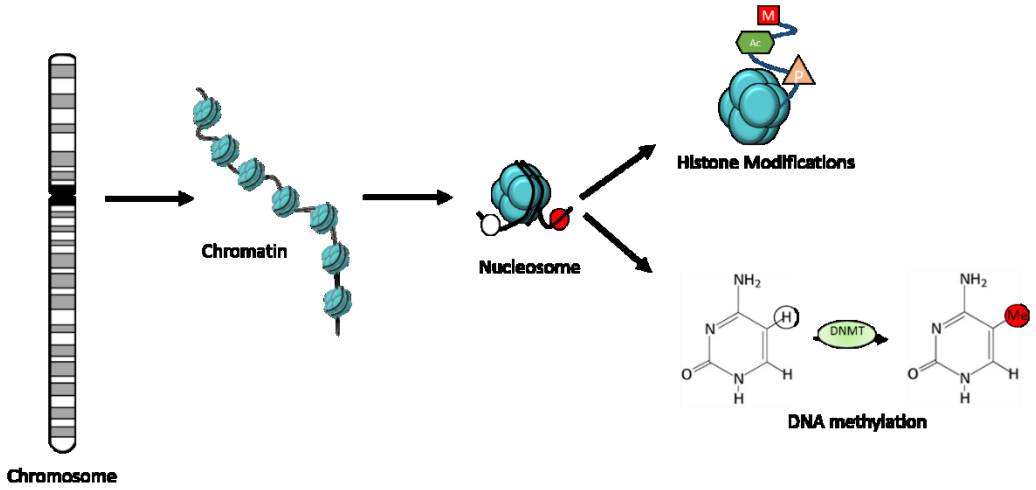


Figure 25. Chromosomal organisation and modifications. The fundamental subunit of the chromosome is the nucleosome, which consists of a DNA helix wrapped around core histones. Individual nucleosomes are further folded into a string of interconnected structures called chromatins. Further compaction leads to the formation of individual chromosomes which only exist during some stages during the cell cycle. The accessibility of the DNA sequences, and the structure of the chromatin fibres can be modified by two main chemical modifications: histone tail post-translational modification and DNA modification mainly methylation.

3.3.1.2. DNA Methylation

DNA methylation in mammals primarily occurs at the CG residues, and non-CG methylation only occurs in the actively transcribed region in stem cells [379, 380]. Cytosine methylation of the DNA is a critical epigenetic modification that plays essential roles in cellular functions including differentiation, embryonic development and even the maintenance of genome integrity [381]. Throughout the genome, approximately 60-80% of the CG residues are highly methylated, except CpG islands and actively transcribed regions where only 10% of the CGs are methylated [380]. Upon the addition of the methyl group on the CG residues, the promoters/genes are transcriptionally repressed.

In mammals, DNMT1, DNMT3A and DNMT3B are the enzymes responsible for the addition and maintenance of the methylation status of the genome. They all perform a slightly different function in the process. DNMT1 mainly function as a maintenance methyltransferase, while DNMT3A and DNMT3B are responsible for *de novo* methylation [382]. However, in certain circumstances such as at certain repetitive elements and single-copy sequences in ESCs, DNMT1 can exhibit considerable *de novo* methylation activity, and both DNMT3A and DNMT3B may also be required to maintain symmetrical CpG methylation [382]. Despite being chemically and genetically stable, 5-methylcytosine (5mc) can still be reversed to its original state by two different methods. One method occurs through a passive DNA demethylation, in which a lack of functional DNA methyltransferases responsible for maintenance can result in the dilution of the modified cytosine duringg DNA replication [383]. In the second method, TET proteins can mediate the active demethylation of the modified cytosine by iterative oxidation of the 5mc to 5hydroxymethylcytosine (5hmC), 5-formylcytosine (5fc) and 5-carboxylcytosine (5caC) [383].

Several studies in model organisms such as *Neurospora crassa* (fungal model) and *Arabidopsis thaliana* (plant model) provided strong evidence suggesting that DNA methylation is functionally linked to histone H3K9 methylation [384, 385]. As an example, factors such as ubiquitin-like PHD and RING finger domain-containing protein 1 (UHRF1/Np95) are capable of linking H3K9 methylation and hemimethylated DNA to stabilise DNMT1 binding [386].

3.3.1.3. Histone Post-Translational Modifications

In addition to DNA methylation, histone post-translational modifications (PTM) are well accepted as essential signals that carry information that dictate the state of the chromatin and the genes within the cell. The pioneering work on histone modifications by Allfrey *et al.* in the mid-1960s, have led to an explosive development in the field of epigenetic [387]. Since then, a large number of different histone PTMs have been reported and studied (Fig. 26 and Table 10). Histone acetylation, methylation, and phosphorylation are the most common form of histone PTMs.

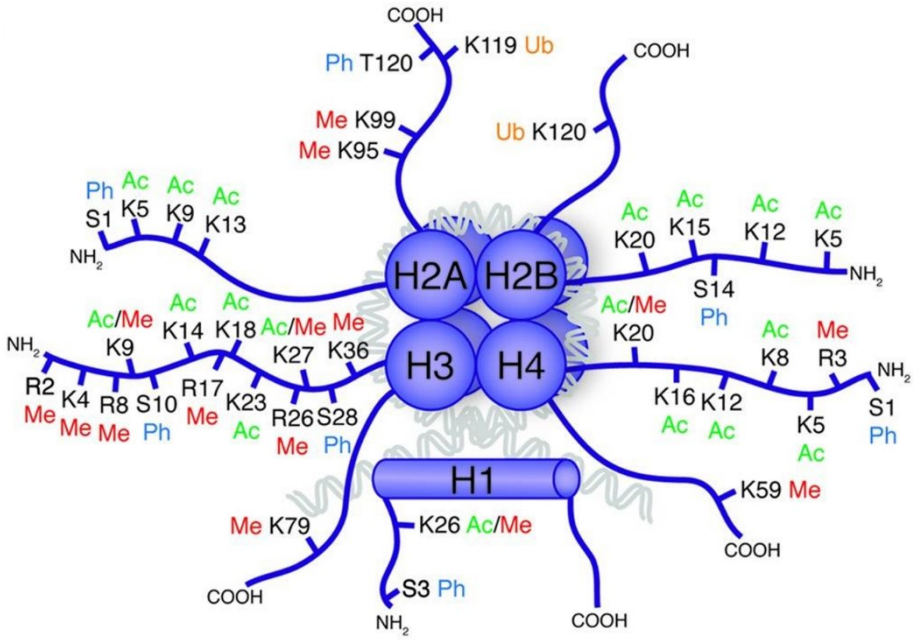


Figure 26. Single nucleosome with histone post-translational modifications. A diagrammatic representation of a nucleosome with the 4-main core-histones (H2A, H2B, H3 and H4) and the linker histone H1. The N-terminal and C-terminal of each histone tail can be subjected to a variety of covalent chemical modification that influence the accessibility and structure of the nucleosome. The covalent PTMs displayed on the figure include methylation (Me), acetylation (Ac), ubiquination (Ub), and phosphorylation (Ph). Figure adapted from [12].

Table 10. Different classes of histones modifications known and their associated functions. K= Lysine, R= Arginine, S= Serine, T= Threonine, E= Glutamic Acid, R= Arginine, P= Proline.

Chromatin modifications	Modified Residues	Functions Regulated
Acetylation	K-ac	Transcription, repair, replication and chromatin condensation
Methylation (lysines)	K-me1, K-me2, K-me3	Transcription and repair
Methylation (arginines)	R-me1, R-me2a, R-me2s	Transcription
Phosphorylation	S-p, T-ph	Transcription, repair and chromatin condensation
Ubiquitylation	K-ub	Transcription and repair
Sumoylation	K-su	Transcription
ADP ribosylation	E-ar	Transcription
Deimination	R>Cit	Transcription
Proline Isomerisation	P-cis>P-trans	Transcription

The acetylation of histones on the lysine residue was first reported by Allfrey *et al.* in 1964. This modification is highly dynamic and regulated by two families of enzymes with opposite functions: histone acetyltransferases (HATs) and histone deacetylases (HDACs) (Fig. 27). The addition of the acetyl group to the lysine side chain is mediated by the HATs, which uses acetyl CoA as a cofactor to catalyse the transfer [388].This modification weakens the interaction between histones and DNA due to the neutralisation of the lysine's positive charge and eventually leads to chromatin adopting a more relaxed state (open chromatin/euchromatin) (Fig. 28). The HATs can be categorised into two major classes: type-A and type-B. The type-A HATs can be further classified into three different sub-groups depending on the conformational structure and the amino-acid sequence homology: GNAT, MYST and

CBP/p300 families [388]. The type-A HATs are often found to be associated in large multiprotein complexes and functioning in numerous transcriptional coactivators [389]. Type-B HATs are highly conserved and are mainly present in the cytoplasm, acetylating free floating histones and not those already incorporated into the chromatin [388].

On the other hand, HDACs enzymes function to remove the acetylation on the lysine residue. The removal of the acetyl-group restores the positive charge of the lysine, and leads to the compaction/stabilisation of the chromatin structure locally and to transcription repression (heterochromatic stage) (Fig. 28). There are four distinct classes of HDAC. Classes I, II, and III, often referred to as sirtuins, require NAD^+ for their enzymatic activity. Class IV only has a single member, HDAC11 [389]. A single HDAC enzyme is capable of deacetylating multiple sites within the histones due to their low target specificity. Similar to HATs, the HDACs are often found to be present in multiple large complexes.

In general, histone phosphorylation occurs on the serine, threonine, and tyrosine residues in the N-terminal histone tails. This process is also highly dynamic, and the levels of phosphorylation in the histones are controlled by kinases and phosphatases that add and remove the phospho-group, respectively [390].

The addition of phosphate group to the hydroxyl group of the target amino-acid side chain by the histone kinases increases the negative charge of the histone, and this modification potentially alters the structure of the chromatin. It is not entirely clear how the kinases are successfully recruited to the target site on the chromatin. In some cases, the kinases might have a built-in DNA-binding domain with which it is bound to the DNA, or perhaps the enzymes may be recruited through association with other chromatin-associated factors before theydirectly interacts with the DNA [388].

The function and mode of action of the histone phosphatases arenot well understood. It is postulated that the level of histone phosphatase must be quite high within the nucleus given the rapid turnover of the phosphorylation status.

Unlike the other histone PTMs, the methylation of histone does not lead to alteration in the charge of histone proteins. The main sites for histone methylation are the lysine and arginine residues. Furthermore, the lysine residues can either be mono-, di-, or tri-methylated, whereas the arginines can be mono-, and symmetrically or asymmetrically di-methylated (Fig.

27). The status of histone methylation is tightly regulated by methyl-transferases and demethylases which add and remove the methyl group, respectively (Fig. 29).

The majority of histone methyltransferases methylate lysines within the N-terminal tails and posses a SET-domain which act as the enzymatic core, except for Dot1 enzyme which adds the methyl group within the globular core of H3K79 and does not possess a SET-domain. The addition of the methyl group mostly leads to transcriptional repression but in some instances the addition of methyl group can lead to transcriptional activation.

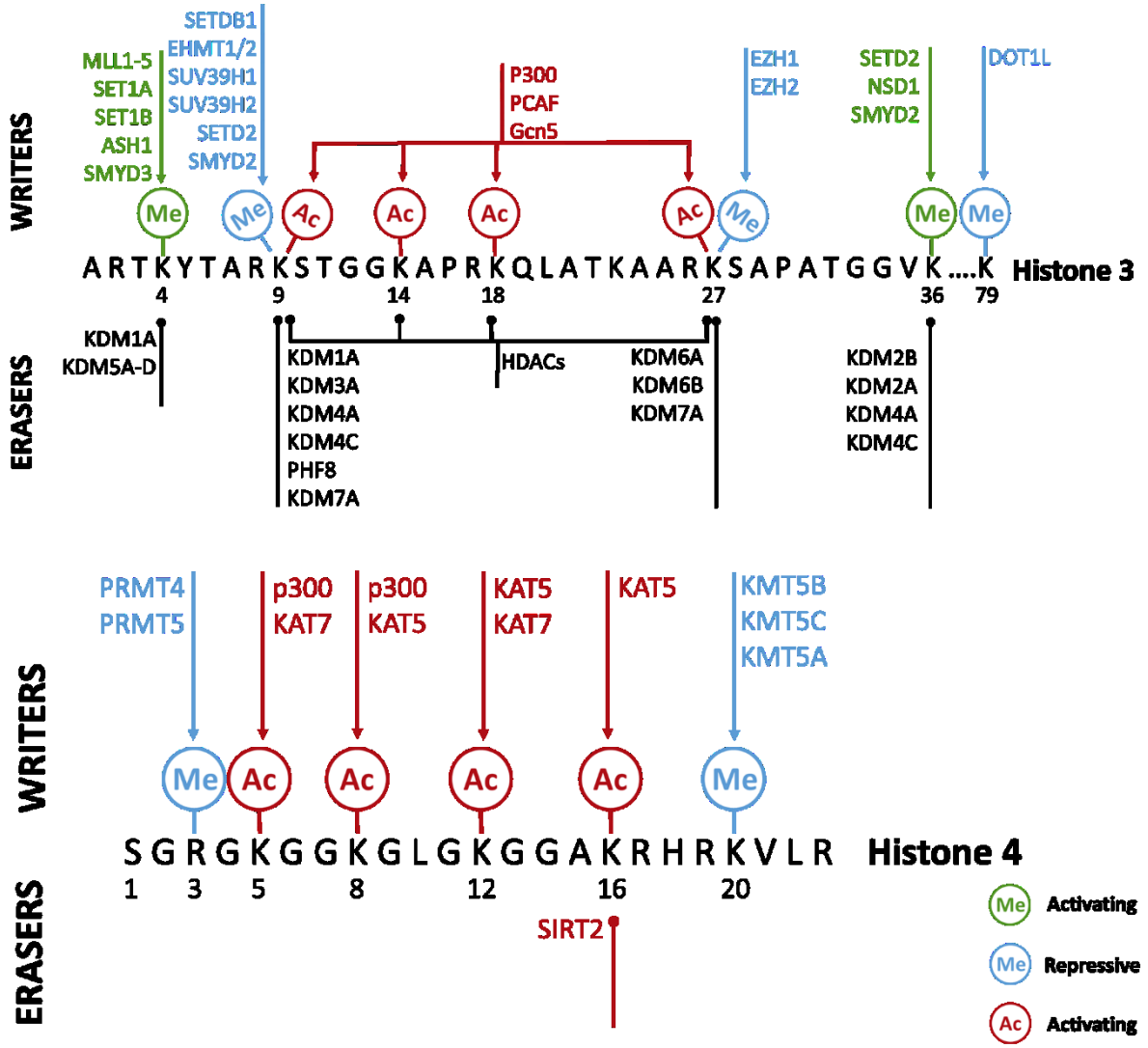


Figure 27. Histone post-translational modifications and their histone modifying enzymes. The histone modifications at the tail of histone 3 and histone 4, and the enzymes involved in the addition (writers) or removal (erasers) of the specific activating or repressing histone marks at the tail of histone 3 and 4.

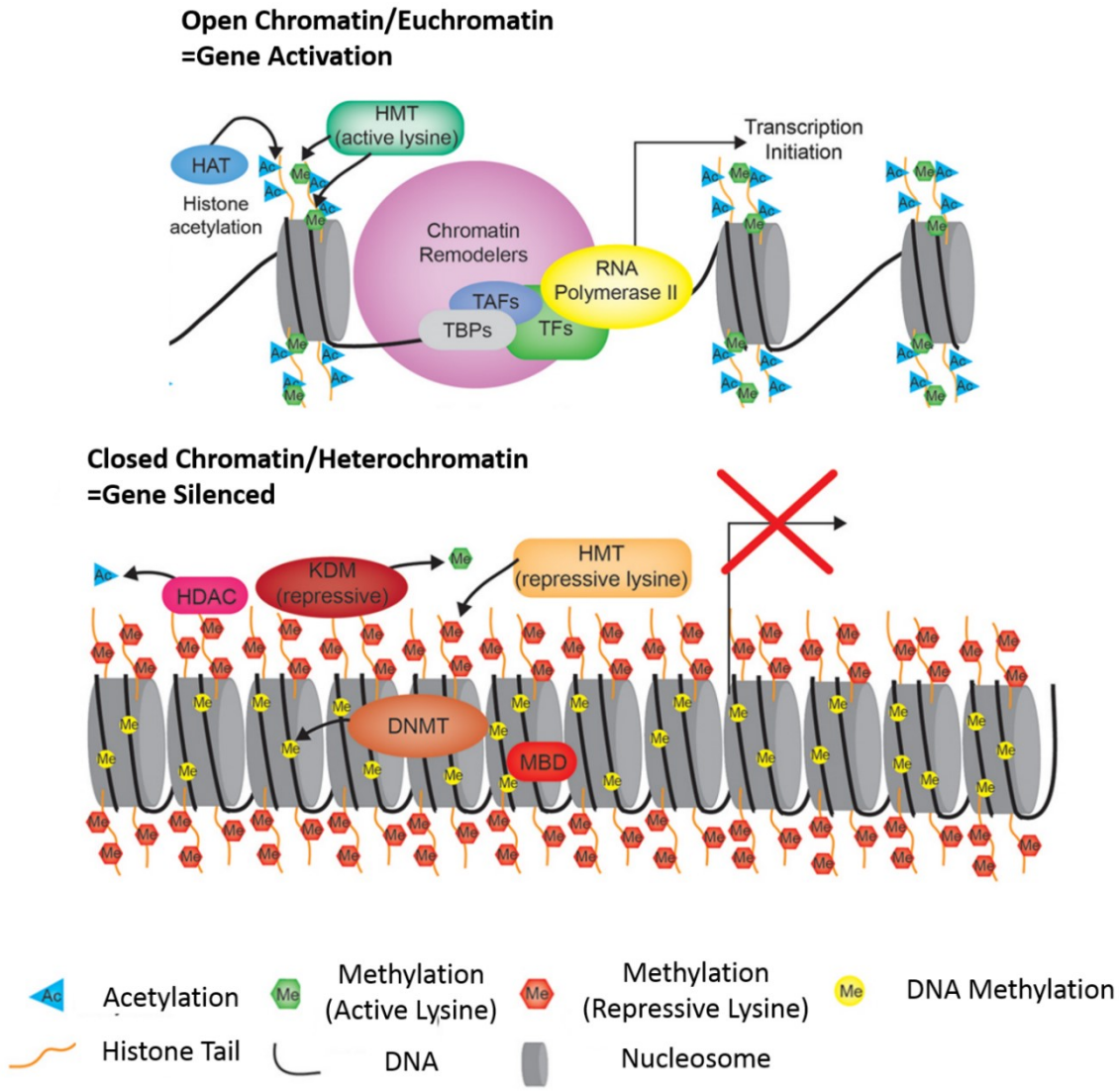


Figure 28. Chromatin status. Diagrammatic representation of an open relaxed chromatin (top section), decorated with a high level of histone acetylation and active lysine methylation markers. The chemical modifications lead to structural changes to the chromatin structure and enable further chromatin remodelling proteins and transcriptional machinery to bind to the DNA and initiate transcription of target genes. On the other hand (bottom section), a densely packed chromatin structure is associated with a silenced gene expression. The nucleosomes are densely packed and the histones tail are chemically modified with repressive methylation marks. The DNA is also methylated by DNA methyltransferases (DNMT). HMT: Histone Methyltransferase, HAT: Histone Acetyltransferase, TAF: TBP associated factors, TF: Transcription Factor, HDAC: Histone Deacetylase, KDM: Lysine (K) - specific Demethylase, MBD: methyl-CpG Binding Domain. Figure adapted from [14].

3.3.2 The Effects of Biophysical Cues on Chromatin

The nuclear envelope is directly linked to the cellular membrane through a series of cytoskeletal components which implies that any mechanical forces applied will have a direct effect on the nucleus. Within the nucleus, individual chromosomes occupy a specific territory based on its size and gene richness.

Heterochromatin (gene poor, transcriptionally repressed) tends to be closely associated with the nuclear lamina at the periphery of the nucleus, whereas euchromatin (gene-rich, transcriptionally active) typically localise at the centre of the nucleus. The positioning and configuration of these components within the nuclear space can also be useful to the identity the behaviour of a cell. Thus any physical forces imparted onto cells might change the organisation of the chromatin, accessibility of DNA for transcription, and chromatin location. For example, specific section of the chromatin might be pushed away from or into transcriptionally repressive regions, thus activating or suppressing gene expression.

As an example, as migrating immune cells [391] and cancer cells [392] move through the *in vivo* environment, they undergo extensive deformation of the cell shape in order to squeeze through tight interstitial spaces between cells or dense extracellular matrix. Several studies demonstrated that along with an alteration in cell shape, cells also experience frequent and transitory nuclear envelope ruptures, which led to chromatin rearrangements including herniation of the chromatin across the nuclear envelope into the cytoplasm [391, 392]. The transient nuclear ruptures caused by the manoeuvres are rapidly repaired by the endosomal sorting complexes required for transport (ESCRT) membrane-remodelling complexes.

Additionally, modifications of histone proteins via PTM such as methylation or acetylation have also been shown to strongly correlate with alteration in chromatin states. Recent work by Jain *et al.* demonstrated that histones modifications could be directly influenced by cell shape [393]. Through the use of micro-contact printing, they were able to pattern cells into various geometries and influenced the cell's histone profile and gene expression. Moreover, during cellular differentiation, simultaneous changes happen the in nuclear shape and structure. For example, embryonic stem cells display dynamic changes in chromatin compaction, reduction in chromatin mobility and upregulation of lamin-type A as they adopt a more specific cellular identity.

In recent years, increasing evidence suggests that different mechanical cues can influence gene expression profiles and cellular functions via epigenetic modulations in DNA methylation and histone PTMs. Most of these studies were conducted in the context of fluid flow in vasculature models. As an example, exposure to shear stress in endothelial cells can lead to the chemical modifications of both histones H3 and H4 which result in the change in eNOS gene expression [394, 395]. The effect of hemodynamic force on epigenetic modification in the cardiovascular system has also been extensively studied. It appears that different types of flow, such as laminar and oscillatory, induce a different type of epigenetic alterations. A study by Zeng *et al.* demonstrated that exposure to laminar flow increased the activity of class I HDACs, in particular, HDAC1 was shown to deacetylate p53 at Lys-320 and Lys-373 leading to cell cycle arrest in endothelial cells [396]. The application of oscillatory flow was shown to upregulate the expression and activity of both class I and class II HDACs. Class I HDACs were shown to regulate the proliferation of endothelial cells in response to disturbed flow while class II HDACs play a role in regulating the cells oxidative responses [397].Furthermore, class III HDACs were found to provide a protective role in atherosclerosis by downregulating the expression of a wide range of pro-inflammatory cytokines, preventingt the formation of foam cell and suppressing the expression of thrombotic factors [398]. A study by Zhou *et al.* demonstrated that non-directional oscillatory shear flow induces the overexpression and nuclear translocation of DNMT1 which eventally lead to DNA hypermethylation, however, this phenomenon was not observed in the sample treated with the unidirectional pulsatile shear flow [399]. DNA hypermethylation has recently been linked to the progression and overexpression of atherosclerosis promoting genes [400].

New techniques such as chromosomal painting pioneered by the Cremer's lab has further provided information regarding the three-dimensional organisation of individualchromosomes within the cell nucleus during interphase. The development and adaptation of chromatin immunoprecipitation (ChIP), chromosome conformation capture (3C), 4C, 5C and Hi-C along with the advancement in sequencing technologies enable methods to explore and understand the impact of chromatin positioning on gene expression and the overall cell phenotype in response to external stimuli including mechanical stimuli. Thus, through the manipulation of the extracellular microenvironment, it is possible to regulate the cellular geometry which has a significant impact on the chromatin structure. Furthermore,

the biophysically induced alteration in chromatin states could be essential in determining fundamental cellular behaviours and the establishment of cellular identity.

3.3.3 Biophysical Regulation of Epigenetic State in Cell Reprogramming

Cellular reprogramming represents one of the significant scientific advancement in the field of cell biology in the past decade and has widespread benefits in regenerative medicine, disease modelling and drug screening. Since the first-ever report on iPSC generation [185],researchers have used numerous methods to improve the efficiency of the reprogramming process and have discovered new methods to reprogram and convert cells into distinct cell types. In particular, the use of transcription factors (refer to [401] for an extensive review on this subject) and chemical compounds have been extensively explored. For example, valproic acid (VPA), a well known HDAC inhibitor, was shown to increase the percentage of $Oct4^{+}$ cells generated during iPSCs reprogramming [402]. Also, tranylcypromine hydrochloride, a potent inhibitor of lysine-specific demethylase, was also reported to improve the efficiency of reprogramming significantly [403]. Interestingly, the use of VPA in combination with the overexpression of a miR302/267 cluster in mouse fibroblasts has been shown to promote transcription-factor-free iPSCs reprogramming [404]. It is well known that these type of cellular conversion involves epigenetic modifications and these studies and others further support the crucial role of histone modifications and other epigenetic factors in cellular reprogramming (Fig. 29).

Extensive studies have been conducted to unravel the roles of transcription factors, miRNAs and small chemical compounds during these process. However, the role of biophysical cues in modulating critical epigenetic modifications in somatic cells, which might facilitate cell reprogramming is still not yet well understood. Further understanding of how biophysical regulation results in changes in gene expression via the modification of a cell's epigenetic state might reveal essential regulatory mechanisms during development, to be used in disease prevention and epigenetic cellular engineering.

In recent years, mechanical biophysical cues have been shown to impact cell behaviour via changes in epigenetic modifications. As an example, the expression and activity of various HDACs are controlled by cyclic mechanical loading in the form of oscillatory or pulsatile flow

in vascular endothelial cells, which results in an alteration in the cells migratory and replication phenotype [405].

Moreover, the culture of MSCs on 10 µm parallel microgroove substrates led to decreased activity of HDACs and subsequently corresponded to an increase in the level of histone acetylation [370]. Additionally, the application of compressive and tensile forces perpendicular to the microgroove substrates resulted in further decrease in HDAC activity. The researchers also demonstrated the importance of lamin proteins in mediating nuclear mechanosensing.

Furthermore, a pivotal study by Downing *et al.* showed that biophysical cues, in the form of nano-patterned parallel microgroove substrate, can replace the effects of small-molecule epigenetic modifiers and significantly improve reprogramming efficiency by fourfold via mechanomodulation of the cell's epigenetic landscape [66]. They seeded adult and embryonic fibroblasts transduced with virus encoding the OSKM reprogramming factors onto microgroove substrate and aligned electrospun nanofibrous scaffolds resulted in changes in cell morphology (more elongated). Alteration in the cell's shape leads to the modulation of the epigenetic state, specifically the decrease in HDAC activity and the upregulation of the WDR5, *i.e.* methyltransferases which lead to increase histone H3 acetylation and methylation. These epigenetic modifications, in turn, promote the cells to undergo a mesenchymal-to-epithelial transition (MET), a process required for the success of the reprogramming procedure. More recently, the same platform was also shown to enhance the trans-differentiation of cardiac progenitors into cardiomyocyte-like cells. The grooved substrate increased the acetylation of H3 and promoted the sumoylation of myocardin, a modification that actively promotes cardiogenic gene activity [226].

The findings discussed in this section highlight the ability of seemingly-subtle material cues to affect a cell's epigenetic state, as well as the functional consequence in priming cells for reprogramming, and subsequent stem cell function. As these recent works build a connection between biophysical regulators and differentiation and pluripotency, they bring into question what other unexplored individual or combined extracellular cues might control intracellular processes.

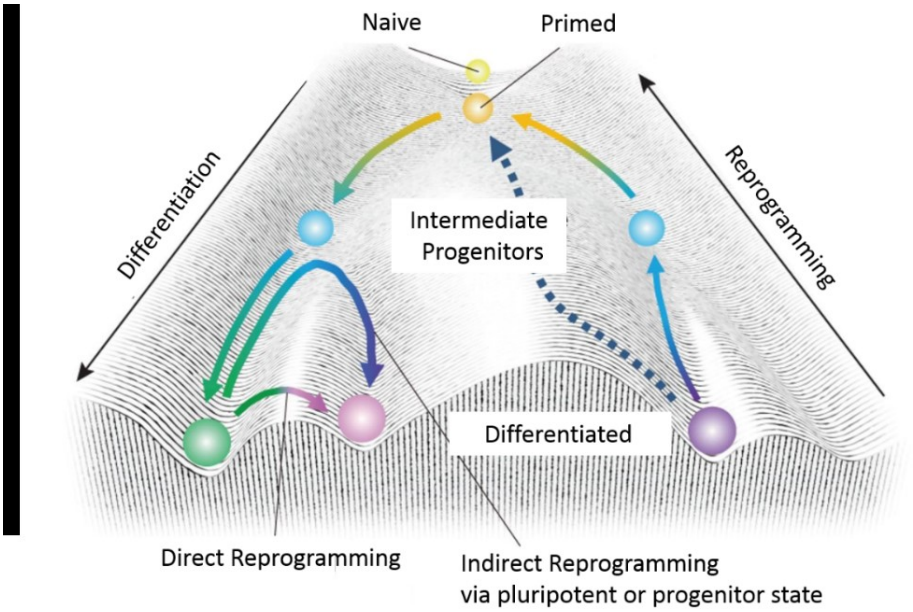


Figure 29. Epigenetic landscape of cellular reprogramming. Pluripotent stem cells (naïve in yellow and primed in orange) can differentiate into any somatic cells (green, pink, purple) through an intermediate state (blue). Cells can also change its cellular identity through direct reprogramming, using various methodologies including transcription factors, miRNAs, and chemical cocktails (green to pink), without going through the intermediate state. Fully differentiated mature cells (purple) can also revert to pluripotency (orange and yellow) via a progenitor state (blue arrow) or directly (dotted arrow). The combination of OSKM overexpression and specific optimal conditions for desired target lineage can be used to convert one cell type to another via a transient pluripotent progenitor state indirect reprogramming). These cell fate changes require extensive changes on the cell epigenetic landscape. Figure adapted from [15].

3.4. Aims

The aim of this study is as follows:

- Firstly, to understand the effect of nanoneedles on the nuclear structure and the remodelling that is induced.
- Secondly, to use a global hypothesis-generating approach to understand the extent of changes that might occur in the transcriptome and proteome of the cells following exposure to nanoneedle.
- Finally, the effect of nanoneedles on the regulation of the cell epigenome was explored.

3.5. Hypotheses

- **Firstly, the use of nanoneedles will not affect the viability of the MEFs.** A combination of fluorescent imaging and FACS techniques is used to validate this point.
- **Secondly, this study proposes that the nNs will influence a wide range of cellular functions, in particular, the cell cytoskeletal components, the defence machinery and the nuclear complexes.** RNA sequencing and global label-free proteomics in conjunction with pathway analysis is used to evaluate the overall changes in the cell signalling on the global scale.
- **Next, the application of nanoneedles might lead to dramatic changes in the nuclear structures and consequently the distribution and organisation of the chromatins.** Fluorescent microscopy including super-resolution imaging techniques is used to validate this point.
- **Finally, the nanoneedle could also modulate histone and DNA modifications and the expression of the enzymes responsible for their fine control.** The expression of the genes and modifications is assessed using standard western blot and quantitative RT-PCR.

3.6. Materials and Methods

3.6.1. Cell Culture

MEFs were used in this study due to their embryonic nature; they are more susceptible to alteration in epigenetic and cellular state. Moreover, MEFs is the standard used in direct reprogramming experients to iPSCs or other cell types. Thus, we can also potentially investigate the effect of nanoneedle on the efficiency of iPSCs generation from MEFs if the results from the study indicates that the presence of nanoneedle can promote the transitional process.

CF1 mouse embryonic fibroblasts were obtained from Amsbio (ASF-1201). MEFs were isolated from 13.5-day old mouse embryos and cultured according to standard mammalian tissue culture protocols and sterile techniques. The CF1 MEFs used in the study were obtained between passage 3 and passage 4. The cells were cultured in high glucose Dulbecco's Modified Eagle Medium supplemented with 10% (v/v) heat-inactivated FBS, 1% (v/v) Pen/Strep and 2 mM L-glutamine. MEFs were seeded at a density of 30,000 cells/cm^2 on a tissue-culture dish, or at 80,000 cells/nN chip. A higher cell density were used to plate on the nN because previous experiments within the group has shown that seeding at this density will lead to simillar cell density post-attachment as in TCP. Since due to the geometry of the nanoneedle substrate some cells might failed to attached.

3.6.2. Cells Viability Assays

MEFs were seeded 24 h prior to the assay on either nN chips or normal tissue culture plastic (TCP) as a control. Following the incubation, nN chips containing MEFs were moved to fresh wells to exclude cells that attached to either the edge or the TCP underneath the substrate. The cells viability were measured using three different method.

Firstly, the viability of the cells cultured on nN chips vs TCP were assessed using flow cytometry with the LIVE/DEAD™ Fixable Violet Dead Cell Stain Kit (405nm excitation) from Invitrogen (L34955). In order to have enough cell numbers for the assay, 5 nN chips were pooled into one biological replicate. The same was performed on cells cultured on TCP. The assays were performed according to the manufacturer's guidance. The samples were analysed with the LSRII flow cytometer (BD, UK) equipped with 405 nm violet excitation laser and 450/50 nm collection filter. The data collected were analysed with FlowJo v10.

Next, the viability of the cells were also assessedusing a fluorescent imaging-based method. The samples were labelled with calcein-AM (green fluorescent) and ethidium homodimer-1 (red fluorescent) to indicate live and dead cells, respectively. The protocol provided by the LIVE/DEAD^{TM} Viability/Cytotoxicity Kit (ThermoFisher, L3224) was used. Samples were imaged live with the Olympus IX 71 fluorescent microscope using a green and red filter cube while maintaining constant acquisition parameters across all chips and times. For each sample, 5 images were acquired in random positions ensuring that both the central and peripheral region of the culture substrate were imaged.

Finally, the level of active caspases was analysed with the Vybrant FAM Poly Caspases Assay Kit (V35117) according to manufacturer's protocol. The samples were analysed with the LSRII flow cytometer (BD, UK) equipped with 488 nm green excitation laser and 530/30 nm collection filter. The data collected were analysed with FlowJo v10.

3.6.3. RNA Expression Analysis

3.6.3.1. RNA Isolation from *In Vitro* Cells

RNA was isolated with TRIzol Reagent (Thermo Fischer Scientific, 15596026) in combination with the Direct-zol Miniprep isolation kit (Zymo Research, R2052). The following modifications were made to the Direct-zol Miniprep isolation procedures. Cell pellets were dissolved in 1 ml TRIzol. The supernatant was immediately snap-frozen on dry ice, and before isolation, the samples were thawed on ice. Following that, 0.2 ml chloroform/isoamyl alcohol 24:1 (Across Organic, ACRO327155000) was added and shaken vigorously for a few seconds, then incubated for 10 min at room temperature (RT). The samples were centrifuged at 12,000 rcf for 15 min at 4°C, and the aqueous phase containing the RNA was carefully removed and transferred to a new DNA lo-bind tube (Eppendorf). An equal volume of absolute ethanol (Across Organic, 10517694) was added to the collected aqueous solution and mixed to form a homogeneous solution. The solution was then applied to the column, and the remaining step of the isolation process was as described in the isolation procedures provided with the kit. The eluted RNA was stored at -80°C.

3.6.3.2. cDNA Synthesis and Quantitative RT-PCR

RNA samples were gently thawed on ice, and the concentration was quantified with a NanoDrop 2000/2000c UV-Vis spectrophotometer (Thermo Fischer Scientific). RNA was reverse transcribed into a single-stranded cDNA with the QuantiTect Reverse Transcription Kit (Qiagen, 205313). Quantitative RT-PCR was carried out with SYBR Green chemistry in 384-well plates in a reaction volume of 10 µl as listed in the table 11. A list of the SYBR Green primers used in the study can be found in table 13.

Table 11. SYBR Green qRT-PCR reaction mix.

SYBR Green-based qRT-PCR reaction	
KiCqStart One-Step ReadyMix, Low ROX	5 µl
Forward Primer (0.5mM)	0.5 µl
Reverse Primer (0.5mM)	0.5 µl
cDNA (10ng)	X µl
Nuclease-free water	10-x µl
Total per reaction	**10 µl**

All quantitative RT-PCR reactions were performed on the QuantStudio 6 Flex Real-Time PCR System (Thermo Fischer Scientific) according to the following thermal cycling profile (Table 12).

Table 12. SYBR Green qRT-PCR thermal cycling profile.

SYBR Green-based reaction	Step1	Step 2	Step 3	Step 4
Cycles	1 x	40 x	40 x	
Temperature (°C)	95	95	60	Melt
Time	30 sec	5 sec	30 sec	Curve

Table 13. SYBR primers used in this study.

Primers	Sequence (5' -> 3')	Primers	Sequence (5' > 3')
F_*GAPDH*	AGGTCGGTGTGAACGGATTTG	**R_*Kat2b***	AGAAGCTGGAGAAACTCGGC
R_*GAPDH*	TGTAGACCATGTAGTTGAGGTCA	**F_*Dnmt1***	ATCCTGTGAAAGAGAACCCTGT
F_*Kmt2d*	GTGGCTGTTCCACACCCAG	**R_*Dnmt1***	CCGATGCGATAGGGCTCTG
R_*Kmt2d*	AGCTTGAGCTTCTCAGCATCG	**F_*Dnmt2***	TACCACCCAAGTTATTGCTGC
F_*Kmt2a*	GCAGATTGTAAGACGGCGAG	**R_*Dnmt2***	TCGTAAAGCACATGGACCTTC
R_*Kmt2a*	GAGAGGGGGTGTTCCTTCCTT	**F_*Dnmt3***	AGCGGGTATGAGGAGTGCAT
F_*Wdr5*	GATCCATCACGGTTGAAATG	**R_*Dnmt3***	GGGAGCATCCTTCGTGTCT
R_*Wdr5*	CAACCTCATCGTCTCAGGGT		G
F_*Ash2l*	TTGCTTCCGGAGAAAGTAGG		
R_*Ash2l*	TGTACAAAATGGTTCACCGC		
F_*Kdm6a*	AGACTCCACTTTCCCTTCAGC		
R_*Kdm6a*	CTTTTCGGGTTCGTGAGGT		
F_*Kdm6b*	TGAAGAACGTCAAGTCCATTGTG		
R_*Kdm6b*	TCCCGCTGTACCTGACAGT		
F_*Kdm2b*	CGAGCTCCTGCTGTTGTTC		
R_*Kdm2b*	TCAGCTGGCCAAAGAAAACT		
F_*Kdm6b*	CCAGACTGCCAGAATCGCTTT		
R_*Kdm6b*	CAGGTGCTTTTTGAGGCCA		
F_*HDAC6*	CAGCAAAGTAAGCTGGGGTG		
R_*HDAC6*	CTTGCTGGTGGCCGTATTAT		
F_*HDAC1*	ATGGTAGCCACCACAAAGGA		
R_*HDAC1*	AGAGAAGCTGCTGTCCGATG		
F_*Kat2b*	CTGGAGGTCTCCTCTTGGTG		

3.6.3.3. RNA Sequencing and Analysis

Total RNA was extracted from cells cultured on either nN chips or TCP after a 24-hour incubation on the respective substrate. A total of 4 biological replicates for each condition were sent to sequencing. RNA was processed for Illumina HiSeq by the gene core facility at the European Molecular Biology Laboratory. The raw data obtained underwent quality

control checks, sequence alignment and differential expression analysis. These checks were performed by the Imperial College Bioinformatics Data Science Group. Ingenuity Pathway Analysis from Qiagen and EnrichR bioinformatics resources v6.8 were used to analyse the differentially expressed genes.

3.6.4. Protein Expression Analysis

3.6.4.1. Protein Isolation

Total protein lysates were isolated using RIPA buffer (Santa Cruz, sc-24948) supplemented with 1x Phosphatase Inhibitors (Roche Applied Biosystems, 04906845001) and 1X Protease Inhibitor Cocktail (Roche Applied Biosystems, 04693159001). The protein lysates were homogenised for 20 sec on ice and centrifuged at 12,000 rcf for 10 min. The supernatant was then transferred to a protein lo-bind tube. The protein concentration was determined by the DC Protein Assay Kits (Bio-Rad, 500-0112).

3.6.4.2. Western Blotting

Protein samples were denatured for 10 min at 95°C in 4x Sample Buffer (Bio-Rad, 1610747) supplemented with 0.1 M β-mercaptoethanol. The proteins were separated by denaturing sodium dodecyl sulfate-polyacrylamide gel electrophoresis (SDS-PAGE) in 4-20% Mini-PROTEAN TGX Precast Protein Gels (Bio-Rad, 4561094) for up to 1 h. Proteins were transferred to a low fluorescence PVDF membrane (Bio-Rad,1704274) with the Trans-Blot Turbo following the protocol recommended by the kit.

The membrane containing proteins were blocked for two hours in Blocking Solution that contains either 5% (v/v) semi-skimmed milk or 5% (v/v) BSA in 0.1% (v/v) TBS-Tween-20 (Sigma, P5927) at RT. Following this step, the respective primary antibody diluted in blocking solution was added to the membrane and was left to incubate overnight at 4°C with gentle agitation. Post incubation with the primary antibody, the membrane was washed five times in 0.1% (v/v) TBS-Tween-20 solution for 5 min each and incubated with the appropriate infrared labelled secondary antibody (LiCor) diluted in the blocking solution for one hour at RT. The membrane was once again washed following the same step as before and scanned and analysed with the Odyssey imaging system and software (LiCor). List of antibodies used in the study is listed in Table 14.

Table 14. Primary antibodies used for immunofluorescence (IF) and western blot (WB)..

Antigen Target	Species Raised	Isotype	Application used (conc in µg/ml)	Company	Product Code
Nuclear Epigenetic Markers					
H3K27me3	Mouse	IgG	WB (1) IF (1)	Abcam	ab6002
H3K4me3	Rabbit	IgG	WB (1) IF (1)	Abcam	ab8580
H3K9/K14ac	Rabbit	IgG	WB (1)	Cell Signalling	9677
H2A.X(Ser139p)	Rabbit	IgG	IF (1)	Cell Signalling	2577
5-Methylcytosine	Mouse	IgG	IF (1)	Active Motif	33D3
Whole Cell Loading Control					
GAPDH	Rabbit	IgG	WB (1)	Santa Cruz	sc-25778

3.6.4.3. Immunostaining

Cells grown on either TCP or nN chips were initially washed with PBS and fixed with freshly prepared 4 % (v/v) paraformaldehyde in PBS (pH 7.4) for 10 min at RT. Then, the cells were washed three times with PBS for 5 min each and permeabilised with 0.4 % (v/v) Triton X-100 (Sigma, X100) for 10 min at RT on a rotating platform. The samples were then blocked for 2 hours in the IF blocking solution (see Table 15) at RT with gentle agitation. Primary antibody diluted in IF blocking solution as shown in Table 14 was added to the samples and left to incubate overnight at 4°C. The samples were washed five times with 0.1% (v/v) PBS-Tween-20 for 5 min each before the addition of species-specific secondary antibody conjugated with Alexa fluorophores (Table 16). After one hour of incubation and wash, the samples were counter-stained with 4 ug/ml 4'6-diamidino-2-phenylindole (DAPI; Sigma, D9542) in PBS for 5 min at RT. A solution containing DAPI was removed and replaced with VECTASHIELD Antifade Mounting Medium (Vector Laboratories, H-1000) to prevent the bleaching of the fluorophores. Samples were covered with aluminium foil and stored at 4°C. Images were

acquired using an Inverted Widefield Axio Observer (Zeiss) and anElyra PS1 (Zeiss) microscope.

Table 15. Immunofluorescence blocking solution recipe

Immunofluorescence Blocking Solution	
5% (v/v) BSA	Invitrogen (B14)
0.1% (v/v) Tween-20	Sigma Aldrich (P1379)
0.3M Glycine	Sigma Aldrich (50046)
PBS	Thermo Fisher Scientific (10010023)

Table 16. Secondary antibodies used for immunofluorescence (IF) and western blot (WB).

Antigen Target	**Species Raised**	**Isotype**	**Application used (conc in µg/ml)**	**Company**	**Product Code**
Anti-mouse IgG, Alexa 488	Goat	IgG	IF (1)	Thermo Fischer	A-11001
Anti-rabbit IgG Alexa 488	Goat	IgG	IF (1)	Thermo Fischer	A-11008

3.6.4.4. Label-Free Mass Spectrometry

For each replicate of the experiments, 10 nanoneedle chips (containing ~8 x 10^4 cells each) were used. The cells were harvested with ice-cold PBS, and lysed in lysis buffer (8 M Urea, 1% (v/v) SDS, 50 mM Tris pH 8.5, 1X PhosphoStop and 1X Complete Protease Inhibitor). Cell lysates were sonicated for 1.5 min at 10% power to destroy the DNA, and further incubated on ice for 15 min. After centrifugation at 15,000 g for 15 min at 4°C, the cleared lysates were transferred to a new tube. The concentration of protein lysates was quantified using the micro BCA. Then, in-solution tryptic digestion, MS/MS experiments, and initial peptide mapping and quantification were performed by the Proteomics Biomedicum core facility at the Department of Medical Biochemistry and Biophysics at Karolinska Institutet.

A list of differentially expressed proteins was then further analysed with Qiagen IPA tools and EnrichR.

3.6.5. Statistical Analysis

Statistical analyses were performed with GraphPad Prism software (version 5). All results are displayed as the mean ± standard deviation (SD). One-way ANOVA analysis followed by Tukey and Bonferroni post-hoc test was used unless stated otherwise.

3.7. Results

The concept of this study and results presented in the following chapter were acquired by the author of this thesis, unless stated otherwise.

3.7.1. The Viability of Cells Cultured on Nanoneedle Chips

Prior to further investigations into cellular behaviours of cells cultured on the nN chips, the viability of the cells on the nN chips versus that on normal TCP were first compared. In general the initial phase of apoptosis occurs relatively fast within hours from the applied stimulus, and late phase apoptosis which includes caspase activation, nuclear condensation and formation of apoptotic bodies occurs from as little as 3-4 hours to 24-48 hours [458]. Moreover, the nanoneedle used in the study will degrade and completely disappear after 24 hr of incubation [9]. To this end, the cells were seeded in either TCP control of nanoneedle substrate for 24 hr and three different assays to assess several aspects of the cellular status were used to give a detailed view cell behaviour on nNs.

Firstly, a dye which covalently binds to intracellular and extracellular amines was utilised to discriminate between cells with intact and compromised membranes. In cells with compromised cellular membranes, the dyes can diffuse into the intracellular space and react with the free amines inside and on the cell surface, resulting in an intense fluorescent signal. Whereas in viable cells, the dyes are only able to react to cell-surface amines, yielding less intense fluorescence. The difference in fluorescent intensity allows for easy discrimination between the two groups. MEFs were seeded on the nN chips and TCP as a control substrate and cultured the cells in the same conditions for 24 hours. Post-incubation, the cells from both substrates were collected and labelled them with the viability dye and analysed them using flow cytometry (Fig. 30 a, b). Cells grown on nN chips and TCP had an average viability of 98.75% and 96.25%, respectively. Suggesting that the use of nN chips as a growth substrate did not seem to affect the viability of the cells in comparison to cells grown on TCP.

To confirm this conclusion, the same experimental setup was performed but changed the dye used to label live and dead cells. Green-fluorescent calcein-AM was used to indicate active intracellular esterase activity, a sign of healthy viable cells, and red fluorescent ethidium homodimer-1 to indicate the loss of plasma membrane integrity, an indicator of dying or dead cells (Fig. 30 c, d). An increase in the percentage of cells positive for the ethidium homodimer-

1 signal was detected when the cells were cultured on the nN chips. However, the changes were not statistically significant. The results from this assay seem to agree with the results from the methods used above. The difference in the percentage of dead cells observed between the two methods could be due to the difference in the targets of the dye used. Green-fluorescent calcein-AM emits high fluorescence upon binding to free amines, while ethidium homodimer-1 only becomes fluorescent upon binding to the DNA.

The nNs might induce slight membrane permeability in the basal membrane of the cells and thus enable the cell impermeable dyes to gain access to the intracellular space and label the cells as dead even though they might be functionally healthy. To address this issue, an assay to detect the level of active caspases in the cells was conducted to determine the number of cells undergoing apoptosis. Using a commercially available kit that is based on a fluorescent inhibitor of caspases (FLICA) methodology, the FLICA molecules have a FAM dye attached to them that is cell permeant and non-cytotoxic. The FLICA molecules bind to the active caspases present inside the cells, and any unbound molecules diffuse out and wash away. The remaining green-fluorescent signal in the cell is a direct measure of the number of active caspases that were present at the time the inhibitor was added. Using this same experimental setup, no significant difference in the percentage of active caspases in cells cultured on the nN chips (Fig. 30 e, f).

Considering the results from the different methods to assess cell viability, it is safe to conclude that the nN chips did not induce any detrimental damages to the cells that can lead to the initiation of apoptosis and cell death within the investigated time point. The assays were only conducted at Thus, the nN chip can be safely used as a substrate to culture MEFs for further investigation.

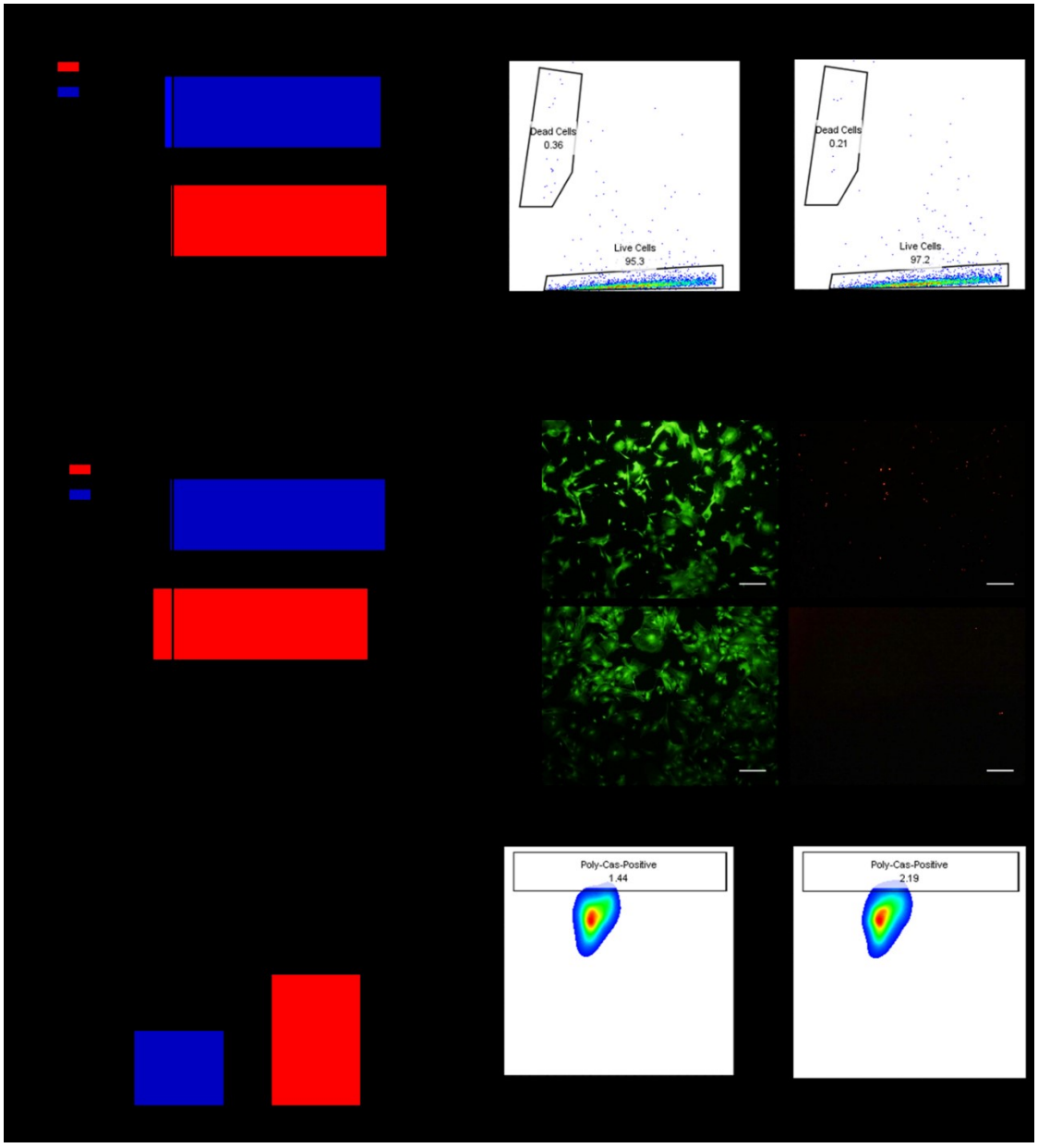


Figure 30. Characterisation of MEFs viability on nanoneedles. (A-B) Flow cytometry results and representative plots showing the percentage of live and dead cells present on cells cultured on nNs versus TCP at 24 hours post-seeding. Mean ± SD, N = 1, n = 2. (C) Percentage of calcein-AM (live cells) and ethidium homodimer-1 (dead cells) positive cells as quantified via flow cytometry. (D) Representative fluorescence microscopy images of live cells (in green) labelled with calcein-AM and dead cells (in red) labelled with ethidium homodimer-1 on nNs and TCP at 24 h post-seeding. Mean ± SD, N = 5, n = 10. Scale bars = 100 µm. (E-F) Flow cytometry analysis and representative plots of the percentage of active caspases in MEFs cultured on nNs and TCP at 24 h post-seeding as a function of cellular viability. The use of nNs as culture substrate did not induce apoptosis and cell death in MEFs. Mean ± SD, N = 3, n =5.

3.7.2. Nanoneedle Induced Nuclear Remodelling

Several studies have shown that the nucleus can adopt different shapes in response to mechanical confinement by arrays of microposts [406-409] and geometrical constraint by micropatterned adhesion molecules [393, 410]. These studies provide insight into how cells can sense and adapt to their microenvironment under prolong nuclear deformation by altering their gene expression profiles, actin cytoskeletal complexes and even differentiation potentials. However, the deformations induced by these materials are on the micrometre scale. In an *in vivo* setting, nuclei exhibit deformations on a much smaller scale (nanometres), such as a compressive force from a single collagen fibre [411] or in nuclei from lamin-A deficient individuals [412].

Advancement in nanotechnology and microfabrication have led to the burgeoning of vertical nanoneedle or nanowire structures. A study by Hanson *et al.* demonstrated that vertical nanopillars could be used to induce nuclear deformation and the extent of the nuclear deformations can be controlled by varying the geometry of the array [100]. The use of transmission electron microscopy also revealed significant nuclear membrane deformation in fibroblasts cultured on vertical nanowires [413].

The nanoneedles might also induced a nuclear membrane deformation and the rearrangement of the nuclear components. To test this hypothesis, MEFs cultured on nanoneedle chips and TCP were fixed and immunolabelled with anti-lamin A (Fig. 31) to reveal the shape of the nuclear envelope. In a three-dimensional confocal scan, the nuclear envelope does not appear on a single optical plane, the nuclear envelope directly on top of each nanoneedle is push further up away from the surface than in neighbouring pixels (Fig. 31a, b). The nuclear envelopes of cells on nanoneedle chips are also highly tortuous, with most cells showing well-resolved lamin A rings in the nucleus over each nanoneedle and a few exhibit trenches in the nucleus perpendicular to the alignment of the nanoneedles. The extent of the nuclear deformation caused by the nanoneedle is visible in a side-view reconstruction of the images (Fig. 31a, b). Furthermore, a DAPI staining was also performed to the MEFs on TCP or nanoneedle chips 24 h post seeding to assess the presence and distribution of heterochromatin foci.

On closer investigation by structured illumination microscopy (SIM), indeed that the nuclear shape deformity results from the mechanical confinement introduced by the presence of the vertical nanoneedles (Fig. 32a). Quantitative analysis of the nucleus revealed a significant reduction in nucleus area when compared to cells on TCP (Fig. 32a, b). Significant rearrangement of the heterochromatin foci was also observed, with cells on nN chips likely to have approximately a third fewer heterochromatin foci within the nucleus (Fig. 32a, c), and individual foci display higher DAPI intensity (Fig. 32d). However, no change in the average size of the foci was observed (Fig. 32e). Despite the reduction in the number of heterochromatin foci, when normalised to the reduced nuclear size in cells cultured on nN; leads to increase porportion of the nucleus area occupied by the heterochromatin foci (Fig. 32f).

The analysis performed were 2-dimensional in nature, and since the nucleus is a 3-dimensional object; further investigations into the effect of nanoneedle on the volume of the nuclear components might provide extra information into how the cells responds and interacts with the presence of the nanoneedle.

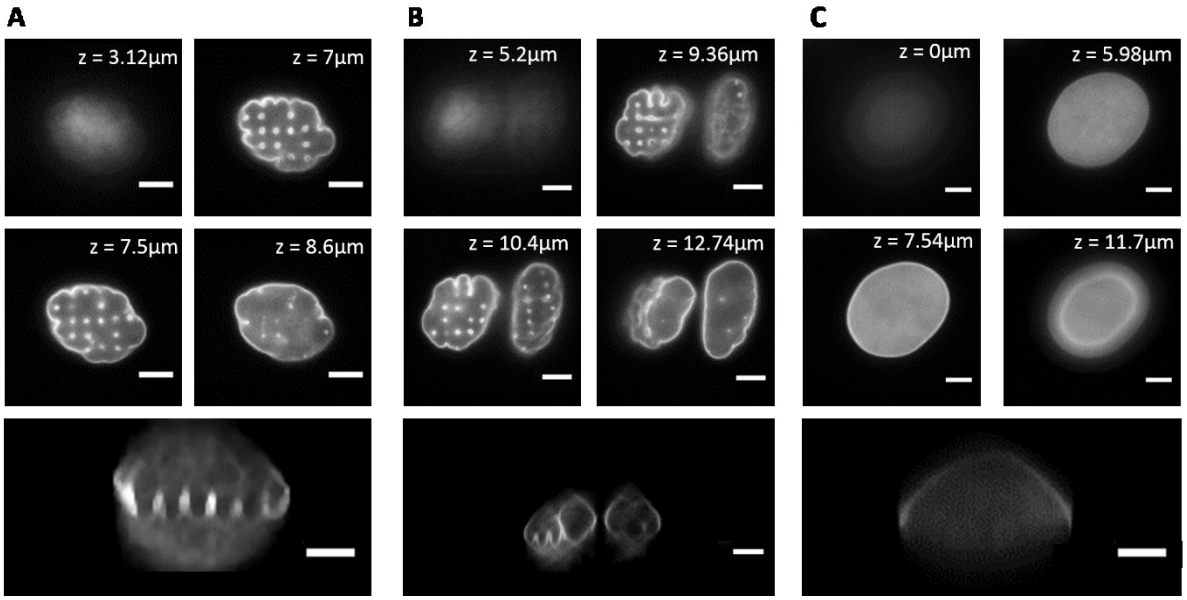


Figure 31. Nanoneedle-induced nuclear deformation. (A, B) Immunostaining of lamin A reveals nuclear deformation in cells cultured on nanoneedles via confocal microscopy. Four optical z slices are shown, beginning from the basal surface of the cell to the apical surface. The reconstructed side view of the confocal scan is also shown (bottom images) (C) MEFs cultured on the TCP control surface did not show any nuclear deformation. The nanoneedle has the following dimensions: 50 nm apical radius, 600 nm basal radius, 2 µm pitch and 5 µm height. Scale bars = 5 µm. Images were acquired by Catherine Hansel.

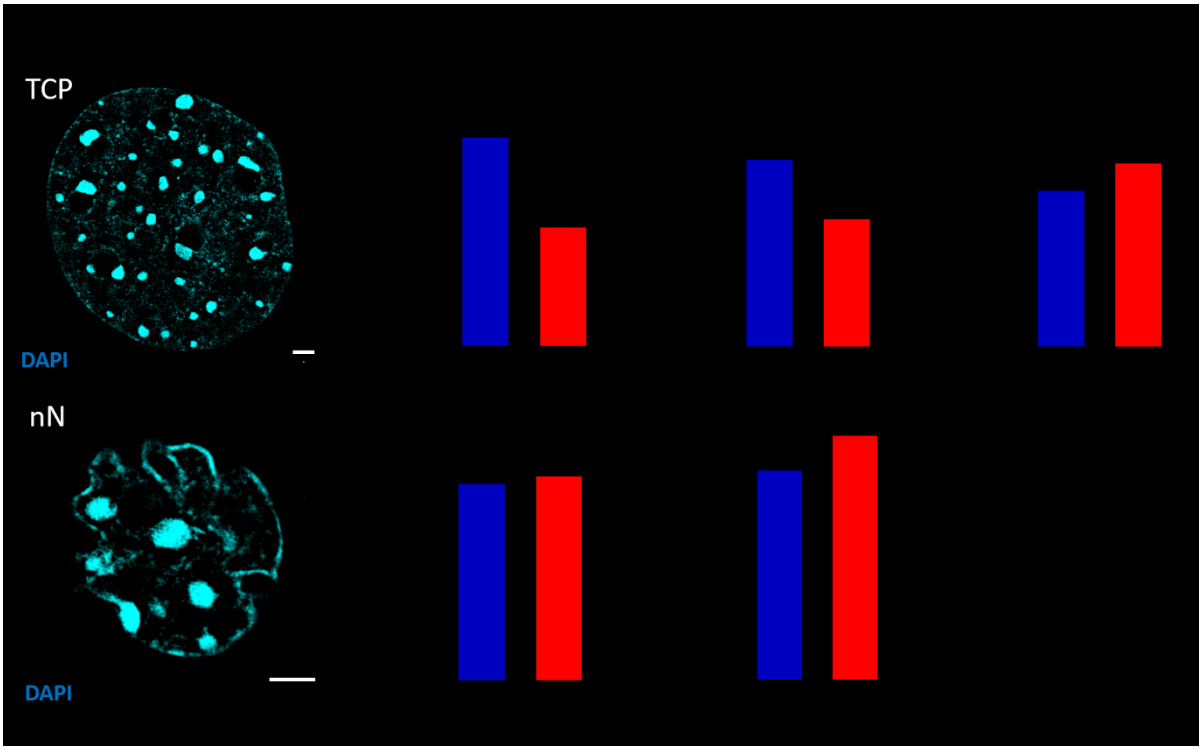


Figure 32. Quantitative analysis of nanoneedle-induced nuclear deformation. (A) DAPI stained nucleus revealed nuclear deformation in SIM. (B) Average nuclear area showing a smaller nuclear size for cells on nN than for cells on TCP. (C) Average number of heterochromatin foci showing less heterochromatin foci in MEFs cultured on nN than on TCP (D) Average intensity of heterochromatin foci revealed that cells on nN chips have a denser heterochromatin foci structure. (E) No difference observed between the average size of heterochromatin foci in cell on TCP and nN. (F) Total area occupied by the heterochromatin foci normalised to nuclear area. Comparisons were analysed with two-tailed, unequal variance Student t-test, corrected for multiple comparisons where necessary. *$p \leq 0.05$, **$p \leq 0.01$, ****$p \leq 0.0001$. Mean± SEM. N = 3. Scale bars = 2 µm. Images were acquired by Catherine Hansel.

To investigate whether nanoneedles induce nuclear condensation, FACS with a DNA intercalating dye was used to investigate the difference in the condensation profile of the cells on the different substrates. The DNA intercalating dye brightly stains the condensed chromatin, but only dimly stains the uncondensed chromatin. The cells were cultured on TCP and nanoneedle chips for 24 hours and labelled with the dye. No difference in the mean fluorescence intensity was found between cells cultured on TCP and nN chips (Fig. 33). These results indicate that nanoneedle-induced nuclear remodelling did not lead to nuclear condensation.

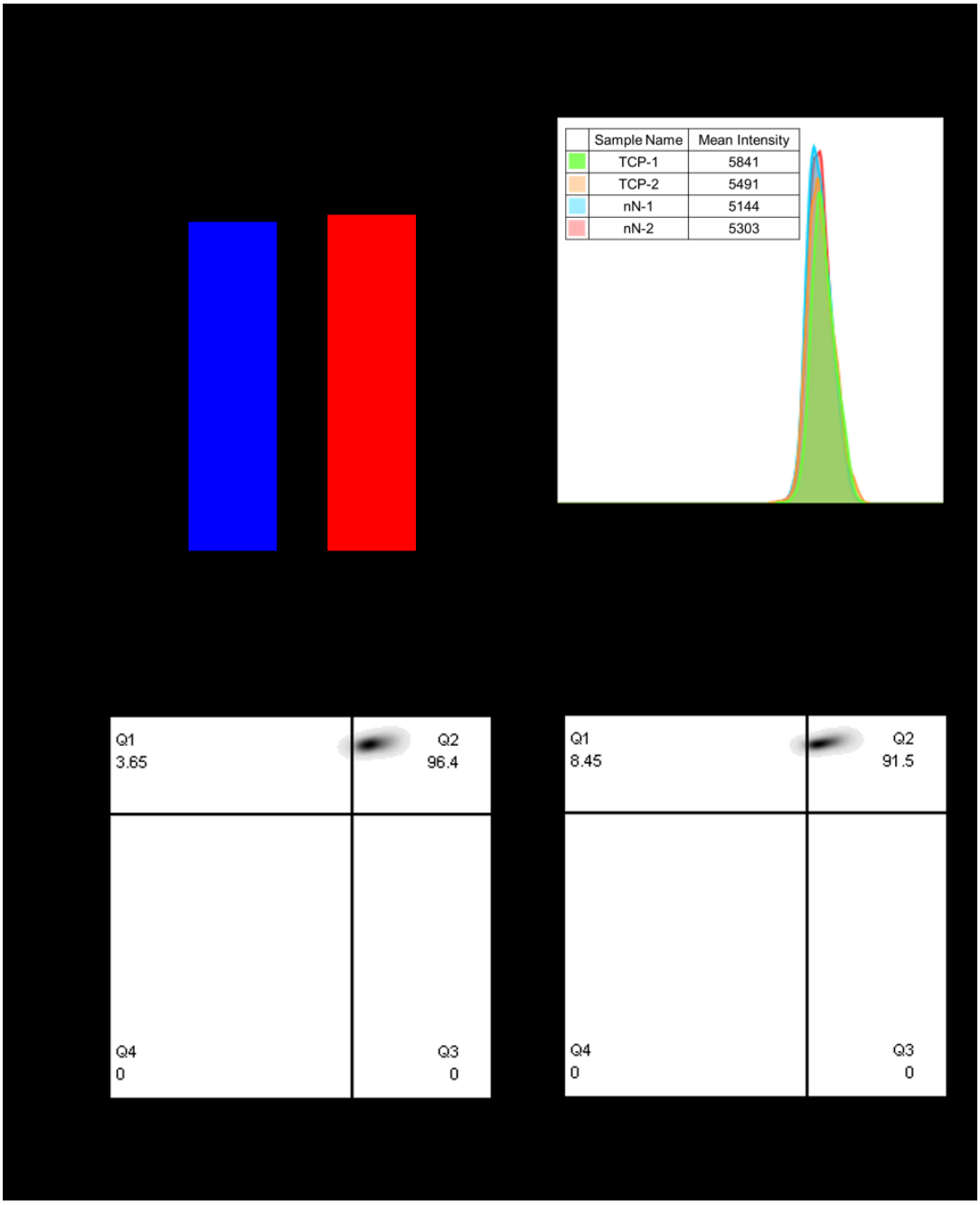


Figure 33. Nanoneedle-induced nuclear deformation did not cause nuclear condensation. (A) Flow cytometry analysis of the intensity of cell nucleus labelled with DNA intercalating dye at 24 h post-seeding on TCP or nNs. The data is reported as a function of nuclear condensation. (B) Representative intensity plot of cells labelled with the intercalating dye post-seeding on TCP or nNs. (C) Representative FACS plot of MEFs stained with DNA intercalating dye at 24 h post-seeding on TCP and nNs as a readout of nuclear condensation. Comparisons were analysed with two-tailed, unequal variance Student t-test, corrected for multiple comparisons where necessary. Mean± SEM. N = 3, n = 6.

The linker histone H1 binds to linker DNA in between the nucleosomes and plays a role in promoting and stabilising chromatin condensation [414]. H1 generally acts as a transcriptional repressor, although there have been several studies which showed H1-specific upregulation of genes transcription [415]. The dissociation of H1 from the nucleosome would leave the linker DNA momentarily accessible to other factors such as transcriptional factors, and histone/chromatin modifying enzymes. The slower re-binding of the histone H1 linker to the linker DNA will allow for the direct, or through subsequent modifications to the chromatin structure, creation of complexes that are stable and persist long enough to allow processes such as gene transcription and DNA repair.

To gain a deeper understanding of cells nuclear dynamics on TCP compared to nNs, transiently expressing H1-GFP MEFs were generated and conducted a fluorescence recovery after photobleaching (FRAP) experiment to measure the kinetics of H1 diffusions. Looking at several representative FRAP recovery curves qualitatively; the H1-GFP fluorescence recovery of cells cultured on TCP versus nN chips seems to be comparable (Fig. 34a, b).

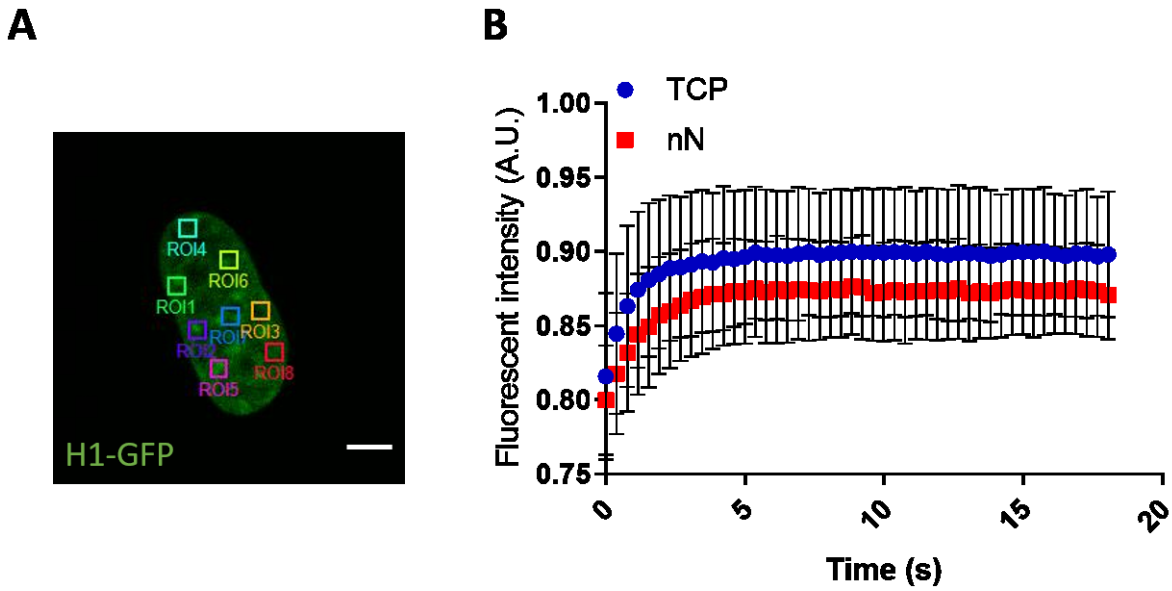


Figure 34. FRAP experiments on H1-GFP diffusion kinetics in the nuclei of cells cultured on TCP and nN chips. (A) Example fluorescence micrographs of H1-GFP-stained MEFs before photobleaching. The squares indicates photobleached area. (B) FRAP recovery curve. H1-GFP MEFs seeded on TCP (blue) and nN (red) were subjected to FRAP analyses. The mean of the relative fluorescent intensity in the bleached area are indicated. (Images used for FRAP analysis was acquired by Catherine Hansel.

3.7.3. Nanoneedle Induced Global Alterations

It is now well accepted that the modulation in cell shape affects the nuclear shape and consequently, the gene expression and cellular function [22]. To investigate the effects of nanoneedle-induced nuclear deformation on cellular functions, the combination of RNA sequencing, mass-spectrometry and pathway analysis tools were used to capture snapshots of the transcriptome and proteome of the cells. MEFs were first seeded on either TCP (control) or nN chips for 24 hours prior to extraction and subsequent procedures.

3.7.3.1. Overview of the Transcriptomic Profile

The first striking observation is that the cells cultured on the nN substrate cluster together and segregate away from the cells cultured on the TCP substrate (Fig. 35). Additionally, the differences in gene expression can be further clustered using cosine distance and average linkage into four main distinct clusters (Fig. 37). Within each cluster cells on nNs have a distinct expression profile compared to cells on TCP. In the first and the fourth clusters the cells on nNs show a reversed expression profile than that of cells cultured on TCP (Fig. 35).

The first cluster appears to contain genes involved in the regulation of skeletal muscle contraction, interstrand cross-link repair, DNA repair, oligodendrocyte differentiation and DNA metabolic process. The second cluster contain genes enriched in processes such as cell cycle regulation, nuclear division, and chromatin remodelling and microtubule organisation during the cell cycle. The genes in the third cluster did not have significant enrichment in any specific biological process. The genes in the fourth cluster are enriched in extracellular matrix organisation functions.

Differentially expressed genes (DEGs) were selected by DESeq2 with conditions of $\log_2$ fold change >1.5 and adjusted *p*-value ≤ 0.01. Comparative analysis revealed 340 and 317 genes in nN samples expressed at significantly higher and lower levels, respectively, compared to those from TCPs (Fig. 36).

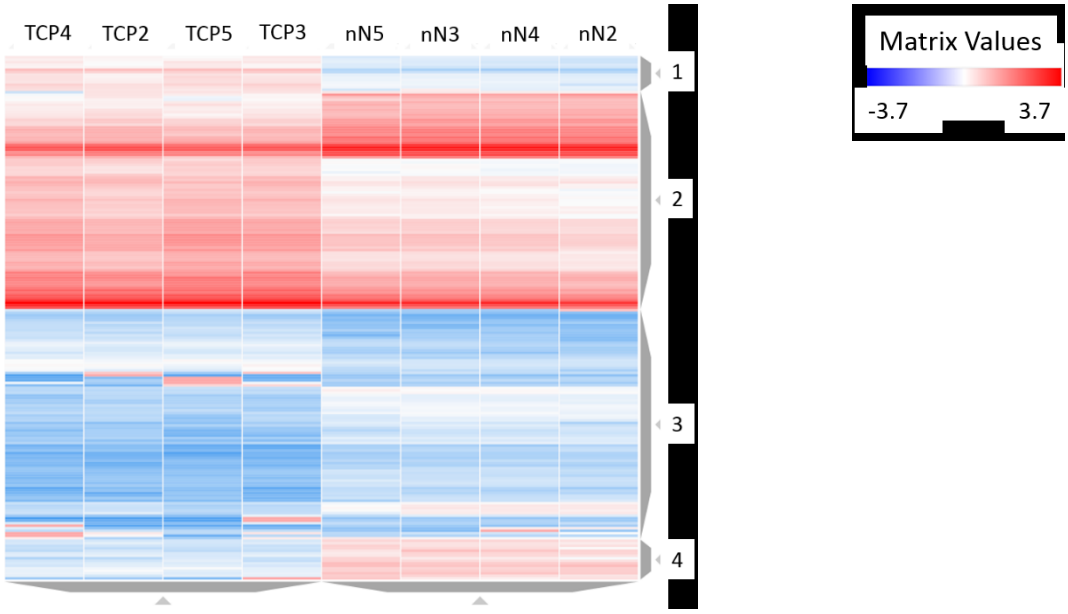


Figure 35. Heat map of gene expression. The samples and the differentially expressed genes have been hierarchically clustered using cosine distance and average linkage. Red/blue cells in the matrix represent positive/negative expression values of genes in individual samples. The analysis revealed that samples from the same culture substrate, *i.e.* TCP or nNs, formed a cluster. In addition, the genes can also be grouped into 4 main clusters.

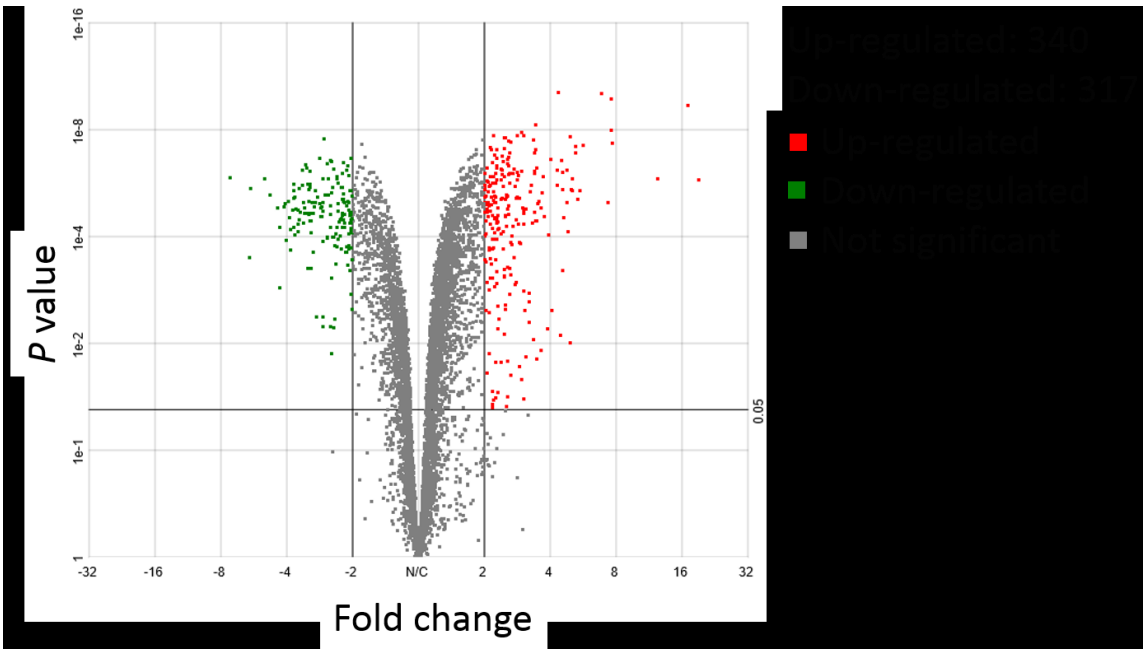


Figure 36. Volcano plot displaying differential expressed genes between nNs and TCP samples. The y-axis corresponds to the mean expression value of log 10 (*p*-value), and the x-axis displays the log2 fold change value. The red dots represent the up-regulated expressed transcripts ($p \leq 0.01$, false discovery rate (FDR) $q \leq 0.01$) between nNs and TCP. The green dots represent the transcripts whose expression was down-regulated ($p \leq 0.01$, FDR $q \leq 0.01$).

3.7.3.2. Overview of the Proteomic Profile

Label-free global proteomics analysis was performed on the cells cultured on either nN chips or TCP control to see if there is any correlation between the alteration in the transcriptome and the proteome. In our samples, a total number of 2189 unique proteins could be identified with high confidence. Principal component analysis (PCA) revealed that all the TCP samples clustered together and were markedly different from nNs (Fig. 37). nN1 and nN2 were slightly further away from the other nN samples but remain more like the nN samples than TCP. This clear separation was still apparent even though the experiments were performed as biologically independent replicates on different days.

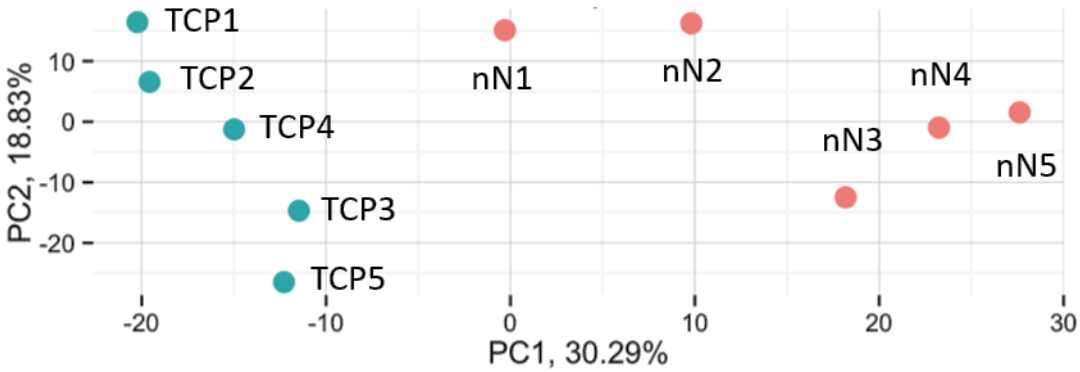


Figure 37. Principal component analysis of the dataset. Scatter plot calculated from the label-free quantification (LFQ) values of all proteins identified in the respective samples: TCP 1-5 and nN 1-5.

Next, hierarchical clustering was performed to visualise the level of the protein expression across all samples. Figure 38 shows the intensities for all the proteins discovered from the samples based on correlation clustering (red represents high intensity, and blue represents low intensity; the proteins are shown in the rows). As the PCA revealed, all biological replicates of the same group strongly clustered together. A closer look on the heat map revealed a large number protein had different intensities in nN samples compared to TCP samples. This further analysis revealed nanoneedle-induced specific proteins expression.

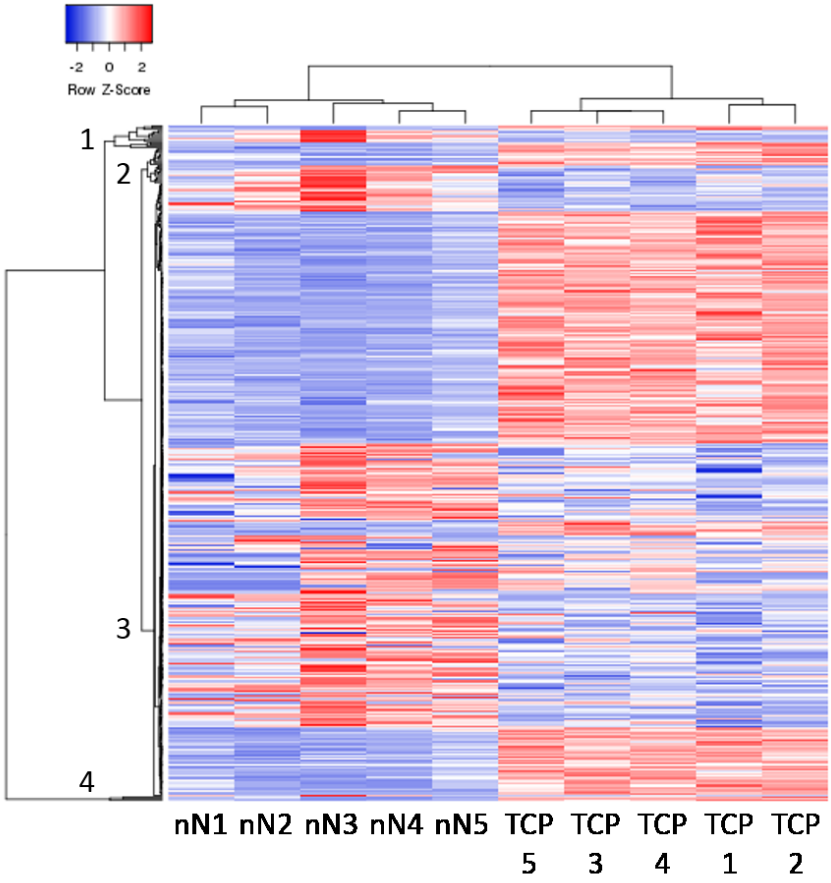


Figure 38. Hierarchical clustering analysis. The rows indicate the correlation for the proteins, and the columns indicate separate samples. The heat map displays log2 LFQ intensities of all the proteins quantified across all the samples (red = high intensity, blue = low intensity).

To further cut down the list and distinguish between background and significantly enriched proteins, a statistical analysis of LFQ intensities of the nN samples compared with the TCP controls was performed. To reveal the significantly enriched proteins and their significance, the log2 ratio of nN/TCP (LFQ intensities) was plotted against the negative log of the *p* value into a volcano plot (Fig. 39). To correct for multiple testing, a permutation-based false discovery rate approach was applied (FDR = 0.05; s0 = 1.5). This analysis separated significant alteration in proteins from the background. Taken together, our dataset revealed 30 significantly up-regulated and 212 significantly down-regulated proteins when comparing samples from nN to TCP.

The top 10% of the up-regulated proteins are: fibromodulin (Fmod) which has a role in the regulation of TGFβ signalling and extracellular matrix assembly, exportin-2 (Cse1l) which may play a role in apoptosis and cell proliferation by controlling the nuclear import and export machinery, and sascin (Sacs) which is a chaperone protein that acts as a regulator of Hsp70 and may be involved in proteasome. The top 10% of the down-regulated proteins are mainly involved in cytoskeletal machinery, cell-cycle and proteins translation pathways.

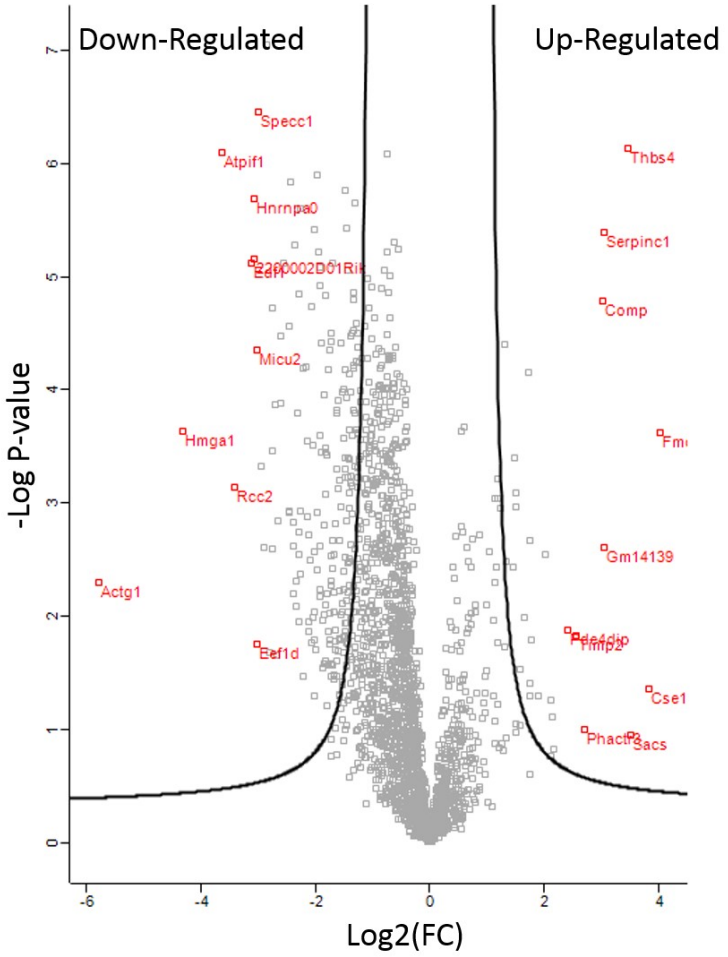


Figure 39. Volcano plot displaying differential expressed proteins between nN and TCP samples. The y-axis corresponds to the mean expression value of -log 10 (*p-value*), and the x-axis displays the log2 fold change value. The left represents the down regulated expressed proteome (log2 (FC) < -1.5, -log 10 (*p-value*) ≤ 0.05); the right represents the proteome whose expression was up regulated (log2 (FC) ≤-1.5, -log 10 (*p-value*) ≤0.05) between nN and TCP. The graph highlights the 10 most up-regulated and down-regulated proteins detected.

3.7.4. Pathway Analysis

3.7.4.1. Transcriptomic Pathway Analysis

To further understand and compare the functions of these DEGs, GO term enrichment analysis was conducted and of the identified 657 DEGs with the threshold value for adjusted *p* value < 0.05. There are three GO domains: biological process (GO_BP), molecular function (GO_MF), and cellular component (GO_CC).

The results of the GO enrichment analysis showed that all up-regulated genes (nN vs TCP) were most significantly enriched in GO terms involved in glutathione metabolic process and extracellular matrix organisations within GO_BP, glutathione transferase and metallopeptidase activities were the two most abundant terms within GO_MF, and no terms were significantly enriched in GO_CC using our selection criteria (Fig. 40).

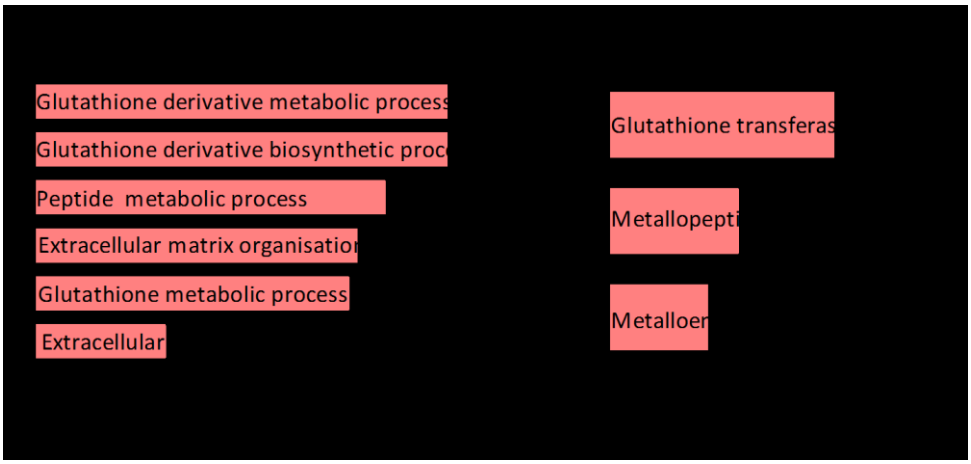


Figure 40. GO enrichment analysis of differentially upregulated expressed genes. (A, B) GO term enrichment analysis of genes that display > 1.5-fold change in expression in cells cultured on nNs compared with cells on TCP. (A) Biological process category; (B) Molecular function. Only the top 10% of terms with enrichment of –log10 (*adjP-value* ≤ 0.05) = 1.3 are displayed

However, all down-regulated genes (nNs vs TCP) were mostly enriched in terms involved in cell cycle including chromatin remodelling, checkpoints regulation and microtubule assembly within GO_BP. Genes with functions associated to the microtubules and histone kinases related to cell cycle regulations were the most highly enriched terms in GO_MF. Lastly, microtubules, spindles and condensed chromosomes were the most highly represented terms in GO_CC (Fig. 41).

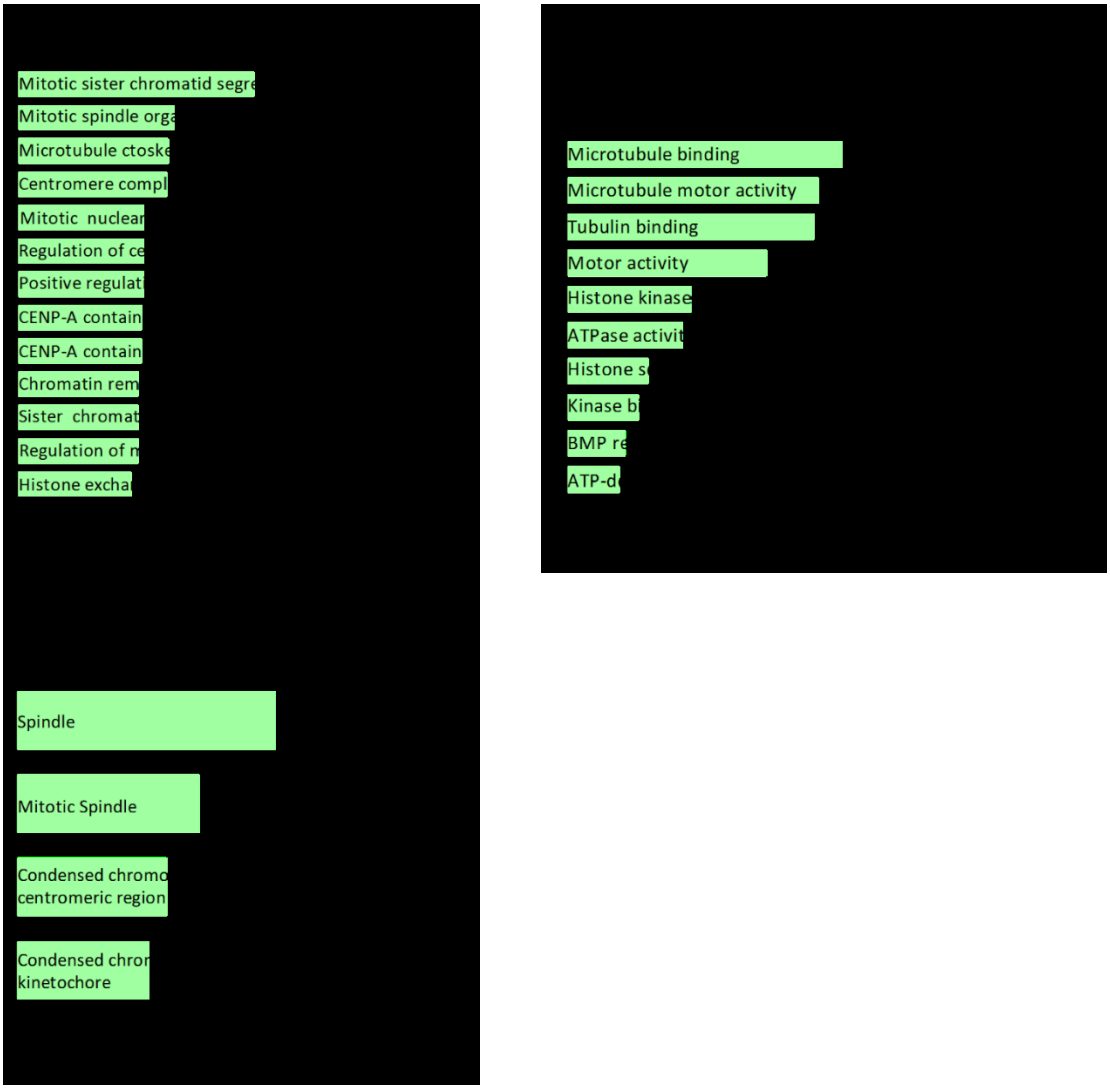


Figure 41. GO enrichment analysis of differentially downregulated expressed genes. (A) The top 10% (13 of 130) GO Biological Process enrich terms. (B) GO Molecular Function enrichment analysis. (C) GO Cellular Component analysis of the downregulated differentially expressed genes. Only the top 10% of terms with a –log10 (*adjP-value* ≤ 0.05) =1.3 are displayed.

To confirm the gene ontology findings and to further investigate the biological function and pathways altered by the presence of the nN, the IPA analysis tool was used. The DEGs were separated into two separate groups, the up-regulated and down-regulated. Genes from the investigated dataset that were associated with biological functions were recorded, and adjusted *p-value* were calculated with B-H Multiple Testing Correction tests. The top molecular and cellular functions, as determined by the adjusted *p-value*, are shown in Fig. 42. These functions might explain or at least partially explain the effects of nNs on cellular function. The functional analysis of the up-regulated DEGs revealed that functions including drug metabolism, molecular transport, cellular function and maintenance and small molecule

biochemistry, are in line with the results observed by the gene ontology analysis. Similarly, genes down-regulated in cells cultured on nNs are associated with cellular and metabolic functions such as, cell cycle, cellular assembly and organisation and DNA replication, recombination and repair directly supporting the results explained above.

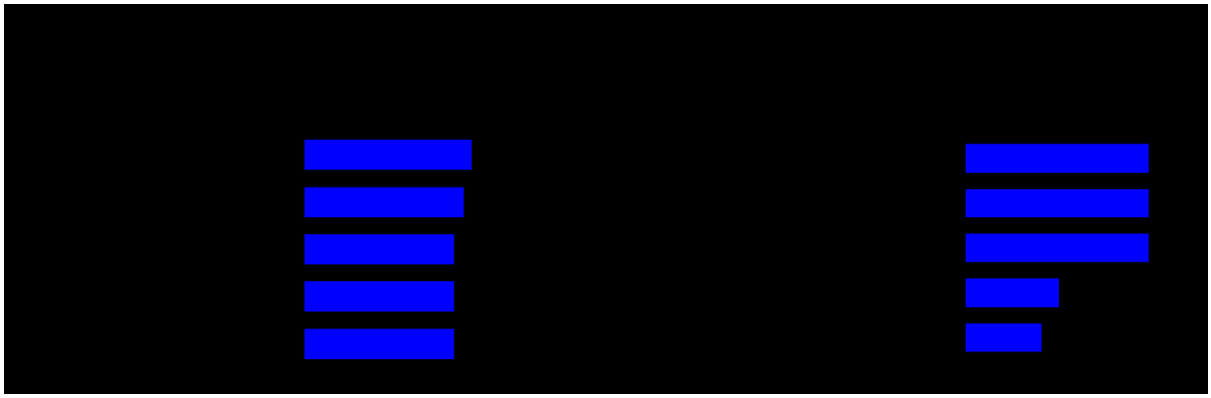


Figure 42. Global functional analysis. The top molecular and cellular functions altered by the presence of the nN chips as culture substrate. (A) Functions from up-regulated DEGs and (B) from down-regulated DEGs. Data sets were analysed by the IPA software. The significant value associated is a measure of likeliness that genes from the investigated data set play a role in the associated function. The data is filtered using the B-H Multiple Testing Correction *p-value* and only the top 5 pathways from the list of pathways with an *adjP-value* ≤ 0.5 are showed.

In addition to the functional annotation, IPA analysis also revealed that the DEGs play a role in essential canonical pathways (Fig. 40 and 41). IPA analysis can also predict the state of the enriched pathways based on the fold change of the genes within the dataset. A positive z-score indicates predictive activation of the enriched pathways, whereas a negative z-score points toward pathway inactivation. A zero z-score indicates that the pathways are neither active nor inactive based on the expression values of the dataset.

In the up-regulated DEGs, top canonical pathways include glutathione-mediated detoxification, xenobiotic metabolism, and NRF2-mediated oxidative stress response (Fig. 43). Both the glutathione signalling and the nuclear factor erythroid 2-related factor 2 (Nrf2) signalling are the two main lines of defence against cellular oxidative stress response [416, 417]. Silicone nanoparticles have been shown to elicit the cells' anti-oxidative stress pathways in response to elevated reactive oxygen species (ROS) and oxidative stress within the cells [418]. Since the nanoneedle chips are made of silicone as they degrade they will release SiO_2 particles directly into the cytosol of the cell. The activation of glutathione and various drug

metabolism pathways and the Nrf2 pathway might indicate an nN-induced stress response. Activation/enrichment of inflammatory pathways including the inhibition of MMPs activity, osteoarthritis pathway and HIF1α signalling were observed (Fig. 43). The activation of inflammatory responses is in line with the working hypothesis that the cells are in a state of oxidative stress.

In the down-regulated DEGs, enrichment in pathways involved in the regulation of the cell cycle such as G2/M DNA damage checkpoint, cyclins and cell cycle regulation and mitotic roles of polo-like kinase were observed (Fig. 44). Additionally, most of the pathways involved in cell cycle checkpoint regulations are predicted to be highly active, while pathways required for the progression of the cell cycle are predicted to be inactive. Taken together the IPA analysis reveals that the presence of the nNs might inhibit cell cycle progression or entry, and might be due to the induction of the oxidative stress response induced by the nN.

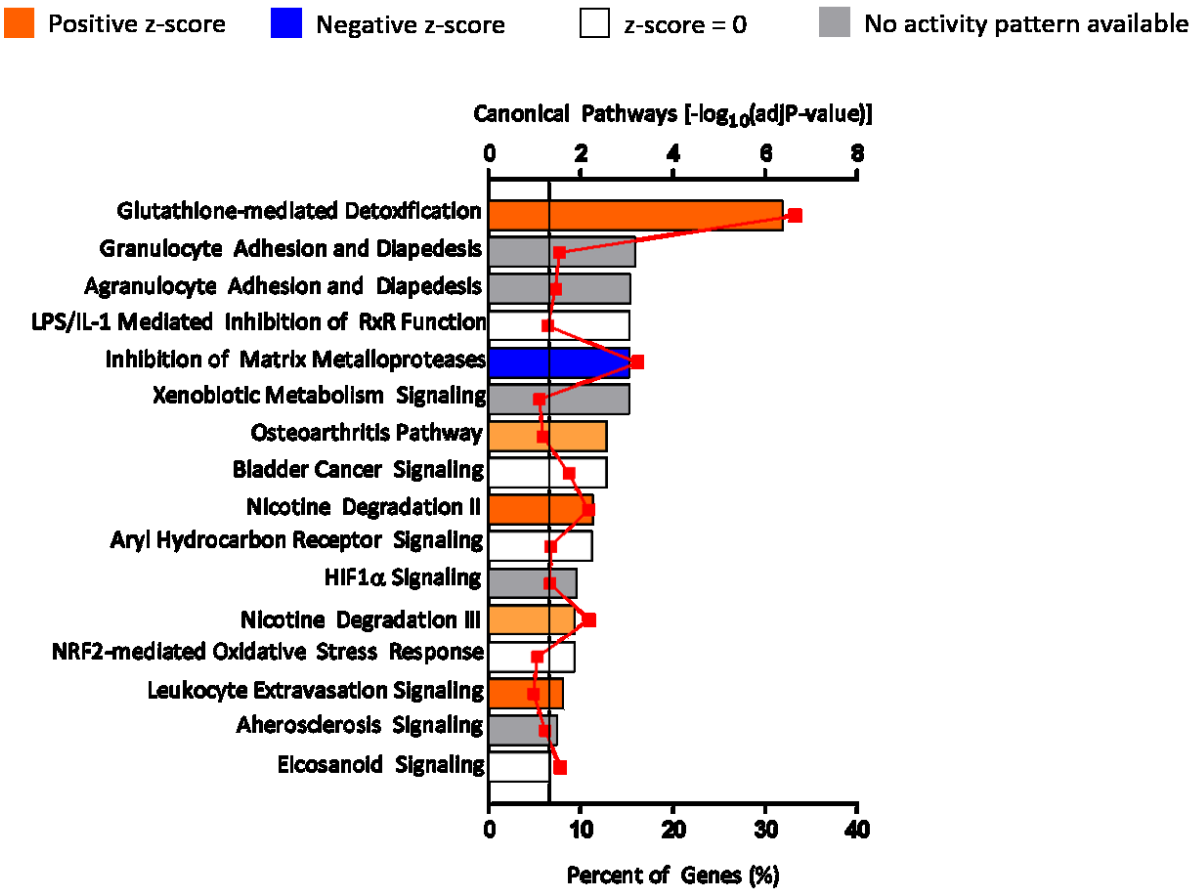


Figure 43. Canonical pathway analysis of upregulated DEGs. Significantly altered canonical pathways associated with cells cultured on nNs compared with cells cultured on TCP. A total of 336 up-regulated transcripts were mapped to the IPA database and then analysed via the core analysis settings on the IPA software to identify the most significantly perturbed canonical pathways. The canonical pathways included in this analysis are shown along the y-axis of the bar chart. The x-axis indicates the statistical significance calculated using the B-H Multiple Testing Correction *p* value. The black threshold line represents the significance cut-off at *adjP-value* ≤ 0.5. The red line represents the number of genes in the data that match with the total number of genes in the specific pathway database.

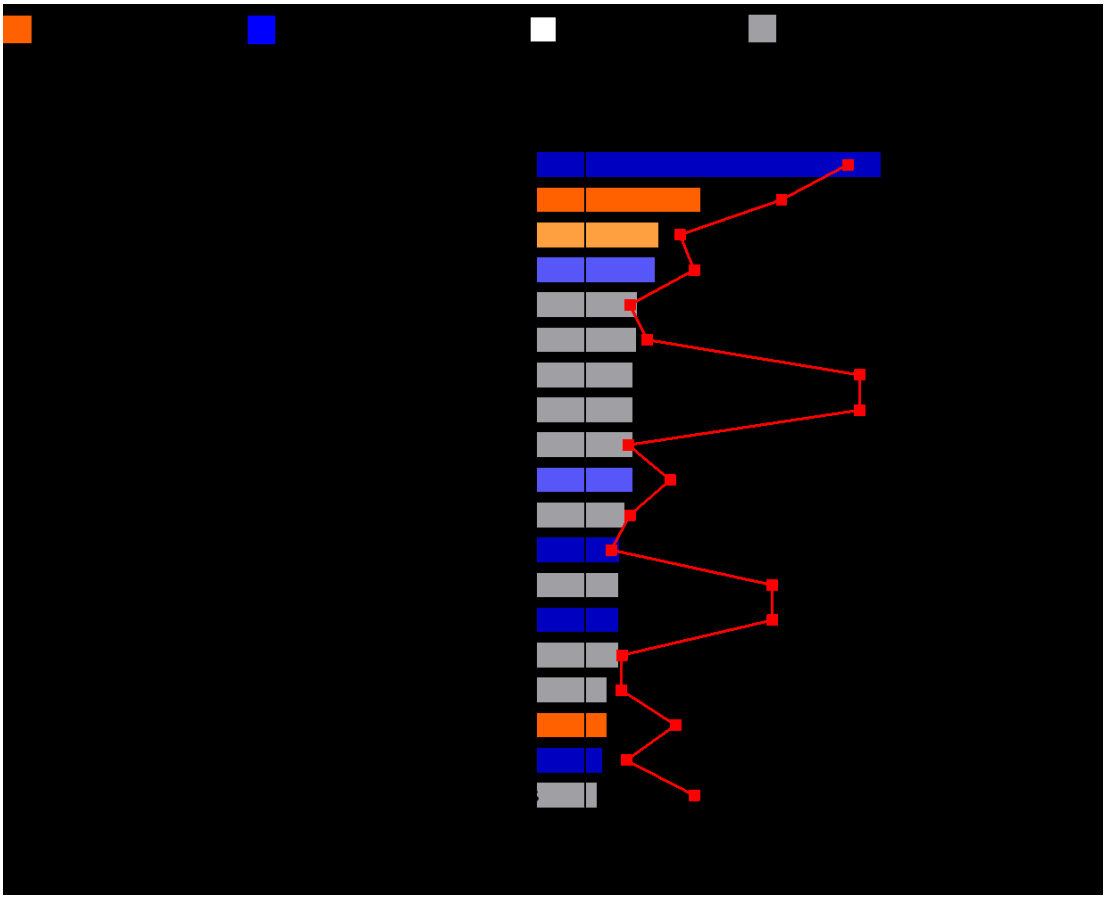


Figure 44. Canonical pathway analysis of downregulated DEGs. Significantly altered canonical pathways associated with cells cultured on nNs compared with cells cultured on TCP. A total of 314 down-regulated transcripts were mapped to the IPA database and then analysed via the core analysis settings on the IPA software to identify the most significantly perturbed canonical pathways. The canonical pathways included in this analysis are shown along the y-axis of the bar chart. The x-axis indicates the statistical significance calculated using the B-H Multiple Testing Correction *p* value. The black threshold line represents the significance cut-off at *adjP-value* ≤ 0.5. The red line running through represents the number of genes in the data that match with the total number of genes in the specific pathway database.

3.7.4.2. Proteomic Pathway Analysis

Multiple studies have demonstrated that mRNA and protein expression data from the same cells under the same conditions do not necessarily have to show a high correlation [419-421]. Thus, in order to gain a fuller understanding of the biological phenomena occuring upon exposure to the nanoneedle chips, the samples were subjected to a label-free global proteomics analysis using mass-spectrometry and analysed the data with several functional enrichment tools. First, the 241 differentially expressed proteins were analysed using EnrichR. The proteins were enriched to Gene Ontology biological process, molecular function, and cellular component categories (Fig. 45). In the biological process category, 75 pathways were found to be statistically enriched ($-\log_{10}$ (*adjP-value* < 0.05) = 1.3) and the most enriched were involved in gene expression from messenger RNA (mRNA) transcription, splicing export and translational process. Interestingly, an enrichment in the mitochondrial electron transport chain (*adjP-value* = 8.63E-05) was observed. 27 molecular functions were found to be statistically enriched in our dataset where the most enriched were RNA binding (87/1388, *adjP-value* = 1.28E-29) and cadherin binding (21/314, *adjP-value* = 3.56E-08). Lastly, 32 terms for cellular component were statistically enriched, and the analysis revealed that the differentially expressed proteins were mainly found in association with the focal adhesion, cytoplasmic components, nucleolus and mitochondrial respiratory chain.

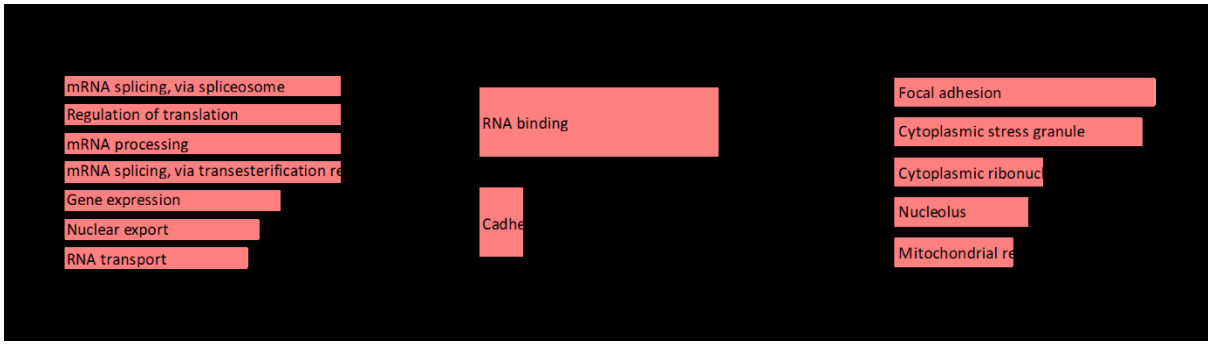


Figure 45. GO enrichment analysis of differentially expressed proteins. (A, B, and C) GO term enrichment analysis of proteins that display >1.5-fold change in expression in cells cultured on nNs compared with cells on TCP. (A) Biological Process category; (B) Molecular Function; (C) Cellular Component. Only the top 10% of terms with enrichment value of –log10 (*adjP-value* ≤ 0.05) = 1.3 are displayed.

The gene ontology enrichment analysis of the differentially expressed proteins revealed existing pathways that were not picked up by the same analysis with the differentially expressed genes dataset. For instance, the proteomic analysis revealed that processes involved in mRNA transcriptions, specifically the splicing mechanism, and translations by the ribosomes were affected by the presence of the nanoneedles. This observation was also supported by the KEGG analysis pathway, which showed the spliceosome pathway to be the most significantly enriched pathway (14/134 proteins, *adjP*-value = 8.805E-08).

3.7.4.3. Integrative Transcriptomic and Proteomic Analysis

When the differentially expressed genes identified via transcriptomic analysis were compared to the differentially expressed proteins detected via mass spectrometry, 41 DEGs have quantitative information on their respective proteins (6.7%) (Fig. 46). Furthermore, a total of 13 genes were detected to be regulated at the level of both transcription (≥ 1.5-fold change and $p \leq 0.01$) and translation (≥ 1.5-fold change and $p \leq 0.05$) levels, and interestingly all these genes have the same direction of change and similar fold change in the two levels (Table. 17).

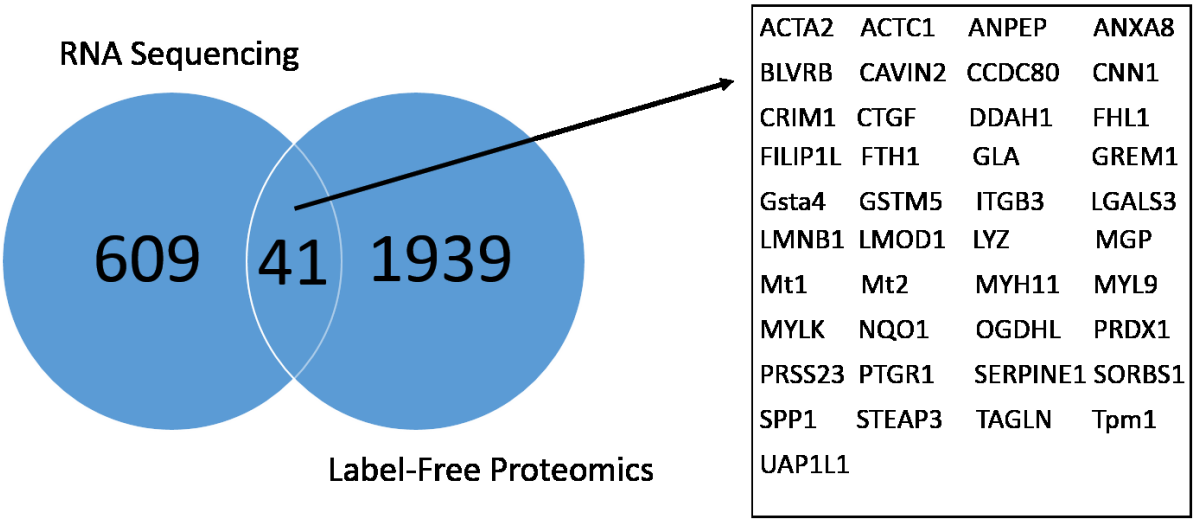


Figure 46. Interactions between mRNA and protein samples. Venn diagram showing the degree of overlap between the two datasets and the differential expressed genes that were also identified in the proteomics dataset.

Table 17. Statistically significant genes regulated at the same level in both mRNA and protein levels.

Gene Symbol	Proteomics		Transcriptomic	
	Log2 Fold Change	*p* value	Log2 Fold Change	*p* value
ACTA2	-2.022	9.26E-03	-1.979	1.47E-19
CAVIN2	-1.758	2.74E-02	-1.898	7.68E-20
CNN1	-2.651	1.43E-03	-2.487	1.08E-26
CTGF	-1.669	9.16E-03	-1.623	1.85E-22
FHL1	-1.354	7.05E-04	-1.754	2.64E-16
FILIP1L	-2.048	1.02E-02	-1.513	2.19E-21
LMOD1	-1.485	5.94E-04	-1.759	1.85E-17
Mt1	2.163	1.49E-01	2.099	3.65E-22
Mt2	1.468	3.67E-03	1.924	8.55E-15
SORBS1	-1.746	1.63E-02	-1.555	2.52E-22
SPP1	1.648	1.02E-02	2.243	9.97E-10
TAGLN	-1.303	1.61E-04	-1.835	1.07E-21
Tpm1	-1.641	1.99E-02	-1.59	9.40E-34

Further investigations into the function of these genes revealed that most are associated with the actin cytoskeleton complex (*adjP*-value = 2.312E-03) and are involved in cellular organisation of the actomyosin structure including the formation of stress fibres and actin bundles (*adjP*-value ranging from = 7.079E-03 – 2.203E-06), and cellular contractility (*adjP*-value = 3.626E-03). Additionally, most of these genes were found to be down-regulated at both mRNA and protein level. This observation fits nicely with the current understanding of cell-nanoneedle interactions [413, 422]. Upon contact with surfaces with nanotopographical features, adherent cells quickly respond and adapt to various parameters including slight changes in the geometry and topography including nanowire density, diameter and height. In general, cells cultured on the high-aspect-ratio nanostructures adopt a rounder morphology with smaller projected cell area than on corresponding flat surface controls. These adaptations in the cell morphology were found to be regulated by the actin cytoskeleton re-

organisations. A study using LifeAct-GFP, recombinant protein for live visualisation of F-actin, observed accumulation of actin fibres around the nanostructures and is often linked to stress fibres [106]. However, in low density, tall and sharp nanostructures like the one used in this study, it has been noticed a lack of stress fibres linked to the lack of adhesion sites available for the cells to grab onto [98, 423]. Thus, overall downregulation of genes involved in this process (Table. 17) might provide clues on the cells morphology on the nanoneedles used in the study.

A comparative functional analysis was also conducted between the differentially expressed genes and the proteins using the IPA tools. The IPA molecular and cellular function enrichment analysis showed that four pathways were significantly differentially regulated at both mRNA and protein level ("Cell Death and Survival", "Cell Morphology", "Cellular Movement" and "Cell Cycle") suggesting that these processes are highly affected when cells are seeded on the nanoneedle chips (Fig. 47). Upon closer look on the proteomic dataset, "cell spreading of fibroblast cell line" functional annotations under the cell morphology was predicted to be inactive (z-score = -0.555). This observation is in line with observations made by previous studies using similar cell lines on nanowires [424]. Like the gene ontology enrichment analysis, the IPA analysis also revealed enrichment in the "RNA Post-Transcriptional Modification" function to be unique to the proteomic dataset.

Furthermore, a comparative canonical pathway analysis identified 4 pathways that are statistically enriched in both the proteomic and transcriptomic dataset (Fig. 48). The enrichment of the "Caveolar-mediated Endocytosis Signalling" pathway is very interesting because vertical nanostructures have been found to induce the formation of stable membrane curvature upon close interaction with the cells. These nanopillars-induced curvatures were also found to enhance the endocytosis pathways significantly and promote the uptake of certain cargoes via the accumulation of proteins involved in the endocytotic pathways around the membrane curvature [106, 425, 426]. Furthermore, the curvature hypothesis proposes that several intracellular proteins might be able to sense the membrane curvatures and further recruit and activate downstream components to modulate cell signalling and behaviour [413].

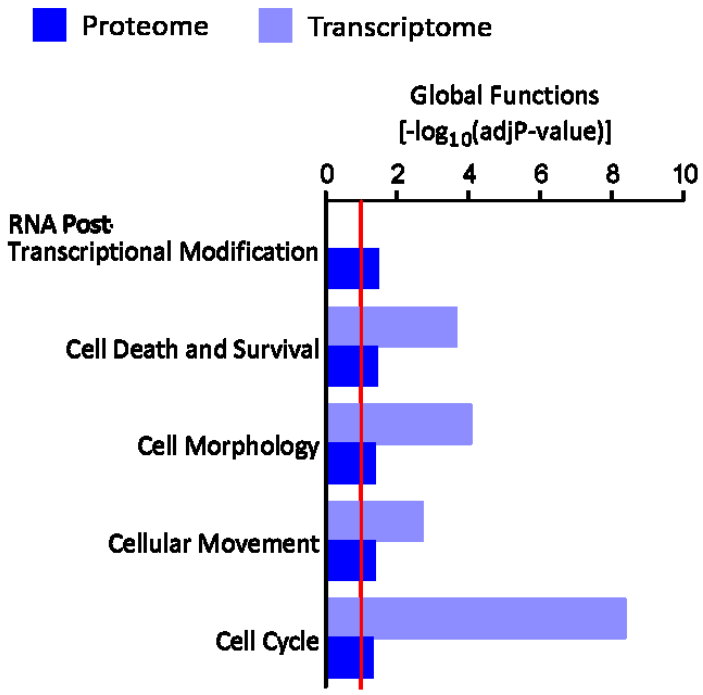


Figure 47. Comparative global functional analysis. The top molecular and cellular functions altered in both mRNA and protein level by the presence of the nN chips as culture substrate. Datasets were analysed by the IPA software. The significant value associated is a measure of the likelihood that genes from the investigated dataset play a role in the associated function. The data is filtered using the B-H Multiple Testing Correction and only pathways with –log10 (*adjP-value* ≤ 0.5) are used in the study.

Thus, some of the alterations in cellular functions in the presence of nanoneedles might be caused by the cells' enhanced endocytotic responses. Additionally, "integrin signalling" was also found to be significantly enriched in both the proteome and the transcriptome dataset. Integrin receptors present on the cell surface play a crucial role in dictating how cells interact with material surfaces [314]. The interaction between integrin and nanotopographical features lead to engagement of the attached cytoskeleton and modulation in downstream signalling pathways [3]. Methods to modulate integrin receptors clustering and activation via nanotopographical cues have been shown to affect not only cellular morphology but also cellular differentiation and cell fate [427-429].

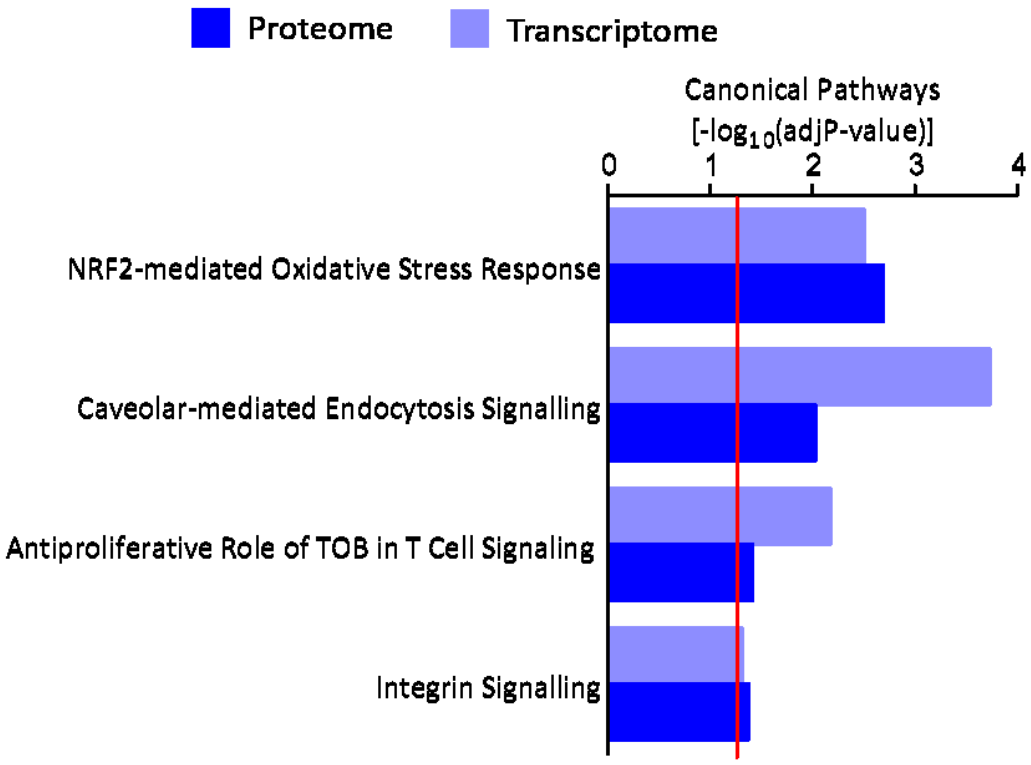


Figure 48. Comparative canonical pathway analysis. The top canonical pathways altered in both mRNA and protein level by the presence of the nN chips. Datasets were analysed by the IPA software. The significant value associated is a measure of the likelihood that genes from the investigated dataset play a role in the associated function. The data is filtered using the B-H Multiple Testing Correction and only pathways with –log10 (*adjP*-value ≤ 0.5) are used in the study.

3.7.5. Oxidative Stress Response on Nanoneedles

In the present study, of all differentially expressed genes, 11 are associated with the oxidative stress response. Genes encoding for the oxidative response, including the members of the glutathione-S-transferases (GSTA3, GSTA4, GSTA5) [fold-change = 5.247, 2.746, 4.764 respectively], prostaglandin synthases (PTGS1, and PTGES) [fold change = 1.3972, 1.637), and G-protein coupled receptor families (AGTR2) [fold change = 2.126] are all up-regulated in the presence of nNs, suggesting an increase in the level of oxidative stress and inflammatory response in the cells compared with the cells cultured on TCP. Glutathione is one of the most critical low-molecular-weight non-protein thiols that function as an intracellular antioxidant by keeping the cellular environment in a reduced state by the reduction of toxic oxygen products [430]. Although the toxic molecules can react with glutathione to form a complex,

the reactions are generally very slow. Members of the GST family can catalyse the reaction and increase the rate of conjugation and elimination of the toxic molecules at about 100 times faster than the non-enzymatic reaction [430]; thus, protecting the cells from the harmful effects of the reactive oxygen species. Moreover, the upregulation of angiotensinogen (AGT) and angiotensin II receptor type 2 (AGTR2) may further indicate the upregulation of the cells protective machinery against oxidative stress. This assumption is consistent with previous findings [431, 432]. Because the increase of the angiotensinogen II precursor AGT may suggest a higher production of angiotensinogen II, and the interaction of angiotensinogen II to the AGTR2 receptors have been demonstrated to provide anti-inflammatory effects in response to high levels of reactive oxygen species in cases such as hypertension and myocardial ischemia [433, 434]. In addition, the upregulation of prostaglandin synthases genes might lead to increased conversion and higher levels of prostaglandin, *i.e.* pro-inflammatory molecules, within the cells [435]. The level of prostaglandins has also been used as a direct biomarker of oxidative stress both *in vitro* and *in vivo* [436].

IPA canonical pathway analysis also supports our hypothesis regarding augmented oxidative stress response and increased inflammatory response in cells cultured on nNs. Several over-represented pathways involved in oxidative stress response are identified in our analysis (Table. 18), and nearly all genes mapped to these pathways are up-regulated. IPA analysis concluded that these pathways are activated in the cells cultured on nNs.

Table 18. Over-represented pathways involved in oxidative stress response.

Canonical pathways involved in oxidative stress response	***ajdP-value***	**Ratio**
Glutathione-mediated Detoxification	4.27E-07	3.33E-0.1
LPS/IL-1 Mediated Inhibition of RXR Function	6.76E-04	6.44E-02
Xenobiotic Metabolism Signalling	8.92E-04	5.51E-02
Nicotine Degradation II	5.63E-03	1.09E-01
Aryl Hydrocarbon Receptor Signalling	5.89E-03	6.72E-02
NRF2-mediated Oxidative Stress Response	1.3E-02	5.29E-02
Nicotine Degradation III	1.3E-02	1.09E-01
Eicosanoid Signalling	4.89E-02	7.81E-02

The NRF2-mediated oxidative stress response is among one of the over-represented pathways in both the differentially expressed gene and the differentially expressed protein canonical pathway analysis (Fig. 49). Moreover, Nrf2 (NFE2L2), a transcription factor, is predicted to be activated in cells cultured on nNs (*P-value*= 2.20E-03; Z-score= 2.678). Nuclear factor-like 2 (NRF2) is a key transcription factor that mediates a wide range of functions in response to oxidative and xenobiotics stress [417] (Fig. 50). Under normal conditions, Nrf2 is rapidly degraded by the ubiquitin-mediated proteasome pathway. However, upon exposure to stimuli such as ROS, cytosolic Nrf2 is activated through phosphatidylinositol 3-kinase (PI3K), RAS and PKC signalling pathways. Upon phosphorylation or association with actin, the stabilised Nrf2 translocate into the nucleus and binds to the antioxidant response elements, and thereby induce expression of protective proteins including antioxidants and ROS detoxifying enzymes [417]. Some of the downstream genes, including members of glutathione S-transferase (GSTA3, GSTA4, GSTA5, GSTM5, and MGST1), aldehyde oxidase 1 (AOX1) [fold-change= 1.794], NAD(P)H quinone dehydrogenase (NQO1) [fold-change= 3.877], aldehyde dehydrogenase 3 family member A1 (ALDH3A1) [fold-change= 3.936], peroxiredoxin (PRDX1) [fold-change= 1.707], and PPARG coactivator 1 alpha (PPARGC1A) [fold-change= 2.206), are differentially expressed in the current study (Fig. 50). Although few genes in the Nrf2 signalling pathway, including Tpm1, GABRB1 and SLC1A1, are down-regulated in cells on nNs. Taken together, the increased expression of the antioxidant and oxidative stress response, suggest a higher level of ROS generated in the presence of nNs.

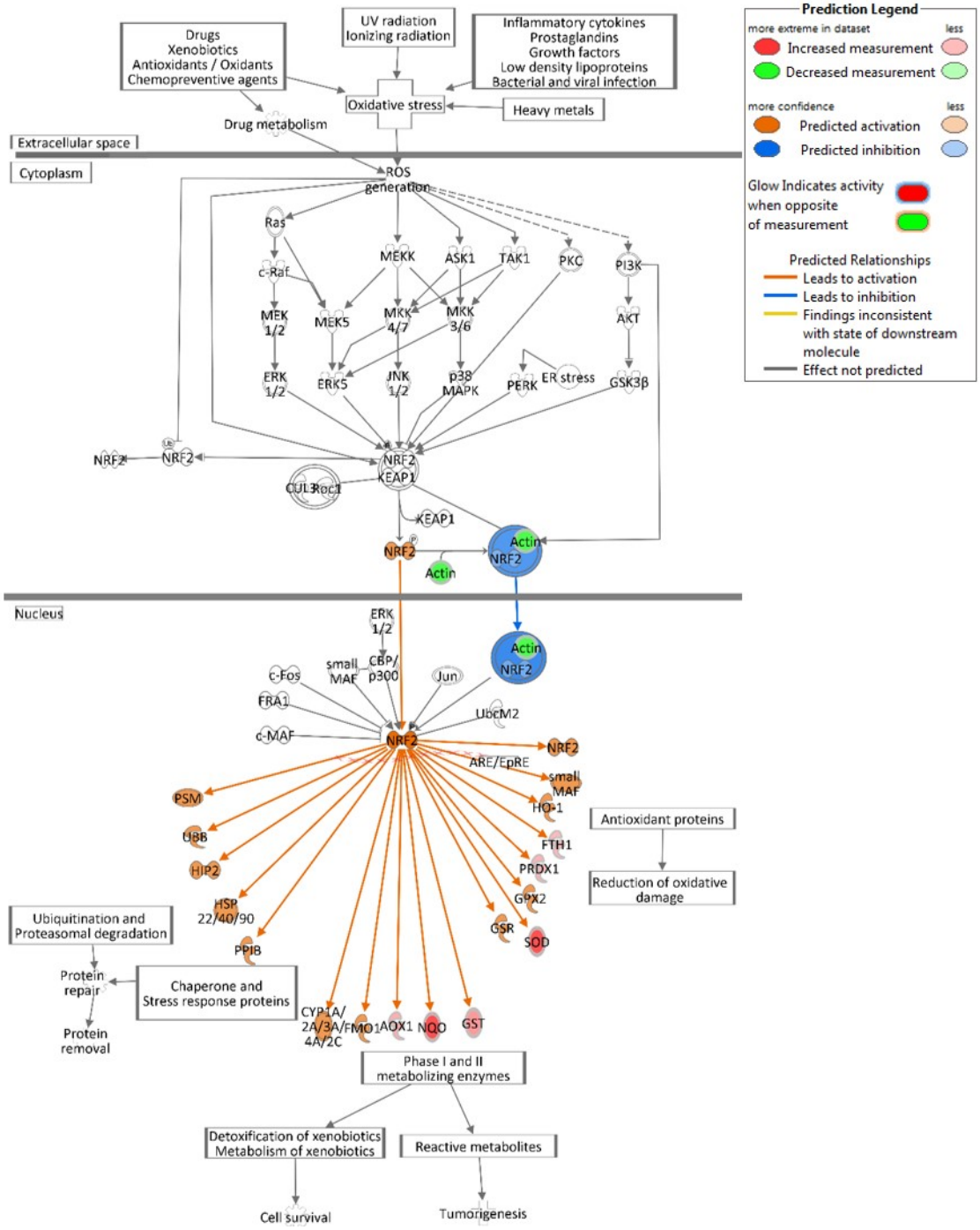


Figure 49. NRF2-mediated oxidative stress response. The Keap1-NRF2 pathway was identified as statistically significant with p = 1.3E-02. Red and green symbols indicate genes up- and down- regulated in the cells on nNs, respectively. The colour intensity is proportional to the degree of fold change.

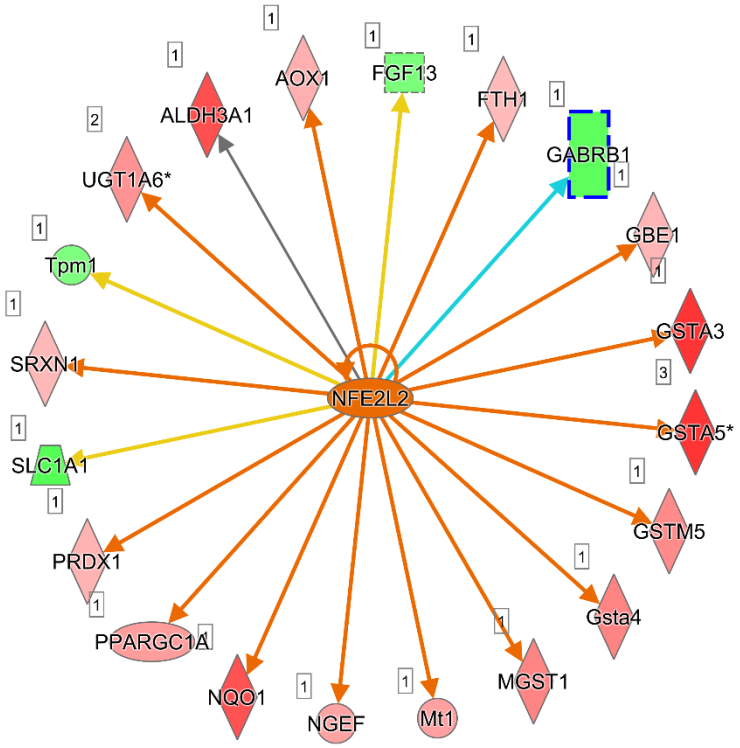


Figure 50. NRF2-Upstream analysis. The NRF2 (NFE2L2) is predicted to be highly activated in cells seeded on nNs. NRF2 controls a range of genes involved in the oxidative stress responses. Red and green symbols indicate genes up- and down- regulated in the cells on nNs, respectively. The colour intensity is proportional to the degree of fold change.

In line with previous findings, several studies have shown that silica nanoparticles (SiO_2) cause oxidative stress [418, 437]. Guo *et al.* [418] showed that the exposure to SiO_2 nanoparticles significantly increased reactive oxygen species after 24 hours, and is also associated with increased activity of antioxidant enzymes (*e.g.* SOD, GSH). Also, they demonstrated that the oxidative stress responses are mediated by MAPK activated NRF2 signalling pathways. As seen in Figure 51, the presence of nNs leads to an increased in ERK phosphorylation and activation. ERK is a key up-stream signalling molecule involved in the activation of the Nrf2 signalling pathway.

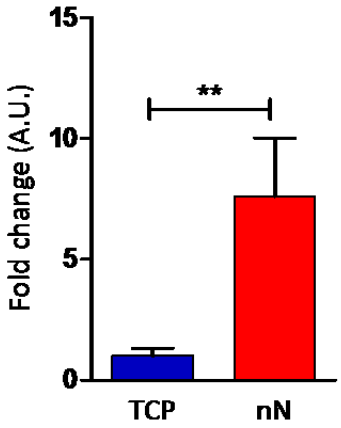


Figure 51. ELISA assay of pERK. The protein levels of phosphorylated ERK measured through ELISA analysis 24 hours post-seeding on either TCP or nN chips. Comparisons were analysed with two-tailed, unequal variance student t-tests. Mean ± SD. N=4; $^{**}p \leq 0.01$.

Also, the antioxidant enzyme microsomal glutathione transferase 1 (MGST1) has also been shown to protect against toxicity induced by silica nanoparticles [427]. MGST1 is a member of the glutathione metabolic pathways and is located mainly in the mitochondrial outer membrane and endoplasmic reticulum. The previous study showed that the overexpression of this protein prevents the peroxidation of cellular lipids induced by the nanoparticles and prevents cellular death [427]. Similarly, the presence of the nNs also leads to the overexpression of the MGST1 protein which further indicates the activation of the cellular defence mechanisms against reactive oxygen species (Fig. 52).

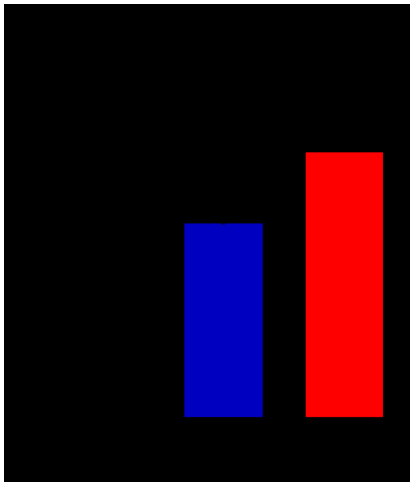


Figure 52. MGST1 differential expression. Expression value of MGST1 in log2 (CPM) from the RNA sequencing data of cells seeded on either TCP or nN chips. Comparisons were analysed with two-tailed, unequal variance Student t-tests. Mean ± SD. N=4; $^{***}p \leq 0.001$.

Moreover, a study demonstrated that fibroblasts cultured on nanowires also exhibit increased reactive oxygen content and DNA damage [424]. They found that increasing the length of the nanowires (to beyond 6.7 µm) allowed the cells to interact with the underlying substrate with a more cytotoxic effect. While using nanowires with a length like the one used in this study (3.8 – 4 µm) the level of ROS and DNA damage increased but not to a significant level. Although the oxidative stress response pathways were upregulated, there were no signs of nanoneedle-induced DNA damage (Fig. 53). In the presence of double-stranded DNA damage, the histone H2AX is phosphorylated into γ-H2AX. Thus, to investigate whether nanoneedles induce any DNA damage, the level of γ-H2AX was measured using immunofluorescence microscopy. MEFs were cultured on normal TCP and nanoneedle chips for 24 hours and labelled for γH2Ax. γH2Ax positive cells were present in both TCP and nN chips (Fig. 53a). Upon further quantification, no significant difference between the numbers of γH2Ax foci present in each nucleus (Fig. 53b). The inherent γH2Ax present in the cells might be the result of the cell isolation procedure.

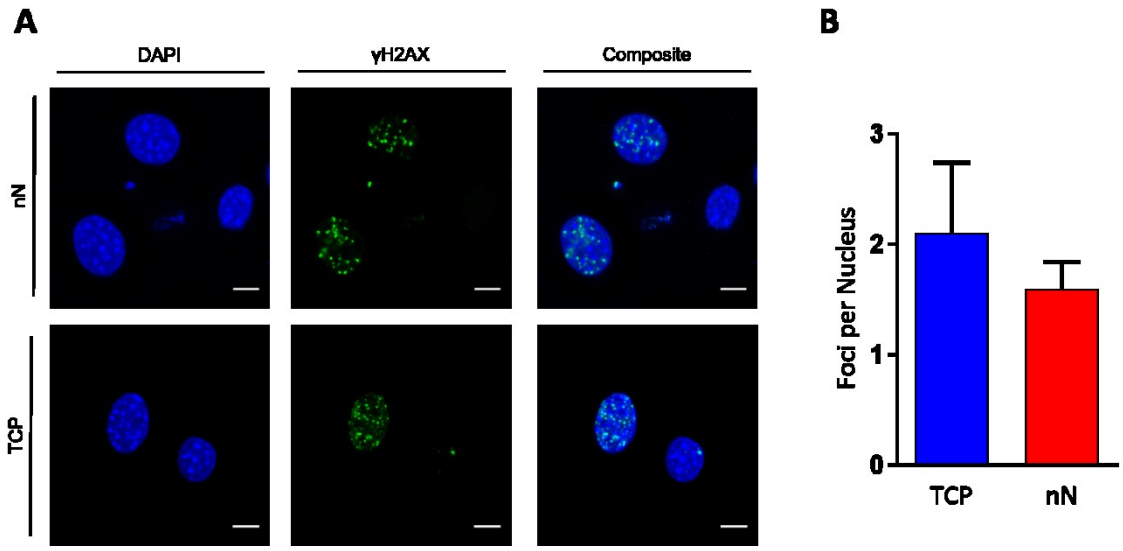


Figure 53. DNA damage investigated by the level of γH2Ax. (A) Immunofluorescent images of MEFs cultured for 24 h on nanoneedle chips or TCP control. Stained with the γH2Ax antibody (green) and DAPI for the nucleus (blue). (B) Quantitative measurement of the number of γH2Ax foci present in each nucleus showing no significant difference between cells cultured on the nanoneedle chips and cells on the TCP control substrate. Mean ± SD. N= 3, n = 614 for TCP, and n = 381 for nN. Scale bars= 10 µm. Images were acquired by Catherine Hansel.

Interestingly in iPSC generation from somatic cell reprogramming, the somatic cells must undergo metabolic reprogramming, shifting from oxidative to glycolytic based energy production [438]. This metabolic switch takes place during the early stages of reprogramming, and even precedes the expression of genes that control self-renewal. Moreover, this metabolic switch is one of the main bottle necks in the reprogramming process, with most cells failing to fully reset their metabolic processes [439].

A study by Hawkins *et al.* demonstrated that an increase in the level of intracellular reactive oxygen species can improve the efficiency of somatic cell reprogramming via the activation of NRF2 signalling pathways [440]. Increased reactive oxygen species leads to the inactivation of Kelch-like ECH-associated protein 1 (KEAP1), a negative regulator of NRF2, allowing NRF2 to evade proteasomal degradation and accumulate in the nucleus to mediate maximal activation of downstream effectors [441]. One of the primary targets of the NRF2 transcription factor is the HIFα signalling. The HIFα signalling is integral to the upregulation of glycolysis in the early stages of iPSC reprogramming. The ectopic upregulation of HIF1α throughout the reprogramming process and HIF2α during the early stages significantly enhance the number of cells that successfully undergo metabolic switch and the number of colonies formed [442].

From these studies, it is clear that the NRF2 transcription factors are at the top of the regulatory chain and play an essential role during the reprogramming process, as the initiator of the metabolic switch, and central defence against oxidative stress. Based on the transcriptomic pathway enrichment analysis conducted in this study, the presence of nanoneedles induces a higher level of reactive oxygen species without causing any detrimental harm to the cells as shown by the live/dead™, caspases and DNA damage analyses. Moreover, the predictive canonical analysis also revealed the robust activation of the NRF2 signalling pathway and the enrichment of HIF1α signalling in cells cultured on the nanoneedles. Thus, it would be interesting to see whether the activation of NRF2 signalling induced by the nanoneedles might positively influence the rate of metabolic conversion and overall efficiency of iPSC reprogramming.

3.7.6. Nanoneedle and Cell Cycle Control

Molecular and cellular function analysis on both the transcriptomic and proteomic datasets also revealed a potential disruption on the cell cycle process (Fig. 47).

The mitotic cell cycle consists of DNA synthesis (S phase) separated by two gap phases (G1 and G2) collectively known as interphase and mitosis (M phase). The cyclin-dependent kinase (CDK)-cyclin complexes play a crucial role in regulating the various events that take place during interphase. Transcription factors such as c-Myc and Ets-1 are responsible for driving the expression of genes required for G1/S phase through the upregulation of the E2F transcription factor [443]. At later stages of S phase, CDK2 activation and progression to G2 phase require the activity and binding of cyclin A2. Furthermore, these processes are highly monitored by various checkpoints that act as sensors to detect possible damages during the S phase and chromosome segregations. Briefly, the presence of DNA damage will activate ataxia-telangiectasia mutated (ATM), ataxia telangiectasia and Rad3-related (ATR), and the checkpoint kinases (CHK1 and CHK2) damage response pathways and prevent the transition to G1/S or G2/M phases [443].

In the transcriptomic dataset in the presence of nanoneedle, “mitotic roles of polo-like kinase”, “G2/M damage checkpoint regulation”, and “ATM Signalling” canonical pathways are significantly enriched (Table 19).

Table 19. Over-represented pathways involved in cell cycle regulation.

Canonical pathways involved in cell cycle regulation	**ajd*P-value***	**Ratio**
Mitotic Roles of Polo-Like Kinase	5.96E-06	2.03E-0.1
Cell Cycle: G2/M DNA Damage Checkpoint Regulation	3.64E-03	1.63E-01
ATM Signalling	1.69E-02	1.12E-01

The “Mitotic Roles of Polo-Like Kinase” and the “Cell Cycle: G2/M DNA Damage Checkpoint Regulation” pathways were predicted to be severely affected (Z-score = -2.11 and 2.121 respectively) based on the expression profile of the genes within the dataset. Studies have shown that the aurora and the polo-like kinases (PLK1) play important roles in the transition from G2 to mitosis. PLK1 regulates a wide range of activities in mitosis and cytokinesis. The phosphorylation of PLK1 by Aurora A kinase activates PLK1 during G2 phase and is essential for cells to re-enter the cell cycle following a DNA damage-induced arrest [444]. Additionally,

the activity of cdc25c phosphatase is also required for the activation of cyclin B-cdc2 kinase (MPF) via the dephosphorylation of inhibitory residues of cdc2. The activation of MPF complex is essential for the progression through the G2/M transition [445]. Since all the genes involved in this pathway were found to be down-regulated, it is possible that the presence of nanoneedles might inhibit the progression from the G2 phase to the start of the mitotic phase via the activation of the G2/M DNA damage checkpoint (Fig. 54). Moreover, the "ATM Signalling" pathway was also found to be enriched and activated (Z-score = 0.378), supporting the previous notion that cells on nanoneedles might be arrested at the G2 phase.

Upon closer look at the 58 and 21 differentially expressed genes and proteins found to be associated with the cell cycle process, most of them were involved in microtubule-associated mitotic process. Some of the differentially expressed genes include the various members of the kinesin-like protein family (KIF11, KIF18, KIF22 and KIF23), members of kinesin-like centrosome-associated protein (CENPE, CENPH, CENPI, and CENPA), kinases that involve microtubule formation (AURKA and AURKB), and other spindle-associated proteins (BUB1, Nsl1, Knl1, NUF2 and PLK1). These are all down-regulated in cells cultured on the nanoneedle chips.

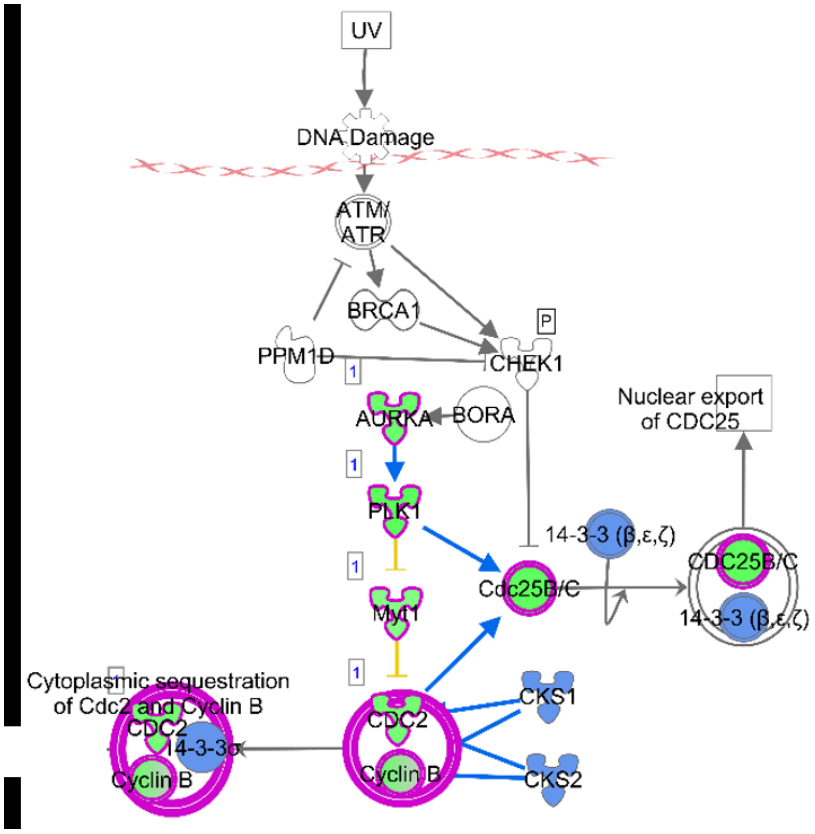


Figure 54. G2/M transition pathway. All the genes involved in the progression of G2 to M phase including, AURKA-PLK1, and cyclin B-cdc2 complex, and cdc25c phosphatase were found to be down regulated in the presence of the nanoneedle chips. Based on the expression profile, IPA canonical analysis predicted the activation of the G2/M DNA damage checkpoint (Z score = 2.121). The observation suggests that cells on nanoneedle chips might not progress to the mitotic phase. Red and green symbols indicate genes up- and down-regulated in the cells on nNs, respectively. Blue symbols represent the predicted downward expression of the genes. The colour intensity is proportional to the degree of fold change.

The centrosome-associated proteins play a crucial role in kinetochore assembly. The kinetochore is a protein complex that sits on the centromere of the chromosomes and connects the chromosomes with microtubules of the spindle to ensure successful segregation of the chromosomes to the daughter cells during mitosis [446]. CENP-A is required to initiate the assembly of the kinetochore complex via the recruitment of CENP-C, CENP-N, and other centromere-associated proteins to form the inner kinetochore subunits. This inner subunit in turn recruits the KMN network which is composed of three sub-complexes (Knl1C (Knl1 and Zwint), Mis12c (Mis12, Nnf1, Dsn1, and Nsl1), and Ndc80c (Ndc80, Nuf2, Spc24 and Spc25)) to form the outer kinetochore complex. These are crucial for microtubule binding and the

spindle assembly checkpoint [447]. Furthermore, studies have shown that CENP-E and CENP-F play a crucial role in mediating the initial attachment of kinetochores to the microtubule lattice, and their inhibition lead to defects in chromosomal alignment, aberrant activation of spindle assembly checkpoints, and mitotic arrest [446]. The gene expression from our study shows downregulation of all these molecules upon exposure to nanoneedle chips, which strongly suggest that the exposure to nanoneedles might inhibit the proper formation of kinetochores and subsequently the successful chromosomal division and mitotic arrest (Fig. 55).

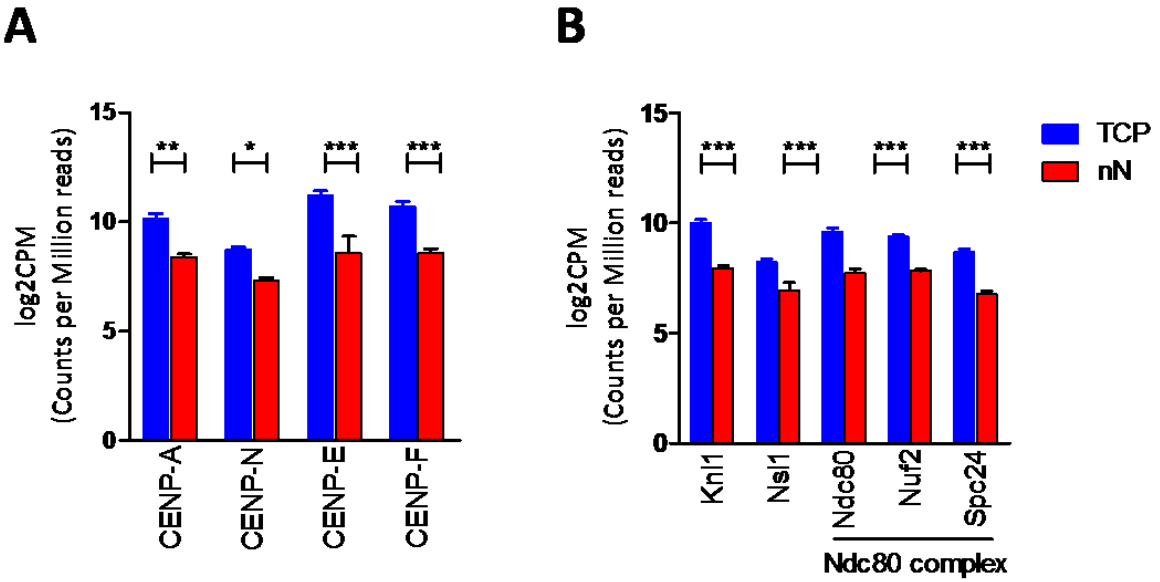


Figure 55. Differential expression of the kinetochore complex. (A) Expression value of centrosome-associated proteins. (B) Expression value of members of the KMN network in log2 (CPM) from the RNA sequencing data of cells seeded on either TCP or nN chips. Comparisons were analysed with two-way anova, Bonferroni post-test. Mean ± SD. N= 4, * ≤ 0.05, ** ≤ 0.01, and *** ≤ 0.001.

The segregation of chromosomes is mediated by the anaphase-promoting complex/cyclosome (APC/C), an E3 ubiquitin ligase responsible for targeting mitotic regulators for degradation, with the help of CDC20 or FZR1 co-factor [443], and is subjected to a screen by the spindle assembly checkpoint (SAC). The SAC is responsible to prevent premature mitotic exit in cells with unattached or improperly attached kinetochore, since errors in this process can lead to chromosomal instability. The interaction between CENP-E and CENP-F with BUB-1 has been shown to be important during the spindle assembly

checkpoint to prevent single chromosome loss. Since depletion of either protein results in metaphase chromosome misalignment and mitotic arrest [448]. In addition to its function during the G2/M checkpoint, Plk1 kinase also plays a role during the mitotic phase and is necessary for the initial formation of a stable kinetochore-microtubule attachment and spindle assembly checkpoints along with Aurora B kinase [449].

To further support the hypothesis that nanoneedle-induced cell cycle disruption primarily affects the mitotic division, a molecular activity prediction analysis was conducted on the "Mitotic Roles of Polo-Like Kinase" canonical pathways using IPA (Fig. 56). In line with the literature, the down regulation of Plk-1 leads to the decrease in the cyclin B-cdc2 complex and subsequently lower EG5 (Kif11) expression, which in-turn is predicted to inhibit/disrupt the separation of the centrosome and the maturation process (Fig. 56a). As shown in figure 55b, the downregulation of APC regulators including Plk-1, Cdc20, cyclin B-cdc2 complex and the mitotic checkpoint complex (Cdc20-mad2l1, Bub1-Bub3) leads to the predicted inhibition of the APC and APC-FZR1 complex required for the metaphase to anaphase transition and the cytokinesis to be completed.

The results are further supported by the gene ontology analysis. The list of genes found to be associated with the cell cycle process was enriched in processes involved in chromosome segregation (21/83, *adjP-value* = 1.24E-16), spindle organisation (16/75, adj*P-value* = 3e-11), and nuclear division (14/75, *adjP-value* = 3.19e-09) during mitosis. Thus, concluding that nanoneedle-induced physical remodelling might have an impact on the microtubule organisation and during the mitotic cell cycle. The cells kick-start defence mechanisms to prevent the rise of chromosomal instabilities or abnormalities on the daughter cells by preventing cell cycle progression. The cells down-regulate all genes required for G2/M transition and predicted to activate the G2/M checkpoint.

Additionally, the physical presence of the nanoneedles might have affected the microtubule structures/dynamics and prevented uneven cellular division due to misaligned chromosomes. The cells also downregulate genes involved in the formation of kinetochores, metaphase to anaphase transition including the SAC complex and mitotic exits.

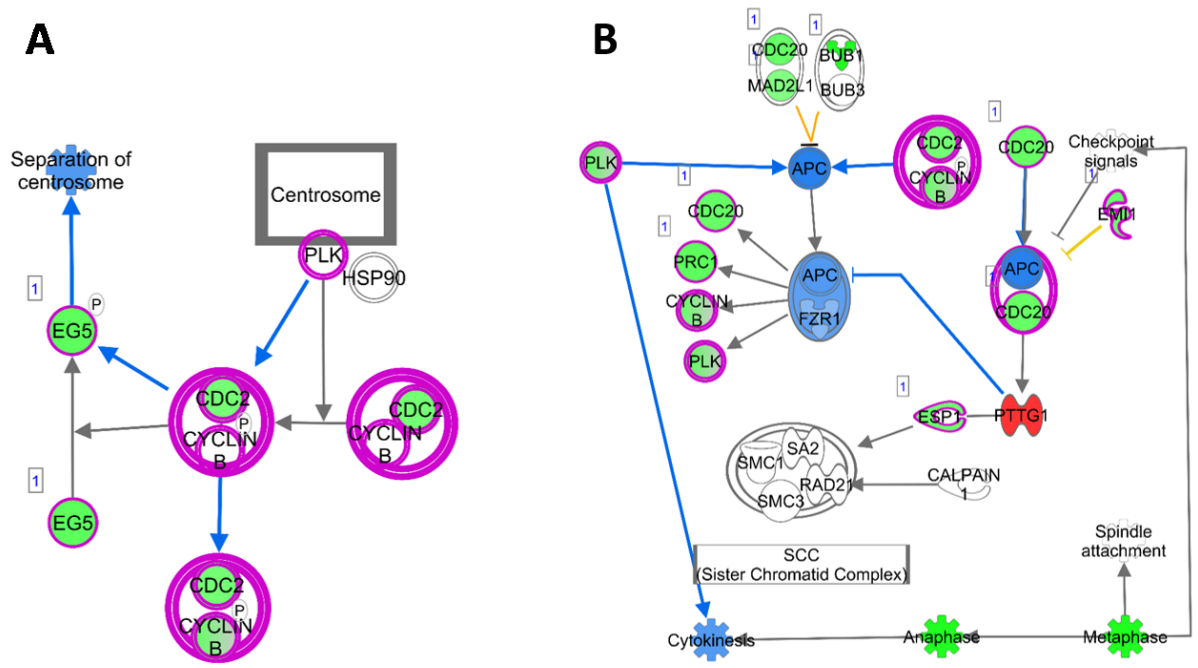


Figure 56. Mitotic pathways. (A) Centrosome separation pathway, and (B) metaphase to anaphase transition and mitotic exit pathway. Both pathways were predicted to be inhibited in the presence on nanoneedle chips. Red and green symbols indicate genes up- and down-regulated in the cells on nN, respectively. Blue symbols represent the predicted downward expression of the genes. The colour intensity is proportional to the degree of fold change.

Studies comparing the level of cellular division and proliferation between nanoneedle chips and control surfaces show wide discrepancies. A study with neurons showed that the percentage of cell cycle antigen (Ki67) detected via immunolabelling was of a similar level on gallium phosphide nanowires and flat control substrate [450]. Bonde *et al.* demonstrated that more HEK293T cells were found to be in S-phase on nanowires than on TCP control based on BrdU labelling [98]. In contrast with our finding, less BrdU positive cells on nanoneedle chips based on immunofluorescent images, and reduced Ki67 expression compared to TCP control (Fig. 57) were observed. They also showed that cells on nanowires were able to form a mitotic spindle required during M-phase and were able to pass through the cell cycle cytokinesis successfully [98]. The discrepancy between the results observed by the studies described above and the results observed in this study might be due to the different cell type used, time-point or physical dimensions.

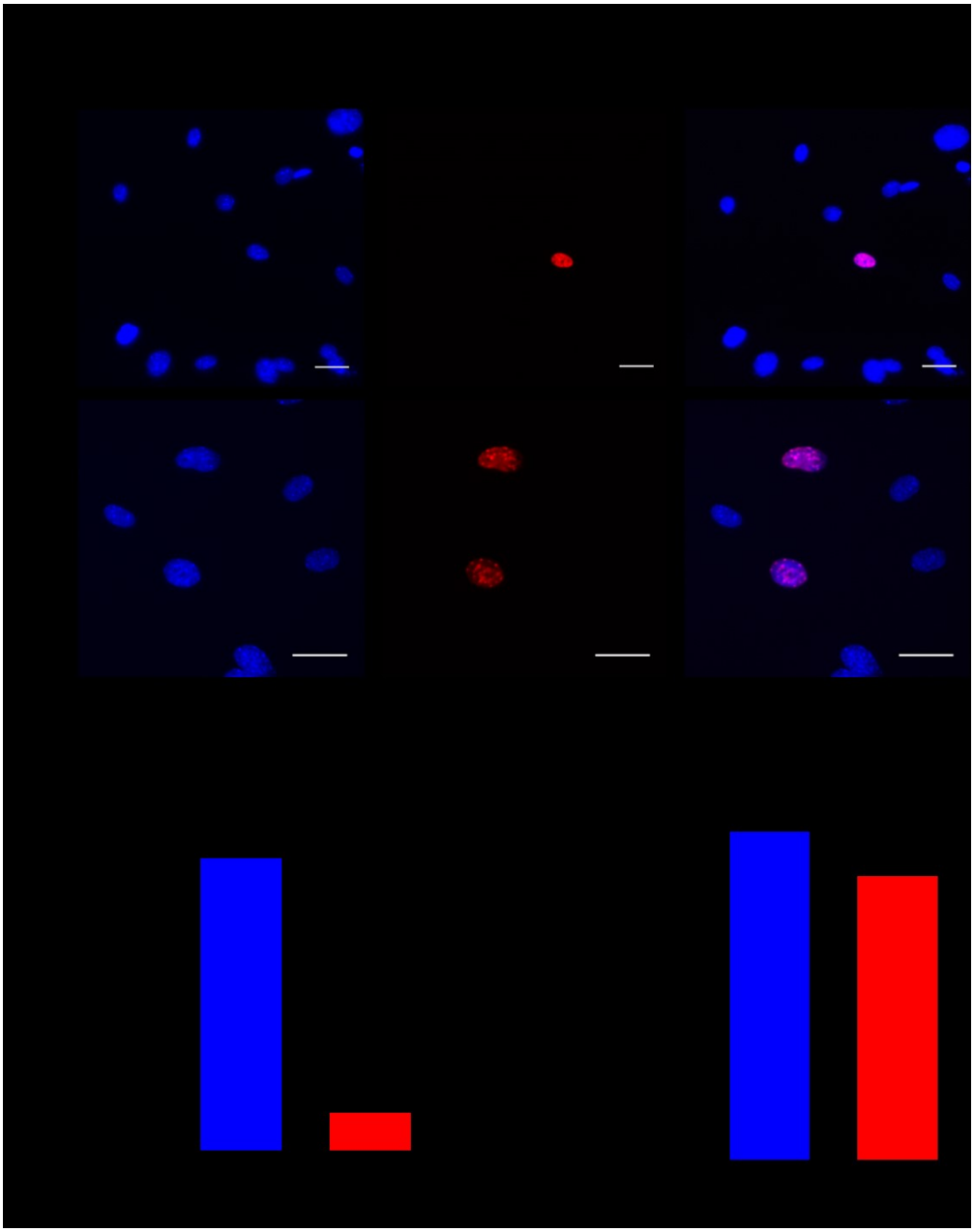


Figure 57. Investigation of cell division. (A) By labelling newly synthesised DNA with the thymidine-analogue BrdU (red), we showed that cells (nuclei, blue) undergo the cell cycle S-phase on both nanoneedle chips and TCP control. Scale bars = 100 µm. Images were acquired by Catherine Hansel (B) Quantitative measurement shows that the number of BrdU positive cells on the nanoneedle chips is significantly decreased compared to TCP control , N = 2. (C) Expression value of Ki67 (cell cycle marker) gene on cells cultured on TCP and nanoneedle chips, N = 4. Statistical significance was analysed with two-tailed, unequal variance student t-tests. ** $p \leq 0.01$, ** $p \leq 0.001$.

In contrast, the cellular division has been reported to be perturbed in L929 fibroblasts cultured on vertical gallium phosphide nanowires [424]. They observed that on nanowires the cells could initiate the process of cellular division, but the process is often either aborted or resulted in aberrant multinucleated cells, especially on the medium (3.8 μm) and long (6.7 μm) length nanowire substrates. The results from our pathway analysis are in line with the results observed by Persson et al. in which the inhibition of genes required for kinetochores assembly and microtubule spindles formation leads to disruption in chromosomal separation during anaphase and cytokinesis and thus resulted in the increased proportion of multinuclear cells on the nanowire substrates. However, no multinucleated cells were observed on the nanoneedle chips following a 24 hours culture. Since Persson et al. only observed cells with abnormal karyotype after 96 hours of culture, it might be possible that during the first 24 hours the cells protective machinery are still able to cope with the disturbances caused by the presence of the nanoneedles by activating the various cell cycle checkpoints and preventing cells to transition through the cell cycle. However, after a certain period, these regulatory elements might fail and allow cells to transition through the different stages of the cell cycle without a proper check which can lead to aberrations such as multinuclear cells and chromosomal instability. Since the nanoneedle chips are degraded following 24 hr incubation, we are unable to monitor the long-term effect the nanoneedle. To identify the molecules that could potentially explain the observed changes, an upstream regulator analysis was performed. Upstream regulators include transcription factors, some cell signalling molecules, such as cytokines and growth factors, as well as enzymes. They can function either as activators or inhibitors for the genes or pathways. Only the upstream regulators with a p value overlap of ≤ 0.01, and either a positive or negative Z-score were considered. The analysis reveals that several transcription factors involved in cell cycle control are perturbed in cells cultured on nanoneedle chips (Fig. 60). As a primary regulator of cell cycle, Myc is predicted as being inactivated in cells cultured on nanoneedle chips (p value = 9.56E-05, Z-score = -3.255).

Myc regulates cell cycle by regulating the expression of target genes many of which are pivotal positive regulators of the cell cycle [451]. Prominent examples of these Myc target genes include, cyclin D2, cyclin E1, Cdc25A, and E2F1. Myc can regulate the levels of active cyclin/Cdks complexes and E2F transcription factors required for cell cycle progression not

only through binding to the respective promoters and transactivating their expressions, but also by elevating the expression of Cdk regulators such as Cdc25, CAK, and Wee1 [451]. Additionally, downregulation of Myc expression results in impaired cell cycle progression via negative regulation of the genes involved in the Cdk/Rb/E2F pathway [452]. A study revealed that the depletion of Myc leads to arrest at either the G0/G1 phase or G2/M phase, and may be dependent upon the expression pattern of oncogene suppressors such as Rb or p53 [453]. The decreased expression of genes downstream of Myc and upregulation of Myc negative regulator (RBL2) in our dataset are in-line with Myc activity being inactivated (Fig. 58).

Apart from Myc, as a main transcriptional factor in cell cycle regulation, the forkhead transcription factor 1 (FOXM1), is also predicted to be responsible for the alterations observed upon exposure to nanoneedle chips. FOXM1 is also predicted to be inactivated (*p*--value = 3.86E-04, Z-score = -2.607) and is downregulated by 1.738-fold in cells cultured on nanoneedle chips. The main role of FOXM1 transcription factors is cell-cycle regulation, in particular, the G2/M transition.

CHIP-seq demonstrates that FOXM1 binds directly to the cell cycle gene homology region and regulates a group of genes involved in the G2 and M phases including Plk1, and Ccnb2 [454]. Downregulation of FOXM1 leads to downregulation of the genes involved during the G2/M transition, further supporting the notion that cells cultured on the nanoneedle chips are likely to be arrested at the G2/M phase of the cell cycle.

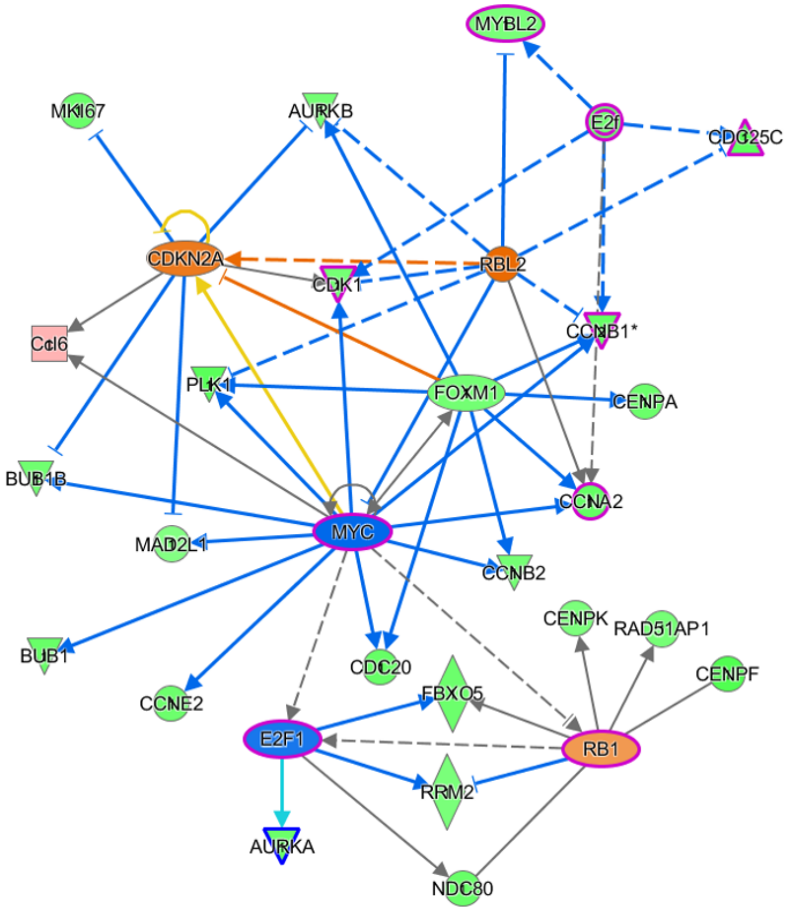


Figure 58. Cell cycle upstream regulators. Transcription factor Myc is predicted to be inactivated and is responsible for the observed alteration in the cell cycle regulation in the presence of the nanoneedles. Myc functions through several intervening regulators such as the Foxm2, Rb1 and E2F family transcription factors to bring about the changes observed in the gene expression. Red and green indicates upregulation and downregulation of gene expression, respectively. The regulators are coloured based on their predicted activation state: orange (activated) or blue (repressed). The intensity of the colour corresponds to the level of activity or expression. The edges connecting the nodes are coloured orange when leading to activation of the downstream node, blue when leading to its inhibition, and yellow if the findings underlying the relationship are inconsistent with the state of the downstream node.

3.7.7. Histones and DNA Modifications on Nanoneedle Chips

As discussed in the literature review of this chapter, the alteration in cell and nuclear shape can lead to epigenetic modifications. More specifically, extracellular mechanical signals derived from topographical cues have been reported to increase the level of histone acetylation and promote cellular reprogramming in both mouse embryonic fibroblasts [66] and mesenchymal stem cells [370]. To test whether the alteration in nuclear structure observed in cells cultured on nanoneedle chips also leads to modifications of the epigenetic codes, western blotting and immunofluorescence analysis on MEFs cultured on either nanoneedle chips or TCP control for 24 hours were performed.

Firstly, qPCR arrays to screen for alterations in the expression levels of various histone modifying enzymes were conducted (Fig. 59). The screen focused on enzymes responsible for the modulation of classical histone markers, methylation and acetylation. From the analysis, a general decrease in the expression of a histone methyltransferase in cells cultured on nanoneedles compared to TCP was observed. An increase in the expression of UTX, *i.e.* a histone H3 demethylase was observed too. Except for the significant increase in the level of HDAC11 expression no other changes in the expression of other histone acetylation modifying enzymes assayed were detected. Lastly, a significant downregulation of a component of the SWI/SNF chromatin remodelling complex, BRG1 was observed. The results suggest a possible alteration in the level of histone methylation and acetylation.

To provide further evidence that the nanoneedle chips might induce a general histone remodelling, the level of several histone post-translational modifications at the global level were investigated. First, the level of histone methylations were determined, in particular the level of active-associated histone marks H3K4me3. Immunofluorescence imaging and subsequent analysis revealed that the level of H3K4me3 on MEFs cultured on nanoneedle chips are significantly higher compared to the TCP control (Fig. 60). The western blotting analysis further confirmed the results (Fig. 61). However, the increase of the H3K4me3 signal on the nanoneedle samples was not statistically significant based on the WB analysis.

Nevertheless, the increase in global H3K4me3 corroborates previously published findings suggesting that a reduced nuclear area/volume might be linked to the increase in this histone marker even though different topographical cues were used in those studies [66, 226].

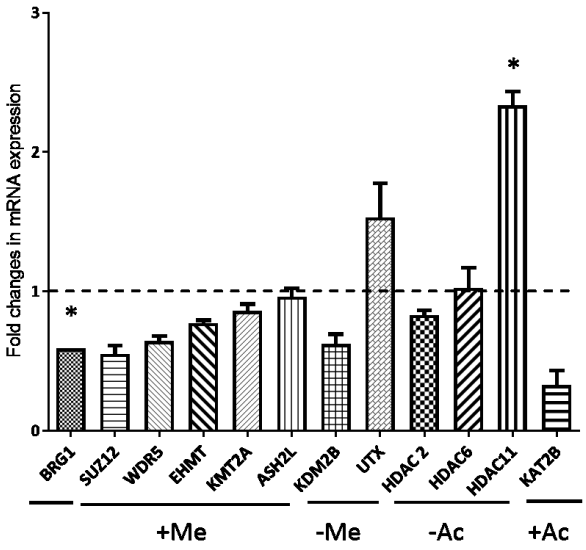


Figure 59. Screen of histone modifying enzymes. The expression level of histone modifying enzymes in cells cultured on nanoneedle chips compared to the TCP control. Chromatin remodelling enzyme (BRG1), histone methyltransferases (SUZ12, WDR5, EHMT, KMT2A, and ASH2L), histone demethylases (KDM2B, and UTX), histone deacetylases (HDAC2, HDAC6 and HDAC11), and histone acetyltransferase (KAT2B). Statistical significance was analysed with two-tailed, unequal variance Student t-tests. Mean ± SD, N= 1, n= 3, * $p \leq 0.05$.

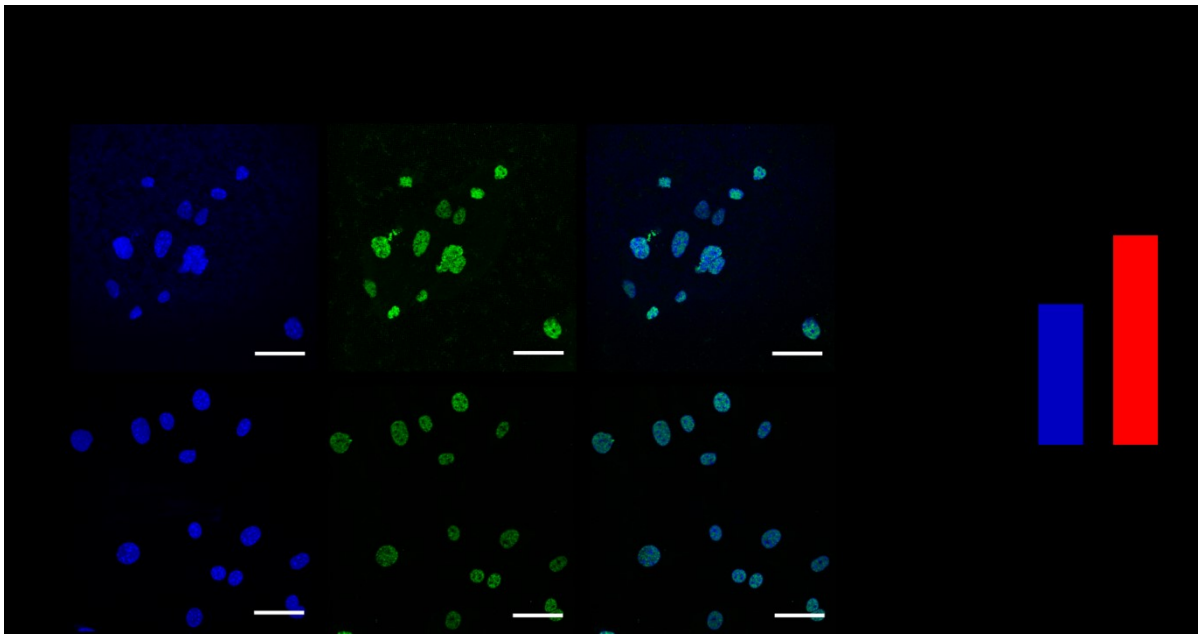


Figure 60. H3K4me3 immunofluorescence. (A) Representative images of MEFs cultured on nanoneedle chips or TCP control stained with DAPI (blue), H3K4me3 (green). Scale bars = 25 µm. Images were acquired by Catherine Hansel (B) Quantitative measurement of the mean fluorescent intensity of the H3K4me3, showed significant upregulation in the active histone marker in cells cultured on nN. Statistical significance was analysed with two-tailed, unequal variance Student t-tests. Mean ± SD, N=3, * $p \leq 0.05$.

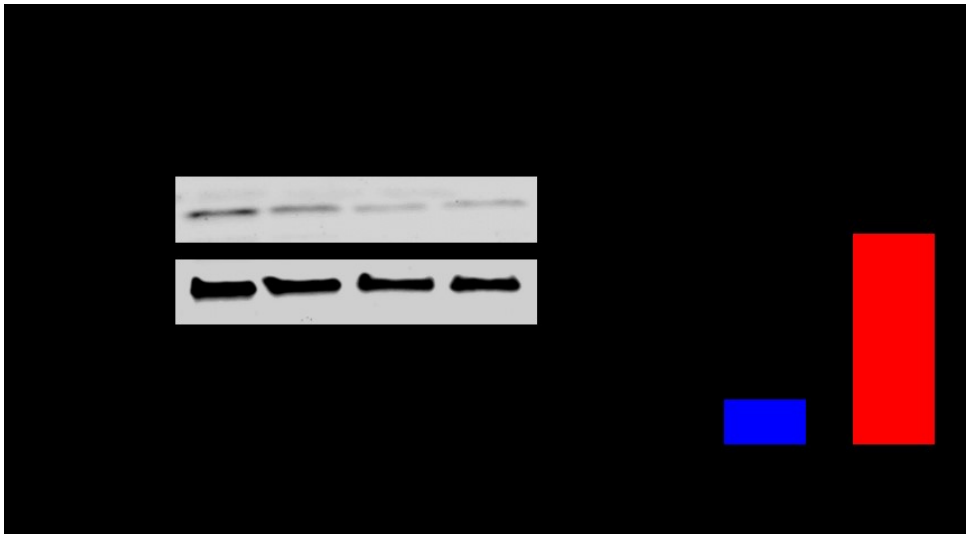


Figure 61. Quantification of H3K4me3. (A) Associated representative immunoblot of the H3K4me3 and GAPDH control. (B) Western blot quantification of H3K4me3 level in MEFS on nanoneedle chips and TCP control. Mean ± SD, N = 3, n = 6.

To further investigate whether the changes in the level of the H3K4me3 were associated with a modification in the expression level of the corresponding modifying enzymes, quantitative RT-PCR analysis on several members of the histone methyltransferase family were performed (Fig. 62). Upregulation in KMT2D (formerly known as MLL2) and KMT2A (formerly known as MLL1) were detected. These two genes are the core component of the MLL1/MLL complex. They contain the SET domain which catalyses the addition of methyl group to the H3K4. However, no difference in the expression of WDR5 and ASH2L, transcriptional activators that belong to the same complex were detected. Furthermore, no change in the level of KDM2B, a H3K4 specific demethylase (Fig. 62).

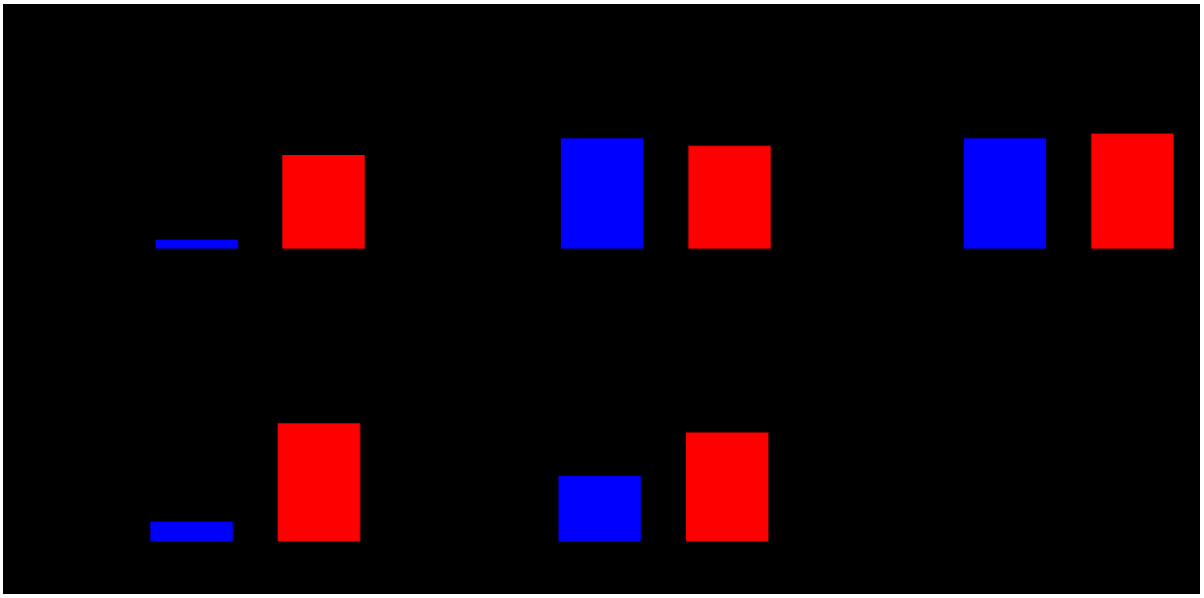


Figure 62. Quantification of H3K4me3 modifying enzymes. qRT-PCR of genes that catalyse the addition or removal of methyl group to the histone H3K4 24 hours post seeding on either nanoneedle chips or TCP control shows the upregulation of the core catalytic subunits of the complex, KMT2D and KMT2A. Statistical significance was analysed with two-tailed, unequal variance Student t-tests. Mean ± SD, N = 3, n = 5, * $p \leq 0.05$, ** $p \leq 0.01$.

A general increase in H3K4me3 level could suggest an increase in chromatin accessibility, and in general this change might be accompanied by a global decrease of the heterochromatin-associated histone marker. To test this hypothesis immunofluorescent imaging and western blotting analysis were used in combination to study the global level of H3K27me3, a marker associated with inactive chromatin. Representative relative quantification of the immunofluorescence images revealed significant difference in the level of H3K27me3 between cells cultured on TCP vs nN based on the mean fluorescence intensity (Fig. 63b). There appeared to be high level of variation in the intensity of the H3K27me3 signal especially in samples cultured on nN. The use of more sensitive technique, western blot analysis revealed a significant reduction of the histone H3K27me3 level globally on the cells cultured on nanoneedle chips (Fig. 64). Thus concludes the effect of nanoneedle in promoting a more open chromatin status through the upregulation of histone active marker, H3K4me3, and simultaneous reduction in the level of repressive histone marker, H3K27me3.

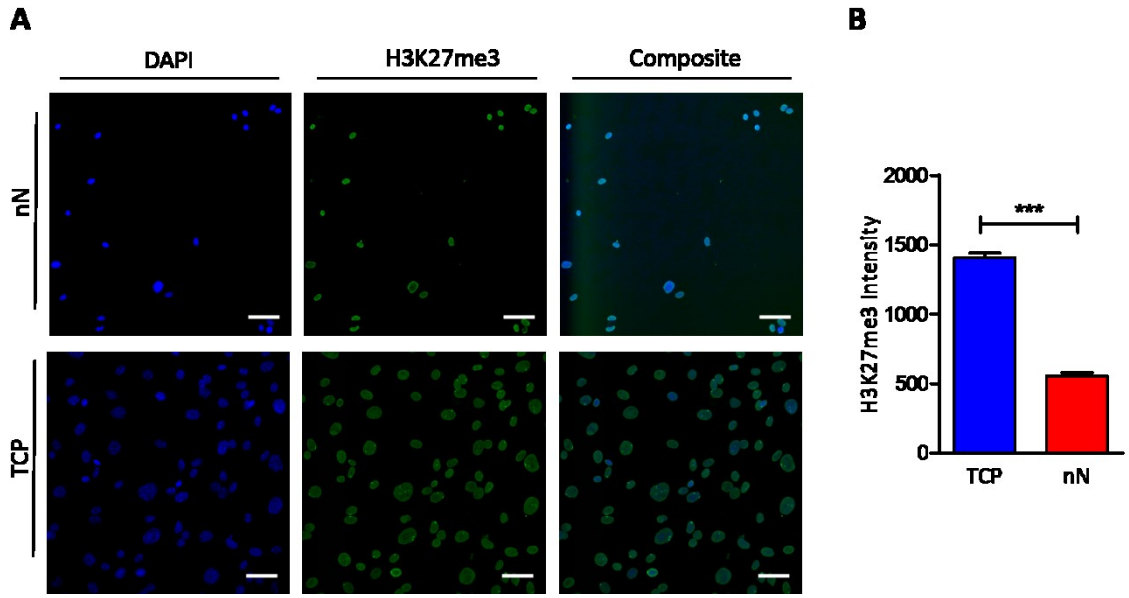


Figure 63. H3K27me3 immunofluorescence. (A) Representative images of MEFs cultured on nanoneedle chips or TCP control stained with DAPI (blue), H3K27me3 (green). Scale bars = 50 µm. Images were acquired by Catherine Hansel (B) Representative quantitative measurement of the mean fluorescent intensity of the H3K27me3, statistical significant difference between cells on TCP vs nN. Statistical significance was analysed with two-tailed, unequal variance Student t-tests. Mean ± SD, N = 1, TCP= 70 cells, nN= 48 cells.

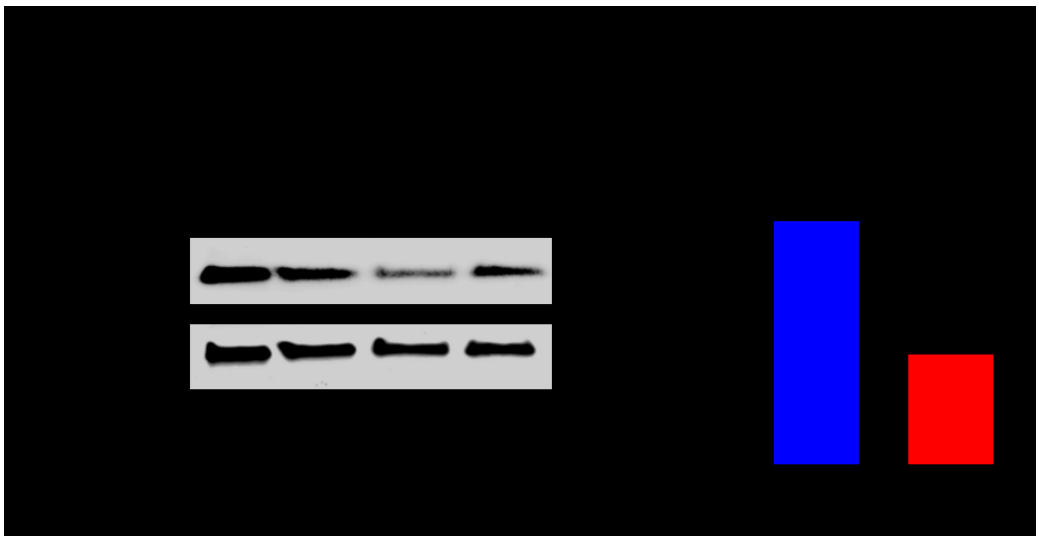


Figure 64. Quantification of H3K27me3. (A) Associated representative immunoblot of the H3K27me3 and GAPDH control. (B) Western blot quantification of H3K27me3 level in MEFS on nanoneedle chips and TCP control. Statistical significance was analysed with two-tailed, unequal variance Student t-tests. Mean ± SD, N =3, n =6, ***$p \leq 0.001$.

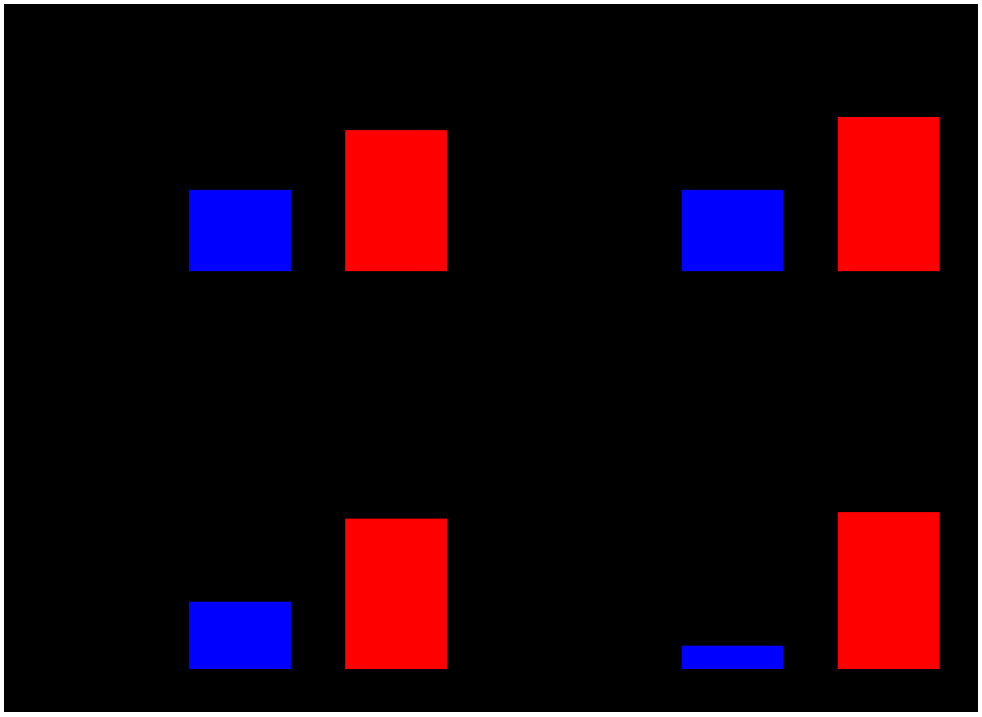


Figure 65. Quantification of H3K27me3 modifying enzymes. qRT-PCR of genes that catalyses the addition or removal of methyl group to the histone H3K27 24 hours post seeding on either nanoneedle chips or TCP control. The analysis shows the upregulation of the two core subunits of the H3K27 demethylases and an upregulation of KMT6B histone methyltransferases. Statistical significance was analysed with two-tailed, unequal variance Student t-tests. Mean ± SD, N = 4, n = 10, $**p \leq 0.01$, $***p \leq 0.001$.

qRT-PCR analysis of the H3K27me3 modifying enzymes were conducted to understand whether the alteration in the H3K27me3 levels was the result of decreased methyltransferase and increased demethylase expression (Fig. 65). A significant upregulation of KMT6B also known as EZH1 was observed. This gene belongs to the polycomb repressive complex 2 (PRC2) along with SUZ12 and is the primary catalytic component of the PRC2 complex. This complex is responsible for catalysing the addition of H3K27me3 and leads to epigenetic silencing of target sequences. Furthermore, the two specific enzymes responsible for the demethylation of Lys-27 of histone H3 were found to be significantly up-regulated. Based on the observed reduction in the global level of the H3K27me3, it may be possible that the overexpression of the H3K27 demethylases might off-set the effect of an increase in the level of the methyltransferase.

The level of histone H3 acetylation was also investigated using western blot analysis. The results showed that the nanoneedles did not have any effect on the level of the histone H3K4/K19 acetylation (Fig. 66).

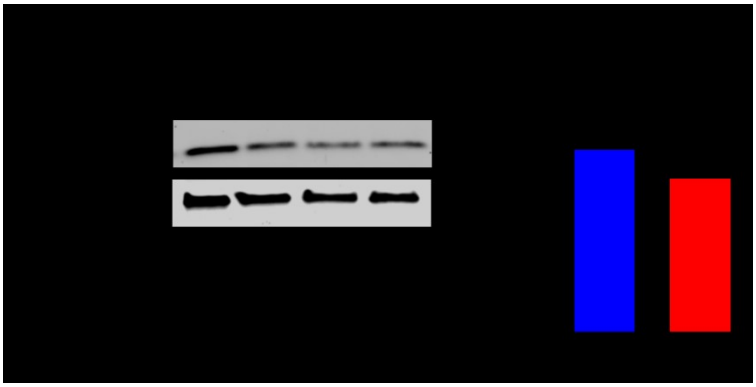


Figure 66. Quantification of H3K4/K19Ac. (A) Associated representative immunoblot of the H3K4/K19Ac and GAPDH control. (B) Western blot quantification of H3K4/K19Ac level in MEFS on nanoneedle chips and TCP control. Mean ± SD, N = 3, n = 6.

Surprisingly, a robust upregulation in the level of HDAC11 was observed, the only member of the class IV HDAC family (Fig. 67). This HDAC is one of the least characterised HDACs. It has been shown that in cells exiting the cell cycle or arresting, the level of HDAC11 mRNA accumulates in the cells [455]. Through an overexpression study, Bagui *et al.* further demonstrated that the upregulation of HDAC11 prevents the cell cycle progression in mouse fibroblasts [455]. Thus, HDAC11 upregulation in cells cultured on nanoneedle chips provides further support and might be partially responsible for the observed/postulated increase in the number of cells exiting the cell cycle at the G2/M phase and failing to progress through the cell cycle process.

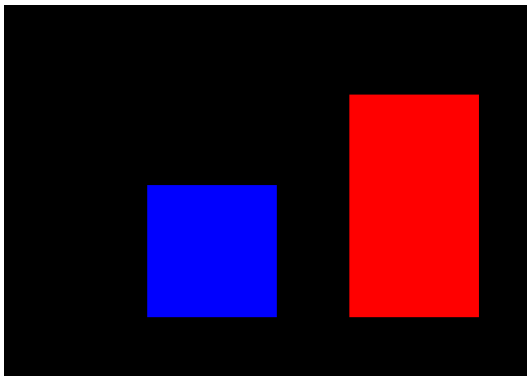


Figure 67. mRNA level of HDAC11. qRT-PCR of HDAC11, a class IV histone deacetylase, 24 hours post seeding on either nanoneedle chips or TCP control shows robust upregulation. Statistical significance was analysed with two-tailed, unequal variance Student t-tests. Mean ± SD, N = 4, n = 11, ** $p \leq 0.01$.

Another vital aspect of epigenetic regulation is DNA methylation. It is involved in various functions in mammalian cells including cell cycle regulation and development. However, the extent to which DNA methylation changes in response to external mechanical cues is currently not well known. Next, the effect of nanoneedles on the level of DNA methylation in the cells was investigated (Fig. 68). Based on the immunofluorescent images, the level of DNA 5-mc were found to be slightly reduced in nN samples compare to TCP but the difference was not significant (Fig. 68a, b).

qRT-PCR were also performed to analyse the level of DNA methyltransferases in the cell (Fig. 69). Significant reduction in the level of the maintenance methyltransferase, DNMT1, and no change in the expression profile of the two methyltransferases responsible for *de novo* methylation were observed. These results suggest that the reduction in global DNA 5mc could potentially be due to an increased turnover of the 5mc marks by the DNA demethylases, the lack of DNMT1 activity to preserve the existing DNA 5mc marks, and no increase in the speed or number of new DNA 5mc.

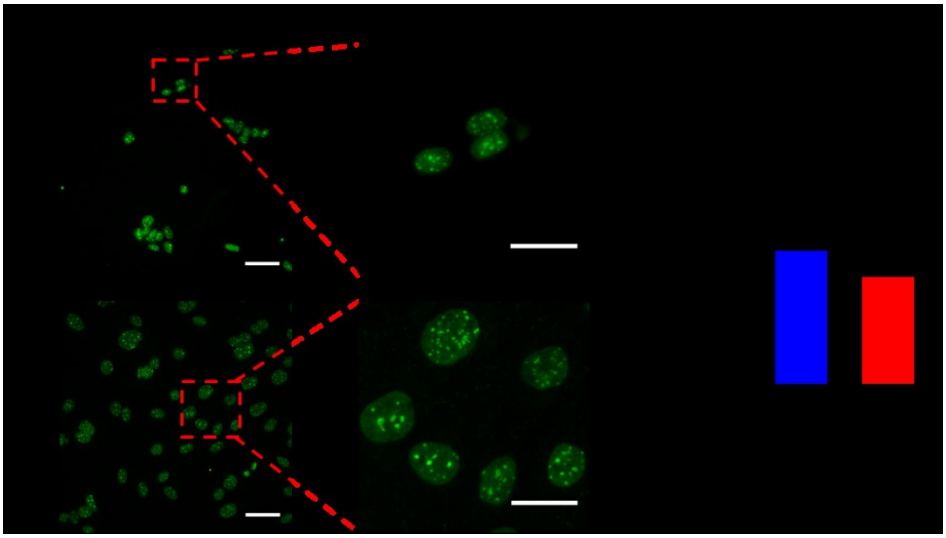


Figure 68. Effect of nanoneedles on the level of DNA 5-mc. (A) Representative immunofluorescence micrographs of MEFs cultured on nanoneedle chips or TCP control stained with antibody specific to DNA 5-mc (green). The panels on the right correspond to the area highlighted by the red dotted box. Scale bars = 50 µm (left), 25 µm (right). Images were acquired by Catherine Hansel (B) Quantitative measurement of the mean fluorescent intensity of the DNA 5-mc. Mean ± SD, N = 2. Statistical significance was analysed with two-tailed, unequal variance Student t-tests.

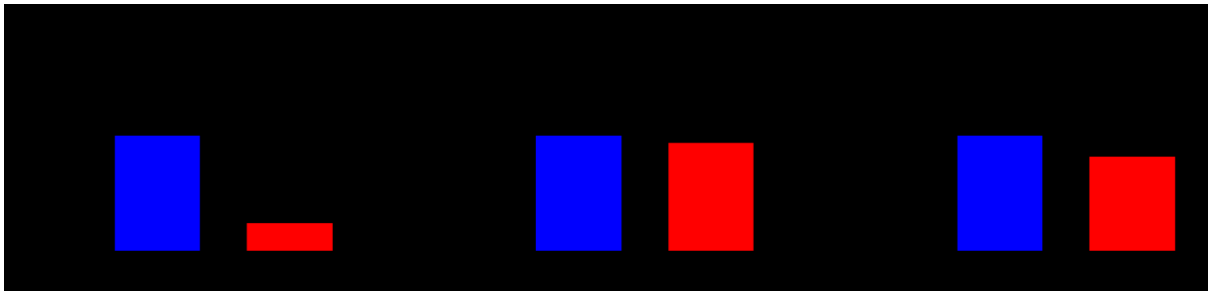


Figure 69. Expression levels of DNMTs. qRT-PCR of the three DNMTs: DNMT1, DNMT3a, and DNMT3b, 24 hours post seeding on either nanoneedle chips or TCP control show significant downregulation of DNMT1 expression on nanoneedle samples. Statistical significance was analysed with two-tailed, unequal variance Student t-tests. Mean ± SD, N = 3, n = 7, $^{**}p \leq 0.01$.

3.8. Disscussion

Extensive progress has been made in the past two decades on the field of mechanobiology. The notion that mechanical cues present in the cellular microenvironment play an essential role in influencing cells decision-making processes are well supported. The relationship between a cell and its surrounding microenvironment is very dynamic, *i.e.* a cell will respond to alteration in extracellular cues by secreting signalling molecules which can alter the composition of the matrix. The growing importance of mechanical cues in regulating biological processes including cell growth, differentiation and cellular fate, has led researchers to further investigate the mechanosensitive pathways.

In parallel to the tremendous progress made in the field of mechanobiology, the fields of bioengineering and biomaterial science have also generated a lot of progress. Various material based *in vitro* model systems have been established to provide dynamic modulation and stimulation of various biochemical and biophysical signals to the cells. This advancement in biomaterial sciences has aided researchers in further understanding the interaction between cell and their surroundings. In recent years micro- and nano-engineered functional biomaterials have been of great help. The ability to tune patterns, geometries, compositions and functionality of materials allow researchers to understand the effects of biophysical cues such as cell shape, stiffness, topography, and geometry in detail. An emerging class of high aspect ratio nanomaterials with diverse tuneable properties have been shown to have a wide range of biological applications. These include the delivery of cell-impermeable biomolecules, electrophysiological recording, and biosensors *in vitro* and *in vivo*.

Owing to their growing use as an investigative and therapeutic tool, the effects of nanostructure materials on cultured cells were particularly of interests. In particular, the effect of high-aspect-ratio porous biodegradable SiO_2 nanoneedles in mouse embryonic fibroblasts (MEFs) behaviour were investigated.

The nanoneedles closely interact with the cells and induced a significant alteration in the cell nuclear structure, owing to the geometrical constraint, nanoscale dimensions, and high aspect ratio. Cells cultured on nanoneedles have a highly tortuous nuclear lamina with lamin rings formed around the individual nanoneedles from the basal to the apical layer. Moreover, a significant reduction in the size of the nucleus, and rearrangement of the intranuclear components such as a decrease in the number of heterochromatin foci were observed. All this massive rearrangement did not seem to affect cell viability and chromatin compactability.

To gain a better understanding of the detailed molecular changes that occur upon exposure to nanoneedles, global hypothesis-generating approach was applied using a combination of RNAseq and label-free MS to map the cells' transcriptome and proteome, respectively. Initial analysis of both datasets revealed that the cells cultured on nanoneedle chips are distinct from the TCP control counterpart. The presence of nanoneedles seems to have induced an extensive and unforeseen global remodelling at both mRNA and protein levels that were not apparent through the initial viability experiments and imaging studies.

Although initial viability experiments showed in Fig 30 did not show any significant activation of cellular apoptosis pathways; the presence of nanoneedles appears to activate the cellular oxidative stress response according to the pathway analysis of the –omics datasets.

It appears that the SiO_2 released because of the biodegradation of the nanoneedles structure leads to the activation of NRF2 transcription factors signalling pathways. NRF2 acts at the top of the regulatory chain that controls the cell main defence mechanism against oxidative stress. The activation of NRF2 leads to the upregulation of genes involved in the glutathione-mediated detoxifications, xenobiotic metabolism and HIF1α signalling such as GSTA3, MGST1, PTGES2, and PTGR2. All these genes are involved in protecting the cells against harmful genotoxic molecules. It seems that the activation of these pathways might be responsible in preventing DNA damage, as no increase in the level of γH2Ax, active caspases or dead cells was observed.

Furthermore, the –omics analysis revealed that cells cultured on the nanoneedle chips are arrested at the G2/M and the metaphase to anaphase transition. Significant downregulation in genes involved in the G2/M transition and in genes required for the formation of stable kinetochore and microtubule spindle structure for proper chromosomal separations were observed. The *in-silico* analysis was partially confirmed by the reduction in the level of BrdU positive cells and the level of Ki67 gene expression.

Further analysis revealed that the transcription factor c-MYC was responsible for the observed changes. The expression of this significant cell cycle regulator was predicted to be downregulated and thus leads to inhibition of cell cycle progression.

Finally, since alteration in nuclear shape has been shown to affect cellular reprogramming, differentiation and cell fate via epigenetic remodelling, some of the canonical epigenetic markers linked to reprogramming were also observed. Our analysis revealed a significant downregulation in the histone repressive marker H3K27me3, and an increase, albeit not to a significant level, in the expression of histone active marker H3K4me3. Furthermore, slight downregulation in the level of repressive DNA marker 5-mc was also detected. These changes in the post-translational modifications were accompanied by the alteration in the expression level of the genes encoding the enzymes responsible for the maintenance, addition or removal of these codes.

Taken together the results from the epigenetic markers and nuclear structures provide compelling evidence that nanoneedles might be able to induce a global epigenetic remodelling and disruption of heterochromatin. The nanoneedles might even promote the chromatins to be more accessible and perhaps enhance cellular reprogramming via epigenetic remodelling and activation of cellular signalling such as the NRF2 pathways that have been shown to promote reprogramming.

The alterations observed especially in the epigenetic and nuclear structure provide some evidence that the physical interaction between the cell and the nanoneedle structure are responsible for some of the changes observed. Since, cells undergoing cellular stress or apoptosis would be in a highly repressed epigenetic state and have a condensed nuclear structure [459, 460]; as oppose to the increase euchromatin and more relaxed nucleus observed in cells cultured on the nanoneedle substrate. Although, we can't rule out the contributions of free-floating SiO_2 induced cellular stress to the observed alterations in

cellular status. It might be possible that the combination of physical constraints induced cytoskeletal remodelling, and the elevated stress response caused by the nanoneedles might be responsible for the observed changes.

So, it is also worth comparing the transcriptomic and proteomic profiles of cells cultured on nN to cells undergoing induced apoptosis and cells cultured on non-degradable nanoneedle. As the results from the comparisons would be able to tell us more specifically if certain changes observed when cells were cultured on the nanoneedle were solely due to the physical constrain applied by the nanoneedle structures or the stress responses activated by the release of SiO_2 from the nanoneedles as they degrade.

Further studies will be needed to investigate in detail the feasibility of nanoneedle-enhanced cellular reprogramming hypothesis. Unfortunately, at the time of writing, results from the MEFs to iPSCs reprogramming on the nanoneedle were not yet available. However, to fully decipher and grasp the underlying mechanisms of the changes observed, high-resolution chromatin immunoprecipitation followed by sequencing (CHIP-seq) will ultimately be needed. Knowing the exact location where the epigenetic markers are enriched will tremendously support the ability to draw reliable conclusions on the potential applications of this material. Besides, a combination of full metabolic activity and metabolomics screening might be beneficial to support the claim generated by the *in-silico* study and guide the clinical usage of SiO_2 based nanomaterials. Being able to fully understand the exact mode of action and the changes caused by the nanoneedles might inform the creation of next-generation nanomaterial systems for clinical and research purposes.

Chapter 4: Conclusions

The field of biomaterial science is currently advancing rapidly, combining progress in technology and biology to develop constructs that are valuable in a variety of areas of biology and medicine. Canonically, biomaterials have been used in regenerative medicine to aid the development of life-like tissues and organs replacement. However, biomaterials also have an important role to play in drug-delivery as biomaterials allow users to tailor the properties in fine-detail to match the required applications, offer a way to deliver biomolecules in a targeted and efficient manner *in vivo* and in conventional *in vitro* experiments. More recently, thanks to the fast-evolving field of microfabrication, this technology is allowing researchers to incorporate the physical structures present in the cellular microenvironment to reproduce a physiologically relevant microenvironment in an *in vitro* setting to replace traditional culture techniques. This offers a way to aid fundamental biological research to understand the complex two-way relationship between cells and their native environment.

Considering the progress in tailored biomaterials and microfabrication it is possible to ask whether we could use these new materials to address some of the most pressing medical and fundamental research problems.

To that end, we utilised a microfabricated porous silicon nanoneedle array as a culture substrate [10]. The geometry of the nanoneedle array has been optimised to meet the requirements for intracellular delivery. The nanoneedles were made porous to increase the surface area to allow maximum loading of biomolecules. The porosity also makes the nanoneedles biodegradable, which is an essential property for *in vivo* applications. The physical properties of the same nanoneedles have also been customised to provide isolated and specific systems to mimic naturally occurring biophysical cues and understand their effect on cellular function. Owing to the nanoscale dimensions and high aspect ratio of the nanoneedle, the nanoneedles can form strong intimate interaction with the cell membrane and the intracellular space of the cells without causing substantial damage.

We propose nanoneedle-mediated delivery as an effective and unique strategy to specifically target gene therapy to epicardial cells *in vivo* for cardiac applications. The limited regeneration capacity of the adult mammalian heart poses a real threat following MI. Gene therapy specifically by direct cardiac reprogramming represents a promising approach for cardiac regeneration and have been shown in various models to restore cardiac function.

Recent studies demonstrated that the epicardium is a promising target for these therapies as it harbours a population of progenitor cells (EPDCs) that plays crucial roles in response to injury. The EPDCs activate post-injury, undergo rapid expansion and contribute to myocardial repair through both paracrine signallings and differentiating into vascular cells, myocytes and fibroblasts. Several studies have demonstrated the feasibility to induce greater involvement of the EPDCs in cardiac repair.

We aimed to explore the possibility to directly reprogram EPDCs into cardiomyocytes *in vivo* to restore heart function. We used the nanoneedle-mediated delivery (nanoinjection) to target gene therapy to the epicardial cells as a promising approach that has not been investigated before.

This study developed a method to efficiently load and rapidly release pDNA from the nanoneedles to mediate efficient transfection. This was achieved through surface chemistry modification via oxygen plasma treatment and the use of optimised buffers that match the pk value of pDNA. Also, we utilise the transposon/transposase system to encode, deliver and integrate the cardiac reprogramming factor MGT. The three cardiac reprogramming genes were combined into a single polycistronic transposon-based plasmid to enable the simultaneous transfer of the three large genes, and overcoming the low co-expression generally observed when genes are delivered using multiple vectors.

We also tested the potential of nanoneedles for integrative gene therapy. Gene expression analysis confirmed sustained expression of transgenes over 30 days and genetic analysis of the genomic DNA indicated the successful integration of the transgenes in the nanoinjected cultures. Next, we demonstrated that the nanoinjection of the PB-MGT lead to the sustained expression of the transgenes and the upregulation of endogenous early cardiac reprogramming genes such as Nppa, Actnt2, and Tnnt2 in isolated primary epicardial cells by day 18. Upon application of the nN chip loaded with MGT+HaHy to the post-MI epicardium in live rats, histological analysis of samples collected at 30 min showed an initial delivery specifically to the epicardial layer, followed by migration and spreading of the transfected cells to the underlying tissue. Two days post-nanoinjection, the overexpression of the Gata4 and Tbx5 transgenes were observed in 4 out of the 7 animals. However, the analysis of samples collected at day 7 showed reduced overall expression of the transgenes, to a non-significant level. These findings indicate that the nN-mediated intracellular gene delivery to

the heart epicardium was mostly successful, but in the long term the transfection was either not stable, or the transfected cells either suppressed gene expression, died or migrated outside of the collection area.

The reprogrammed epicardial cells in this study did not robustly activate the full cardiac program; and instead only induced expression of early cardiac markers. The inefficient cardiac reprogramming reported was likely caused by several reasons. Firstly, despite adopting an optimal stoichiometry of reprogramming factors (Mef2c-Gata4-Tbx5) in a polycistronic constuct as reported by Wang *et al*., the expression profile of the MGT construct generated in this study showed an inverse expressions (*i.e.* high Tbx5, and Gata4, and low level of Mef2c) compared to construct generated by Wang *et al.* [35]. This discrepancy in expression patterns might be down to the different plasmid backbone, and promoter used in the construct, and perhaps the addition of in-frame dsRED casette at the end of the construct might influence the way the transcription machinery process the information. Consistent with previously published findings that high expression of Tbx5 and Gata4 is associated with low level/inefficient cardiac reprogramming [34, 35, 456].

Secondly, to the best of our knowledge, this study represents the first attempt at direct reprogramming of epicardial derived cells towards iCM both *in vitro* and *in vivo*. Most of the published studies only used fibroblasts from either mouse or human of various sources such as cardiac, tail-tip or embryonic to performed the direct cardiac reprogramming protocols. Since the rat EPDCs were isolated from the post-MI heart without any enrichment or purification steps; one can assume that the culture contains a mix population of cells including fibroblasts and activated epicardial cells ($Wt1^+$, and $TCF21^+$). Thus it is possible that additional factors or different factors might be needed to fully activate the cardiac gene program. As demonstrated by several studies, the MGT transcription factors are enough to reprogram neonatal mouse fibroblasts into cardiomyocyte, but the same factors are far than optimal in adult of human fibroblasts [204-206].

While our work did not aim at establishing the ideal protocol for epicardial cell reprogramming, our data reveal that these factors can induce and initiate the early stages of the cardiac reprogramming factors. Further studies are necessary to establish the cellular identities of the cells that were transfected in the epicardium layer of the heart. The information obtained could help design excellent reprogramming cocktails. Additionally, the

nanoneedles enable the loading of different types of cargoes simultaneously, including nucleic acids and chemical inhibitors and allow to specifically target the epicardium. Future studies exploring the use of nanoneedles to deliver the TF-based reprogramming factors along with small molecules inhibitors that have been shown to promote cardiac reprogramming could provide far superior results. Lastly, a further optimisation into the strategy for interfacing nanoneedles with the epicardium might provide more uniform and higher rate of transfection.

In the second part of the study, we proposed to use the nanoneedle chips to provide external mechanical cues and investigate the global changes that occur within the cell. Phyicomechanical signals from the extracellular environment play a crucial role in dictating cells decision-making processes. Biophysical cues can regulate processes including, cell growth, differentiation and cellular fate. These discoveries have led researchers to further investigate various mechanosensitive pathways. High-aspect-ratio porous biodegradable nanoneedles generated from SiO_2 have been successfully used in various investigative and therapeutic tools. As such, we sought to investigate the effects nanoneedles have on MEFs.

The presence of nanoneedles induces extensive nuclear remodelling which includes significant reduction in nuclear size and rearragement of the intranuclear component. The nuclear lamina of cells cultured on nanoneedles were highly warped. Interestingly, the nuclear lamin forms a ring around the individual nanoneedle from the basal to apical layer. Despite the extensive membrane deformities, the nuclear envelope remained intact. Using nanoneedle structure of similar dimeter as the one used in this study, several studies have observed similar morphological changes [11, 100, 413]. However, cell viability and nuclear membrane integrity were negatively influence by an increased in nanoneedle diameter over 200 nm [457]. This phenomenon is possibly because of the fluidity of the membrane to adopt to the nanoneedle structure up until 200 nm. We also observed a marked decrease in the number of heterochromatin foci. However, we did not observe any alteration in chromatin compactibility.

Using RNA sequencing, label-free MS and subsequent pathway analysis, we reveal that the presence of the nanoneedles activate the cellular oxidative stress response, inhibit cell cycle progression, and induce membrane and cytoskeletal remodelling.

Upstream regulators analysis revealed NRF2 transcription factors as the main factor responsible for the activation of the oxidative stress response. The activation of NRF2 leads to the expression of genes involved in the glutathione-mediated detoxifications, xenobiotic metabolism and HIF1α. The activation of these pathways was found to be effective at preventing DNA damage, as no increase in the level of γH2Ax, active caspases or dead cells were found.

In line with previous findings, several studies have shown that silica nanoparticles (SiO_2) cause oxidative stress [418, 437]. Moreover, a study demonstrated that fibroblasts cultured on nanowires also exhibit increased ROS and DNA damage [424]. However, the dimension of nanoneedle used in this study is still within the acceptable range, since no increase in DNA damage was observed, unlike in the study conducted by Persson *et al.* Thus, as the nanoneedle degrade and release the SiO_2 directly into the cells' cytosol; it comes as no surprise that the cell will upregulate the expression of genes and activate pathways involved in oxidative stress-responses. Moreover, the pathway analysis performed in this study further supports the role of NRF2 signalling pathways in mediating the oxidative stress response [418].

Moreover, our analysis reveals that cells cultured on nanoneedle chips are arrested at the G2/M and the metaphase to anaphase transition. Genes involved in the G2/M transition and genes required for the formation of stable kinetochore and microtubule spindle structure for proper chromosomal separations were found to be downregulated. The low level of Brdu staining and decreased Ki67 mRNA expression level in cells cultured on nanoneedle chips further supports the notion that the presence of nanoneedles cause a disruption in the cell cycle progression. The downregulation of c-MYC expression was found to be responsible for the disruption in cell cycle. However, studies comparing the level of cellular division and proliferation in nanoneedle chips show wide inconsistencies. A study showed that the level of Ki67 was unchanged in the presence of nanowires [450], and Bonde *et al.* demonstrated that more cells were found to be in S-phase on nanowires based on the BrdU labelling [98]. Furthermore, Bonde *et al.* showed that cells on nanowires could form mitotic spindle required during M-phase, inconsistent with the results of the pathways analysis conducted. On the other hand, cellular division has been reported to be perturbed in L929 fibroblasts cultured on vertical gallium phosphide nanowires [424]. They observed that on nanowires the cells

could initiate the process of cellular division, but the process is often either aborted or resulted in aberrant multinucleated cells. Persson *et al.* also observed inhibition of genes required for kinetochores assembly and microtubule spindles formation, similar to the results observed in this study. In their study the downregulation of the genes led to disruption in chromosomal separation during anaphase and cytokinesis and resulted in the increased proportion of multinuclear cells on the nanowire substrates. However, no multinucleated cells were observed on the nanoneedle chips used in this study following a 24 hours culture. The discrepancy between the results observed by published studies and the results observed in this study might be due to the different cell type used, time-point or physical dimensions.

Analysis of the histones PTMs and DNA methylation revealed a significant downregulation in the repressive markers, H3K27me3, and an increase albeit not to a significant level of the expression of histone active marker H3K4me3. These changes in the post-translational modifications were also accompanied by the alteration in the expression level of the genes encoding the enzymes responsible for the maintenance, addition or removal of these codes. In conjunction, the results from the epigenetic markers and nuclear structures provide compelling evidence that nanoneedles might be able to induce global epigenetic remodelling and disruption of heterochromatin.

We hypothesise that the presence of the nanoneedles might enhance the efficiency of iPSCs reprogramming from MEFs by inducing chromatin remodelling towards a more open status, and activation of reprogramming promoting signalling pathways, such as the NRF2. Unfortunately, at the time of writing, results from the MEFs to iPSCs reprogramming on the nanoneedle were not yet available. However, to fully decipher and grasp the underlying mechanisms of the changes observed high-resolution chromatin immunoprecipitation followed by sequencing (CHIP-seq) would ultimately be needed. Knowing the exact location that the epigenetic markers are enriched will tremendously support the ability to draw reliable conclusions on the potential applications of this material. Besides, a combination of full metabolic activity and metabolomics screening might be beneficial to support the claim generated by the *in-silico* study and guide the clinical usage of SiO_2 based nanomaterials.

In summary, the most impactful results of the present body of work are:

- Nanoneedle chips can be used to deliver stable integrative constructs into cells *in vitro* and *in vivo* in a highly specialised and defined manner.
- The overexpression of the MGT cardiac reprogramming factor can initiate the early stages of direct cardiac reprogramming from EPDCs.
- Cells cultured on nanoneedle chips undergo extensive nuclear rearrangement including alteration in nuclear structure and distribution of intranuclear components.
- Nanoneedles can induce a global dramatic chromatin remodelling characterised in MEFs by a massive disruption of heterochromatic features.
- The activation of oxidative stress response by cells on nanoneedles acts as a protective mechanism against excessive ROS.
- The physical confinement of the cell shape and disruption of cytoskeletal components including microtubules by the presence of nanoneedles lead to impaired cell cycle progression.

References

1. Sadahiro, T., S. Yamanaka, and M. Ieda, *Direct cardiac reprogramming: progress and challenges in basic biology and clinical applications.* Circ Res, 2015. **116**(8): p. 1378-91.
2. Tsimbouri, P.M., *Adult Stem Cell Responses to Nanostimuli.* J Funct Biomater, 2015. **6**(3): p. 598-622.
3. Sun, Z., S.S. Guo, and R. Fassler, *Integrin-mediated mechanotransduction.* J Cell Biol, 2016. **215**(4): p. 445-456.
4. McMurray, R.J., M.J. Dalby, and P.M. Tsimbouri, *Using biomaterials to study stem cell mechanotransduction, growth and differentiation.* J Tissue Eng Regen Med, 2015. **9**(5): p. 528-39.
5. Swift, J., et al., *Nuclear lamin-A scales with tissue stiffness and enhances matrix-directed differentiation.* Science, 2013. **341**(6149): p. 1240104.
6. Guilluy, C., et al., *Isolated nuclei adapt to force and reveal a mechanotransduction pathway in the nucleus.* Nat Cell Biol, 2014. **16**(4): p. 376-81.
7. Simoes, F.C. and P.R. Riley, *The ontogeny, activation and function of the epicardium during heart development and regeneration.* Development, 2018. **145**(7).
8. Dupont, S., et al., *Role of YAP/TAZ in mechanotransduction.* Nature, 2011. **474**(7350): p. 179-83.
9. Chiappini, C., et al., *Biodegradable silicon nanoneedles delivering nucleic acids intracellularly induce localized in vivo neovascularization.* Nat Mater, 2015. **14**(5): p. 532-9.
10. Chiappini, C., et al., *Biodegradable nanoneedles for localized delivery of nanoparticles in vivo: exploring the biointerface.* ACS Nano, 2015. **9**(5): p. 5500-9.
11. Buch-Manson, N., et al., *Mapping cell behavior across a wide range of vertical silicon nanocolumn densities.* Nanoscale, 2017. **9**(17): p. 5517-5527.
12. Tollervey, J.R. and V.V. Lunyak, *Epigenetics: judge, jury and executioner of stem cell fate.* Epigenetics, 2012. **7**(8): p. 823-40.
13. Liehn, E.A., et al., *Repair after myocardial infarction, between fantasy and reality: the role of chemokines.* J Am Coll Cardiol, 2011. **58**(23): p. 2357-62.
14. Layman, W.S. and J. Zuo, *Epigenetic regulation in the inner ear and its potential roles in development, protection, and regeneration.* Front Cell Neurosci, 2014. **8**: p. 446.
15. Takahashi, K. and S. Yamanaka, *A developmental framework for induced pluripotency.* Development, 2015. **142**(19): p. 3274-85.
16. Tajik, A., et al., *Transcription upregulation via force-induced direct stretching of chromatin.* Nat Mater, 2016. **15**(12): p. 1287-1296.
17. Cho, S., J. Irianto, and D.E. Discher, *Mechanosensing by the nucleus: From pathways to scaling relationships.* J Cell Biol, 2017. **216**(2): p. 305-315.
18. Maharana, S., et al., *Chromosome intermingling-the physical basis of chromosome organization in differentiated cells.* Nucleic Acids Res, 2016. **44**(11): p. 5148-60.

19. Uhler, C. and G.V. Shivashankar, *Nuclear Mechanopathology and Cancer Diagnosis.* Trends Cancer, 2018. **4**(4): p. 320-331.

20. Bhat, S. and A. Kumar, *Biomaterials and bioengineering tomorrow's healthcare.* Biomatter, 2013. **3**(3).

21. Huebsch, N. and D.J. Mooney, *Inspiration and application in the evolution of biomaterials.* Nature, 2009. **462**(7272): p. 426-32.

22. Crowder, S.W., et al., *Material Cues as Potent Regulators of Epigenetics and Stem Cell Function.* Cell Stem Cell, 2016. **18**(1): p. 39-52.

23. Navarro, M., et al., *Biomaterials in orthopaedics.* J R Soc Interface, 2008. **5**(27): p. 1137-58.

24. Lam, M.T. and J.C. Wu, *Biomaterial applications in cardiovascular tissue repair and regeneration.* Expert Rev Cardiovasc Ther, 2012. **10**(8): p. 1039-49.

25. Domenech, M., et al., *Tissue Engineering Strategies for Myocardial Regeneration: Acellular Versus Cellular Scaffolds?* Tissue Eng Part B Rev, 2016. **22**(6): p. 438-458.

26. Sharma, K., *Nanomaterials for Drug Delivery*, in *Advances in Personalized Nanotherapeutics*, A. Kaushik, R.D. Jayant, and M. Nair, Editors. 2017, Springer International Publishing: Cham. p. 57-77.

27. Ingber, D.E., N. Wang, and D. Stamenovic, *Tensegrity, cellular biophysics, and the mechanics of living systems.* Rep Prog Phys, 2014. **77**(4): p. 046603.

28. Hill, A.B., et al., *Overcoming Gene-Delivery Hurdles: Physiological Considerations for Nonviral Vectors.* Trends Biotechnol, 2016. **34**(2): p. 91-105.

29. Matkar, P.N., H. Leong-Poi, and K.K. Singh, *Cardiac gene therapy: are we there yet?* Gene Ther, 2016. **23**(8-9): p. 635-48.

30. Keeler, A.M., M.K. ElMallah, and T.R. Flotte, *Gene Therapy 2017: Progress and Future Directions.* Clin Transl Sci, 2017. **10**(4): p. 242-248.

31. Lukashev, A.N. and A.A. Zamyatnin, Jr., *Viral Vectors for Gene Therapy: Current State and Clinical Perspectives.* Biochemistry (Mosc), 2016. **81**(7): p. 700-8.

32. Ieda, M., et al., *Direct reprogramming of fibroblasts into functional cardiomyocytes by defined factors.* Cell, 2010. **142**(3): p. 375-86.

33. Qian, L., et al., *In vivo reprogramming of murine cardiac fibroblasts into induced cardiomyocytes.* Nature, 2012. **485**(7400): p. 593-8.

34. Inagawa, K., et al., *Induction of cardiomyocyte-like cells in infarct hearts by gene transfer of Gata4, Mef2c, and Tbx5.* Circ Res, 2012. **111**(9): p. 1147-56.

35. Wang, L., et al., *Stoichiometry of Gata4, Mef2c, and Tbx5 influences the efficiency and quality of induced cardiac myocyte reprogramming.* Circ Res, 2015. **116**(2): p. 237-44.

36. Katz, M.G., et al., *Gene therapy delivery systems for enhancing viral and nonviral vectors for cardiac diseases: current concepts and future applications.* Hum Gene Ther, 2013. **24**(11): p. 914-27.

37. Cavazzana-Calvo, M., *Basic research tries to decrease the risks of translational medicine.* Gene Ther, 2009. **16**(3): p. 309-10.

38. Newman, C.M. and T. Bettinger, *Gene therapy progress and prospects: ultrasound for gene transfer.* Gene Ther, 2007. **14**(6): p. 465-75.

39. Bekeredjian, R., et al., *Ultrasound-targeted microbubble destruction can repeatedly direct highly specific plasmid expression to the heart.* Circulation, 2003. **108**(8): p. 1022-6.

40. Kondo, I., et al., *Treatment of acute myocardial infarction by hepatocyte growth factor gene transfer: the first demonstration of myocardial transfer of a "functional" gene using ultrasonic microbubble destruction.* J Am Coll Cardiol, 2004. **44**(3): p. 644-53.

41. Mehier-Humbert, S. and R.H. Guy, *Physical methods for gene transfer: improving the kinetics of gene delivery into cells.* Adv Drug Deliv Rev, 2005. **57**(5): p. 733-53.

42. Heilmann, C.A., et al., *Transmyocardial laser revascularization combined with vascular endothelial growth factor 121 (VEGF121) gene therapy for chronic myocardial ischemia--do the effects really add up?* Eur J Cardiothorac Surg, 2003. **23**(1): p. 74-80.

43. Li, W., et al., *Enhanced thoracic gene delivery by magnetic nanobead-mediated vector.* J Gene Med, 2008. **10**(8): p. 897-909.

44. Kamimura, K., et al., *Advances in Gene Delivery Systems.* Pharmaceut Med, 2011. **25**(5): p. 293-306.

45. Ko, Y.T., et al., *Gene delivery into ischemic myocardium by double-targeted lipoplexes with anti-myosin antibody and TAT peptide.* Gene Ther, 2009. **16**(1): p. 52-9.

46. Sun, L., et al., *The use of cationic microbubbles to improve ultrasound-targeted gene delivery to the ischemic myocardium.* Biomaterials, 2013. **34**(8): p. 2107-16.

47. Ji, J., et al., *Ultrasound-targeted transfection of tissue-type plasminogen activator gene carried by albumin nanoparticles to dog myocardium to prevent thrombosis after heart mechanical valve replacement.* Int J Nanomedicine, 2012. **7**: p. 2911-9.

48. Kim, H., et al., *Dexamethasone-conjugated polyethylenimine as an efficient gene carrier with an anti-apoptotic effect to cardiomyocytes.* J Gene Med, 2009. **11**(6): p. 515-22.

49. Lee, Y., et al., *Human erythropoietin gene delivery for cardiac remodeling of myocardial infarction in rats.* J Control Release, 2013. **171**(1): p. 24-32.

50. Riley, M.K. and W. Vermerris, *Recent Advances in Nanomaterials for Gene Delivery-A Review.* Nanomaterials (Basel), 2017. **7**(5).

51. Obataya, I., et al., *Mechanical sensing of the penetration of various nanoneedles into a living cell using atomic force microscopy.* Biosens Bioelectron, 2005. **20**(8): p. 1652-5.

52. Shalek, A.K., et al., *Vertical silicon nanowires as a universal platform for delivering biomolecules into living cells.* Proc Natl Acad Sci U S A, 2010. **107**(5): p. 1870-5.

53. Shalek, A.K., et al., *Nanowire-mediated delivery enables functional interrogation of primary immune cells: application to the analysis of chronic lymphocytic leukemia.* Nano Lett, 2012. **12**(12): p. 6498-504.

54. Chiappini, C., et al., *Mapping Local Cytosolic Enzymatic Activity in Human Esophageal Mucosa with Porous Silicon Nanoneedles.* Adv Mater, 2015. **27**(35): p. 5147-52.

55. Robinson, J.T., et al., *Vertical nanowire electrode arrays as a scalable platform for intracellular interfacing to neuronal circuits.* Nat Nanotechnol, 2012. **7**(3): p. 180-4.

56. Na, Y.R., et al., *Probing enzymatic activity inside living cells using a nanowire-cell "sandwich" assay.* Nano Lett, 2013. **13**(1): p. 153-8.

57. Suyatin, D.B., et al., *Nanowire-based electrode for acute in vivo neural recordings in the brain.* PLoS One, 2013. **8**(2): p. e56673.

58. Xu, X., et al., *Precision-Guided Nanospears for Targeted and High-Throughput Intracellular Gene Delivery.* ACS Nano, 2018. **12**(5): p. 4503-4511.

59. Faia-Torres, A.B., et al., *Osteogenic differentiation of human mesenchymal stem cells in the absence of osteogenic supplements: A surface-roughness gradient study.* Acta Biomater, 2015. **28**: p. 64-75.

60. Yang, W., et al., *Surface topography of hydroxyapatite promotes osteogenic differentiation of human bone marrow mesenchymal stem cells.* Mater Sci Eng C Mater Biol Appl, 2016. **60**: p. 45-53.

61. Takeuchi, K., et al., *Enhanced intrinsic biomechanical properties of osteoblastic mineralized tissue on roughened titanium surface.* J Biomed Mater Res A, 2005. **72**(3): p. 296-305.

62. de Oliveira, P.T. and A. Nanci, *Nanotexturing of titanium-based surfaces upregulates expression of bone sialoprotein and osteopontin by cultured osteogenic cells.* Biomaterials, 2004. **25**(3): p. 403-13.

63. Abagnale, G., et al., *Surface topography enhances differentiation of mesenchymal stem cells towards osteogenic and adipogenic lineages.* Biomaterials, 2015. **61**: p. 316-26.

64. Wang, P.Y., et al., *Modulation of osteogenic, adipogenic and myogenic differentiation of mesenchymal stem cells by submicron grooved topography.* J Mater Sci Mater Med, 2012. **23**(12): p. 3015-28.

65. Lu, D., et al., *Microgrooved Surface Modulates Neuron Differentiation in Human Embryonic Stem Cells.* Methods Mol Biol, 2016. **1307**: p. 281-7.

66. Downing, T.L., et al., *Biophysical regulation of epigenetic state and cell reprogramming.* Nat Mater, 2013. **12**(12): p. 1154-62.

67. Yim, E.K., S.W. Pang, and K.W. Leong, *Synthetic nanostructures inducing differentiation of human mesenchymal stem cells into neuronal lineage.* Exp Cell Res, 2007. **313**(9): p. 1820-9.

68. Fiedler, J., et al., *The effect of substrate surface nanotopography on the behavior of multipotnent mesenchymal stromal cells and osteoblasts.* Biomaterials, 2013. **34**(35): p. 8851-9.

69. You, M.H., et al., *Synergistically enhanced osteogenic differentiation of human mesenchymal stem cells by culture on nanostructured surfaces with induction media.* Biomacromolecules, 2010. **11**(7): p. 1856-62.

70. Sjostrom, T., et al., *Fabrication of pillar-like titania nanostructures on titanium and their interactions with human skeletal stem cells.* Acta Biomater, 2009. **5**(5): p. 1433-41.

71. Dalby, M.J., et al., *The control of human mesenchymal cell differentiation using nanoscale symmetry and disorder.* Nat Mater, 2007. **6**(12): p. 997-1003.

72. VanDersarl, J.J., A.M. Xu, and N.A. Melosh, *Nanostraws for Direct Fluidic Intracellular Access.* Nano Letters, 2012. **12**(8): p. 3881-3886.

73. Yin, Z., et al., *Electrospun scaffolds for multiple tissues regeneration in vivo through topography dependent induction of lineage specific differentiation.* Biomaterials, 2015. **44**: p. 173-85.

74. Pelham, R.J., Jr. and Y. Wang, *Cell locomotion and focal adhesions are regulated by substrate flexibility.* Proc Natl Acad Sci U S A, 1997. **94**(25): p. 13661-5.

75. Yeung, T., et al., *Effects of substrate stiffness on cell morphology, cytoskeletal structure, and adhesion.* Cell Motil Cytoskeleton, 2005. **60**(1): p. 24-34.

76. Jacot, J.G., A.D. McCulloch, and J.H. Omens, *Substrate stiffness affects the functional maturation of neonatal rat ventricular myocytes.* Biophys J, 2008. **95**(7): p. 3479-87.

77. Hazeltine, L.B., et al., *Effects of substrate mechanics on contractility of cardiomyocytes generated from human pluripotent stem cells.* Int J Cell Biol, 2012. **2012**: p. 508294.

78. Mittal, N., et al., *Substrate Stiffness Modulates the Maturation of Human Pluripotent Stem-Cell-Derived Hepatocytes.* ACS Biomaterials Science & Engineering, 2016. **2**(9): p. 1649-1657.

79. Engler, A.J., et al., *Matrix elasticity directs stem cell lineage specification.* Cell, 2006. **126**(4): p. 677-89.

80. Yang, M.T., et al., *Assaying stem cell mechanobiology on microfabricated elastomeric substrates with geometrically modulated rigidity.* Nature Protocols, 2011. **6**(2): p. 187-213.

81. Sant, S., et al., *Biomimetic Gradient Hydrogels for Tissue Engineering.* Can J Chem Eng, 2010. **88**(6): p. 899-911.

82. Zaari, N., et al., *Photopolymerization in Microfluidic Gradient Generators: Microscale Control of Substrate Compliance to Manipulate Cell Response.* Advanced Materials, 2004. **16**(23-24): p. 2133-2137.

83. Frey, M.T. and Y.L. Wang, *A photo-modulatable material for probing cellular responses to substrate rigidity.* Soft Matter, 2009. **5**(9): p. 1918-1924.

84. Guvendiren, M. and J.A. Burdick, *Stiffening hydrogels to probe short- and long-term cellular responses to dynamic mechanics.* Nature Communications, 2012. **3**.

85. Khetan, S., et al., *Degradation-mediated cellular traction directs stem cell fate in covalently crosslinked three-dimensional hydrogels.* Nature Materials, 2013. **12**(5): p. 458-465.

86. Kloxin, A.M., M.W. Tibbitt, and K.S. Anseth, *Synthesis of photodegradable hydrogels as dynamically tunable cell culture platforms.* Nature Protocols, 2010. **5**(12): p. 1867-1887.

87. Nasrollahi, S., et al., *Past matrix stiffness primes epithelial cells and regulates their future collective migration through a mechanical memory.* Biomaterials, 2017. **146**: p. 146-155.

88. Eyckmans, J. and C.S. Chen, *STEM CELL DIFFERENTIATION Sticky mechanical memory.* Nature Materials, 2014. **13**(6): p. 542-543.

89. Yang, C., et al., *Mechanical memory and dosing influence stem cell fate.* Nature Materials, 2014. **13**(6): p. 645-652.

90. Yan, Z.Q., et al., *Histone deacetylases modulate vascular smooth muscle cell migration induced by cyclic mechanical strain.* J Biomech, 2009. **42**(7): p. 945-8.

91. Kearney, E.M., et al., *Tensile Strain as a Regulator of Mesenchymal Stem Cell Osteogenesis.* Annals of Biomedical Engineering, 2010. **38**(5): p. 1767-1779.

92. Li, Y., et al., *Moderate dynamic compression inhibits pro-catabolic response of cartilage to mechanical injury, tumor necrosis factor-alpha and interleukin-6, but accentuates degradation above a strain threshold.* Osteoarthritis and Cartilage, 2013. **21**(12): p. 1933-1941.

93. DeForest, C.A. and D.A. Tirrell, *A photoreversible protein-patterning approach for guiding stem cell fate in three-dimensional gels.* Nature Materials, 2015. **14**(5): p. 523-531.

94. Huebsch, N., et al., *Harnessing traction-mediated manipulation of the cell/matrix interface to control stem-cell fate.* Nature Materials, 2010. **9**(6): p. 518-526.

95. Parekh, S.H., et al., *Modulus-driven differentiation of marrow stromal cells in 3D scaffolds that is independent of myosin-based cytoskeletal tension.* Biomaterials, 2011. **32**(9): p. 2256-2264.

96. Fong, A.H., et al., *Three-Dimensional Adult Cardiac Extracellular Matrix Promotes Maturation of Human Induced Pluripotent Stem Cell-Derived Cardiomyocytes.* Tissue Engineering Part A, 2016. **22**(15-16): p. 1016-1025.

97. Chiappini, C., *Nanoneedle-Based Sensing in Biological Systems.* ACS Sens, 2017. **2**(8): p. 1086-1102.

98. Bonde, S., et al., *Tuning InAs nanowire density for HEK293 cell viability, adhesion, and morphology: perspectives for nanowire-based biosensors.* ACS Appl Mater Interfaces, 2013. **5**(21): p. 10510-9.

99. Felipe, V., et al., *Biomechanical Cell Regulation by High Aspect Ratio Nanoimprinted Pillars.* Advanced Functional Materials, 2016. **26**(31): p. 5599-5609.

100. Hanson, L., et al., *Vertical nanopillars for in situ probing of nuclear mechanics in adherent cells.* Nat Nanotechnol, 2015. **10**(6): p. 554-62.

101. Hallstrom, W., et al., *Fifteen-piconewton force detection from neural growth cones using nanowire arrays.* Nano Lett, 2010. **10**(3): p. 782-7.

102. Hanson, L., et al., *Characterization of the cell-nanopillar interface by transmission electron microscopy.* Nano Lett, 2012. **12**(11): p. 5815-20.

103. Berthing, T., et al., *Cell membrane conformation at vertical nanowire array interface revealed by fluorescence imaging.* Nanotechnology, 2012. **23**(41): p. 415102.

104. Xu, A.M., et al., *Quantification of nanowire penetration into living cells.* Nat Commun, 2014. **5**: p. 3613.

105. Aalipour, A., et al., *Plasma membrane and actin cytoskeleton as synergistic barriers to nanowire cell penetration.* Langmuir, 2014. **30**(41): p. 12362-7.

106. Zhao, W., et al., *Nanoscale manipulation of membrane curvature for probing endocytosis in live cells.* Nat Nanotechnol, 2017. **12**(8): p. 750-756.

107. Wang, Y., et al., *Poking cells for efficient vector-free intracellular delivery.* Nat Commun, 2014. **5**: p. 4466.

108. Matsumoto, D., et al., *Oscillating high-aspect-ratio monolithic silicon nanoneedle array enables efficient delivery of functional bio-macromolecules into living cells.* Sci Rep, 2015. **5**: p. 15325.

109. Elnathan, R., et al., *Engineering vertically aligned semiconductor nanowire arrays for applications in the life sciences.* Nano Today, 2014. **9**(2): p. 172-196.

110. Kawamura, R., et al., *High efficiency penetration of antibody-immobilized nanoneedle thorough plasma membrane for in situ detection of cytoskeletal proteins in living cells.* Journal of Nanobiotechnology, 2016. **14**(1): p. 74.

111. Steinberg, B.A., et al., *Global outcomes of ST-elevation myocardial infarction: comparisons of the Enoxaparin and Thrombolysis Reperfusion for Acute Myocardial Infarction Treatment-Thrombolysis In Myocardial Infarction study 25 (ExTRACT-TIMI 25) registry and trial.* Am Heart J, 2007. **154**(1): p. 54-61.

112. Jennings, R.B. and K.A. Reimer, *The Cell Biology of Acute Myocardial-Ischemia.* Annual Review of Medicine, 1991. **42**: p. 225-246.

113. Murry, C.E., H. Reinecke, and L.M. Pabon, *Regeneration gaps - Observations on stem cells and cardiac repair.* Journal of the American College of Cardiology, 2006. **47**(9): p. 1777-1785.

114. Mann, D.L., *The emerging role of innate immunity in the heart and vascular system: for whom the cell tolls.* Circ Res, 2011. **108**(9): p. 1133-45.

115. Nian, M., et al., *Inflammatory cytokines and postmyocardial infarction remodeling.* Circ Res, 2004. **94**(12): p. 1543-53.

116. Mann, D.L. and F.G. Spinale, *Activation of matrix metalloproteinases in the failing human heart: breaking the tie that binds.* Circulation, 1998. **98**(17): p. 1699-702.

117. Sun, Y., et al., *Infarct scar as living tissue.* Basic Res Cardiol, 2002. **97**(5): p. 343-7.

118. Poss, K.D., L.G. Wilson, and M.T. Keating, *Heart regeneration in zebrafish.* Science, 2002. **298**(5601): p. 2188-90.

119. Jopling, C., et al., *Zebrafish heart regeneration occurs by cardiomyocyte dedifferentiation and proliferation.* Nature, 2010. **464**(7288): p. 606-9.

120. Kikuchi, K., et al., *Primary contribution to zebrafish heart regeneration by gata4(+) cardiomyocytes.* Nature, 2010. **464**(7288): p. 601-5.

121. Bergmann, O., et al., *Evidence for cardiomyocyte renewal in humans.* Science, 2009. **324**(5923): p. 98-102.

122. Haubner, B.J., et al., *Functional Recovery of a Human Neonatal Heart After Severe Myocardial Infarction.* Circ Res, 2016. **118**(2): p. 216-21.

123. Polizzotti, B.D., et al., *Neuregulin stimulation of cardiomyocyte regeneration in mice and human myocardium reveals a therapeutic window.* Sci Transl Med, 2015. **7**(281): p. 281ra45.

124. Mahmoud, A.I., et al., *Meis1 regulates postnatal cardiomyocyte cell cycle arrest.* Nature, 2013. **497**(7448): p. 249-253.

125. Hsieh, P.C., et al., *Evidence from a genetic fate-mapping study that stem cells refresh adult mammalian cardiomyocytes after injury.* Nat Med, 2007. **13**(8): p. 970-4.

126. Senyo, S.E., et al., *Mammalian heart renewal by pre-existing cardiomyocytes.* Nature, 2013. **493**(7432): p. 433-6.

127. Malliaras, K., et al., *Cardiomyocyte proliferation and progenitor cell recruitment underlie therapeutic regeneration after myocardial infarction in the adult mouse heart.* EMBO Mol Med, 2013. **5**(2): p. 191-209.

128. D'Uva, G., et al., *ERBB2 triggers mammalian heart regeneration by promoting cardiomyocyte dedifferentiation and proliferation.* Nat Cell Biol, 2015. **17**(5): p. 627-38.

129. Beltrami, A.P., et al., *Adult cardiac stem cells are multipotent and support myocardial regeneration.* Cell, 2003. **114**(6): p. 763-76.

130. Oh, H., et al., *Cardiac progenitor cells from adult myocardium: homing, differentiation, and fusion after infarction.* Proc Natl Acad Sci U S A, 2003. **100**(21): p. 12313-8.

131. Matsuura, K., et al., *Adult cardiac Sca-1-positive cells differentiate into beating cardiomyocytes.* J Biol Chem, 2004. **279**(12): p. 11384-91.

132. Hierlihy, A.M., et al., *The post-natal heart contains a myocardial stem cell population.* FEBS Lett, 2002. **530**(1-3): p. 239-43.

133. Martin, C.M., et al., *Persistent expression of the ATP-binding cassette transporter, Abcg2, identifies cardiac SP cells in the developing and adult heart.* Dev Biol, 2004. **265**(1): p. 262-75.

134. Pfister, O., et al., *CD31- but Not CD31+ cardiac side population cells exhibit functional cardiomyogenic differentiation.* Circ Res, 2005. **97**(1): p. 52-61.

135. Messina, E., et al., *Isolation and expansion of adult cardiac stem cells from human and murine heart.* Circ Res, 2004. **95**(9): p. 911-21.

136. Smith, R.R., et al., *Regenerative potential of cardiosphere-derived cells expanded from percutaneous endomyocardial biopsy specimens.* Circulation, 2007. **115**(7): p. 896-908.

137. Davis, D.R., et al., *Validation of the cardiosphere method to culture cardiac progenitor cells from myocardial tissue.* PLoS One, 2009. **4**(9): p. e7195.

138. Urbanek, K., et al., *Stem cell niches in the adult mouse heart.* Proc Natl Acad Sci U S A, 2006. **103**(24): p. 9226-31.

139. Schaefer, A., et al., *Impact of intracoronary bone marrow cell transfer on diastolic function in patients after acute myocardial infarction: results from the BOOST trial.* Eur Heart J, 2006. **27**(8): p. 929-35.

140. Erbs, S., et al., *Restoration of microvascular function in the infarct-related artery by intracoronary transplantation of bone marrow progenitor cells in patients with acute myocardial infarction: the Doppler Substudy of the Reinfusion of Enriched Progenitor Cells and Infarct Remodeling in Acute Myocardial Infarction (REPAIR-AMI) trial.* Circulation, 2007. **116**(4): p. 366-74.

141. Liu, B., et al., *Effectiveness and safety of selected bone marrow stem cells on left ventricular function in patients with acute myocardial infarction: a meta-analysis of randomized controlled trials.* Int J Cardiol, 2014. **177**(3): p. 764-70.

142. Janssens, S., et al., *Autologous bone marrow-derived stem-cell transfer in patients with ST-segment elevation myocardial infarction: double-blind, randomised controlled trial.* Lancet, 2006. **367**(9505): p. 113-21.

143. Lunde, K., et al., *Intracoronary injection of mononuclear bone marrow cells in acute myocardial infarction.* N Engl J Med, 2006. **355**(12): p. 1199-209.

144. de Jong, R., et al., *Intracoronary stem cell infusion after acute myocardial infarction: a meta-analysis and update on clinical trials.* Circ Cardiovasc Interv, 2014. **7**(2): p. 156-67.

145. Higuchi, A., et al., *Stem cell therapies for myocardial infarction in clinical trials: bioengineering and biomaterial aspects.* Lab Invest, 2017. **97**(10): p. 1167-1179.

146. Spees, J.L., R.H. Lee, and C.A. Gregory, *Mechanisms of mesenchymal stem/stromal cell function.* Stem Cell Res Ther, 2016. **7**(1): p. 125.

147. Lee, J.W., et al., *A randomized, open-label, multicenter trial for the safety and efficacy of adult mesenchymal stem cells after acute myocardial infarction.* J Korean Med Sci, 2014. **29**(1): p. 23-31.

148. Hare, J.M., et al., *A randomized, double-blind, placebo-controlled, dose-escalation study of intravenous adult human mesenchymal stem cells (prochymal) after acute myocardial infarction.* J Am Coll Cardiol, 2009. **54**(24): p. 2277-86.

149. Menasche, P., *Cell therapy trials for heart regeneration - lessons learned and future directions.* Nat Rev Cardiol, 2018.

150. Bolli, R., et al., *Cardiac stem cells in patients with ischaemic cardiomyopathy (SCIPIO): initial results of a randomised phase 1 trial.* Lancet, 2011. **378**(9806): p. 1847-57.

151. Malliaras, K., et al., *Intracoronary cardiosphere-derived cells after myocardial infarction: evidence of therapeutic regeneration in the final 1-year results of the CADUCEUS trial (CArdiosphere-Derived aUtologous stem CElls to reverse ventricUlar dySfunction).* J Am Coll Cardiol, 2014. **63**(2): p. 110-22.

152. van Berlo, J.H., et al., *c-kit+ cells minimally contribute cardiomyocytes to the heart.* Nature, 2014. **509**(7500): p. 337-41.

153. Koninckx, R., et al., *Mesenchymal stem cells or cardiac progenitors for cardiac repair? A comparative study.* Cell Mol Life Sci, 2011. **68**(12): p. 2141-56.

154. Laflamme, M.A., et al., *Formation of human myocardium in the rat heart from human embryonic stem cells.* Am J Pathol, 2005. **167**(3): p. 663-71.

155. van Laake, L.W., et al., *Human embryonic stem cell-derived cardiomyocytes survive and mature in the mouse heart and transiently improve function after myocardial infarction.* Stem Cell Res, 2007. **1**(1): p. 9-24.

156. van Laake, L.W., et al., *Improvement of mouse cardiac function by hESC-derived cardiomyocytes correlates with vascularity but not graft size.* Stem Cell Res, 2009. **3**(2-3): p. 106-12.

157. Zwi-Dantsis, L., et al., *Derivation and cardiomyocyte differentiation of induced pluripotent stem cells from heart failure patients.* Eur Heart J, 2013. **34**(21): p. 1575-86.

158. Chong, J.J., et al., *Human embryonic-stem-cell-derived cardiomyocytes regenerate non-human primate hearts.* Nature, 2014. **510**(7504): p. 273-7.

159. Carvalho, E., et al., *Myocardial infarction: stem cell transplantation for cardiac regeneration.* Regen Med, 2015. **10**(8): p. 1025-43.

160. Meyer, G.P., et al., *Intracoronary bone marrow cell transfer after myocardial infarction: eighteen months' follow-up data from the randomized, controlled BOOST (BOne marrOw transfer to enhance ST-elevation infarct regeneration) trial.* Circulation, 2006. **113**(10): p. 1287-94.

161. Schachinger, V., et al., *Bone-marrow-derived progenitor cell therapy in need of proof of concept: design of the REPAIR-AMI trial.* Nat Clin Pract Cardiovasc Med, 2006. **3 Suppl 1**: p. S23-8.

162. Assmus, B., et al., *Clinical outcome 2 years after intracoronary administration of bone marrow-derived progenitor cells in acute myocardial infarction.* Circ Heart Fail, 2010. **3**(1): p. 89-96.

163. Makkar, R.R., et al., *Intracoronary cardiosphere-derived cells for heart regeneration after myocardial infarction (CADUCEUS): a prospective, randomised phase 1 trial.* Lancet, 2012. **379**(9819): p. 895-904.

164. Serpooshan, V., et al., *The effect of bioengineered acellular collagen patch on cardiac remodeling and ventricular function post myocardial infarction.* Biomaterials, 2013. **34**(36): p. 9048-55.

165. Chiu, L.L. and M. Radisic, *Controlled release of thymosin beta4 using collagen-chitosan composite hydrogels promotes epicardial cell migration and angiogenesis.* J Control Release, 2011. **155**(3): p. 376-85.

166. Christman, K.L., et al., *Fibrin glue alone and skeletal myoblasts in a fibrin scaffold preserve cardiac function after myocardial infarction.* Tissue Eng, 2004. **10**(3-4): p. 403-9.

167. Christman, K.L., et al., *Injectable fibrin scaffold improves cell transplant survival, reduces infarct expansion, and induces neovasculature formation in ischemic myocardium.* J Am Coll Cardiol, 2004. **44**(3): p. 654-60.

168. Kochupura, P.V., et al., *Tissue-engineered myocardial patch derived from extracellular matrix provides regional mechanical function.* Circulation, 2005. **112**(9 Suppl): p. I144-9.

169. Efraim, Y., et al., *Biohybrid cardiac ECM-based hydrogels improve long term cardiac function post myocardial infarction.* Acta Biomater, 2017. **50**: p. 220-233.

170. Wang, T., et al., *Bone marrow stem cells implantation with alpha-cyclodextrin/MPEG-PCL-MPEG hydrogel improves cardiac function after myocardial infarction.* Acta Biomater, 2009. **5**(8): p. 2939-44.

171. Wang, T., et al., *Novel thermosensitive hydrogel injection inhibits post-infarct ventricle remodelling.* Eur J Heart Fail, 2009. **11**(1): p. 14-9.

172. Mayfield, A.E., et al., *The effect of encapsulation of cardiac stem cells within matrix-enriched hydrogel capsules on cell survival, post-ischemic cell retention and cardiac function.* Biomaterials, 2014. **35**(1): p. 133-42.

173. Ye, L., et al., *Cardiac repair in a porcine model of acute myocardial infarction with human induced pluripotent stem cell-derived cardiovascular cells.* Cell Stem Cell, 2014. **15**(6): p. 750-61.

174. Zimmermann, W.H., et al., *Engineered heart tissue grafts improve systolic and diastolic function in infarcted rat hearts.* Nat Med, 2006. **12**(4): p. 452-8.

175. Tiburcy, M., et al., *Defined Engineered Human Myocardium With Advanced Maturation for Applications in Heart Failure Modeling and Repair.* Circulation, 2017. **135**(19): p. 1832-1847.

176. Gnecchi, M., et al., *Paracrine action accounts for marked protection of ischemic heart by Akt-modified mesenchymal stem cells.* Nat Med, 2005. **11**(4): p. 367-8.

177. Takahashi, M., et al., *Cytokines produced by bone marrow cells can contribute to functional improvement of the infarcted heart by protecting cardiomyocytes from ischemic injury.* Am J Physiol Heart Circ Physiol, 2006. **291**(2): p. H886-93.

178. Valadi, H., et al., *Exosome-mediated transfer of mRNAs and microRNAs is a novel mechanism of genetic exchange between cells.* Nat Cell Biol, 2007. **9**(6): p. 654-9.

179. Ibrahim, A.G., K. Cheng, and E. Marban, *Exosomes as critical agents of cardiac regeneration triggered by cell therapy.* Stem Cell Reports, 2014. **2**(5): p. 606-19.

180. Khan, M., et al., *Embryonic stem cell-derived exosomes promote endogenous repair mechanisms and enhance cardiac function following myocardial infarction.* Circ Res, 2015. **117**(1): p. 52-64.

181. Kervadec, A., et al., *Cardiovascular progenitor-derived extracellular vesicles recapitulate the beneficial effects of their parent cells in the treatment of chronic heart failure.* J Heart Lung Transplant, 2016. **35**(6): p. 795-807.

182. El Harane, N., et al., *Acellular therapeutic approach for heart failure: in vitro production of extracellular vesicles from human cardiovascular progenitors.* Eur Heart J, 2018. **39**(20): p. 1835-1847.

183. Davis, R.L., H. Weintraub, and A.B. Lassar, *Expression of a single transfected cDNA converts fibroblasts to myoblasts.* Cell, 1987. **51**(6): p. 987-1000.

184. Takahashi, K., et al., *Induction of pluripotent stem cells from adult human fibroblasts by defined factors.* Cell, 2007. **131**(5): p. 861-72.

185. Takahashi, K. and S. Yamanaka, *Induction of pluripotent stem cells from mouse embryonic and adult fibroblast cultures by defined factors.* Cell, 2006. **126**(4): p. 663-76.

186. Feng, R., et al., *PU.1 and C/EBPalpha/beta convert fibroblasts into macrophage-like cells.* Proc Natl Acad Sci U S A, 2008. **105**(16): p. 6057-62.

187. Sekiya, S. and A. Suzuki, *Direct conversion of mouse fibroblasts to hepatocyte-like cells by defined factors.* Nature, 2011. **475**(7356): p. 390-3.

188. Vierbuchen, T., et al., *Direct conversion of fibroblasts to functional neurons by defined factors.* Nature, 2010. **463**(7284): p. 1035-41.

189. Riddell, J., et al., *Reprogramming committed murine blood cells to induced hematopoietic stem cells with defined factors.* Cell, 2014. **157**(3): p. 549-64.

190. Srivastava, D. and M. Ieda, *Critical factors for cardiac reprogramming.* Circ Res, 2012. **111**(1): p. 5-8.

191. Song, K., et al., *Heart repair by reprogramming non-myocytes with cardiac transcription factors.* Nature, 2012. **485**(7400): p. 599-604.

192. Chen, O. and L. Qian, *Direct Cardiac Reprogramming: Advances in Cardiac Regeneration.* Biomed Res Int, 2015. **2015**: p. 580406.

193. Protze, S., et al., *A new approach to transcription factor screening for reprogramming of fibroblasts to cardiomyocyte-like cells.* J Mol Cell Cardiol, 2012. **53**(3): p. 323-32.

194. Christoforou, N., et al., *Transcription factors MYOCD, SRF, Mesp1 and SMARCD3 enhance the cardio-inducing effect of GATA4, TBX5, and MEF2C during direct cellular reprogramming.* PLoS One, 2013. **8**(5): p. e63577.

195. Addis, R.C., et al., *Optimization of direct fibroblast reprogramming to cardiomyocytes using calcium activity as a functional measure of success.* Journal of Molecular and Cellular Cardiology, 2013. **60**(0): p. 97-106.

196. Hirai, H., et al., *Accelerated direct reprogramming of fibroblasts into cardiomyocyte-like cells with the MyoD transactivation domain.* Cardiovasc Res, 2013. **100**(1): p. 105-13.

197. Jayawardena, T.M., et al., *MicroRNA-mediated in vitro and in vivo direct reprogramming of cardiac fibroblasts to cardiomyocytes.* Circ Res, 2012. **110**(11): p. 1465-73.

198. Fu, Y., et al., *Direct reprogramming of mouse fibroblasts into cardiomyocytes with chemical cocktails.* Cell Res, 2015. **25**(9): p. 1013-24.

199. Wang, H., et al., *Small molecules enable cardiac reprogramming of mouse fibroblasts with a single factor, Oct4.* Cell Rep, 2014. **6**(5): p. 951-60.

200. Ifkovits, J.L., et al., *Inhibition of TGFbeta signaling increases direct conversion of fibroblasts to induced cardiomyocytes.* PLoS One, 2014. **9**(2): p. e89678.

201. Muraoka, N., et al., *MiR-133 promotes cardiac reprogramming by directly repressing Snai1 and silencing fibroblast signatures.* EMBO J, 2014. **33**(14): p. 1565-81.

202. Nam, Y.J., et al., *Reprogramming of human fibroblasts toward a cardiac fate.* Proc Natl Acad Sci U S A, 2013. **110**(14): p. 5588-93.

203. Wada, R., et al., *Induction of human cardiomyocyte-like cells from fibroblasts by defined factors.* Proc Natl Acad Sci U S A, 2013. **110**(31): p. 12667-72.

204. Fu, J.D., et al., *Direct reprogramming of human fibroblasts toward a cardiomyocyte-like state.* Stem Cell Reports, 2013. **1**(3): p. 235-47.

205. Islas, J.F., et al., *Transcription factors ETS2 and MESP1 transdifferentiate human dermal fibroblasts into cardiac progenitors.* Proc Natl Acad Sci U S A, 2012. **109**(32): p. 13016-21.

206. Cao, N., et al., *Conversion of human fibroblasts into functional cardiomyocytes by small molecules.* Science, 2016. **352**(6290): p. 1216-20.

207. Mathison, M., et al., *"Triplet" polycistronic vectors encoding Gata4, Mef2c, and Tbx5 enhances postinfarct ventricular functional improvement compared with singlet vectors.* J Thorac Cardiovasc Surg, 2014. **148**(4): p. 1656-1664 e2.

208. Mathison, M., et al., *In vivo cardiac cellular reprogramming efficacy is enhanced by angiogenic preconditioning of the infarcted myocardium with vascular endothelial growth factor.* J Am Heart Assoc, 2012. **1**(6): p. e005652.

209. Srivastava, D., et al., *Cardiac repair with thymosin beta4 and cardiac reprogramming factors.* Ann N Y Acad Sci, 2012. **1270**: p. 66-72.

210. Jayawardena, T.M., et al., *MicroRNA induced cardiac reprogramming in vivo: evidence for mature cardiac myocytes and improved cardiac function.* Circ Res, 2015. **116**(3): p. 418-24.

211. Ma, H., et al., *In vivo cardiac reprogramming using an optimal single polycistronic construct.* Cardiovasc Res, 2015. **108**(2): p. 217-9.

212. Liu, Z., et al., *Re-patterning of H3K27me3, H3K4me3 and DNA methylation during fibroblast conversion into induced cardiomyocytes.* Stem Cell Res, 2016. **16**(2): p. 507-18.

213. Karamboulas, C., et al., *HDAC activity regulates entry of mesoderm cells into the cardiac muscle lineage.* J Cell Sci, 2006. **119**(Pt 20): p. 4305-14.

214. Chen, H.P., et al., *HDAC inhibition promotes cardiogenesis and the survival of embryonic stem cells through proteasome-dependent pathway.* J Cell Biochem, 2011. **112**(11): p. 3246-55.

215. Dal-Pra, S., et al., *Demethylation of H3K27 Is Essential for the Induction of Direct Cardiac Reprogramming by miR Combo.* Circ Res, 2017. **120**(9): p. 1403-1413.

216. Hirai, H. and N. Kikyo, *Inhibitors of suppressive histone modification promote direct reprogramming of fibroblasts to cardiomyocyte-like cells.* Cardiovasc Res, 2014. **102**(1): p. 188-90.

217. Zhou, Y., et al., *Bmi1 Is a Key Epigenetic Barrier to Direct Cardiac Reprogramming.* Cell Stem Cell, 2016. **18**(3): p. 382-95.

218. Liu, L., et al., *Targeting Mll1 H3K4 methyltransferase activity to guide cardiac lineage specific reprogramming of fibroblasts.* Cell Discov, 2016. **2**: p. 16036.

219. Zhao, Y., et al., *High-efficiency reprogramming of fibroblasts into cardiomyocytes requires suppression of pro-fibrotic signalling.* Nat Commun, 2015. **6**: p. 8243.

220. Mohamed, T.M., et al., *Chemical Enhancement of In Vitro and In Vivo Direct Cardiac Reprogramming.* Circulation, 2017. **135**(10): p. 978-995.

221. Zhou, H., et al., *Akt1/protein kinase B enhances transcriptional reprogramming of fibroblasts to functional cardiomyocytes.* Proc Natl Acad Sci U S A, 2015. **112**(38): p. 11864-9.

222. Abad, M., et al., *Notch Inhibition Enhances Cardiac Reprogramming by Increasing MEF2C Transcriptional Activity.* Stem Cell Reports, 2017. **8**(3): p. 548-560.

223. Yamakawa, H., et al., *Fibroblast Growth Factors and Vascular Endothelial Growth Factor Promote Cardiac Reprogramming under Defined Conditions.* Stem Cell Reports, 2015. **5**(6): p. 1128-1142.

224. Chopra, A., et al., *Reprogramming cardiomyocyte mechanosensing by crosstalk between integrins and hyaluronic acid receptors.* J Biomech, 2012. **45**(5): p. 824-31.

225. Sia, J., et al., *Effect of biophysical cues on reprogramming to cardiomyocytes.* Biomaterials, 2016. **103**: p. 1-11.

226. Morez, C., et al., *Enhanced efficiency of genetic programming toward cardiomyocyte creation through topographical cues.* Biomaterials, 2015. **70**: p. 94-104.

227. Kong, Y.P., et al., *Matrix identity and tractional forces influence indirect cardiac reprogramming.* Sci Rep, 2013. **3**: p. 3474.

228. Li, Y., et al., *Tissue-engineered 3-dimensional (3D) microenvironment enhances the direct reprogramming of fibroblasts into cardiomyocytes by microRNAs.* Sci Rep, 2016. **6**: p. 38815.

229. Smart, N. and P.R. Riley, *The epicardium as a candidate for heart regeneration.* Future Cardiol, 2012. **8**(1): p. 53-69.

230. Duenas, A., A.E. Aranega, and D. Franco, *More than Just a Simple Cardiac Envelope; Cellular Contributions of the Epicardium.* Front Cell Dev Biol, 2017. **5**: p. 44.

231. Dettman, R.W., et al., *Common epicardial origin of coronary vascular smooth muscle, perivascular fibroblasts, and intermyocardial fibroblasts in the avian heart.* Dev Biol, 1998. **193**(2): p. 169-81.

232. Masters, M. and P.R. Riley, *The epicardium signals the way towards heart regeneration.* Stem Cell Res, 2014. **13**(3 Pt B): p. 683-92.

233. Burns, C.G. and C.E. Burns, *Development. A crowning achievement for deciphering coronary origins.* Science, 2014. **345**(6192): p. 28-9.

234. Boyd, N.L., et al., *Dissecting the role of human embryonic stem cell-derived mesenchymal cells in human umbilical vein endothelial cell network stabilization in three-dimensional environments.* Tissue Eng Part A, 2013. **19**(1-2): p. 211-23.

235. Trembley, M.A., L.S. Velasquez, and E.M. Small, *Epicardial Outgrowth Culture Assay and Ex Vivo Assessment of Epicardial-derived Cell Migration.* J Vis Exp, 2016(109).

236. Zhou, B., et al., *Epicardial progenitors contribute to the cardiomyocyte lineage in the developing heart.* Nature, 2008. **454**(7200): p. 109-13.

237. Cai, C.L., et al., *A myocardial lineage derives from Tbx18 epicardial cells.* Nature, 2008. **454**(7200): p. 104-8.

238. Christoffels, V.M., et al., *Tbx18 and the fate of epicardial progenitors.* Nature, 2009. **458**(7240): p. E8-9; discussion E9-10.

239. Zeng, B., et al., *Developmental patterns and characteristics of epicardial cell markers Tbx18 and Wt1 in murine embryonic heart.* J Biomed Sci, 2011. **18**: p. 67.

240. Rudat, C. and A. Kispert, *Wt1 and epicardial fate mapping.* Circ Res, 2012. **111**(2): p. 165-9.

241. Kikuchi, K., et al., *tcf21+ epicardial cells adopt non-myocardial fates during zebrafish heart development and regeneration.* Development, 2011. **138**(14): p. 2895-902.

242. Gonzalez-Rosa, J.M., M. Peralta, and N. Mercader, *Pan-epicardial lineage tracing reveals that epicardium derived cells give rise to myofibroblasts and perivascular cells during zebrafish heart regeneration.* Dev Biol, 2012. **370**(2): p. 173-86.

243. Perez-Pomares, J.M., et al., *Origin of coronary endothelial cells from epicardial mesothelium in avian embryos.* Int J Dev Biol, 2002. **46**(8): p. 1005-13.

244. Mikawa, T. and D.A. Fischman, *Retroviral analysis of cardiac morphogenesis: discontinuous formation of coronary vessels.* Proc Natl Acad Sci U S A, 1992. **89**(20): p. 9504-8.

245. Red-Horse, K., et al., *Coronary arteries form by developmental reprogramming of venous cells.* Nature, 2010. **464**(7288): p. 549-53.

246. Grieskamp, T., et al., *Notch signaling regulates smooth muscle differentiation of epicardium-derived cells.* Circ Res, 2011. **108**(7): p. 813-23.

247. Riley, P.R. and N. Smart, *Vascularizing the heart.* Cardiovasc Res, 2011. **91**(2): p. 260-8.

248. Kang, J.O. and H.M. Sucov, *Convergent proliferative response and divergent morphogenic pathways induced by epicardial and endocardial signaling in fetal heart development.* Mech Dev, 2005. **122**(1): p. 57-65.

249. Stuckmann, I., S. Evans, and A.B. Lassar, *Erythropoietin and retinoic acid, secreted from the epicardium, are required for cardiac myocyte proliferation.* Dev Biol, 2003. **255**(2): p. 334-49.

250. Chen, T., et al., *Epicardial induction of fetal cardiomyocyte proliferation via a retinoic acid-inducible trophic factor.* Dev Biol, 2002. **250**(1): p. 198-207.

251. Brade, T., et al., *Retinoic acid stimulates myocardial expansion by induction of hepatic erythropoietin which activates epicardial Igf2.* Development, 2011. **138**(1): p. 139-48.

252. Porrello, E.R., et al., *Transient regenerative potential of the neonatal mouse heart.* Science, 2011. **331**(6020): p. 1078-80.

253. Lavine, K.J., et al., *Endocardial and epicardial derived FGF signals regulate myocardial proliferation and differentiation in vivo.* Dev Cell, 2005. **8**(1): p. 85-95.

254. Morabito, C.J., et al., *Positive and negative regulation of epicardial-mesenchymal transformation during avian heart development.* Dev Biol, 2001. **234**(1): p. 204-15.

255. Ieda, M., et al., *Cardiac fibroblasts regulate myocardial proliferation through beta1 integrin signaling.* Dev Cell, 2009. **16**(2): p. 233-44.

256. Wills, A.A., et al., *Regulated addition of new myocardial and epicardial cells fosters homeostatic cardiac growth and maintenance in adult zebrafish.* Development, 2008. **135**(1): p. 183-92.

257. Eid, H., et al., *Role of epicardial mesothelial cells in the modification of phenotype and function of adult rat ventricular myocytes in primary coculture.* Circ Res, 1992. **71**(1): p. 40-50.

258. Smart, N., et al., *Thymosin beta4 induces adult epicardial progenitor mobilization and neovascularization.* Nature, 2007. **445**(7124): p. 177-82.

259. Bock-Marquette, I., et al., *Thymosin β4 mediated PKC activation is essential to initiate the embryonic coronary developmental program and epicardial progenitor cell activation in adult mice in vivo.* Journal of Molecular and Cellular Cardiology, 2009. **46**(5): p. 728-738.

260. van Wijk, B., et al., *Cardiac regeneration from activated epicardium.* PLoS One, 2012. **7**(9): p. e44692.

261. Zhou, B., et al., *Adult mouse epicardium modulates myocardial injury by secreting paracrine factors.* J Clin Invest, 2011. **121**(5): p. 1894-904.

262. Lepilina, A., et al., *A dynamic epicardial injury response supports progenitor cell activity during zebrafish heart regeneration.* Cell, 2006. **127**(3): p. 607-19.

263. Wang, J., et al., *Fibronectin is deposited by injury-activated epicardial cells and is necessary for zebrafish heart regeneration.* Dev Biol, 2013. **382**(2): p. 427-35.

264. Mercer, S.E., S.J. Odelberg, and H.G. Simon, *A dynamic spatiotemporal extracellular matrix facilitates epicardial-mediated vertebrate heart regeneration.* Dev Biol, 2013. **382**(2): p. 457-69.

265. Huang, G.N., et al., *C/EBP transcription factors mediate epicardial activation during heart development and injury.* Science, 2012. **338**(6114): p. 1599-603.

266. Ramjee, V., et al., *Epicardial YAP/TAZ orchestrate an immunosuppressive response following myocardial infarction.* J Clin Invest, 2017. **127**(3): p. 899-911.

267. Limana, F., et al., *Myocardial infarction induces embryonic reprogramming of epicardial c-kit(+) cells: role of the pericardial fluid.* J Mol Cell Cardiol, 2010. **48**(4): p. 609-18.

268. Bollini, S., et al., *Re-activated adult epicardial progenitor cells are a heterogeneous population molecularly distinct from their embryonic counterparts.* Stem Cells Dev, 2014. **23**(15): p. 1719-30.

269. Smart, N., et al., *Thymosin beta4 facilitates epicardial neovascularization of the injured adult heart.* Ann N Y Acad Sci, 2010. **1194**: p. 97-104.

270. Shrivastava, S., et al., *Thymosin beta4 and cardiac repair.* Ann N Y Acad Sci, 2010. **1194**: p. 87-96.

271. Smart, N., et al., *De novo cardiomyocytes from within the activated adult heart after injury.* Nature, 2011. **474**(7353): p. 640-4.

272. Zhou, B., et al., *Thymosin beta 4 treatment after myocardial infarction does not reprogram epicardial cells into cardiomyocytes.* J Mol Cell Cardiol, 2012. **52**(1): p. 43-7.

273. Rui, L., et al., *Extending the time window of mammalian heart regeneration by thymosin beta 4.* J Cell Mol Med, 2014. **18**(12): p. 2417-24.

274. Vieira, J.M., et al., *BRG1-SWI/SNF-dependent regulation of the Wt1 transcriptional landscape mediates epicardial activity during heart development and disease.* Nat Commun, 2017. **8**: p. 16034.

275. Xiang, F.L., et al., *Cardiac-specific overexpression of human stem cell factor promotes epicardial activation and arteriogenesis after myocardial infarction.* Circ Heart Fail, 2014. **7**(5): p. 831-42.

276. Urayama, K., et al., *Prokineticin receptor-1 induces neovascularization and epicardial-derived progenitor cell differentiation.* Arterioscler Thromb Vasc Biol, 2008. **28**(5): p. 841-9.

277. Foglio, E., et al., *Exosomal clusterin, identified in the pericardial fluid, improves myocardial performance following MI through epicardial activation, enhanced arteriogenesis and reduced apoptosis.* Int J Cardiol, 2015. **197**: p. 333-47.

278. Wei, K., et al., *Epicardial FSTL1 reconstitution regenerates the adult mammalian heart.* Nature, 2015. **525**(7570): p. 479-85.

279. Wang, Q.L., et al., *Mesenchymal stem cell-loaded cardiac patch promotes epicardial activation and repair of the infarcted myocardium.* J Cell Mol Med, 2017. **21**(9): p. 1751-1766.

280. Zhou, B. and W.T. Pu, *Isolation and characterization of embryonic and adult epicardium and epicardium-derived cells.* Methods Mol Biol, 2012. **843**: p. 155-68.

281. Esser, K.-H., W.H. Marx, and T. Lisowsky, *maxXbond: first regeneration system for DNA binding silica matrices.* Nature Methods, 2006. **3**: p. 68.

282. Chuong, E.B., N.C. Elde, and C. Feschotte, *Regulatory activities of transposable elements: from conflicts to benefits.* Nat Rev Genet, 2017. **18**(2): p. 71-86.

283. Garcia-Garcia, L., et al., *Long-Term PEDF Release in Rat Iris and Retinal Epithelial Cells after Sleeping Beauty Transposon-Mediated Gene Delivery.* Mol Ther Nucleic Acids, 2017. **9**: p. 1-11.

284. Kren, B.T., et al., *Nanocapsule-delivered Sleeping Beauty mediates therapeutic Factor VIII expression in liver sinusoidal endothelial cells of hemophilia A mice.* J Clin Invest, 2009. **119**(7): p. 2086-99.

285. Tipanee, J., et al., *Preclinical and clinical advances in transposon-based gene therapy.* Biosci Rep, 2017. **37**(6).

286. Woodard, L.E. and M.H. Wilson, *piggyBac-ing models and new therapeutic strategies.* Trends Biotechnol, 2015. **33**(9): p. 525-33.

287. Provenzano, P.P. and P.J. Keely, *Mechanical signaling through the cytoskeleton regulates cell proliferation by coordinated focal adhesion and Rho GTPase signaling.* J Cell Sci, 2011. **124**(Pt 8): p. 1195-205.

288. Discher, D.E., P. Janmey, and Y.L. Wang, *Tissue cells feel and respond to the stiffness of their substrate.* Science, 2005. **310**(5751): p. 1139-43.

289. Isenberg, B.C., et al., *Vascular smooth muscle cell durotaxis depends on substrate stiffness gradient strength.* Biophys J, 2009. **97**(5): p. 1313-22.

290. Lachowski, D., et al., *Substrate Rigidity Controls Activation and Durotaxis in Pancreatic Stellate Cells.* Sci Rep, 2017. **7**(1): p. 2506.

291. Lo, C.M., et al., *Cell movement is guided by the rigidity of the substrate.* Biophys J, 2000. **79**(1): p. 144-52.

292. Klein, E.A., et al., *Cell-cycle control by physiological matrix elasticity and in vivo tissue stiffening.* Curr Biol, 2009. **19**(18): p. 1511-8.

293. Hadjipanayi, E., V. Mudera, and R.A. Brown, *Close dependence of fibroblast proliferation on collagen scaffold matrix stiffness.* J Tissue Eng Regen Med, 2009. **3**(2): p. 77-84.

294. Wang, H.B., M. Dembo, and Y.L. Wang, *Substrate flexibility regulates growth and apoptosis of normal but not transformed cells.* Am J Physiol Cell Physiol, 2000. **279**(5): p. C1345-50.

295. Heisenberg, C.P. and Y. Bellaiche, *Forces in tissue morphogenesis and patterning.* Cell, 2013. **153**(5): p. 948-62.

296. Mammoto, T. and D.E. Ingber, *Mechanical control of tissue and organ development.* Development, 2010. **137**(9): p. 1407-20.

297. Chua, K.N., et al., *Surface-aminated electrospun nanofibers enhance adhesion and expansion of human umbilical cord blood hematopoietic stem/progenitor cells.* Biomaterials, 2006. **27**(36): p. 6043-51.

298. Kurth, I., et al., *Hematopoietic stem and progenitor cells in adhesive microcavities.* Integr Biol (Camb), 2009. **1**(5-6): p. 427-34.

299. Saha, S., et al., *Inhibition of human embryonic stem cell differentiation by mechanical strain.* J Cell Physiol, 2006. **206**(1): p. 126-37.

300. Heo, K.S., K. Fujiwara, and J. Abe, *Shear stress and atherosclerosis.* Mol Cells, 2014. **37**(6): p. 435-40.

301. Simmons, R.D., S. Kumar, and H. Jo, *The role of endothelial mechanosensitive genes in atherosclerosis and omics approaches.* Arch Biochem Biophys, 2016. **591**: p. 111-31.

302. Spyropoulou, A., K. Karamesinis, and E.K. Basdra, *Mechanotransduction pathways in bone pathobiology.* Biochim Biophys Acta, 2015. **1852**(9): p. 1700-8.

303. Kim, J.H., et al., *Matrix cross-linking-mediated mechanotransduction promotes posttraumatic osteoarthritis.* Proc Natl Acad Sci U S A, 2015. **112**(30): p. 9424-9.

304. Broders-Bondon, F., et al., *Mechanotransduction in tumor progression: The dark side of the force.* The Journal of Cell Biology, 2018.

305. Lammerding, J., et al., *Lamin A/C deficiency causes defective nuclear mechanics and mechanotransduction.* J Clin Invest, 2004. **113**(3): p. 370-8.

306. Dahl, K.N., et al., *Distinct structural and mechanical properties of the nuclear lamina in Hutchinson-Gilford progeria syndrome.* Proc Natl Acad Sci U S A, 2006. **103**(27): p. 10271-10276.

307. Scaffidi, P. and T. Misteli, *Lamin A-dependent nuclear defects in human aging.* Science, 2006. **312**(5776): p. 1059-63.

308. Vogel, V. and M. Sheetz, *Local force and geometry sensing regulate cell functions.* Nat Rev Mol Cell Biol, 2006. **7**(4): p. 265-75.

309. Hynes, R.O. and A. Naba, *Overview of the matrisome--an inventory of extracellular matrix constituents and functions.* Cold Spring Harb Perspect Biol, 2012. **4**(1): p. a004903.

310. Humphrey, J.D., E.R. Dufresne, and M.A. Schwartz, *Mechanotransduction and extracellular matrix homeostasis.* Nat Rev Mol Cell Biol, 2014. **15**(12): p. 802-12.

311. Schwartz, M.A., M.D. Schaller, and M.H. Ginsberg, *Integrins: emerging paradigms of signal transduction.* Annu Rev Cell Dev Biol, 1995. **11**: p. 549-99.

312. Humphries, J.D., A. Byron, and M.J. Humphries, *Integrin ligands at a glance.* J Cell Sci, 2006. **119**(Pt 19): p. 3901-3.

313. Vicente-Manzanares, M. and A.R. Horwitz, *Adhesion dynamics at a glance.* J Cell Sci, 2011. **124**(Pt 23): p. 3923-7.

314. Dalby, M.J., N. Gadegaard, and R.O. Oreffo, *Harnessing nanotopography and integrin-matrix interactions to influence stem cell fate.* Nat Mater, 2014. **13**(6): p. 558-69.

315. Janmey, P.A., et al., *From tissue mechanics to transcription factors.* Differentiation, 2013. **86**(3): p. 112-20.

316. Mitra, S.K., D.A. Hanson, and D.D. Schlaepfer, *Focal adhesion kinase: in command and control of cell motility.* Nat Rev Mol Cell Biol, 2005. **6**(1): p. 56-68.

317. del Rio, A., et al., *Stretching single talin rod molecules activates vinculin binding.* Science, 2009. **323**(5914): p. 638-41.

318. Grashoff, C., et al., *Measuring mechanical tension across vinculin reveals regulation of focal adhesion dynamics.* Nature, 2010. **466**(7303): p. 263-6.

319. Sawada, Y., et al., *Force sensing by mechanical extension of the Src family kinase substrate p130Cas.* Cell, 2006. **127**(5): p. 1015-26.

320. Khatiwala, C.B., et al., *The regulation of osteogenesis by ECM rigidity in MC3T3-E1 cells requires MAPK activation.* J Cell Physiol, 2007. **211**(3): p. 661-72.

321. Hamamura, K., et al., *RhoA-mediated signaling in mechanotransduction of osteoblasts.* Connect Tissue Res, 2012. **53**(5): p. 398-406.

322. Birukov, K.G., *Small GTPases in mechanosensitive regulation of endothelial barrier.* Microvasc Res, 2009. **77**(1): p. 46-52.

323. Holle, A.W., et al., *In situ mechanotransduction via vinculin regulates stem cell differentiation.* Stem Cells, 2013. **31**(11): p. 2467-77.

324. le Duc, Q., et al., *Vinculin potentiates E-cadherin mechanosensing and is recruited to actin-anchored sites within adherens junctions in a myosin II-dependent manner.* J Cell Biol, 2010. **189**(7): p. 1107-15.

325. Tzima, E., et al., *A mechanosensory complex that mediates the endothelial cell response to fluid shear stress.* Nature, 2005. **437**(7057): p. 426-31.

326. Makino, A., et al., *G protein-coupled receptors serve as mechanosensors for fluid shear stress in neutrophils.* Am J Physiol Cell Physiol, 2006. **290**(6): p. C1633-9.

327. Martinac, B., *Mechanosensitive ion channels: an evolutionary and scientific tour de force in mechanobiology.* Channels (Austin), 2012. **6**(4): p. 211-3.

328. O'Conor, C.J., et al., *TRPV4-mediated mechanotransduction regulates the metabolic response of chondrocytes to dynamic loading.* Proc Natl Acad Sci U S A, 2014. **111**(4): p. 1316-21.

329. Matthews, B.D., et al., *Ultra-rapid activation of TRPV4 ion channels by mechanical forces applied to cell surface beta1 integrins.* Integr Biol (Camb), 2010. **2**(9): p. 435-42.

330. Head, B.P., H.H. Patel, and P.A. Insel, *Interaction of membrane/lipid rafts with the cytoskeleton: impact on signaling and function: membrane/lipid rafts, mediators of cytoskeletal arrangement and cell signaling.* Biochim Biophys Acta, 2014. **1838**(2): p. 532-45.

331. Das, J., et al., *Hemodynamic shear stress induces protective autophagy in HeLa cells through lipid raft-mediated mechanotransduction.* Clin Exp Metastasis, 2018.

332. Corriden, R. and P.A. Insel, *New insights regarding the regulation of chemotaxis by nucleotides, adenosine, and their receptors.* Purinergic Signal, 2012. **8**(3): p. 587-98.

333. Solon, J., et al., *Fibroblast adaptation and stiffness matching to soft elastic substrates.* Biophys J, 2007. **93**(12): p. 4453-61.

334. Jungbauer, S., et al., *Two characteristic regimes in frequency-dependent dynamic reorientation of fibroblasts on cyclically stretched substrates.* Biophys J, 2008. **95**(7): p. 3470-8.

335. Faust, U., et al., *Cyclic stress at mHz frequencies aligns fibroblasts in direction of zero strain.* PLoS One, 2011. **6**(12): p. e28963.

336. Na, S., et al., *Rapid signal transduction in living cells is a unique feature of mechanotransduction.* Proc Natl Acad Sci U S A, 2008. **105**(18): p. 6626-31.

337. Martins, R.P., et al., *Mechanical regulation of nuclear structure and function.* Annu Rev Biomed Eng, 2012. **14**: p. 431-55.

338. Khatau, S.B., et al., *A perinuclear actin cap regulates nuclear shape.* Proc Natl Acad Sci U S A, 2009. **106**(45): p. 19017-22.

339. Rhee, S., et al., *Microtubule function in fibroblast spreading is modulated according to the tension state of cell-matrix interactions.* Proc Natl Acad Sci U S A, 2007. **104**(13): p. 5425-30.

340. Ng, D.H., et al., *Microtubule-dependent modulation of adhesion complex composition.* PLoS One, 2014. **9**(12): p. e115213.

341. Minin, A.A. and M.V. Moldaver, *Intermediate vimentin filaments and their role in intracellular organelle distribution.* Biochemistry (Mosc), 2008. **73**(13): p. 1453-66.

342. Shabbir, S.H., et al., *Geometric control of vimentin intermediate filaments.* Biomaterials, 2014. **35**(5): p. 1359-66.

343. Ketema, M., et al., *Nesprin-3 connects plectin and vimentin to the nuclear envelope of Sertoli cells but is not required for Sertoli cell function in spermatogenesis.* Mol Biol Cell, 2013. **24**(15): p. 2454-66.

344. Gasparri, F., et al., *Thymidine kinase 1 expression defines an activated G1 state of the cell cycle as revealed with site-specific antibodies and ArrayScan assays.* Eur J Cell Biol, 2009. **88**(12): p. 779-85.

345. Eckes, B., et al., *Impaired mechanical stability, migration and contractile capacity in vimentin-deficient fibroblasts.* J Cell Sci, 1998. **111 (Pt 13)**: p. 1897-907.

346. Clark, K., et al., *Myosin II and mechanotransduction: a balancing act.* Trends Cell Biol, 2007. **17**(4): p. 178-86.

347. Ridley, A.J., et al., *Cell migration: integrating signals from front to back.* Science, 2003. **302**(5651): p. 1704-9.

348. Van Haastert, P.J. and P.N. Devreotes, *Chemotaxis: signalling the way forward.* Nat Rev Mol Cell Biol, 2004. **5**(8): p. 626-34.

349. McBeath, R., et al., *Cell shape, cytoskeletal tension, and RhoA regulate stem cell lineage commitment.* Dev Cell, 2004. **6**(4): p. 483-95.

350. Paszek, M.J., et al., *Tensional homeostasis and the malignant phenotype.* Cancer Cell, 2005. **8**(3): p. 241-54.

351. Shin, J.W., et al., *Contractile forces sustain and polarize hematopoiesis from stem and progenitor cells.* Cell Stem Cell, 2014. **14**(1): p. 81-93.

352. Lombardi, M.L., et al., *The interaction between nesprins and sun proteins at the nuclear envelope is critical for force transmission between the nucleus and cytoskeleton.* J Biol Chem, 2011. **286**(30): p. 26743-53.

353. Starr, D.A. and H.N. Fridolfsson, *Interactions between nuclei and the cytoskeleton are mediated by SUN-KASH nuclear-envelope bridges.* Annu Rev Cell Dev Biol, 2010. **26**: p. 421-44.

354. Maniotis, A.J., C.S. Chen, and D.E. Ingber, *Demonstration of mechanical connections between integrins, cytoskeletal filaments, and nucleoplasm that stabilize nuclear structure.* Proc Natl Acad Sci U S A, 1997. **94**(3): p. 849-54.

355. Wang, N., J.D. Tytell, and D.E. Ingber, *Mechanotransduction at a distance: mechanically coupling the extracellular matrix with the nucleus.* Nat Rev Mol Cell Biol, 2009. **10**(1): p. 75-82.

356. Guilluy, C. and K. Burridge, *Nuclear mechanotransduction: forcing the nucleus to respond.* Nucleus, 2015. **6**(1): p. 19-22.

357. Athirasala, A., N. Hirsch, and A. Buxboim, *Nuclear mechanotransduction: sensing the force from within.* Curr Opin Cell Biol, 2017. **46**: p. 119-127.

358. Swift, J. and D.E. Discher, *The nuclear lamina is mechano-responsive to ECM elasticity in mature tissue.* J Cell Sci, 2014. **127**(Pt 14): p. 3005-15.

359. Eckersley-Maslin, M.A., et al., *Lamin A/C is expressed in pluripotent mouse embryonic stem cells.* Nucleus, 2013. **4**(1): p. 53-60.

360. Pajerowski, J.D., et al., *Physical plasticity of the nucleus in stem cell differentiation.* Proc Natl Acad Sci U S A, 2007. **104**(40): p. 15619-24.

361. Lammerding, J., et al., *Abnormal nuclear shape and impaired mechanotransduction in emerin-deficient cells.* J Cell Biol, 2005. **170**(5): p. 781-91.

362. Ihalainen, T.O., et al., *Differential basal-to-apical accessibility of lamin A/C epitopes in the nuclear lamina regulated by changes in cytoskeletal tension.* Nat Mater, 2015. **14**(12): p. 1252-1261.

363. Jia, Q., et al., *Downregulation of YAP-dependent Nupr1 promotes tumor-repopulating cell growth in soft matrices.* Oncogenesis, 2016. **5**: p. e220.

364. Ho, C.Y., et al., *Lamin A/C and emerin regulate MKL1-SRF activity by modulating actin dynamics.* Nature, 2013. **497**(7450): p. 507-11.

365. Garcia, A., J.F. Rodriguez Matas, and M.T. Raimondi, *Modeling of the mechano-chemical behaviour of the nuclear pore complex: current research and perspectives.* Integr Biol (Camb), 2016. **8**(10): p. 1011-1021.

366. Feuerborn, A. and P.R. Cook, *Why the activity of a gene depends on its neighbors.* Trends Genet, 2015. **31**(9): p. 483-90.

367. Lanctot, C., et al., *Dynamic genome architecture in the nuclear space: regulation of gene expression in three dimensions.* Nat Rev Genet, 2007. **8**(2): p. 104-15.

368. Bolzer, A., et al., *Three-dimensional maps of all chromosomes in human male fibroblast nuclei and prometaphase rosettes.* PLoS Biol, 2005. **3**(5): p. e157.

369. Neelam, S., et al., *Direct force probe reveals the mechanics of nuclear homeostasis in the mammalian cell.* Proc Natl Acad Sci U S A, 2015. **112**(18): p. 5720-5.

370. Li, Y., et al., *Biophysical regulation of histone acetylation in mesenchymal stem cells.* Biophys J, 2011. **100**(8): p. 1902-9.

371. Poh, Y.C., et al., *Dynamic force-induced direct dissociation of protein complexes in a nuclear body in living cells.* Nat Commun, 2012. **3**: p. 866.

372. Wang, Y., et al., *Orientation and repositioning of chromosomes correlate with cell geometry-dependent gene expression.* Mol Biol Cell, 2017. **28**(14): p. 1997-2009.

373. Enyedi, B., M. Jelcic, and P. Niethammer, *The Cell Nucleus Serves as a Mechanotransducer of Tissue Damage-Induced Inflammation.* Cell, 2016. **165**(5): p. 1160-1170.

374. De Vos, W.H., et al., *Repetitive disruptions of the nuclear envelope invoke temporary loss of cellular compartmentalization in laminopathies.* Hum Mol Genet, 2011. **20**(21): p. 4175-86.

375. Tamiello, C., et al., *Soft substrates normalize nuclear morphology and prevent nuclear rupture in fibroblasts from a laminopathy patient with compound heterozygous LMNA mutations.* Nucleus, 2013. **4**(1): p. 61-73.

376. Kornberg, R.D. and J.O. Thomas, *Chromatin structure; oligomers of the histones.* Science, 1974. **184**(4139): p. 865-8.

377. Kornberg, R.D., *Chromatin structure: a repeating unit of histones and DNA.* Science, 1974. **184**(4139): p. 868-71.

378. Felsenfeld, G. and M. Groudine, *Controlling the double helix.* Nature, 2003. **421**(6921): p. 448-53.

379. Meissner, A., et al., *Genome-scale DNA methylation maps of pluripotent and differentiated cells.* Nature, 2008. **454**(7205): p. 766-70.

380. Lister, R., et al., *Human DNA methylomes at base resolution show widespread epigenomic differences.* Nature, 2009. **462**(7271): p. 315-22.

381. Guenatri, M., et al., *Mouse centric and pericentric satellite repeats form distinct functional heterochromatin.* J Cell Biol, 2004. **166**(4): p. 493-505.

382. Arand, J., et al., *In vivo control of CpG and non-CpG DNA methylation by DNA methyltransferases.* PLoS Genet, 2012. **8**(6): p. e1002750.

383. Wu, X. and Y. Zhang, *TET-mediated active DNA demethylation: mechanism, function and beyond.* Nat Rev Genet, 2017. **18**(9): p. 517-534.

384. Tamaru, H. and E.U. Selker, *A histone H3 methyltransferase controls DNA methylation in Neurospora crassa.* Nature, 2001. **414**(6861): p. 277-83.

385. Jackson, J.P., et al., *Control of CpNpG DNA methylation by the KRYPTONITE histone H3 methyltransferase.* Nature, 2002. **416**(6880): p. 556-60.

386. Cheng, X., *Structural and functional coordination of DNA and histone methylation.* Cold Spring Harb Perspect Biol, 2014. **6**(8).

387. Allfrey, V.G., R. Faulkner, and A.E. Mirsky, *Acetylation and Methylation of Histones and Their Possible Role in the Regulation of Rna Synthesis.* Proc Natl Acad Sci U S A, 1964. **51**: p. 786-94.

388. Bannister, A.J. and T. Kouzarides, *Regulation of chromatin by histone modifications.* Cell Res, 2011. **21**(3): p. 381-95.

389. Yang, X.J. and E. Seto, *HATs and HDACs: from structure, function and regulation to novel strategies for therapy and prevention.* Oncogene, 2007. **26**(37): p. 5310-8.

390. Oki, M., H. Aihara, and T. Ito, *Role of histone phosphorylation in chromatin dynamics and its implications in diseases.* Subcell Biochem, 2007. **41**: p. 319-36.

391. Raab, M., et al., *ESCRT III repairs nuclear envelope ruptures during cell migration to limit DNA damage and cell death.* Science, 2016. **352**(6283): p. 359-62.

392. Denais, C.M., et al., *Nuclear envelope rupture and repair during cancer cell migration.* Science, 2016. **352**(6283): p. 353-8.

393. Jain, N., et al., *Cell geometric constraints induce modular gene-expression patterns via redistribution of HDAC3 regulated by actomyosin contractility.* Proc Natl Acad Sci U S A, 2013. **110**(28): p. 11349-54.

394. Illi, B., et al., *Shear stress-mediated chromatin remodeling provides molecular basis for flow-dependent regulation of gene expression.* Circ Res, 2003. **93**(2): p. 155-61.

395. Fish, J.E., et al., *The expression of endothelial nitric-oxide synthase is controlled by a cell-specific histone code.* J Biol Chem, 2005. **280**(26): p. 24824-38.

396. Zeng, L., et al., *The role of p53 deacetylation in p21Waf1 regulation by laminar flow.* J Biol Chem, 2003. **278**(27): p. 24594-9.

397. Lee, D.Y., et al., *Role of histone deacetylases in transcription factor regulation and cell cycle modulation in endothelial cells in response to disturbed flow.* Proc Natl Acad Sci U S A, 2012. **109**(6): p. 1967-72.

398. Stein, S. and C.M. Matter, *Protective roles of SIRT1 in atherosclerosis.* Cell Cycle, 2011. **10**(4): p. 640-7.

399. Zhou, J., et al., *Epigenetic Mechanism in Regulation of Endothelial Function by Disturbed Flow: Induction of DNA Hypermethylation by DNMT1.* Cell Mol Bioeng, 2014. **7**(2): p. 218-224.

400. Lund, G., et al., *DNA methylation polymorphisms precede any histological sign of atherosclerosis in mice lacking apolipoprotein E.* J Biol Chem, 2004. **279**(28): p. 29147-54.

401. Xu, J., Y. Du, and H. Deng, *Direct lineage reprogramming: strategies, mechanisms, and applications.* Cell Stem Cell, 2015. **16**(2): p. 119-34.

402. Huangfu, D., et al., *Induction of pluripotent stem cells by defined factors is greatly improved by small-molecule compounds.* Nat Biotechnol, 2008. **26**(7): p. 795-7.

403. Li, Y., et al., *Generation of iPSCs from mouse fibroblasts with a single gene, Oct4, and small molecules.* Cell Res, 2011. **21**(1): p. 196-204.

404. Anokye-Danso, F., et al., *Highly efficient miRNA-mediated reprogramming of mouse and human somatic cells to pluripotency.* Cell Stem Cell, 2011. **8**(4): p. 376-88.

405. Chen, L.J., S.Y. Wei, and J.J. Chiu, *Mechanical regulation of epigenetics in vascular biology and pathobiology.* J Cell Mol Med, 2013. **17**(4): p. 437-48.

406. Badique, F., et al., *Directing nuclear deformation on micropillared surfaces by substrate geometry and cytoskeleton organization.* Biomaterials, 2013. **34**(12): p. 2991-3001.

407. Davidson, P.M., et al., *Microstructured Surfaces Cause Severe but Non-Detrimental Deformation of the Cell Nucleus.* Advanced Materials, 2009. **21**(35): p. 3586-3590.

408. Pan, Z., et al., *Control of cell nucleus shapes via micropillar patterns.* Biomaterials, 2012. **33**(6): p. 1730-5.

409. Liu, X., et al., *Subcellular cell geometry on micropillars regulates stem cell differentiation.* Biomaterials, 2016. **111**: p. 27-39.

410. Versaevel, M., T. Grevesse, and S. Gabriele, *Spatial coordination between cell and nuclear shape within micropatterned endothelial cells.* Nat Commun, 2012. **3**: p. 671.

411. Wolf, K. and P. Friedl, *Mapping proteolytic cancer cell-extracellular matrix interfaces.* Clin Exp Metastasis, 2009. **26**(4): p. 289-98.

412. Goldman, R.D., et al., *Accumulation of mutant lamin A causes progressive changes in nuclear architecture in Hutchinson-Gilford progeria syndrome.* Proc Natl Acad Sci U S A, 2004. **101**(24): p. 8963-8.

413. Lou, H.Y., et al., *The Role of Membrane Curvature in Nanoscale Topography-Induced Intracellular Signaling.* Acc Chem Res, 2018. **51**(5): p. 1046-1053.

414. Flanagan, T.W. and D.T. Brown, *Molecular dynamics of histone H1.* Biochim Biophys Acta, 2016. **1859**(3): p. 468-75.

415. Stasevich, T.J., et al., *Dissecting the binding mechanism of the linker histone in live cells: an integrated FRAP analysis.* EMBO J, 2010. **29**(7): p. 1225-34.

416. Siritantikorn, A., et al., *Protection of cells from oxidative stress by microsomal glutathione transferase 1.* Biochem Biophys Res Commun, 2007. **355**(2): p. 592-6.

417. Ma, Q., *Role of nrf2 in oxidative stress and toxicity.* Annu Rev Pharmacol Toxicol, 2013. **53**: p. 401-26.

418. Guo, C., et al., *Silica nanoparticles induce oxidative stress, inflammation, and endothelial dysfunction in vitro via activation of the MAPK/Nrf2 pathway and nuclear factor-kappaB signaling.* Int J Nanomedicine, 2015. **10**: p. 1463-77.

419. Ghazalpour, A., et al., *Comparative analysis of proteome and transcriptome variation in mouse.* PLoS Genet, 2011. **7**(6): p. e1001393.

420. Pascal, L.E., et al., *Correlation of mRNA and protein levels: cell type-specific gene expression of cluster designation antigens in the prostate.* BMC Genomics, 2008. **9**: p. 246.

421. Yeung, E.S., *Genome-wide correlation between mRNA and protein in a single cell.* Angew Chem Int Ed Engl, 2011. **50**(3): p. 583-5.

422. Bonde, S., et al., *Exploring arrays of vertical one-dimensional nanostructures for cellular investigations.* Nanotechnology, 2014. **25**(36): p. 362001.

423. Kuo, S.W., et al., *Regulation of the fate of human mesenchymal stem cells by mechanical and stereo-topographical cues provided by silicon nanowires.* Biomaterials, 2012. **33**(20): p. 5013-22.

424. Persson, H., et al., *Fibroblasts cultured on nanowires exhibit low motility, impaired cell division, and DNA damage.* Small, 2013. **9**(23): p. 4006-16, 3905.

425. Dalby, M.J., et al., *Attempted endocytosis of nano-environment produced by colloidal lithography by human fibroblasts.* Exp Cell Res, 2004. **295**(2): p. 387-94.

426. Teo, B.K., et al., *The effect of micro and nanotopography on endocytosis in drug and gene delivery systems.* Biomaterials, 2011. **32**(36): p. 9866-75.

427. Yim, E.K., et al., *Nanotopography-induced changes in focal adhesions, cytoskeletal organization, and mechanical properties of human mesenchymal stem cells.* Biomaterials, 2010. **31**(6): p. 1299-306.

428. McMurray, R.J., et al., *Nanoscale surfaces for the long-term maintenance of mesenchymal stem cell phenotype and multipotency.* Nat Mater, 2011. **10**(8): p. 637-44.

429. Chen, W., et al., *Nanotopography influences adhesion, spreading, and self-renewal of human embryonic stem cells.* ACS Nano, 2012. **6**(5): p. 4094-103.

430. Forman, H.J., H. Zhang, and A. Rinna, *Glutathione: overview of its protective roles, measurement, and biosynthesis.* Mol Aspects Med, 2009. **30**(1-2): p. 1-12.

431. Benigni, A., P. Cassis, and G. Remuzzi, *Angiotensin II revisited: new roles in inflammation, immunology and aging.* EMBO Mol Med, 2010. **2**(7): p. 247-57.

432. Steckelings, U.M., E. Kaschina, and T. Unger, *The AT2 receptor--a matter of love and hate.* Peptides, 2005. **26**(8): p. 1401-9.

433. Wu, L., et al., *Roles of angiotensin II type 2 receptor stimulation associated with selective angiotensin II type 1 receptor blockade with valsartan in the improvement of inflammation-induced vascular injury.* Circulation, 2001. **104**(22): p. 2716-21.

434. Chang, Y. and W. Wei, *Angiotensin II in inflammation, immunity and rheumatoid arthritis.* Clin Exp Immunol, 2015. **179**(2): p. 137-45.

435. Ricciotti, E. and G.A. FitzGerald, *Prostaglandins and inflammation.* Arterioscler Thromb Vasc Biol, 2011. **31**(5): p. 986-1000.

436. Teppner, M., et al., *Quantitative profiling of prostaglandins as oxidative stress biomarkers in vitro and in vivo by negative ion online solid phase extraction - Liquid chromatography-tandem mass spectrometry.* Anal Biochem, 2016. **498**: p. 68-77.

437. Lin, C., et al., *Transcriptional activation of follistatin by Nrf2 protects pulmonary epithelial cells against silica nanoparticle-induced oxidative stress.* Sci Rep, 2016. **6**: p. 21133.

438. Panopoulos, A.D., et al., *The metabolome of induced pluripotent stem cells reveals metabolic changes occurring in somatic cell reprogramming.* Cell Res, 2012. **22**(1): p. 168-77.

439. Park, S.J., et al., *Metabolome Profiling of Partial and Fully Reprogrammed Induced Pluripotent Stem Cells.* Stem Cells Dev, 2017. **26**(10): p. 734-742.

440. Hawkins, K.E., et al., *NRF2 Orchestrates the Metabolic Shift during Induced Pluripotent Stem Cell Reprogramming.* Cell Rep, 2016. **14**(8): p. 1883-91.

441. Baird, L., et al., *Regulatory flexibility in the Nrf2-mediated stress response is conferred by conformational cycling of the Keap1-Nrf2 protein complex.* Proc Natl Acad Sci U S A, 2013. **110**(38): p. 15259-64.

442. Mathieu, J., et al., *Hypoxia-inducible factors have distinct and stage-specific roles during reprogramming of human cells to pluripotency.* Cell Stem Cell, 2014. **14**(5): p. 592-605.

443. Malumbres, M. and M. Barbacid, *Cell cycle, CDKs and cancer: a changing paradigm.* Nat Rev Cancer, 2009. **9**(3): p. 153-66.

444. Bruinsma, W., et al., *Inhibition of Polo-like kinase 1 during the DNA damage response is mediated through loss of Aurora A recruitment by Bora.* Oncogene, 2017. **36**(13): p. 1840-1848.

445. Peter, M., et al., *Initial activation of cyclin-B1-cdc2 kinase requires phosphorylation of cyclin B1.* EMBO Rep, 2002. **3**(6): p. 551-6.

446. Ciossani, G., et al., *The kinetochore proteins CENP-E and CENP-F directly and specifically interact with distinct BUB mitotic checkpoint Ser/Thr kinases.* J Biol Chem, 2018. **293**(26): p. 10084-10101.

447. Zhou, X., et al., *Phosphorylation of CENP-C by Aurora B facilitates kinetochore attachment error correction in mitosis.* Proc Natl Acad Sci U S A, 2017. **114**(50): p. E10667-E10676.

448. Guo, Y., et al., *CENP-E--dependent BubR1 autophosphorylation enhances chromosome alignment and the mitotic checkpoint.* J Cell Biol, 2012. **198**(2): p. 205-17.

449. Godek, K.M., L. Kabeche, and D.A. Compton, *Regulation of kinetochore-microtubule attachments through homeostatic control during mitosis.* Nat Rev Mol Cell Biol, 2015. **16**(1): p. 57-64.

450. Piret, G., M.T. Perez, and C.N. Prinz, *Neurite outgrowth and synaptophysin expression of postnatal CNS neurons on GaP nanowire arrays in long-term retinal cell culture.* Biomaterials, 2013. **34**(4): p. 875-87.

451. Bretones, G., M.D. Delgado, and J. Leon, *Myc and cell cycle control.* Biochim Biophys Acta, 2015. **1849**(5): p. 506-16.

452. Niu, Z., et al., *Knockdown of c-Myc inhibits cell proliferation by negatively regulating the Cdk/Rb/E2F pathway in nasopharyngeal carcinoma cells.* Acta Biochim Biophys Sin (Shanghai), 2015. **47**(3): p. 183-91.

453. Wang, H., et al., *c-Myc depletion inhibits proliferation of human tumor cells at various stages of the cell cycle.* Oncogene, 2008. **27**(13): p. 1905-15.

454. Chen, X., et al., *The forkhead transcription factor FOXM1 controls cell cycle-dependent gene expression through an atypical chromatin binding mechanism.* Mol Cell Biol, 2013. **33**(2): p. 227-36.

455. Bagui, T.K., et al., *Proliferative status regulates HDAC11 mRNA abundance in nontransformed fibroblasts.* Cell Cycle, 2013. **12**(21): p. 3433-41.

456. Chen, J.X., et al., *Inefficient reprogramming of fibroblasts into cardiomyocytes using Gata4, Mef2c, and Tbx5.* Circ Res, 2012. **111**(1): p. 50-5.

457. Kim, W., et al., *Interfacing silicon nanowires with mammalian cells.* J Am Chem Soc, 2007. **129**(23): p. 7228-9.

458. Ward, M.W. et al., Real Time Single Cell Analysis of Bid Cleavage and Bid Translocation during Caspase-dependent and Neuronal Caspase-independent Apoptosis. Journal of Biological Chemistry, 2006. **281**(9): p. 5837-44.

459. Prokhorova, E.A. et al., Role of the nucleus in apoptosis:signaling and execution.Cell Mol Life Sci. 2015. **72**(23): p. 4593-612.

460. Fahrenkrog, B. Histone modifications as regulators of life and death in Saccharomyces cerevisiae. Microb Cell. 2016. **3**(1): p1-13.